

Lecture Notes in Chemistry 96

Jianyong Zhang

Ya Hu

Yongguang Li

# Gel Chemistry

Interactions, Structures and Properties



Springer

# Lecture Notes in Chemistry

Volume 96

## Series editors

Barry Carpenter, Cardiff, UK  
Paola Ceroni, Bologna, Italy  
Barbara Kirchner, Bonn, Germany  
Katharina Landfester, Mainz, Germany  
Jerzy Leszczynski, Jackson, USA  
Tien-Yau Luh, Taipei, Taiwan  
Eva Perlt, Bonn, Germany  
Nicolas C. Polfer, Gainesville, USA  
Reiner Salzer, Dresden, Germany

## The Lecture Notes in Chemistry

The series Lecture Notes in Chemistry (LNC) reports new developments in chemistry and molecular science-quickly and informally, but with a high quality and the explicit aim to summarize and communicate current knowledge for teaching and training purposes. Books published in this series are conceived as bridging material between advanced graduate textbooks and the forefront of research. They will serve the following purposes:

- provide an accessible introduction to the field to postgraduate students and nonspecialist researchers from related areas,
- provide a source of advanced teaching material for specialized seminars, courses and schools, and
- be readily accessible in print and online

The series covers all established fields of chemistry such as analytical chemistry, organic chemistry, inorganic chemistry, physical chemistry including electrochemistry, theoretical and computational chemistry, industrial chemistry, and catalysis. It is also a particularly suitable forum for volumes addressing the interfaces of chemistry with other disciplines, such as biology, medicine, physics, engineering, materials science including polymer and nanoscience, or earth and environmental science.

Both authored and edited volumes will be considered for publication. Edited volumes should however consist of a very limited number of contributions only. Proceedings will not be considered for LNC.

The year 2010 marks the relaunch of LNC.

More information about this series at <http://www.springer.com/series/632>

Jianyong Zhang · Ya Hu  
Yongguang Li

# Gel Chemistry

Interactions, Structures and Properties

 Springer

Jianyong Zhang  
School of Materials Science and Engineering  
Sun Yat-sen University  
Guangzhou, Guangdong  
China

Yongguang Li  
School of Chemistry and Chemical  
Engineering  
Sun Yat-sen University  
Guangzhou, Guangdong  
China

Ya Hu  
School of Materials Science and Engineering  
Sun Yat-sen University  
Guangzhou, Guangdong  
China

ISSN 0342-4901

ISSN 2192-6603 (electronic)

Lecture Notes in Chemistry

ISBN 978-981-10-6880-5

ISBN 978-981-10-6881-2 (eBook)

<https://doi.org/10.1007/978-981-10-6881-2>

Library of Congress Control Number: 2017962035

© Springer Nature Singapore Pte Ltd. 2018

This work is subject to copyright. All rights are reserved by the Publisher, whether the whole or part of the material is concerned, specifically the rights of translation, reprinting, reuse of illustrations, recitation, broadcasting, reproduction on microfilms or in any other physical way, and transmission or information storage and retrieval, electronic adaptation, computer software, or by similar or dissimilar methodology now known or hereafter developed.

The use of general descriptive names, registered names, trademarks, service marks, etc. in this publication does not imply, even in the absence of a specific statement, that such names are exempt from the relevant protective laws and regulations and therefore free for general use.

The publisher, the authors and the editors are safe to assume that the advice and information in this book are believed to be true and accurate at the date of publication. Neither the publisher nor the authors or the editors give a warranty, express or implied, with respect to the material contained herein or for any errors or omissions that may have been made. The publisher remains neutral with regard to jurisdictional claims in published maps and institutional affiliations.

Printed on acid-free paper

This Springer imprint is published by Springer Nature

The registered company is Springer Nature Singapore Pte Ltd.

The registered company address is: 152 Beach Road, #21-01/04 Gateway East, Singapore 189721, Singapore

# Contents

<b>1</b>	<b>Introduction</b>	1
1.1	Components of Gels	1
1.2	Driving Force	3
1.3	Characterization	4
	References	6
<b>2</b>	<b>Supramolecular Gels</b>	9
2.1	Heat/Temperature Responsive Gels	10
2.2	Light Responsive Gels	16
2.2.1	Conformational Changes	16
2.2.2	Coupling Reactions	22
2.2.3	Electrocyclic Reactions	23
2.3	Sonication and Mechanical Stress Responsive Gels	29
2.3.1	Ultrasound	30
2.3.2	Mechanical Stress	34
2.4	Chemical Responsive Gels	37
2.4.1	Acid and Base	37
2.4.2	Redox	40
2.4.3	Ion	42
2.4.4	Neutral Species	48
2.5	Conclusions	51
	References	51
<b>3</b>	<b>Metal–Organic Gels</b>	61
3.1	Discrete Gelators	62
3.1.1	Metal–Organic Gelators with Monodentate Ligands	62
3.1.2	Metal–Organic Gelators with Chelate Ligands	65
3.1.3	Organometallic Gelators	70

3.1.4	Metal–Organic Gelators Based on Tripyridine and Tridentate Ligands . . . . .	72
3.1.5	Coordination Cages . . . . .	76
3.2	Coordination Polymer Gelators . . . . .	81
3.2.1	Metal–Carboxylate Gels . . . . .	81
3.2.2	Metal–Heterocycle Polymer Gels . . . . .	89
3.2.3	Coordination Polymer Gels with Hybrid Donors . . . . .	95
3.3	Applications . . . . .	101
3.3.1	Gels as Crystallization Media . . . . .	101
3.3.2	Post-modification of Organogels by Metal Ions . . . . .	103
3.3.3	Metal–Organic Gels for Sorption . . . . .	105
3.3.4	Metal–Organic Gels as Template . . . . .	106
3.3.5	Metal–Organic Gels as Catalyst . . . . .	108
	References . . . . .	111
<b>4</b>	<b>Dynamic Covalent Gels</b> . . . . .	<b>119</b>
4.1	Discrete Gelators . . . . .	121
4.1.1	Imine/Acylhydrazone Gels . . . . .	121
4.1.2	Imine/Acylhydrazone Gels and Metal Ions . . . . .	128
4.1.3	Borate Gels . . . . .	135
4.1.4	Conversions Between Anthracene and Its Dimer . . . . .	139
4.1.5	Dynamic Covalent Cycles and Cages . . . . .	139
4.2	Dynamic Covalent Polymer Gelators . . . . .	141
4.2.1	Imine Gels . . . . .	143
4.2.2	Calix[4]Arene-Derived Acylhydrazone Gels . . . . .	145
	References . . . . .	148
<b>5</b>	<b>Polymer Gels</b> . . . . .	<b>153</b>
5.1	Introduction to Polymer Gels . . . . .	153
5.1.1	Cross-Linking of Polymer Chains . . . . .	154
5.1.2	Traditional Polymer Gels . . . . .	155
5.2	Fundamental Aspects . . . . .	157
5.2.1	Concepts . . . . .	157
5.2.2	Mechanical Properties . . . . .	158
5.2.3	Swelling and Shrinking Properties . . . . .	158
5.3	Nature of Cross-Linking Leading to the Formation of Polymer Gels . . . . .	162
5.3.1	Hydrogen-Bonded Polymer Gels . . . . .	162
5.3.2	Metal–Organic Coordination Polymer Gels . . . . .	165
5.3.3	Polymer Gels Based on Dynamic Covalent Chemistry . . . . .	171
5.3.4	Hybrid Polymer and Low Molecular Weight Gels . . . . .	178
	References . . . . .	185

<b>6 Inorganic Gels</b> .....	191
6.1 Sol–Gel Process for Gel Formation .....	192
6.2 Silica-Based Gels .....	194
6.3 Chalcogels .....	199
6.4 Other Inorganic Gels .....	204
References .....	206
<b>Index</b> .....	209

# Chapter 1

## Introduction

**Abstract** A brief introduction of gels, their components, driving force and characterization is given in this chapter.

**Keywords** Gels · Supramolecular interactions · Characterization

A gel is “a soft, solid or solid-like material consisting of two or more components one of which is a liquid, present in substantial quantity” according to Kramer’s definition [1–3]. Gels often consist of two continuous phases which interpenetrate on the macroscopic scale. Gels consist mainly of a liquid (e.g. water, alcohol) which interpenetrates with a persistent network structure, formed by a second species, the gelator. Solvent is the major component, up to about 99% by weight of the gel, while the remaining 1% is the gelator [4]. The persistent gelator network prevents the liquid constituent from flowing freely due to its attraction to the liquid, although the molecules of the liquid continue to diffuse throughout the structure. Therefore, gels exhibit some rheological properties like those of a solid.

### 1.1 Components of Gels

Gelators may be discrete small molecules, polymers, inorganic particles or colloidal particles (Fig. 1.1). The gelators aggregate via various supramolecular interactions to form one-dimensional (1D), 2D and 3D structures. For discrete small molecules, 1D structures (e.g. fibres) may be formed via intermolecular–supramolecular interactions such as hydrogen bonding,  $\pi\cdots\pi$  stacking, van der Waals attraction, solvophobic effects, forming supramolecular gels. When polymer chains are cross-linked via various interactions, polymer gels may be obtained. In inorganic gels, precursors react to form inorganic colloidal particles and the particles are further cross-linked to form inorganic gel matrix. When bridging molecular

---

Jianyong Zhang and Yongguang Li contributed together to this chapter.

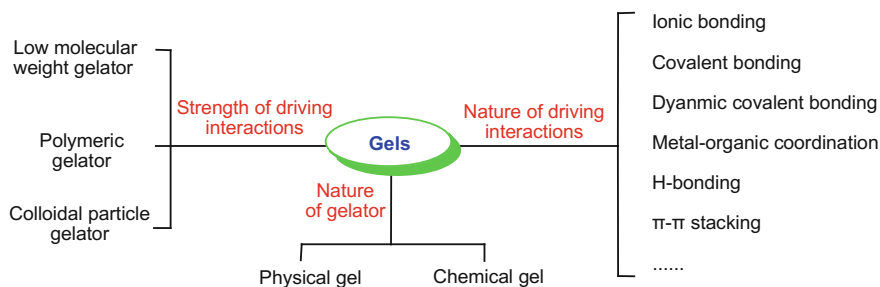


**Fig. 1.1** Classification of gels by nature of driving interactions, strength of driving interaction and nature of gelator

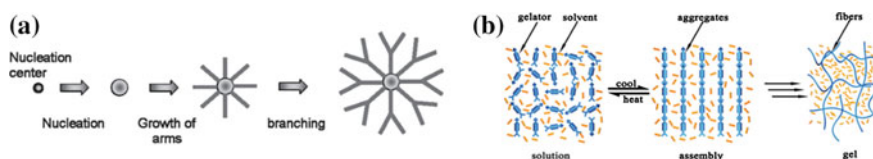


**Fig. 1.2** Schematic illustration of **a** fibre network formation through nucleation and growth of fibre and **b** the self-assembly of low molecular weight gelators into one-dimensional aggregates and the subsequent formation of an entangled network. Reprinted with the permission from Ref. [9]. Copyright 2015 American Chemical Society

precursors are used, oligomeric/polymeric aggregates may be formed. If the initially formed aggregates have a proper solubility in solution, the aggregates may grow in one direction to form fibres or are interconnected via interactions to form a network structure, finally leading to gelation.

The instinctive property of solvent is of great importance during the gelation process. For example, the polarity, viscosity, functional groups of solvents are usually influential to the framework of the gels. The balance of gelator-solvent and gelator-gelator interactions is influenced by the polarity, viscosity, as well as the temperature. Solvents assist the nucleation and growth in the processes of self-assembly and subsequent gelation [5–7]. In fact, at the initial stages, the primary nucleation among the gelators occurs in the supersaturation solution with the formation of fibres. Then, the alternating and branching of fibrous arms are growing spontaneously. Finally, the nucleation and growth process converts into kinetically stable fibrous aggregates, entrapped an extra of solvent molecules in the gelation process [8] (Fig. 1.2). During the whole procedure, supersaturation-mediated nucleation and growth is found to be the driving force for the gel nanostructure formation [8, 9]. Additionally, the unique properties of gels can be exploited when introducing functional molecule precursors into the liquid phase. For example, the gel network is able to template porous materials with specific morphologies [10].

## 1.2 Driving Force

Intermolecular forces are responsible for the assembled way of discrete molecular building blocks. Although gelation is the result of a subtle balance between a multitude of non-covalent interactions, one or some interactions may be identified to be crucial as the driving force(s). In gels, the driving forces range from strong chemical bonds to weak intermolecular interactions (Fig. 1.1).

Traditional covalent bond is irreversible, and the reactions are performed under kinetic control. For supramolecular gelation, “error correction” and “proof-reading” should be allowed in the self-assembly of gelator molecules. The corresponding reactions should be reversible, and the products should be under thermodynamic control. Dynamic covalent chemistry has been developed based on reversible reactions, such as imine-type exchange and disulphide exchange reactions [11, 12]. Its advantages include the combination of robust covalent chemical bonds and the reactions under thermodynamic control. To realize a dynamic covalent process, catalyst is usually needed. Dynamic covalent exchange is generally slower than other dynamic processes. However, switching a dynamic covalent system from dynamic to inert is possible upon activation or deactivation of the catalyst.

Metal–organic bonds are acid–base interactions based on the Lewis theory of acid–base interactions of electron pair donation and acceptance. Their stability may be explained by the hard–soft interaction principle. Soft electron donors (e.g. S, P) form more stable complexes with soft metal ions such as  $\text{Ag}^+$  or  $\text{Pt}^{2+}$ . Metal ions having high charge and small size (e.g.  $\text{Al}^{3+}$ ,  $\text{Fe}^{3+}$ ,  $\text{Cr}^{3+}$ ) are hard Lewis acids and bond best to hard electron donors (e.g.  $\text{H}_2\text{O}$ ,  $\text{NH}_3$ ). The chelate compound is more stable, called the chelate effect. The chelate effect is an entropy effect. Moreover, chelate rings having five or six members are generally more stable than those of other sizes.

Hydrogen bonding, abbreviated as  $\text{X}-\text{H}\cdots\text{A}$  (X, donor; A, acceptor), is the most popular non-covalent interactions using for construction of the gels. Conventional hydrogen bonding is often described as an electronic dipolar–dipolar interaction, and contribution from the Coulomb energy is important. The energy ( $10\text{--}120\text{ kJ mol}^{-1}$ ) is much stronger than that of van der Waal interaction, but weaker than that of covalent bonds. Charge-assisted interactions are usually stronger than hydrogen bonding involving neutral species. More importantly, owing to its two characteristics, directional and saturable property, hydrogen bonding is usually chosen as driven force to construct supramolecular architecture. Carboxylic acid dimer is one of the most well-known hydrogen-bonding motifs. Besides conventional hydrogen bonding, weaker hydrogen bonding is also known, including  $\text{X}-\text{H}/\pi$ ,  $\text{C}-\text{H}/n$  and  $\text{C}-\text{H}/\pi$  interactions ( $2\text{--}20\text{ kJ mol}^{-1}$ ).

Another important driving force is  $\pi$ – $\pi$  interaction, which exists among aromatic and other  $\pi$ -delocalized moieties. Substitution of electron-donating or electron-withdrawing atoms or groups leads to  $\pi$ -delocalized molecules with electron-donor and electron-acceptor properties. Combination of donors and acceptors may lead to partial charge transfer from donor to acceptor. Offset

face-to-face and edge-to-face geometrical motifs are prevalent for pairs of equivalent molecules, while eclipsed face-to-face motif is favoured by pairs with complementary donor and acceptor properties. For offset face-to-face motif, the plane separation is 3.4–3.6 Å. The stabilizing energy is about 9 kJ mol<sup>-1</sup> for a pair of benzene molecules, and the involvement of charged species increases the stabilizing energy.

Furthermore, van der Waals, halogen bonding, cation- $\pi$  and metallophilic (e.g. aurophilic) interactions as well as solvophobic effect play important roles in the formation process of supramolecular gels. Among them, the solvophobic effect is related to functional moieties in the gelator molecule showing poor solubility in the solvent, resulting in gelation.

In the following chapters, gels have been classified into five general catalogues according to the driving force, supramolecular gels, metal-organic gels, dynamic covalent gels, polymer gels and inorganic gels.

### 1.3 Characterization

Various techniques can be used to gain structural information on different scales. There are two basic parameters, the critical gelator concentration (CGC) and gel-to-sol transition temperature ( $T_{\text{gel}}$ ), which are extensively used to characterize the capacity of the gels. The CGC means the minimum concentration of the gelator molecule to form a gel at a certain temperature (usually at room temperature). The popular visual identified method, inversion test, is adopted to characterize a gel. The inversion test, also named bottom-up method, is the simple visual way to assess the gels behaviour by dissolving a gelator molecule in a certain solvent or mixed solvents to form clear solutions (sol form) under heating process, and cooling the solutions to get a stable gel by using a thermocontrolled oil bath. And then,  $T_{\text{gel}}$  is determined, however, to a certain extent, and the stability of the gel is dependent on the container size resulting in relatively low accuracy of the  $T_{\text{gel}}$ . So, the dropping ball method is developed. A metal ball is placed onto the gel surface; after conversion to the sol form, the ball would be dropped. The temperature is recorded as the  $T_{\text{gel}}$ . Differential scanning calorimetry (DSC) provides a direct instrumental method to measure  $T_{\text{gel}}$  during the heating and cooling process. When the sample undergoes gel-to-sol transition, more energy will be needed to flow than that of the reference. During the cooling process, the sample undergoes sol-to-gel phase transition, and less energy will be needed to flow. So, the phase transition enthalpy can also be collected to take insight into the thermodynamic behaviours of gels. The DSC data can help further take insight into the intrinsic behaviour of the gels.

The structures and morphologies of gels have been elucidated by conventional imaging techniques such as scanning electron microscopic (SEM), transmission electron microscopic (TEM) and atom force microscopic (AFM) at the microscopic level. The preparation of xerogels is pivotal for the study of the morphology of gels

[13]. In order to avoid the collapse of the aggregate framework, the gels are handled by a supercritical drying method that the solvent molecules are removed by using liquid  $\text{CO}_2$ , which can be converted to a gas via a supercritical fluid state with the formation of destructive phase boundaries [14]. As an alternative method, cryoscopic TEM and SEM can be applied in which the sample is prepared by rapidly freezing it to liquid  $\text{N}_2$  temperatures to preserve the original structure and imaging performed at low temperature. And at the nanoscale, X-ray diffraction (XRD), small-angle neutron scattering (SANS) and small-angle X-ray scattering (SAXS) are required to investigate the structures and packing model of gels. Specifically, comparison of the XRD patterns given by a gelator in its crystalline form with that from its gel can help identify the gel's molecular packing [15]. Additionally, IR and NMR spectroscopies can give information on the presence of the local environments and motions of functional groups, e.g. hydrogen bonding. Absorption and emission spectroscopies can give information on the packing of gelator molecules, e.g. stacking of aromatic groups.

Rheological study can give various parameters of gels. The stress and strain, for instance, are usually measured to judge the viscoelastic behaviour of the gels. As a kind of viscoelastic materials, rheological property [16] is often used to study the response of the gels to an applied stress. In rheological experiment, the elastic storage modulus ( $G'$ , the contribution of elastic, i.e. solid-like, behaviour to the complex dynamic modulus) and elastic loss modulus ( $G''$ , the contribution of viscous, i.e. liquid-like, behaviour to the complex modulus) are two key parameters to reflect the behaviours and structures of gel materials. Commonly, if the amount of deformation of the material is proportional to applied force or stress, the material is said to be elastic (like a rubber band). In purely elastic materials, the stress and strain are in phase. On the contrary, for viscous materials, the strain lags behind the stress by a  $90^\circ$  phase angle (also called the loss angle,  $\delta$ ). The immediate stress responds to the applied strain, and viscoelastic materials have a strain lag between  $0^\circ$  and  $90^\circ$ . The complex dynamic modulus ( $G$ ) is used to quantify the stress-strain relationship (Eq. 1.1).

$$G = G' + iG'' \quad (1.1)$$

The storage and loss moduli are related to the quantities  $\sigma_0$  and  $\varepsilon_0$ , the amplitudes of stress and strain, respectively, and the phase shift ( $\delta$ ) between them as shown in Eqs. (1.2) and (1.3).

$$G' = \frac{\sigma_0}{\varepsilon_0} \cos \delta \quad (1.2)$$

$$G'' = \frac{\sigma_0}{\varepsilon_0} \sin \delta \quad (1.3)$$

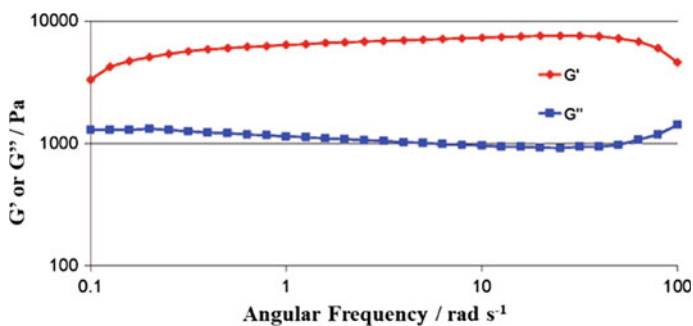


**Fig. 1.3** Frequency sweep rheometry data for a supramolecular gel. Reprinted with the permission from Ref. [17]. Copyright 2009 American Chemical Society

For most supramolecular gels, the elastic modulus ( $G'$ ) should be invariant with frequency up to a particular yield point and should exceed elastic loss modulus ( $G''$ ) by at least an order of magnitude (Fig. 1.3).

## References

- Almdal K, Dyre J, Hvidt S, Kramer O (1993) Towards a phenomenological definition of the term 'gel'. *Polym Gels Netw* 1:5–17
- Flory PJ (1974) Introductory lecture, Faraday discuss. *Chem Soc* 57:7–18
- Weiss RG, T  rech P (2006) Molecular gels. In: Weiss RG, T  rech P (eds) *Materials with self-assembled fibrillar networks*. Springer, Netherlands, pp 1–13
- Estroff LA, Hamilton AD (2004) Water gelation by small organic molecules. *Chem Rev* 104:1201–1218
- Zhu G, Dordick JS (2006) Solvent effect on organogel formation by low molecular weight molecules. *Chem Mater* 18:5988–5995
- Jonkheijm P, van der Schoot P, Schenning APHJ, Meijer EW (2006) Probing the solvent-assisted nucleation pathway in chemical self-assembly. *Science* 313:80–83
- Stepanenko V, Li XQ, Gershberg J, Wurthner F (2013) Evidence for kinetic nucleation in helical nanofiber formation directed by chiral solvent for a perylene bisimide organogelator. *Chem Eur J* 19:4176–4183
- Li JL, Liu XY (2010) Architecture of supramolecular soft functional materials: from understanding to micro-/nanoscale engineering. *Adv Funct Mater* 20:3196–3216
- Liu M, Zhang L, Wang T (2015) Supramolecular chirality in self-assembled systems. *Chem Rev* 115:7304–7397
- van Bommel KJC, Friggeri A, Shinkai S (2003) Organic templates for the generation of inorganic materials. *Angew Chem Int Ed* 42:980–999
- Jin YH, Yu C, Denman RJ, Zhang W (2013) Recent advances in dynamic covalent chemistry. *Chem Soc Rev* 42:6634–6654
- Wilson A, Gasparini G, Matile S (2014) Functional systems with orthogonal dynamic covalent bonds. *Chem Soc Rev* 43:1948–1962
- Sangeetha NM, Bhat S, Choudhury AR, Maitra U, Terech P (2004) Properties of hydrogels derived from cationic analogues of bile acid: remarkably distinct flowing characteristics. *J Phys Chem B* 108:16056–16063

14. Shi C, Huang Z, Kilic S, Xu J, Enick RM, Beckman EJ, Carr AJ, Melendez RE, Hamilton AD (1999) The gelation of CO<sub>2</sub>: a sustainable route to the creation of microcellular materials. *Science* 286:1540–1543
15. Ostuni E, Kamaras P, Weiss RG (1996) Novel X-ray method for in situ determination of gelator strand structure: polymorphism of cholesteryl anthraquinone-2-carboxylate. *Angew Chem Int Ed* 35:1324–1326
16. Mezger T (2006) *The rheology handbook*, 2nd edn. William Andrew publishing, Norwich
17. Piepenbrock MO, Lloyd GO, Clarke N, Steed JW (2010) Metal- and anion-binding supramolecular gels. *Chem Rev* 110:1960–2004

## Chapter 2

# Supramolecular Gels

**Abstract** Supramolecular gels constructed by the assembly of small molecules have been extensively investigated. The gels bearing functional groups also exhibit intelligent and potential applications in the fields of tissue engineering and wound healing, drug delivery, templating or transcribing self-assembly morphology, molecular electronics, sensing and so forth. Due to various kinds of weak non-covalent interactions, abundant architectures are constructed and are smart to the external stimuli, such as temperature, light, mechanical stress, chemical, pH value. Therefore, supramolecular gels are sorted and stated according to different stimuli in this chapter.

**Keywords** Supramolecular gels · Non-covalent interaction · Driving force  
Stimuli-responsive gels

Supramolecular gels consist of three-dimensional networks that are formed by molecular self-assembly. In the process of gelation, the gelator molecules self-assemble to form fibrous architectures in nanometre scale through intermolecular non-covalent interactions. They in turn build up a micrometer-scale entangled three-dimensional network entrapping/immobilizing large organic solvent molecules, preventing the solvent molecules from flowing with the formation of viscoelastic materials as supramolecular gels. Hence, a gel could be defined as “a colloidal network that is expanded throughout its whole volume by a fluid”.

Strong hydrogen bonding such as urea and amide is widely explored to construct fibrous structures, as well as other driving forces, including  $\pi$ - $\pi$  stacking interaction, donor-acceptor interaction, metal coordination, solvophobic forces (hydrophobic forces for gels in water) and van der Waals interactions, could also interlink between small molecules for self-assembly into various architectures. Subsequently, the architectures twist and knit into three-dimensional network with the formation of gels (Fig. 2.1) [1–3]. Importantly, once the supramolecular gels prepared from small gelator molecules with few functional groups exhibit intelli-

---

Yongguang Li and Yeye Ai contributed together to this chapter.

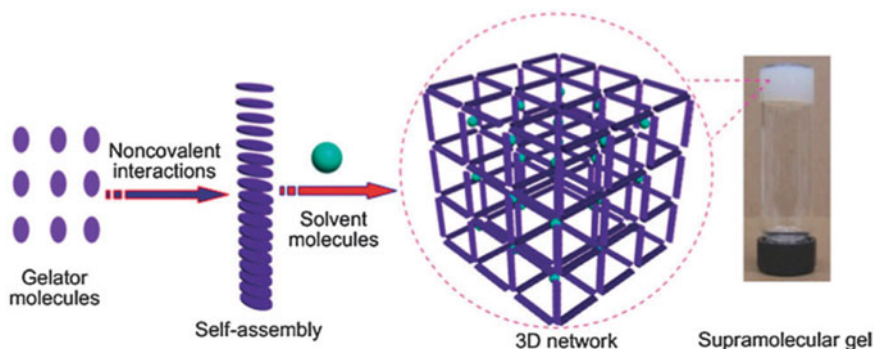


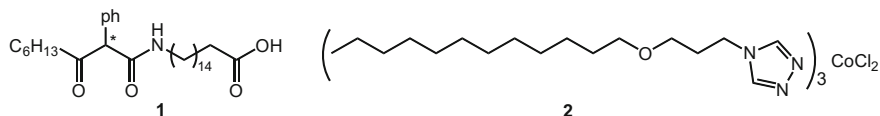
**Fig. 2.1** Schematic representation of the formation of a supramolecular gel. Reprinted with the permission from Ref. [9]. Copyright 2013 Royal Society of Chemistry

gent and potential applications in the fields of tissue engineering and wound healing, drug delivery, templating or transcribing self-assembly morphology, molecular electronics, sensing and so forth [4–7].

An obvious advantage of supramolecular gels compared with the chemically cross-linked polymeric gels is that the gelation is usually reversible. This is due to three-dimensional networks that are formed by self-assembly through non-covalent interactions. The reversible gel-to-sol phase transition exhibits high sensitivity to external stimuli that is an intrinsic behaviour of supramolecular gels. In addition to the commonly thermo-responsive property, plenty of supramolecular gels are also responsive to external stimuli such as light, sound, pH value, chemicals, ions and mechanical stress which make the gels become “smart”. Based on this unique characteristic, it is widely used in diverse fields of regenerative medicine, drug delivery, sensors, logic gates, actuators, cosmetic, foods, environmental remediation and nanoelectronic, etc. [8].

## 2.1 Heat/Temperature Responsive Gels

In the preparation of thermoreversible supramolecular gels, firstly, the solubility of the gelator molecules increases as the temperature raises. Subsequently, the supersaturated solution is obtained and the gelator molecules would be aggregate into nanoparticles for most commonly nanofibres upon cooling process, which further twist and knit with the formation of 3D network enwrapped solvent resulting in supramolecular gels. The threshold temperature  $T_{\text{gel}}$  is usually used to assess the stability of thermoreversible gels. To a great extent, the  $T_{\text{gel}}$  value is affected by the strength of the intermolecular interactions (or non-covalent interactions) in the gels, which is highly sensitive to the structure of the gelators. For example, the threshold temperature  $T_{\text{gel}}$  can be largely effected by differences in the length of alkyl chain



**Scheme 2.1** Chemical structures of racemic **1** and complex **2**

[10], the number and positions of functional groups [11–13] and enantiomeric excess [14, 15]. The differences result in the distinction of molecular characteristics such as solubility, polarity, flexibility and further influence the nucleation and growth process. Žinić and co-workers demonstrated that the enantiomeric assemblies by different diastereomeric aggregation show different morphologies and stability of gel networks. This is reflected in sometimes dramatically different gelator effectiveness values ( $G_{\text{eff}}$ ), for instant, racemic **1** can form a 70 times more effective gelator of *p*-xylene than its (*R*)-enantiomer (Scheme 2.1) [11].

A gel-to-sol phase transition will occur associated with enthalpy changes upon increasing the temperature. Complete reversal behaviour example was first reported by Kimizuka and co-workers. A blue gel is formed after the gelator **2** ( $\text{Co}^{2+}$  coordinated-4-alkyl triazole complex) (Fig. 2.2) is dissolved in chloroform at room temperature. Surprisingly, the blue gel turns to a pink colour solution upon decreasing the temperature to 0 °C, which could be recovered once the temperature increases to room temperature. The unique thermoresponsive properties are due to the transformation configuration from tetrahedral complexes in the gel state to the metastable octahedral complexes in solution state upon cooling. Essentially, the gel-to-sol transition is enthalpically driven as a result of an entropically-favoured molecular transformation (Fig. 2.2) [16].

As an important driven force in self-assembly in supramolecular gels, the hydrogen bonding is sensitive to temperature, and it becomes weak and disappears gradually upon increasing the temperature. Percec and co-workers reported helical

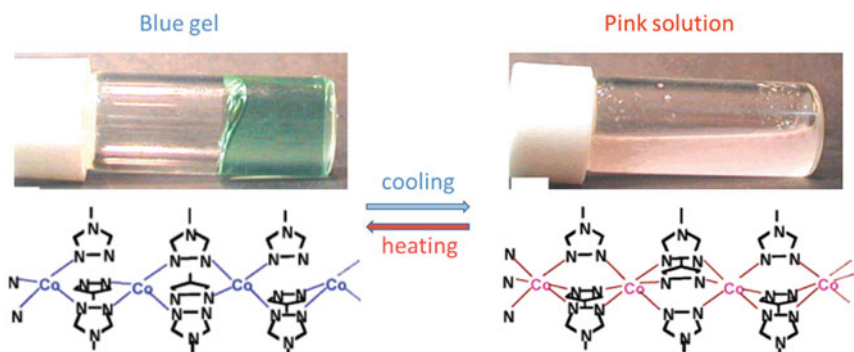


**Fig. 2.2** Thermally-induced gelation of complex **2** and schematic illustrations of transformation in polymeric  $T_d$  complex and  $O_h$  complex packing modes. Reprinted with the permission from Ref. [16]. Copyright 2004 American Chemical Society

supramolecular columns constructed by  $C_3$ -symmetric dendrimers via trisesters and trisamides of 1,3,5-benzenetricarboxylic acid [17]. The thermal reversible inversion of chirality was realized, negative chirality for 2D and 3D phases with triangular symmetry and positive chirality for 2D and 3D phases with rectangular symmetry.

Kasha and co-workers proposed an explanation of aggregation effects for optical property changes [18, 19]. The dimerization replaces the vibronic state with one higher and another lower in energy, which responds to the two possible configurations of transition dipoles (Fig. 2.3). A blue shift is termed a hypsochromic effect and attributed to the H-aggregation adopted to an overlapping aggregation, while a red shift with bathochromic effect is indicative of J-aggregation adopted to a side-on aggregation [18]. Commonly, the thermoresponsive gels show variable absorption. For example, Das and co-workers reported a series of cogels prepared from dialkoxynaphthalene and naphthalene diimide derivatives in non-polar solvents present variable adsorption states, in which due to the alternating stacked fashion with different naphthalene moieties. The cogels appear bright red or orange at 0 °C, while get permanent yellow colorations as warmed to room temperature, because the gelators separate into single-component gels [20].

The  $\pi$  system gels with stacking of aromatic rings can lead to exchange of excitation energy by thermally-induced structural changes resulting in fluorescence changes. Generally, the gel-to-sol transition upon heating reduces fluorescence due to the promoting quenching effects by molecular vibration, solvent collisions and disaggregation of the gel networks [21, 22]. On the contrary, the aggregation-induced-enhanced emission (AIEE) phenomenon occurs in a variety of supramolecular gel systems, which take effect during the aggregation when the fluorescent formed or retained [23, 24]. However, in aryl  $\pi$ -conjugated system, the

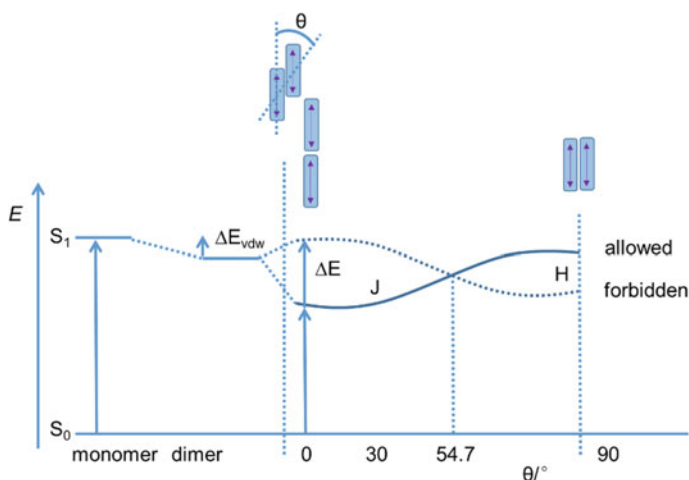


**Fig. 2.3** Schematic diagram showing the variation in energy of the allowed and forbidden  $S_1$  states as the angle between molecules,  $\theta$ , is varied. Note that splitting does not affect  $\Delta E_{vdw}$ , the average energy of dimer states relative to the monomer

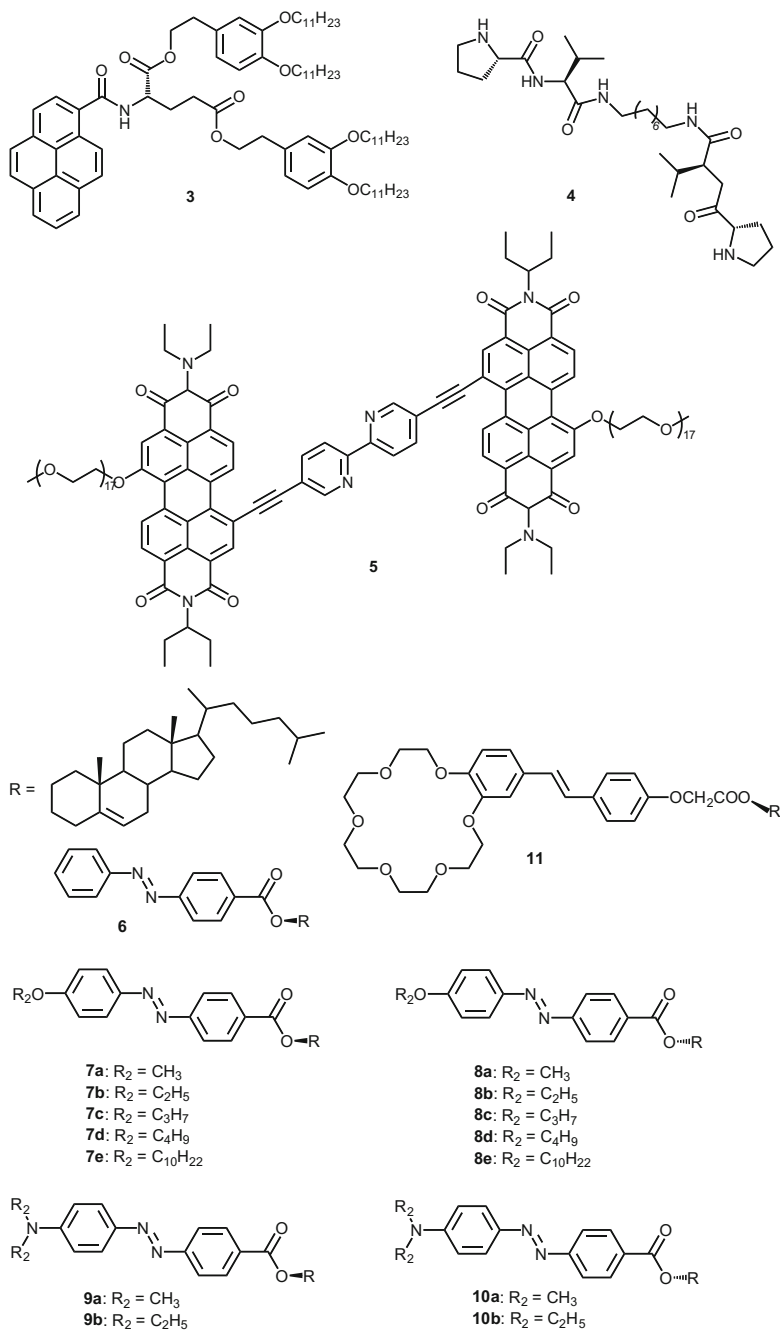
pyrene-based aggregates are common to promote excimer formation through  $\pi$ - $\pi$  stacking interaction, causing aggregation-caused quenching (ACQ) [24, 25]. Decreasing the  $\pi$ - $\pi$  coupling is the general method to avoid ACQ, and balancing with strengthening other interactions such as the H bonds of gelator **3** (Scheme 2.2 and Fig. 2.4) [25, 26].

The reversibility of the sol-gel transitions of supramolecular gels can be exploited in diverse applications, such as supports for catalytic particles, enzymes, quantum dots or controlling crystallization nanofabrication processes [27–30]. In the liquid- and gas-processes, the supramolecular gels as temporary catalyst supports have been successfully prepared in situ growth of gold, palladium and platinum nanoparticles [31, 32]. For example, Rodríguez-Llansola and co-workers demonstrated that gelator **4** can be used as catalyst for Henry nitroaldol reactions with high efficiency only in the gel state. Upon raising the temperature to dissolve the gel, both the efficiencies of the conversion and selectivity are decreased. Proton transfer between proline residues in the gel promotes deprotonation of the nitroalkane reagent, which may subsequently react with an aldehyde to yield a nitroaldol product. In solution, the catalyst is considerably less basic and thus acts as a soft nucleophile, directly attacking the aldehyde to form an imine (Fig. 2.5) [33].

Upon heating, the thermoresponsive gels also exhibit variable physical properties before reverting to sol state. The intrinsic size and shape of gel networks as well as the interactions with solvent molecules are likely affected by the raising temperature. And the changes cause substantial amounts of liquid to enter or leave the material, further producing swelling and deswelling effects [34]. And the supramolecular interactions present in the gel are dependent on the heating. Typically, upon raising temperature the gels forming of hydrophobic gelators and a polar solvent undergo deswelling process, due to the entropic disfavour of ordering of the solvent molecules around the gel networks. Conversely, gel fibres comprising hydrogen bonds exist swelling effects, because the hydrogen bonding is weakened by heating, inducing uptake of solvent molecules [35, 36].

A simple method of inducing a deswelling response is to remove solvent molecules from the gel, generally, by heating or decreased pressure. As for avoiding the collapse of frameworks of gels, supercritical drying is the most common method to prepare porous materials from small-molecule gels. Shi and co-workers obtained the aerogels by dealing the bis(urea) gelators with perfluorinated end groups can gel with supercritical drying with carbon dioxide directly at concentrations of 1–6 wt% and a pressure of 300 atm. The target xerogel exhibiting microsized pores shows ideal supports for heterogeneous catalysis or molecular sensing applications [37, 38].

Generally, the expulsion of solvent molecules in the gel is linked to two kinds of variation, including reducing solubility of the gelator or increased aggregation of the gel fibres. Krieg and co-workers reported a kind of swelling supramolecular gelator **5** based on a perylene diimide chromophore (PDI) decorated with polyethylene glycol groups. Gelator **5** forms gels in the mixture of tetrahydrofuran and water. In the formation process of elongated fibres,  $\pi$ - $\pi$  stacking of the planar pyrene moieties plays a pivotal role. The supramolecular self-assembly gels are stable even at 100 °C. At higher temperature, the conformational flexibility of



**Scheme 2.2** Molecular structures of gelators 3–11

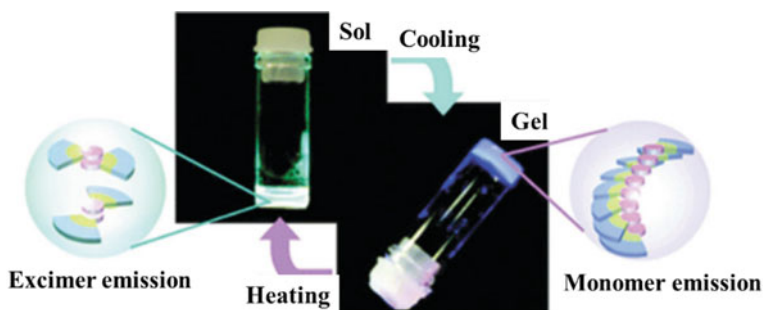


**Fig. 2.4** Photograph of the fluorescent gel and sol of **3** and schematic illustration of the self-assembly in the gel state and excimer formation in the sol state, respectively. Reprinted with the permission from Ref. [25]. Copyright 2007 American Chemical Society

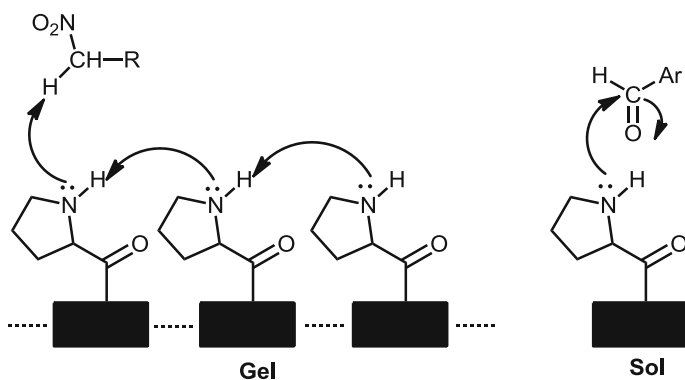


**Fig. 2.5** Catalytic reaction schemes illustrating the dominant reaction pathways in its gels and sols

polyethylene glycol (PEG) chains increases, inducing the lower polarity, and the PEG chains further predominate the adjacent fibres interact [39]. Therefore, the fibres become more hydrophobic, resulting in increasing aggregation and expulsion of solvent molecules beyond 70 °C. And temperature triggered deswelling of the gel leads to the (reversible) expulsion of a large fraction of the aqueous solvent (Fig. 2.6) [40].

Due to the controlled manner, swelling of supramolecular gels composed of LMWGs has been exploited in drug release, especially in topical applications [41, 42]. LMWGs possess a number of advantages: simple to synthesis, rapid low-temperature interconversion in gel-sol transition, controllably modified to realize specific interactions with target molecules [35, 43, 44]. However, it is hard to design sufficiently stable and biocompatible supramolecular gels with specific properties, and the widespread use of LMWGs in medical products has yet to be realized [45].

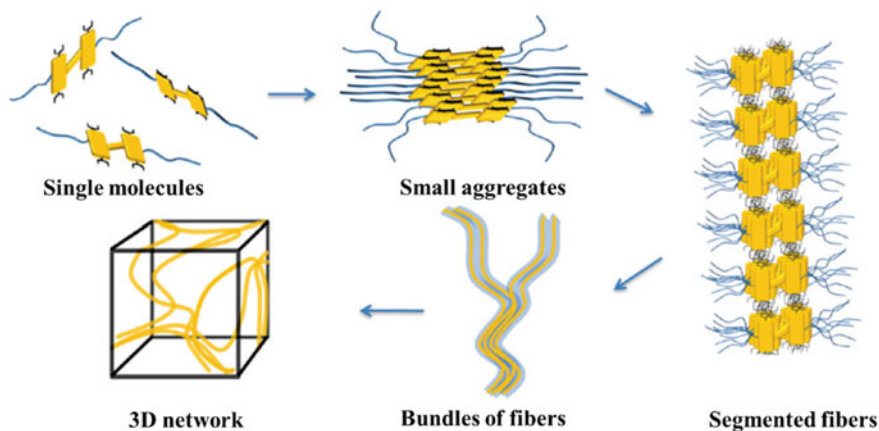


**Fig. 2.6** Schematic representation of and the assembly hierarchy for gelator **5**. Reprinted with the permission from Ref. [40]. Copyright 2009 American Chemical Society

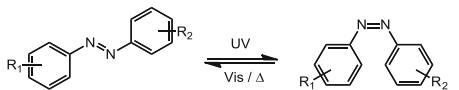
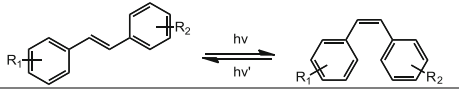
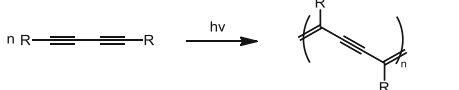
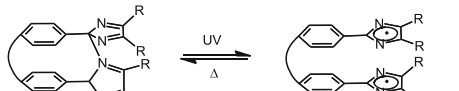
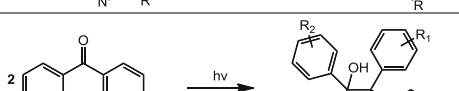
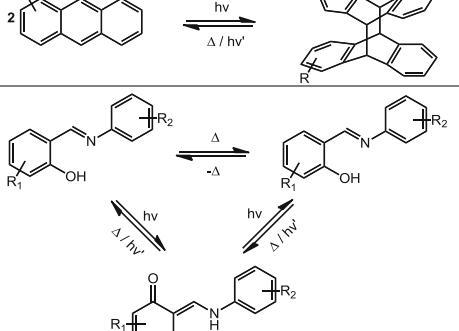
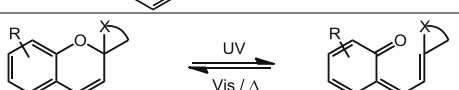
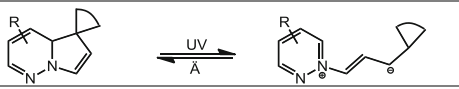
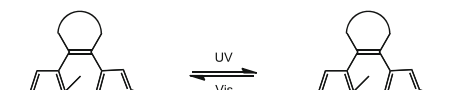
## 2.2 Light Responsive Gels

Supramolecular gels based on photoresponsive chromophores have attracted much attention since the modulation of their properties can be realized by using light as an external trigger. Generally, the *trans*–*cis* isomerization, 2+2 dimerization, photoscission, photopolymerizations of the chromophore derived gelators can be realized. The common patterns of reactivity based on LMWGs are listed in Table 2.1. Upon photoirradiation, the changes at microlevel based on the supramolecular interactions such as  $\pi$ – $\pi$  stacking and hydrogen bonding and so on can result in the transformation of self-assembly manners of gelators. Further, the properties of gels produce changes, such as the change of viscosity and polarity, the modulation of the size and shape of the xerogel morphology, electronic properties. Such processes can be sorted as conformational changes, coupling reactions, intramolecular proton transfer and electrocyclic reactions of the photoresponsive chromophores. And the most commonly used photoresponsive chromophores include azobenzene, stilbene, diarylethene and spiropyran.

### 2.2.1 Conformational Changes

In supramolecular gels, the changes of molecular conformation are quite common, generally, in which, the bond angles vary while the connectivity of the atoms remains fixed. In this process, gelators with flexibility can get access to different packing modes with comparable energies. And *cis*–*trans* isomerization is particularly popular, because they have a reversible conversion between the two fixed

**Table 2.1** Examples of photoresponsive functionalities that have been incorporated into LMWGs

Reaction class	Example	Equation
<i>Trans-cis</i> ( <i>E-Z</i> ) isomerization	Azobenzene	
	Stilbene	
Polymerization	Diacetylene	
Dimerization	Imidazole	
	Benzophenone	
Cycloaddition	Anthracene	
Tautomerization	<i>N</i> -salicylidene aniline (anil)	
Electrocyclic reaction	Spiropyran	
	Dihydroindolizine	
	Dithienylethene (DTE)	

R groups indicate common derivatization patterns but are not exhaustive

conformations and similar chemical states. The relative photoresponsive chromophores mainly include azobenzene, stilbene and butadienes [46–49].

### 2.2.1.1 Azobenzenes

Azobenzene derivatives have been investigated for the design of photoresponsive gels for several decades. The trans-azobenzene exists an absorbance at near 360 nm originating from the  $\pi$ - $\pi^*$  state, and the cis-azobenzene generates a decreasing of  $\pi$ - $\pi^*$  band, while increasing of the  $n$ - $\pi^*$  band at near 290 and 460 nm, respectively, when the trans–cis reaction occurs by UV radiation. The reverse cis–trans reaction is realized by visible light radiation or just keeping under dark condition at room temperature for several hours [50–52].

As for azobenzene derived gelators, Shinkai and his co-workers have made significant contributions. The gelation properties of two types of gelators **6**–**11** with cholesterol groups having the natural (*S*) or inverted (*R*) configuration have been studied (Scheme 2.2). Among them, the gelators **7** and **8** with *p*-alkoxy azobenzene moiety show better gelation ability, and gelate non-polar solvents or polar [53–55] to “read-out” the sol–gel transition and the supramolecular chirality by CD spectra and SEM images [56, 57].

Trans–cis isomerization may affect the structure or stability of gels. Given that most azobenzene-based gelators strongly favour a trans configuration under ambient condition, conversion to cis configuration will alter the shape of a molecule and the interactions of self-assembly. Such changes will induce dissolution of the gel and cause gel–sol transition, which is generally reversible. Liu and co-workers demonstrated that the gelator **12** shows a positive CD activity and an inverted CD signal in polar solvents and non-polar solvents, respectively (Fig. 2.7). Detailed chiroptical studies and semiempirical quantum mechanical calculations reveal that the difference in azobenzene moiety interaction plays a vital role under the relevant conditions. In polar solvents, the gelator forms H-type self-assembly aggregates with strong  $\pi$ - $\pi$  interaction of azobenzene moiety. While the gelator self-assembled into the same H-type aggregate with an interdigitated stacking mode through weak  $\pi$ - $\pi$  interaction and strong hydrogen bonding in non-polar solvents. The gels both show responsive to heat and photoirradiation stimulus [58].

Yagai and co-workers have studied the cooperative gelation properties of the azobenzene functionalized melamine (**13**) and the complementary H-bonding barbiturate (**B1**) or cyanurate (**C1**) derivatives to fabricate photoresponsive rosette assemblies (Fig. 2.8). The experiment results show that a rosette containing barbiturate (**B1**) cannot hierarchically organize into higher-order columnar aggregates in aliphatic solvents due to the steric bulk of tridodecyloxyphenyl substituent. However, the sterically non-demanding *N*-dodecylcyanurate **C1** forms gels with hierarchically organized elongated columnar fibrous aggregates through  $\pi$ - $\pi$  stacking and hydrogen bonding interaction in cyclohexane. Dynamic light scattering (DLS) and UV–Vis spectra studies revealed that the dissociation and the

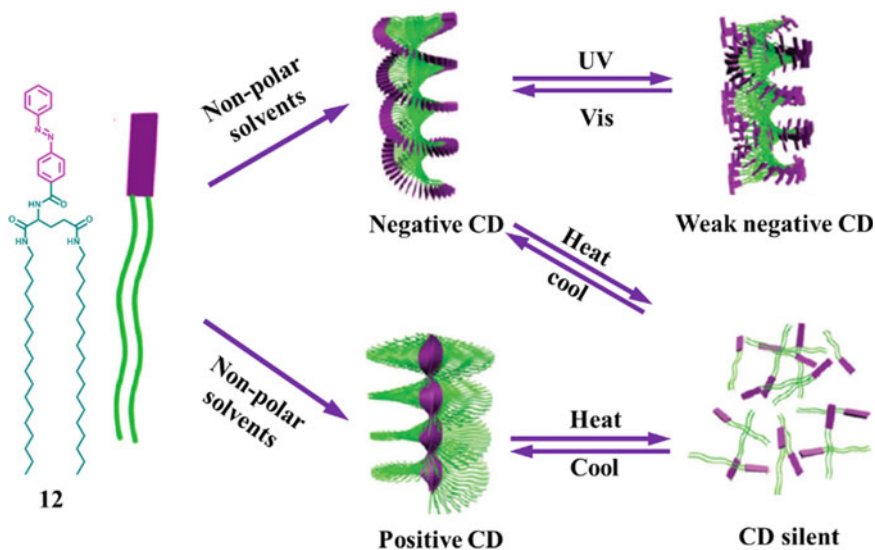


**Fig. 2.7** Illustration of the multichannel supramolecular chiroptical switches composed by gelator **12**. Reprinted with the permission from Ref. [58]. Copyright 2011 American Chemical Society

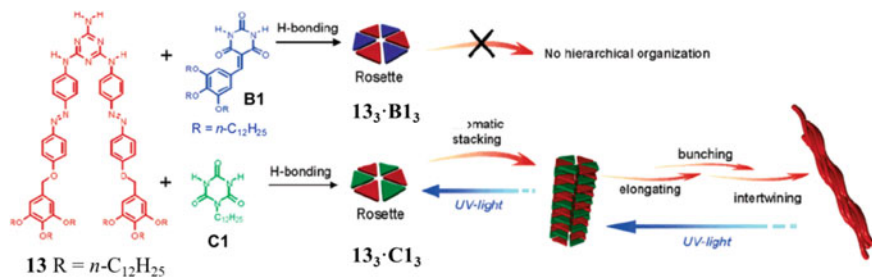


**Fig. 2.8** Schematic representation showing aggregation of the melamine-azobenzene conjugate (**13**) with barbiturate (**B1**) and cyanurate (**C1**) derivatives. Reprinted with the permission from Ref. [51]. Copyright 2005 American Chemical Society

reformation of columnar aggregates controlled by the trans-cis isomerization of the azobenzene moiety are realized by UV irradiation [51].

The gel-sol transition via photoisomerization may change the aggregate and modulate the interactions between gelator and the surrounding solvent molecules, which induce swelling or contraction of the gel, as encapsulate bulk liquid depending on the solvent-gel interface energy. It is worth noting that while light-induced swollen and deswelling transition is similar with those induced by heating; the microstructural changes in these processes can be obviously different. Xie and co-workers demonstrated that coassembled gel of the dentron gelator **14** and azobenzene derivative **15**

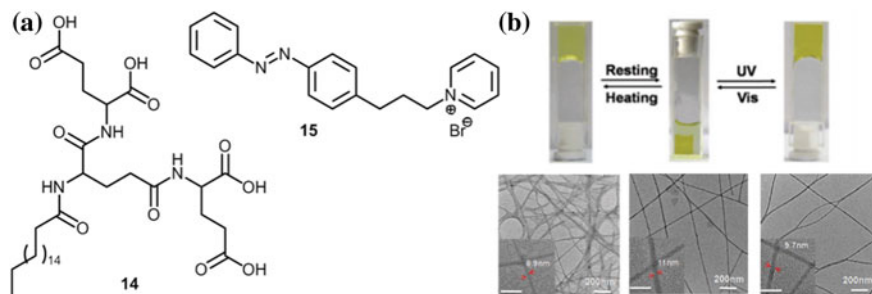


**Fig. 2.9** **a** Molecular structures of gelator **14** and **15**, and **b** reversible deswelling and swelling transitions of a mixed hydrogel of **14** and **15**, on resting and after exposure to UV light. Reprinted with the permission from Ref. [50]. Copyright 2016 Royal Society of Chemistry

shows thermally reversible deswelling at 20 °C, but return to the swollen state after photoisomerization. The swollen gels with similar appearance can be obtained upon heating or UV irradiation, but the fibrous structure of the latter is obviously wider and more twisted, larger diminished the supramolecular chirality (Fig. 2.9) [50].

In addition to change of the conformation of a molecular, the trans–cis isomerization may alter the polarity, because the C-shaped cis-form of an azobenzene moiety tends to be larger polar than the S-shaped trans-form [59], and the gel–sol transition upon UV irradiation may lead to the precipitation of gelators in a non-polar solvent [60]. So it is possible to realize sol–gel transition in a non-polar solvent upon UV irradiation leading to trans–cis photoisomerization due to the suitable gelation aggregate as the reduction in solubility.

### 2.2.1.2 Stilbenes

Stilbenes are recognized as another important photoisomerization systems. Like azobenzene compounds, they show reversible photoinduced trans–cis photoisomerization while with relatively high conversions, and they are suitable for the design of “smart” gelators [61, 62]. For most of stilbenes derivatives, the thermal activation barrier is around 154 kJ mol<sup>-1</sup>. Even though stilbenes in the cis-form are not thermally stable enough and return to the trans-form in the dark, the large activation barrier precludes thermal relaxation at ambient condition to a certain extent, and their photochemical and self-assembly properties have attracted much attention.

The trans–cis photoisomerization may affect the stability of the gels, facilitate the gel–sol transition and the aggregation transformation. Xu and co-workers demonstrated the aggregation controlled by stilbene photoisomerization. Stilbene gelator **16** favours a Z form at ambient condition and induce a quantitative conversion from the E form to the Z upon irradiation at 387 nm, while the reverse reaction is realized by UV irradiation at 360 nm. The gelator can form fibrous aggregates in either form while with different mechanisms of self-assembly. Only

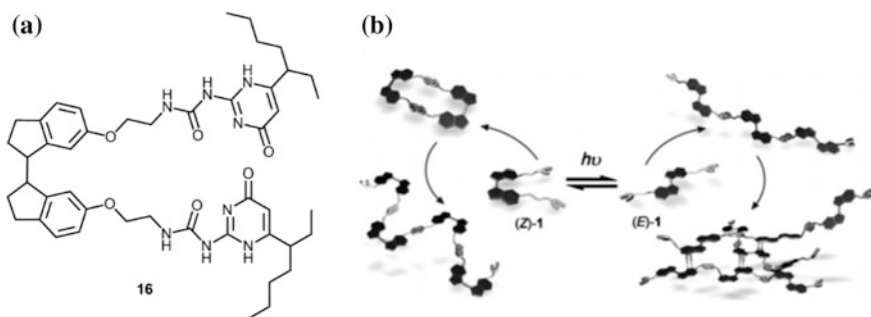


**Fig. 2.10** **a** Molecular structure of gelator **16**, and **b** schematic representation of the self-assembly mechanism of stilbene **16**. Reprinted with the permission from Ref. [63]. Copyright 2013 John Wiley & Sons, Inc.

fibres of *E* form can form stable gels with fine fibrous gel network due to the isodesmic polymerization, while *Z* form aggregates via a two-stage ring-chain pathway and cannot form gels, due to a lack of  $\pi$ - $\pi$  stacking between fibres hindered by the proximity of the molecule's bulky side chains (Fig. 2.10) [63]. Another stilbene isomerization delivering a useful gel-sol transition to realize the spatially controllable by the optical and rheological properties of gels was demonstrated by Draper and co-workers [64].

The photoisomerization of stilbenes may exhibit changes in fluorescence and provide the tuneable emission in bio-imaging applications. Zhu and co-workers reported that naphthalimide-functionalized cyanostilbene **17** with UV irradiation can shift fluorescence from yellow to blue, and dye HeLa cells as a medium [65]. Due to the *Z*-to-*E* photoisomerization of the cyanostilbene unit, the initial emission attributed to the naphthalimide moiety increases in emission wavelength. The self-assembly disorder and the dual fluorescent properties are utilized to achieve the conversion from yellow, green, to blue. Computational studies show that the *E* form presents fluorescence enhancement contributing to AIEE phenomena, because steric hindrance prevents the twisted intramolecular charge transfer (TICT) state, and disfavours radiative relaxation (Fig. 2.11).

Notwithstanding, the photochemical and self-assembly properties of azobenzene and stilbene-based compounds have been exploited in many studies, there are still some limitations in the molecular switches. As for azobenzene isomerization, a complete conversion of the *trans*-to-*cis* isomer cannot generally be accomplished, and usually proceeds with quantum yields below 30%. And the environment of the switchable groups within the aggregate needs to be considered. And the lack of vacant space and strong interactions may disfavour the conformational changes bonding [66, 67]. Similarly, neighbouring functional groups may restrain the photoisomerization of the stilbene moiety, instead may facilitate the irreversible formation of cyclic structures [50, 68]. Additionally, the thermal back isomerization of azobenzene and stilbene-based systems make it hard to realize a photochemical control on the relative properties.

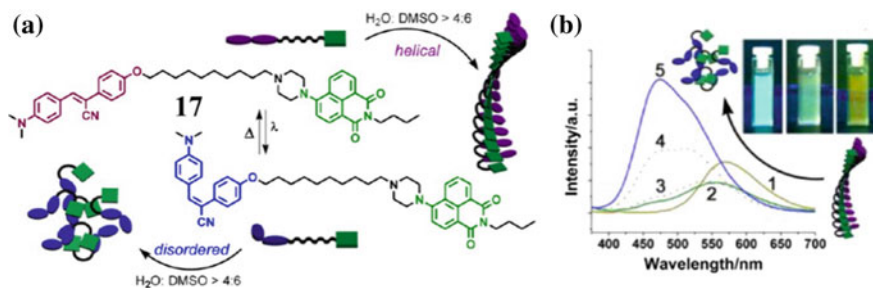


**Fig. 2.11** **a** Schematic representation of the corresponding helical and disordered assemblies of the *Z*-isomer and *E*-isomer of gelator of naphthalimide-functionalized cyanostilbene **17**, **b** emission spectra ( $\lambda_{\text{ex}} = 365$  nm) of compound **17** in DMSO with 90% water at (1) initial state and after photoirradiation at 254 nm for (2) 2 h, (3) 3 h, (4) 5 h and (5) 8 h, and photograph images (right-to-left) of the corresponding states 1, 2 and 5 under a UV light ( $\lambda = 365$  nm). Reprinted with the permission from Ref. [65]. Copyright 2013 American Chemical Society

## 2.2.2 Coupling Reactions

### 2.2.2.1 Diacetylenes

In recent years, the self-assembly of diacetylene derivatives has attracted much attention due to the covalent fixation of supramolecular assembly of polydiacetylenes by photopolymerization reactions. Diacetylene gelators are particularly interesting because the gel network can be permanently supported by the formation of covalent cross-links between gelator molecules under photoirradiation conditions, which is generally stabilized by non-covalent interactions. And the morphological characteristics are retained with the increasing of the stiffness and thermal stability of the gels, which indicates that the polymerization is generally irreversible [69, 70]. One popular application of gel-based polymerization is to fabricate conductive arrays of conjugated  $\pi$  bonds. Néabo and co-workers reported that a toluene gel **18** comprising columnar stacks realized topochemical coupling upon photoirradiation, and the reaction takes place at solvent-free condition. The rigid and highly extended  $\pi$  network is achieved by the polymerization and represents a lower optical band gap than its linear counterpart and provides the potential strategy for preparing low-bandgap nanowires (Fig. 2.12) [71].

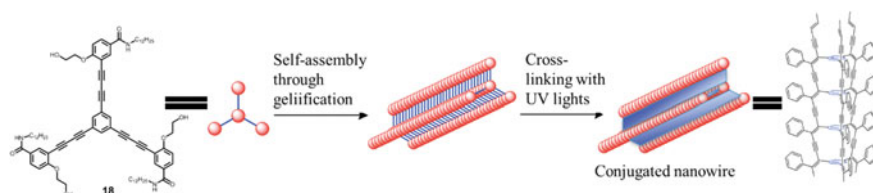


**Fig. 2.12** Schematic illustration of the preparation of covalently linked, conjugated nanowires from compounds **18**. Reprinted with the permission from Ref. [71]. Copyright 2013 American Chemical Society

Generally, the incorporate structural motifs of diacetylene may affect the polymerization and self-assembly processes. It is important to note that the gelation ability is affected by stereostructural effect, like diacetylene gelators **19**, they exhibit a good gelation ability with enantiomers, while the racemic mixtures of diastereomers cannot form gels at all. In addition, they represent a prominent odd-even effect with respect to the photopolymerization in the gel state, and further affect the colour of the resulted photopolymers. The cyclohexane gels with odd numbers of carbon atom spacers show thermally stability and obvious colour changes from orange ( $n = 3$ ) to blue-purple ( $n = 7$ ) upon photoirradiation, while gels with even  $n$  are non-photoreactive. Simple gas-phase modelling results show that the geometric differences at the molecular level may have a crucial effect on the bulk photopolymerization properties (Fig. 2.13) [72]. Furthermore, the gelators **20** similarly exhibit an odd-even effect on the polymer obtained with various colour from red to dark blue. And the carbon atoms of the aliphatic chains control the planarity of the polymers and reveal the changes on the self-assembly manners (Scheme 2.3) [73].

### 2.2.3 Electrocyclic Reactions

Electrocyclic reactions are the most currently reported intramolecular photoreactions in LWMGs. Due to the changes of planarity linked with the loss or gain of  $sp^2$  centres, ring closing and opening processes have a pronounced effect on the

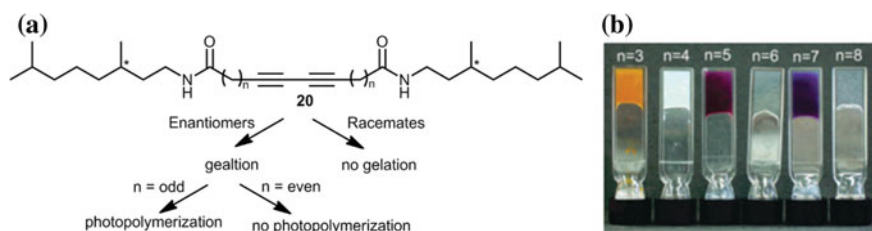
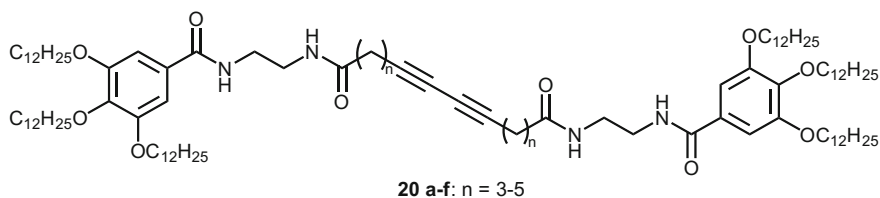


**Fig. 2.13** a Illustration of gelation ability of gelators **19**, and b photographs of the photoirradiated cyclohexane gels. Reprinted with the permission from Ref. [72]. Copyright 2004 American Chemical Society



**Scheme 2.3** Molecular structure of gelators **20**

self-assembly properties. The most commonly used photoresponsive functionalities for the light-induced electrocyclic reactions include spiropyrans, spirooxazines, and dithienylethenes.

### 2.2.3.1 Spiropyran and Spirooxazines

The photochromic reaction of spiropyrans and closely related spirooxazines occurs reversible photochemical cleavage of the C–O bond within a six-membered heterocycle to generate a new double bond and a ketone moiety [47, 52, 74–76]. The products containing more  $sp^2$  sites tend to adopt a more planar conformation with increased conjugation and involve the emergence of new optical absorption bands in the range of around 570–750 nm. Due to their intriguing photochromic properties, spiroheterocyclic compounds have been investigated for the design of optical memories, switches and displays [74–76].

In spiropyran system, the supramolecular self-assembly is sensitive to the photoinduced changes in the packing. Qiu and co-workers reported a spiropyran linked to a di-D-alanine moiety molecule **21**. The closed-form spiropyran cannot form gel, while this compound upon UV irradiation to generate merocyanine form in aqueous solution can form dark red fibrous gels at low pH. The gel–sol transition can be realized by the regeneration of the closed-ring system upon visible light irradiation or the addition of one equivalent of vancomycin with strong hydrogen bonding interactions. The ligand–receptor interactions are sensitive to the stereoisomer structures, and the disruption induced by chiral molecular vancomycin only occur when the gelator is based on the D enantiomer alanine rather than the L. It is indicated that the binding of the receptor and ligand is based on a particular combination of hydrogen bonds and  $\pi$ – $\pi$  stacking interactions. And the response proves that the balanced self-assembly base on the  $\pi$ – $\pi$  stacking are interrupted by the induced hydrogen bonding and hydrophilicity interactions (Fig. 2.14) [77].

In fact, the pH sensitivity among gelators formed by photoinduced reactions is common, because the products of ring open are often sufficiently basic to be significantly protonated at moderately low pH. Two kinds of spironaphthoxazine gelators with different length of alkoxy chain **22a–b** have been found by Li and

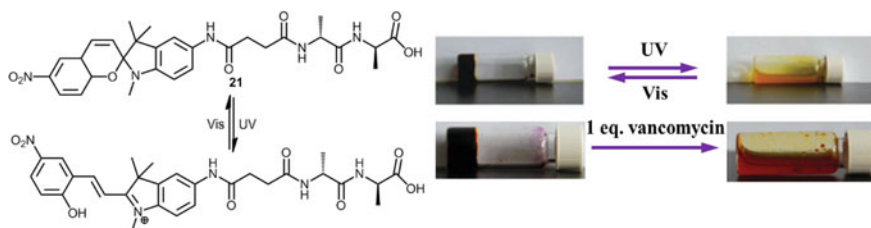
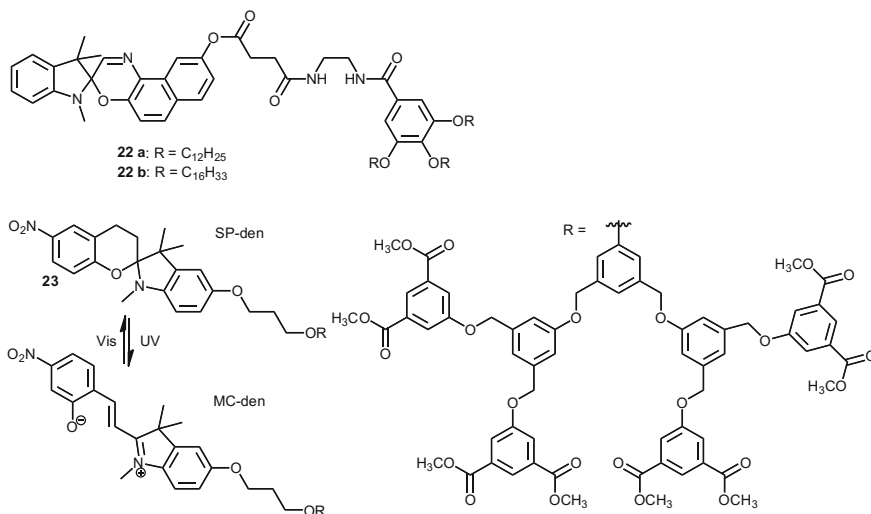


**Fig. 2.14** Illustration of gelator **21** response to photoirradiation and acidic solution. Reprinted with the permission from Ref. [77]. Copyright 2009 Royal Society of Chemistry



**Scheme 2.4** Chemical structures of gelators **22** and **23**

co-workers. The formation of stable organogels at concentrations below that of the critical gelation concentration (c.g.c) can be induced by the addition of *p*-toluenesulfonic acid, meanwhile with an apparent change in colour from colourless to purple (Scheme 2.4) [78].

The spiroindoline-functionalized dendron molecule **23** (Scheme 2.4) shows various self-assembly properties dependent on the processing conditions. By manipulating the cooling process, the toluene solution of **23** shows different self-assembled structures: spherical nano-/microparticles in solution by cooling the hot solution to 30 °C with UV irradiation, while fibrous network within organogel by cooling to 0 °C. Multivalent  $\pi$ - $\pi$  stacking interactions based on the molecule are the important driving force for the gelation. Interestingly, the gel-gel transition can be successfully realized by the reversible switch by UV and visible light irradiation. And the aggregates based on merocyanine form exhibit the fluorescence enhancement (Fig. 2.15) [79].

A drawback of electrocyclic reactions based on spiroindolines and spirooxazines is that their products are short-lived under ambient conditions, because most of the merocyanines are thermally unstable, tending to the back reaction to spiro-form in the dark. Even the photoresponsive products in the gel state with longer lifetime typically occur the loss of products within minutes.

### 2.2.3.2 Dithienylethenes

A more stable photoinduced transition in the electrocyclic switch is the dithienylethene (DTE) functionality. Upon exposure to UV light, the DET groups can

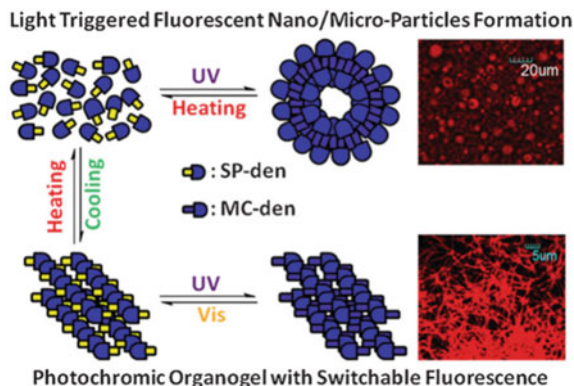


**Fig. 2.15** Schematic representation of the self-assembly of spiropyran-functionalized dendron molecule **23** into particles and network structure within the organogel, and the corresponding transformations under UV and visible irradiation. Reprinted with the permission from Ref. [79]. Copyright 2010 John Wiley & Sons, Inc.

convert to a closed-ring structure, and usually, the ring closure and opening upon UV and visible light, respectively, is reversible. Of course, the nature of the groups around the DTE core plays a pivotal role in the reaction cycle and may inhibit the reaction. Generally, dithio-cyclopentanes and fluorinated derivatives exhibit reliable and reversible photochemical reactions and are thus popular in the study of molecular switches in the gel state [80].

The ring closure of a DTE can involve two kinds of the changes in the molecular conformation properties: reducing the flexibility of the molecule, may favour gelation due to the lowering the entropic cost of aggregation, while generating two  $sp^3$  sites, forces the substituents at these sites to be oriented out of the plane of the molecule. And the ring closure of a DTE system can induce the changes in aggregates, further influence the self-assembly results. DTE gelator **24** functionalized with fluorescent  $\pi$ -conjugated wings (oligo(para-phenylenevinylene) (OPV)) has been demonstrated by Yagai and co-workers [69]. In methylcyclohexane solution, the closed-form compound results a non-fluorescence solution, while produces a highly fluorescence gel by generating the ring opening form under 600 nm light. Molecular modelling results show that the DTE core of photoproduct can regulate the aggregation by the  $\pi$ - $\pi$  stacking interactions. However, the closed isomer forms a disordered structure due to the steric hindrance of methyl groups in the DTE core with fluorescence quenching through the energy transfer within aggregates and the intramolecular energy transfer from the  $\pi$ -conjugated moieties to the diarylethene core (Fig. 2.16).

In most DTE systems, the closed and open forms are both stable enough under ambient conditions with no significant degradation of the relative responsive behaviour upon cycles of UV and visible light irradiation. And it is potentially suited to applications involving the release of an entrapped species. One tactic is to construct porous metallocage gelator incorporating the DTE core. Foster and

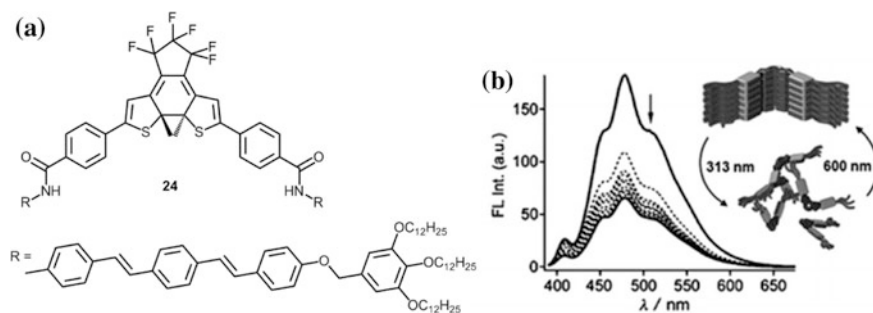


**Fig. 2.16** **a** Molecular structure of DTE-OPV gelator **24**, and **b** schematic representations of the molecular packing in the open (top) and closed (bottom) forms and changes in fluorescence upon ring closing in methylcyclohexane. Reprinted with the permission from Ref. [69]. Copyright 2013 John Wiley & Sons, Inc.

co-workers studied metallocage hydrogels can selectively bind benzene guest in the presence of the similarly sized anisole and release the guest molecules by the addition of competitive agent, such as furan. It is worth noting that the gels with intrinsic porosity enable to control delivery of multiple reagents with differing diffusion rates, and exhibit potential applications in catalysis, drug delivery, chemical purification [81, 82].

Additional investigations by de Jong and co-workers [83] highlight another advantage of DTE moiety: the generation of two chiral centres upon ring closure in molecules that are already chiral can result in diastereomeric products with discrepant optical and aggregation properties. The reversible optical transcription of supramolecular chirality into molecular chirality can be realized by gelator **25**. The dithienylethene molecule **25** exists in two antiparallel interconvertible open forms with *P*- and *M*-helicity, which cyclize in a fully reversible manner upon irradiation with UV light to form two diastereomers of the ring closed products of **25**. The open form **25** can form gels in non-polar solvents. In toluene gels, the gelator self-assembles to helical fibres dependent on the supramolecular self-assembly chirality, consistent with CD and TEM studies. Though there is no stereoselectivity in the solutions, the selective self-assembly of **25** into the gel state shows nearly absolute stereocontrol. Both the open and closed forms of **25** exist in two kinds of chiral gel states, denoted as  $\alpha$  and  $\beta$ , leading to a four-state chiroptical supramolecular switch, achieving a sequence of cycled photochemical reactions (Fig. 2.17). The optical switching between different supramolecular chiral aggregates and the interplay of molecular and supramolecular chirality in these systems is attractive for designing molecular memory systems and smart functional materials.

Since the chirality, physical state, molecular configuration of the DTE systems can be exerted by the permutation of thermal and photonic inputs. The relatively materials with well defined, long lasting, resistant to fatigue over several cycles can be exploited in chemical information storage applications. The system state keeps undisturbed upon the stimulus required for data read-out, which makes DTEs more

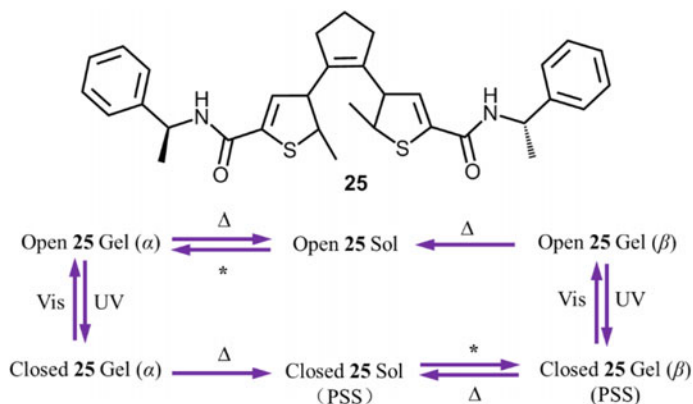


**Fig. 2.17** Structure of gelator **25** and four different chiral aggregated states and the switching processes of the chiroptical supramolecular switch consisting of the open form **25** and the closed form of **25**. UV,  $\lambda = 313$  nm; visible (Vis),  $\lambda > 460$  nm; \* = cooling;  $\Delta$  = heating

superior in effective data storage [84, 85]. Xiao and co-workers present the first example of a fluorescent switch with non-destructive read-out ability in the gel state [84]. Thus, composition of the system may be determined rapidly, reliably and non-invasively, without risk of conversion to an alternative state [80, 86].

Another related use for the DTE moieties is as a component of a molecular logic gate (MLG). MLGs deliver an output signal in the presence of a particular combination of inputs, in accordance with a predefined set of Boolean operations [87]. For example, Xue and co-workers reported a tetrakis(amide) gelator, it is DMSO–water mixture gel system can be constructed as a XNOR gate based on the output of fluorescence intensity at 600 nm in the present of the two inputs of proton and fluoride ions. Due to the gel–sol transitions can afford additional output, a more complicated gate may be expected. The MLGs based on some combination gates can deliver multiple output signals due to their response to multiple chemical stimuli [81]. And the chemical systems are potentially allowed to be modulated in situ without the invasive devices. Chemically addressable MLGs with repeatable responses by using of exclusively non-invasive inputs can achieve cycles of writing and erasing in data storage systems. Selective isomerization of individual photochromes can use absorption and emission properties at different wavelengths as logic outputs and allow design of simple Boolean logic gates and more complex logic devices with all-photonic inputs and outputs. A triad FG-DTE molecule **26** consisting of a dithienylethene and two fulgimides developed by Andréasson and co-workers and constructs effective logic gate. The absorption and fluorescence signals with relative characteristic pattern are induced by the two molecular switches dependent on the ring opening and closure (Fig. 2.18). And it can be configured as AND, XOR, INH, half-adder, half-sub-tractor, multiplexer, demultiplexer, encoder, decoder, keypad lock and logically reversible transfer gate logic devices, all with a common initial state [88].

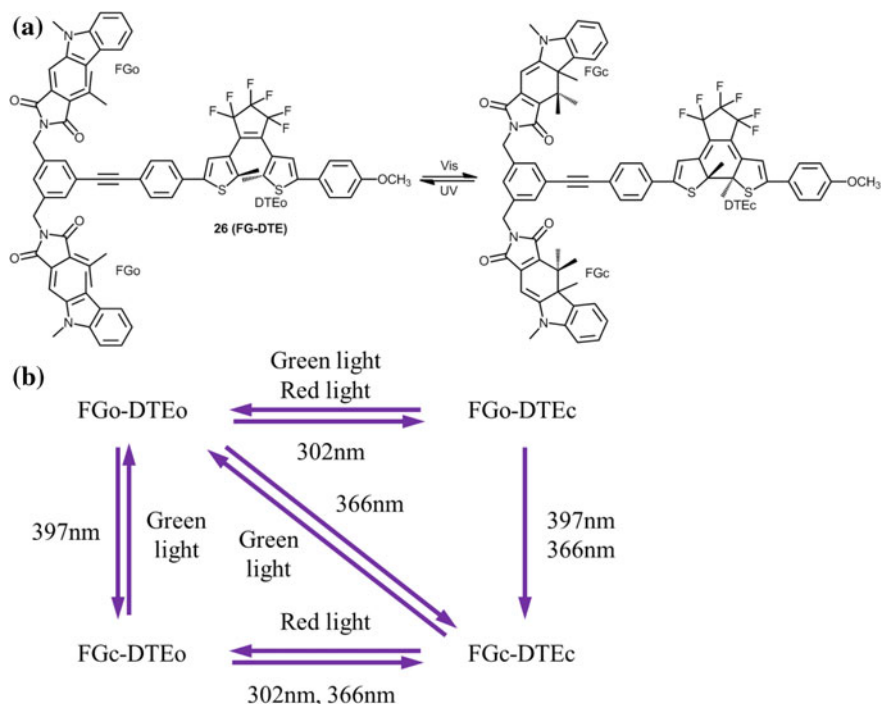


**Fig. 2.18 a** Structure and **b** photochemical interconversions among the four photoisomeric structures of FG-DTE **26**

## 2.3 Sonication and Mechanical Stress Responsive Gels

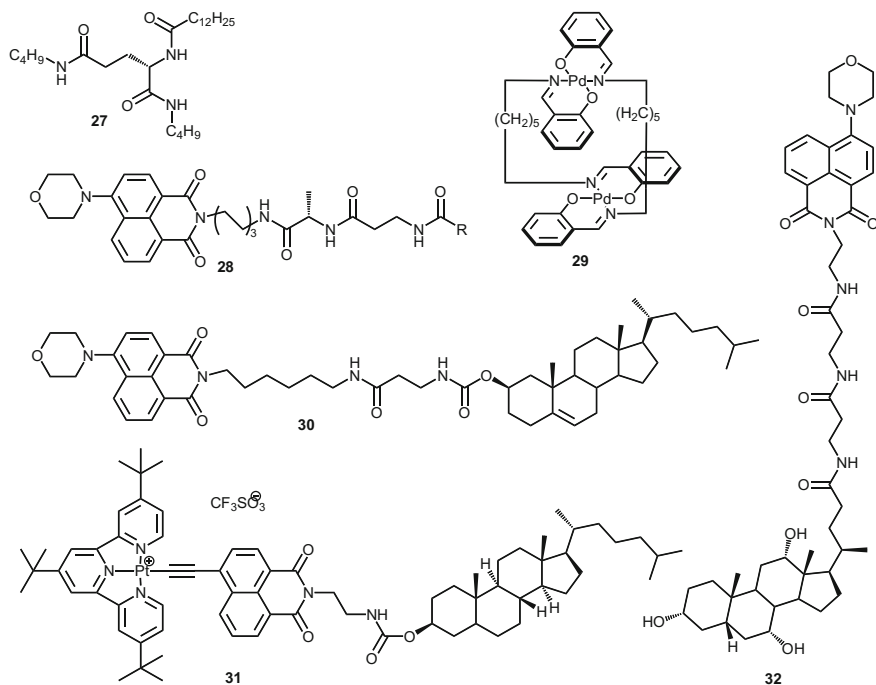
As for two kinds of important physical forces, ultrasound and mechanical stress have efficiently affected and triggered the smart supramolecular gels on the self-assembly processes [89, 90]. Generally, moderate sonication and mechanical stress can modulate the molecular configuration or the self-assembly processes, but not change or destroy the chemical structure of gelator [91, 92]. The mechanical stimulus can be used to overcome the activation barrier or offer access to more viable aggregate pathways in kinetically disfavoured self-assembly. In the physical-stimulus-responsive gels, the balance between non-covalent interactions plays a pivotal role in the formation of nano/microarchitectures, and have been explored applications in many fields, such as wettability switches, hybrid materials, pollutant removal [89, 93–95].

### 2.3.1 *Ultrasound*

Ultrasound waves as a kind of high-frequency mechanical waves propagate in physical medium and generate transient bubbles of vapour which produces abrupt implosion or cavitation. The cavitation effect will provide high energy to induce certain chemical and physical changes due to the short timescale of cavitation leading to temperature of up to 5000 K and pressure of several hundred atmospheres. Surprisingly, the self-assembly can take place under sonication and may promote gel formation at lower concentration, higher temperature, faster rate than in mild conditions, which is hard to achieve the resulting aggregates by other methods [89, 96–98]. And ultrasound may be suitable for stimulating gelation in a kinetically disfavoured self-assembly processes with a high energy barrier.

Solubilization is a common use of ultrasound through breaking up and dissolve materials which are resistant to thermal treatment, and under certain circumstances, provide possibility to gelation process. The ultrasound as a driving force can equilibrate the aggregates between the thermodynamic product and initial kinetic product. Anderson and co-workers present highly insoluble compounds uric acid and melamine with stable  $\pi$ -stacking and strong hydrogen bonding, which partially dissolve in water. Ultrasound-induced dissolution of aggregates under non-equilibrium conditions allows the materials to reaggregate as a stable gel [99].

The effects on nucleation under sonication may further promote gelation. Under ambient conditions, typically, the aggregation processes involve that a relatively small number of nuclei made of the dissolved gelator proceed into dense, highly branched spherulites. However, under sonication treatment, the population of nuclei becomes larger due to increasing of fragments and disperses of the initial aggregates, which vastly accelerated fibre growth. From the microlevel, the environment of separate assemblies is less supersaturated on average, and tend to assemble into smaller, less branched and more interpenetrated spherulites which are better suited to form gel [100, 101]. This phenomenon in gels of **27** (Scheme 2.5) has been studied by Wang and co-workers. Exposure to ultrasound, the CGC of gels reduced from 2.0 to 0.5% (w/v) and the gel strength increased by up to three orders of magnitude compared to thermally generated gels (Fig. 2.19) [101]. In addition, the degree of branching, average fibre diameter and thermodynamic stability of the sonogels can be tuned via the temperature or concentration [98, 102, 103]. Yi and co-workers reported peptide-based ALS gelator **28** (Scheme 2.5). In  $\text{CH}_3\text{CN}$  gels, the gel-to-gel process triggered by sonication with the transformation of the core-shell microspheres into nanoballs, further cross-linked into nanofibers with higher thermostability. In toluene gels, sonication displayed a cutting effect on the fibrous morphology with changes of 100 nm fibre diameter into 20–40 nm (Fig. 2.20) [104]. Amazingly, sonication-triggered morphology changes in the gel state are mostly reversible, and the sonogels return to initial state upon heating-cooling treatment without fatigue. And the gel-to-gel transition shows potential applications in controlled release, functional expression and shape-memory materials.



**Scheme 2.5** Chemical structures of gelators 27–32

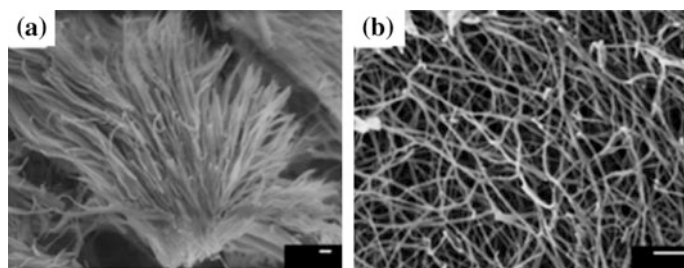


**Fig. 2.19** SEM micrographs of propylene glycol gels of 27, **a** after a heating–cooling cycle and **b** with additional ultrasound treatment (**b**) (scale bars 500 nm). Reprinted with the permission from Ref. [101]. Copyright 2009 American Chemical Society

Sonication-induced conformation transitions may influence the supramolecular interactions and further affect the gelation processes. In one study, Naota and co-workers demonstrated that dinuclear palladium(II) complex gelator **29** (Scheme 2.5) undergoes sol–gel transition with sonication for 3–10 s along with the structural transformation from self-locked intramolecular  $\pi$ – $\pi$  stacking to interlocked intermolecular  $\pi$ – $\pi$  stacking (Fig. 2.21) [105]. In an ALS system, Yi

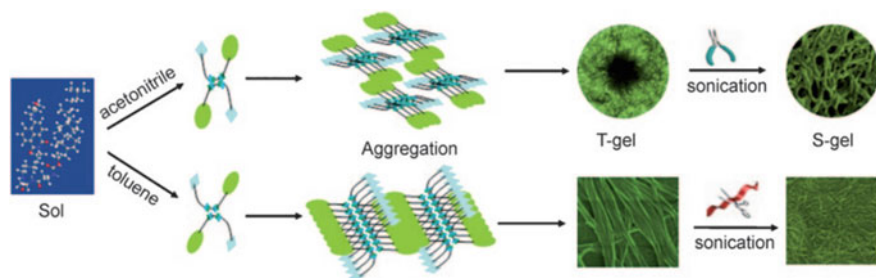


**Fig. 2.20** Schematic representation of the aggregation changes of **28** in acetonitrile and toluene. Reprinted with the permission from Ref. [104]. Copyright 2010 John Wiley & Sons, Inc.

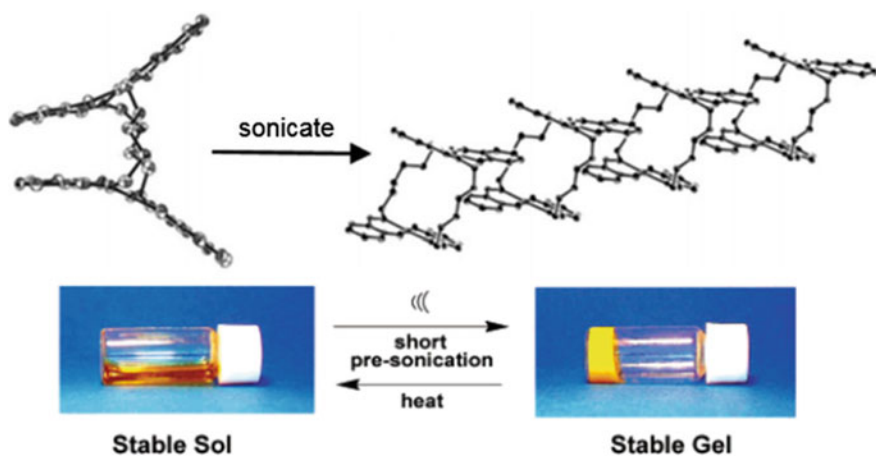


**Fig. 2.21** Schematic representation of structure transformations induced by sonication. Reprinted with the permission from Ref. [105]. Copyright 2005 American Chemical Society

and co-workers reported gelator **30** (Scheme 2.5), the cooperation and relative competition of intra- and intermolecular hydrogen bonds are directed by the sonication or thermal process. Upon sonication irradiation, the conformational transition from intramolecular hydrogen bonding between the  $-C=O$  bond of naphthalic anhydride and  $-NH$  (ethyl imide) to intermolecular hydrogen bonding accompanied by the morphology changes from vesicle to fibres (Fig. 2.22) [93]. Similarly, the (*R*)-*N*-Fmoc-octylglycine cyclohexane gels are induced under sonication with interconnection of nanofibres for the formation of the fibrous network [106]. Complex **31** (Scheme 2.5) as a typical sonication-induced gelator has been studied by Liu and co-workers. The transformation of the conformation converts from a perpendicular mode to a coplanar mode of 1,8-naphthalimide and the platinum(II)-terpyridyl ring accompanied by the precipitate-to-gel transition. The initial vesicles are formed by the hydrophobic interactions between cholesterol groups, aggregate

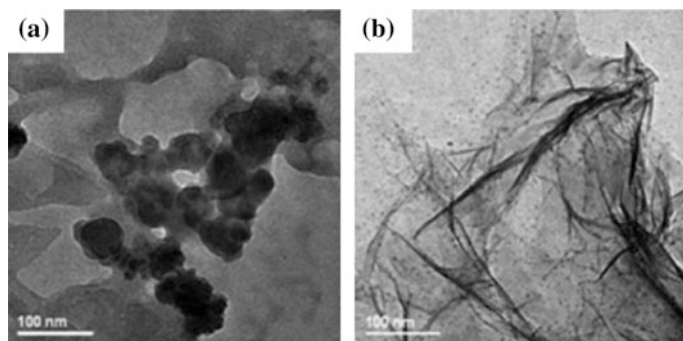


**Fig. 2.22** SEM micrographs of *p*-xylene gels of **30** from **a** S-gel and **b** R-gel (scale bars 100 nm). Reprinted with the permission from Ref. [93]. Copyright 2009 John Wiley & Sons, Inc.

into fibres form with intermolecular interactions (including hydrophobic interactions and ionic dipolar interactions) along with the gel formation (Fig. 2.23) [107].

Sonication as an important method to exploit complex functional materials, one strategy is to generate new materials by self-assembly of gels with other systems [108–110]. David Bardelang and his co-workers firstly induced QDs (quantum dots) into organogels system via ultrasound treatment. Morphological studies revealed that large QDs stick to the surfaces of gel fibres, while not significantly affected the gelation properties and the luminescence of the QDs [111, 112]. Yi and co-workers demonstrated a hybrid gels incorporated peptide-based derivatives **32**

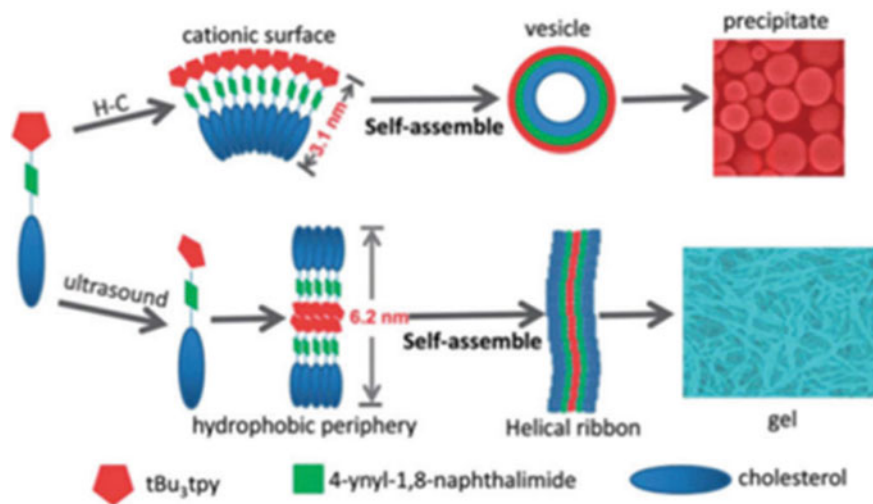


**Fig. 2.23** Schematic mechanism of the gelation of platinum(II) complex **31** via a self-assembly process in heating–cooling (H–C) process and sonication, respectively. Reprinted with the permission from Ref. [107]. Copyright 2013 Royal Society of Chemistry

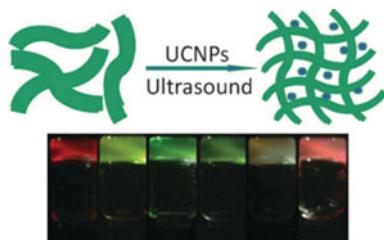


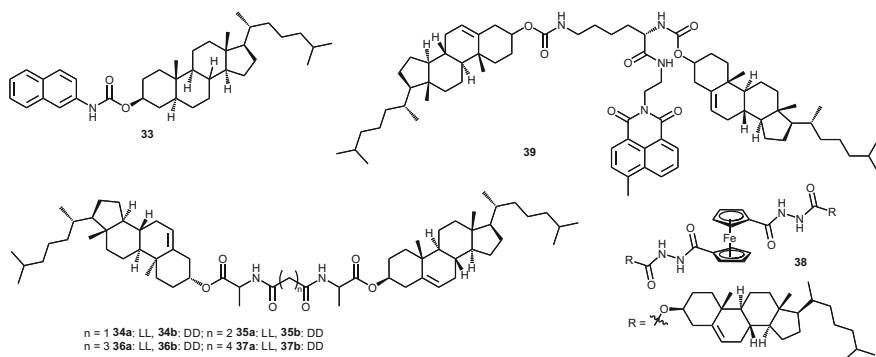
**Fig. 2.24** Chemical structure of **32**. Self-assembly of **32** + UCNP and fluorescent images of **32** + UCNP gels in n-hexanol. Images from left to right: **32** + UCNP-Red, **32** + [UCNP-Red/UCNP-Green (1/1 wt)], **32** + UCNP-Green, **32** + [UCNP-Green/UCNP-Blue (1/1 wt)], **32** + UCNP-Blue, **32** + [UCNP-Blue/UCNP-Red (1/1 wt)] ( $\lambda_{\text{ex}} = 980 \text{ nm}$ ). Reprinted with the permission from Ref. [113]. Copyright 2009 Royal Society of Chemistry

(Scheme 2.5) and up-conversion nanophosphors (UCNPs) that might exhibit multicolour emission through excitation by NIR light [113]. UCNP ( $\text{NaYF}_4$ ) converted to a self-assembled network of a LWMG through physical interactions in a polar solvent via sonication, thereby reinforcing the gel structure and enhancing the stability of the gel. These UCNP nanocomposite gels could fulfil the requirements for colour displays, NIR light absorption materials to generate power, or be modified to function as biological labels (Fig. 2.24).

### 2.3.2 Mechanical Stress

As gentler mechanical stimuli, physical shaking or shearing stress can affect the supramolecular gels properties at micro/macro-levels without changes of molecular conformation. Commonly, LMWGs undergo gel–sol transition under mechanical stress, and the gel can be recovered by heating–cooling treatment. The thixotropic properties of supramolecular gels by internal stimuli after the removal of the external stimuli, are based on the non-covalent bonds with dynamic properties. As third-generation self-healing materials, the thixotropic gels based on supramolecular systems are significant in industry, fracture and fatigue, biomaterials and smart materials [114, 115].

Exposure to mechanical stress generated by shaking or shear stress, the LMWGs usually converted into sol or sol-like state, and the gels state can be recovered after resting, which indicated that some LMWGs exhibit thixotropic properties. The first thixotropic cholesterol-based gels of CNC **33** were reported by Weiss and co-workers. Gelator **33** can form gels with spherulitic SAFINs (self-assembled fibrillar networks) morphology at incubation temperature  $\leq 28 \text{ }^\circ\text{C}$ . The gels can be transformed into sols via shear without significant destruction of the building blocks of the SAFIN structure, and then reassembly into spherulite re-entangle after resting process (Scheme 2.6) [116]. Fang and co-workers demonstrated gelation behaviour of the diacid amides of



**Scheme 2.6** Chemical structures of compounds 33–39

dicholesteryl L(D)-alaninates LS<sub>2</sub> (34–37) can be adjusted by varying the amino acid chirality and the length of the spacer connecting the two cholesteryl moieties (Scheme 2.6). Rheological studies show that the gels are thixotropic, and the mechanical properties of the gels can be adjusted either by altering the spacer length or by changing the gelator concentration, which the relative aggregation mode, the morphology, and the chirality of the network structures of the gels were revealed by XRD, SEM and CD spectroscopy studies [100].

The thixotropic gels triggered by mechanical forces show the phase-selective gelation between water and oil, which indicates that the feasibility of removing oil or pollutants from water sources [117]. The first example of phase-selective gelation with amino acid amphiphiles was reported by Bhattacharya and Krishnan-Ghosh [118]. There are some characteristics in phase-selective gelation: (1) recovery and reuse of the gelator after the phase-selective gelation of the oil in these mixtures [94, 95]; (2) an appropriate extractant with an organic hydrocarbon solvent for a solid-liquid system; (3) the extractant need appropriate selectivity [119]. Recently, Yan and co-workers studied that heptane gels of the ferrocene-containing dicholesterol compound 38 (Scheme 2.6) revealed a fast and fully reversible phase transition (within seconds) upon the shear force without the involvement of heating-cooling cycle [120]. And efficient absorbing and entrapping of the iodine take place in the processes. Based upon the thixotropic molecular gel, a novel separation strategy, which combines the great efficiency of liquid-liquid extraction and the convenience of liquid-solid separation, has been successfully conducted for removing iodine from wastewater with extraction efficiency up to 72% (Fig. 2.25).

By mechanical stress, the thixotropic gels by internal stimuli may involve transformations in phase, morphology, even chirality, which are potential for third-generation self-healing materials. ALS<sub>2</sub> system gelator 39 (Scheme 2.6) was reported by Yi and co-workers. The toluene gels (0.86–1.70 wt%) respond to mechanical stimulus by the ring separating into a biased arc structure to expel the solvent molecules from the gel network, resulting in a gel-to-sol transition, and the gels could be recovered after resting for at least 20 min at room temperature

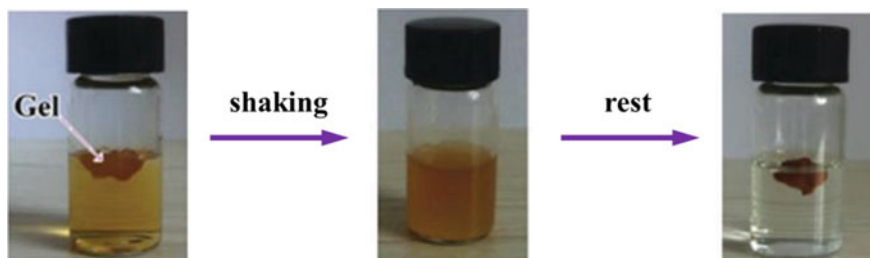


**Fig. 2.25** Heptane gels perform adsorption  $I_2$  from water by shaking–resting processes. Reprinted with the permission from Ref. [120]. Copyright 2015 Elsevier Inc.

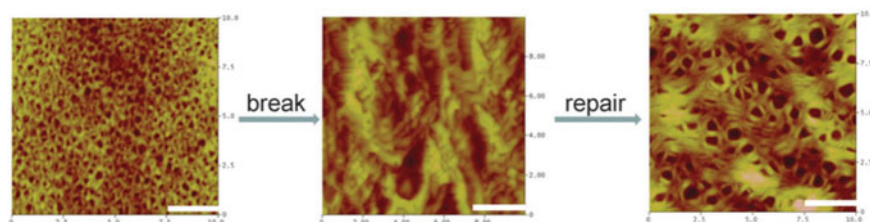


**Fig. 2.26** Chemical structure of gelator **39** and AFM images of gel **39** in its original, broken and repaired state (scale bar, 2.5  $\mu\text{m}$ ). Reprinted with the permission from Ref. [100]. Copyright 2012 Royal Society of Chemistry

(Fig. 2.26) [100]. The self-healing processes based on the gel-to-sol transition induced by mechanical stress can be reversible many times. It is intriguing that the gelation can take place by a simple shaking–resting process in a solvent/solid system at room temperature without a heating–cooling process. The reversible shaking–resting processes as well as breaking–repairing via the disintegration of the distinct rings and reconstitution of the gel network are suggested that the cooperation and competition of the supramolecular assembly among the hydrogen bonding, hydrophobic and aromatic interactions, as well as the spontaneous chirality, contributed to the destruction and the reconstitution of the cross-linked structure.

In fact, the controllability of the rheological properties of fluids during self-healing processes is of practical importance for industrial applications, biomaterials and smart systems [89, 90, 100]. In addition, the high sensitivity to mechanical stress and show switchable rheological properties makes thixotropic organogels potential in applications such as the art cleaning and protection [121] and blood and cell conservation [122].

As for most gel systems, their intriguing physical properties that are sensitive to physical stimuli such as sonication or mechanical stress, have been discovered by serendipity, which is hard to predicable to some extent. Nevertheless, along with the rapid development of instrument techniques such as X-ray diffraction (XRD),

small-angle-X-ray scattering (SAXS), NMR, SEM, TEM, confocal laser scanning microscopy, circular dichroism (CD) and absorption and fluorescent spectroscopy, theoretical calculation, the designing and studying new molecular systems get more guidance that makes gelation more predicted, which are associated with the intrinsic nature of gelation and the corresponding response processes.

## 2.4 Chemical Responsive Gels

Compared to the serendipity of physical stimuli, the structures of the gels controlled by chemical stimuli are more predictable. Through introducing the molecular design functional groups that interact either by covalent or non-covalent interactions with other molecules present in the medium into the systems, the properties of the gels may be altered. Generally, on the one hand, the pre-gelators might be activated by the chemical stimuli to form gels. On the other hand, the gels would be disassembled by solubilization or precipitation processes after stimuli treatment. And the stimuli might product irreversible properties or it may be regenerated by the addition of an antagonist stimuli. According to the type of gelator-stimuli interaction systems, we mainly focus on the acid–base reaction, ion-binding, redox reactions, neutral species.

### 2.4.1 Acid and Base

pH-responsive gelators functionalized with ionizable groups allow the control of gelation processes by acid–base behaviour. Basically, the sol-to-gel transition can be tuned by pH changes. Escuder and co-workers reported a hydrogelator **40** derived from isophthalic acid (Scheme 2.7) [123]. The gelator can be solubilized in basic media and can be formed into a hydrogel at pH = 1 with an addition of HCl solution (Fig. 2.27). As for basic ionizable gelator, it is soluble in acidic media, and can be converted into hydrogels exposure to basic conditions like NaOH solution or ammonia vapours [124]. And the sol–gel transitions are both reversible by the addition of appropriate antagonist stimulus as for as the concentration of gelator remains above CGC. In fact, the reversibility of the sol–gel transformation processes also depends on the present of side products like salts in the medium.

Generally, the physical properties can be sensitive to the rate of addition of the stimulus. Sometimes, the high reproductivity of gel properties is hard to realize, because the heterogeneous gels particles even precipitates might form if the acidic stimulus is added too fast due to the kinetics of mixing being slower than the initial kinetic of gelation. In order to avoid this effect, Adam and co-workers introduce an approach to control the rate of pH changes by using hydrolysatation characteristic of  $\delta$ -gluconolactone to produce homogeneous hydrogels [125].



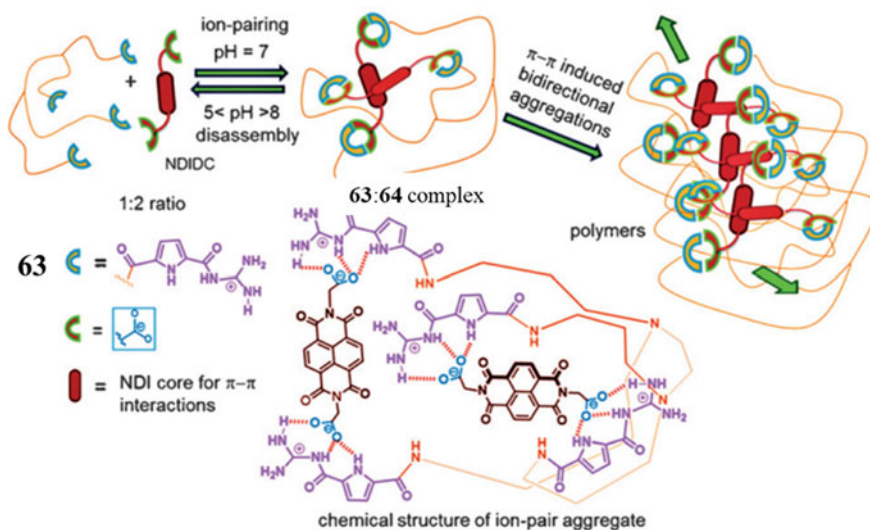


**Fig. 2.28** Proposed model for the two component assemblies of **41** and NDIC **42**. Reprinted with the permission from Ref. [126]. Copyright 2016 John Wiley & Sons, Inc.

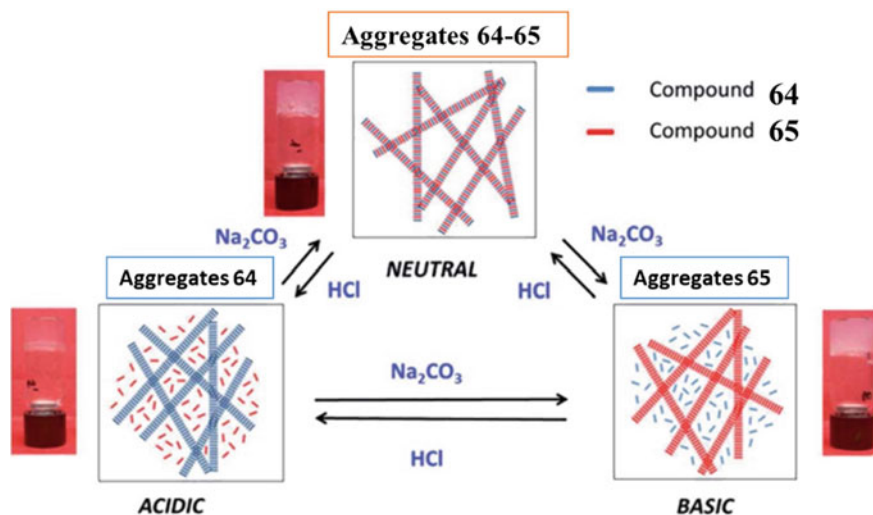


**Fig. 2.29** Scheme of the pH-responsiveness of mixtures **43:44**. Reprinted with the permission from Ref. [127]. Copyright 2014 Royal Society of Chemistry

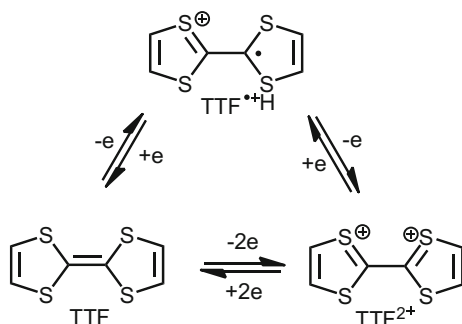
self-assembled nanofibrillar network, selectively interacting with positively charged dyes such as methylene blue and methyl violet 2B. The gel can be regenerated by dissolution in basic water followed by acidification after repetitive extractions with chloroform to remove the dye.

### 2.4.2 Redox

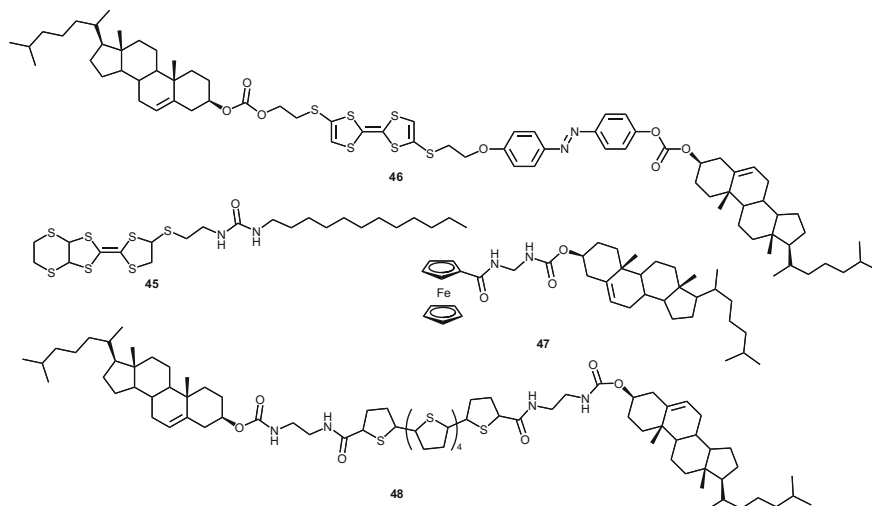
The transformations in the oxidation of the sensitive centre in the redox-sensitive gelators exhibit two different changes. One may involve a dramatic modification of solubility of gelators along with gel–sol transition, and another may product a change of chemical structure of the gelator either by formation of new covalent bonds or destruction of sensitive fragments. And the redox-active units mainly include reversible tetrathiafulvalene (TTF), ferrocene, thiophene and others.

Tetrathiafulvalene (TTF) and its derivatives are reversibly transformed into the respective radical cations ( $\text{TTF}^{\bullet+}$ ) and dications ( $\text{TTF}^{2+}$ ) by chemical redox reactions, and relative gelators show redox responsive (Scheme 2.8) [128, 129]. Zhang and co-workers studied the gelator **45** (Scheme 2.9) containing one TTF and one urea group can self-assemble into networks through hydrogen bonding and shows responsive to redox reaction [130]. The addition of  $\text{Fe}^{3+}$  to the gel can destroy the gel leading to the gel–sol transition due to the TTF unit oxidizing into the corresponding  $\text{TTF}^{\bullet+}$ . In addition, they designed and studied a multi-stimuli-responsive gel **46** (Scheme 2.9) featuring electroactive TTF and photoresponsive azobenzene units [131]. And theredox reactions are reversible by either the addition of  $\text{Fe}^{3+}$  or ascorbic acid (Fig. 2.30).

There are another electroactive units such as ferrocene and thiophene except for TTF group, which can be reversibly transformed into the respective cations by chemical means showing responsiveness to redox reactions. Cholesterol-appended ferrocene derivatives have been reported by Fang and co-workers [132]. The gelator **47** (Scheme 2.9) can form organogels in cyclohexane and the product is responsive to multi-stimuli such as thermal, sonication, mechanical stress and redox reactions, which can efficiently tune the gel–sol transitions (Scheme 2.9). When the gel system is oxidized with  $(\text{NH}_4)_2\text{Ce}(\text{NO}_3)_6$ , the gel dissembles into sol state and the gel state can be restored by addition of hydrazine as reductant. Shinkai and co-workers studied redox-active sexithiophene derivatives bearing two cholesteryl groups at the



**Scheme 2.8** Schematic representation of the transformation of the tetrathiafulvalene (TTF) between the respective radical cations ( $\text{TTF}^{\bullet+}$ ) and dications ( $\text{TTF}^{2+}$ ) by chemical redox reactions



**Scheme 2.9** Chemical structures of gelators **45–48**



**Fig. 2.30** Reversible tuning of the gel formation of **46** in  $\text{CH}_2\text{Cl}_2/\text{MeOH}$  (3/1, v/v) by chemical oxidation and reduction. Reprinted with the permission from Ref. [131]. Copyright 2010 American Chemical Society

$\alpha$ -position gelator **48** (Scheme 2.9) [133]. The 1,1,2,2-tetrachloroethane gels can be formed by the self-assembly of  $\pi$ - $\pi$  stacking and van der Waals forces and show reversible responsiveness to redox reactions along with gel-sol transitions by addition of oxidizing and reducing reagents such as  $\text{FeCl}_3$  and ascorbic acid, respectively (Fig. 2.31).

Except for reversible electroactive units, the irreversible redox-active reactions are also applied for redox-responsive gel systems. Hamachi and co-workers designed and prepared gelators **49** and **50** containing *p*-borono phenylmethoxycarbonyl unit (Bpmoc-FF) and *p*-nitro-phenylmethoxycarbonyl unit (Npmoc-FF) can form stable organogels through the formation of self-assembled nanofibre networks through van der Waals,  $\pi$ - $\pi$ , and hydrogen bonding interactions attributed to the hydrophobic aromatic groups (Fmoc-FF). The introducing moieties are sensitive to redox agents such as  $\text{H}_2\text{O}_2$  and  $\text{Na}_2\text{S}_2\text{O}_4$ , which may cause the removal of a hydrophobic degradation unit from the peptide *N*-terminal. Accordingly, the

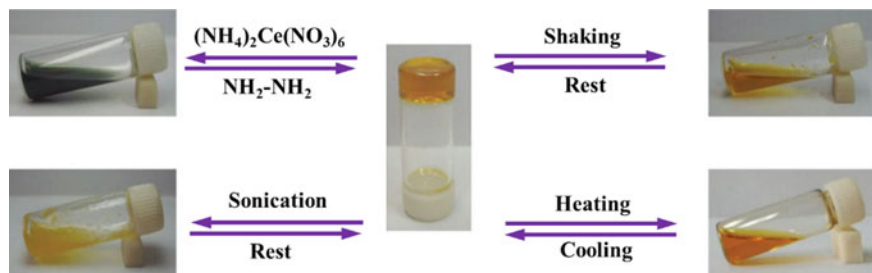


**Fig. 2.31** Reversible sol–gel phase transition of the gel of **48**/cyclohexane triggered by chemical redox reaction, shear stress, sonication, and temperature. Reprinted with the permission from Ref. [132]. Copyright 2008 John Wiley & Sons, Inc.

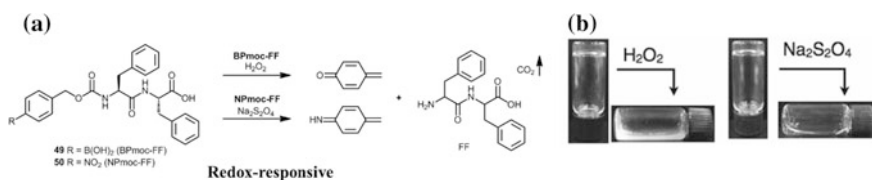


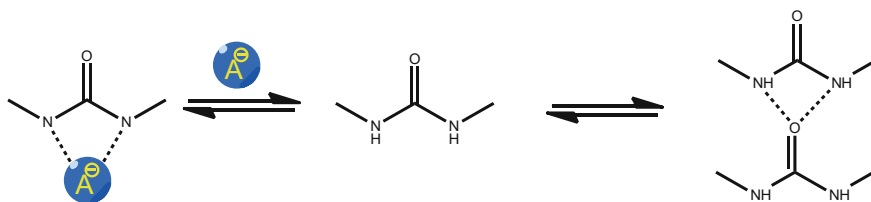
**Fig. 2.32** **a** Redox-responsive degradation mechanisms of **49** (BPmoc-FF), **50** (NPmoc-FF). **b** Photographs of gel-sol transitions of **49** and **50** upon addition of  $\text{H}_2\text{O}_2$  and  $\text{Na}_2\text{S}_2\text{O}_4$  respectively. Reprinted with the permission from Ref. [134]. Copyright 2011 John Wiley & Sons, Inc.

changes of molecular structures should destroy the delicate balance of molecular interactions in the self-assembled nanofiber network, which causes the gel–sol phase transition which is irreversible (Fig. 2.32) [134].

### 2.4.3 Ion

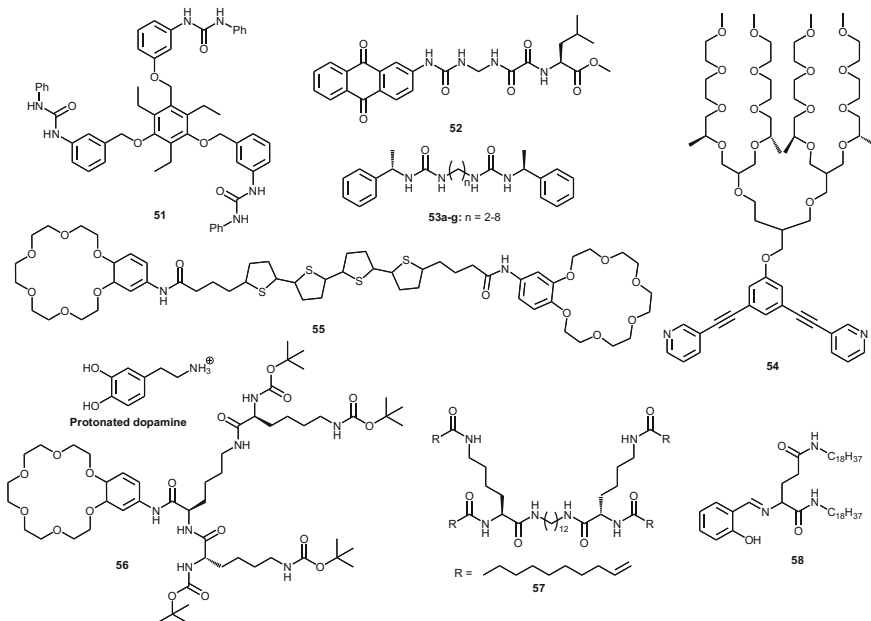
The design of gelators functionalized with binding sites for charged guests allows the tuning of gel properties by binding with anions or cations. Generally, the gelators bearing hydrogen bonding donor groups tend to interact with anions, typically including urea-based systems, and ligand sites for cations have been reported like crown ethers and others.

Based on the hydrogen-bonding functionalities' ability to bind to anions, urea-based systems have been studied widely to bind anions and then tune the gel properties. In one review, Steed and co-workers revealed that the competition between the anion-gelator binding and the gelator self-association can be used to precisely tune the gel properties (Scheme 2.10) [135]. Tris-urea gelator **53** containing anion-binding moieties has been studied by Yamanaka and co-workers, which can form gels in several polar solvents upon sonication irradiation. The



**Scheme 2.10** Tuning of aggregation of urea groups by anion binding

acetone gels of **51** (Scheme 2.11) respond to anions with the formation of tetrabutylammonium salt, resulting in homogeneous solutions, while the addition of  $\text{BF}_4^-$  cannot cause complete phase transition of the gel due to weak binding capacity. And the reversible and repeatable process can be used as a mean to sense or identify fluoride (Fig. 2.33) [136].



**Scheme 2.11** Chemical structures of gelators **51–58**



**Fig. 2.33** Photographs of acetone gel of **51** showing the transitions between gel state and liquid state upon addition of chemical stimuli. Reprinted with the permission from Ref. [136]. Copyright 2007 Elsevier Inc.

From above examples, the gel–sol processes are the results of the dissociation of intermolecular hydrogen bonds by binding of addition of anions typically the binding of fluoride. The strong binding of  $F^-$  anion originates from the high basicity of the anion and results in the deprotonation of the hydrogen bonding moiety. Žinić and co-workers reported an oxalamide-derived anthraquinone gelator **52** (Scheme 2.11), and it can form gels in various solvents with tuning properties by binding anions. In *p*-xylene gels, the fluoride is able to induce gels into reddish solution, and the change in colour and prevention of gelation is caused by the deprotonating of the NH group closest to the anthraquinone unit in gelator **52** by interacting with basic  $F^-$ . However, the ethanol gels keep gel phase with only colour change upon addition of  $TBA^+F^-$  because the fluoride tends to be solvated by polar solvent such as methanol, ethanol and water. A gradual breakdown of the gel over 4 h is realized by simple contact with fluoride with addition of a concentrated  $TBA^+F^-$ -*p*-xylene solution on the top of the gel, which is potential for sensing fluoride with the naked eye (Fig. 2.34) [137].

By the addition of anions to gels, the gel-to-sol transitions are not the only resultant effects and can be used to change the strength of the gel. A series of chiral bis(urea) gelators **53a–g** (Scheme 2.11) with different even and odd chain length have been prepared by Steed and co-workers, and for the even numbered spacers the rheological characteristics can be tuned by the introduction of sub-stoichiometric amounts of anions which compete for the urea hydrogen bonding groups and influence their directionality. And the results in a decrease of  $G'$ ,  $G''$  and the yield stress of the gel suggest that the anions can cause a decrease in the interconnectivity of the individual gel threads for a fixed concentration of gelator. The anion-binding constants are for gelator **53a** decrease in the sequence  $CH_3CO_2^- \geq Cl^- > NO_3^- > BF_4^-$ , which is consistent with the decreases in rheological values, while  $BF_4^-$  anion causes no effect due to weak binding capacity (Fig. 2.35).

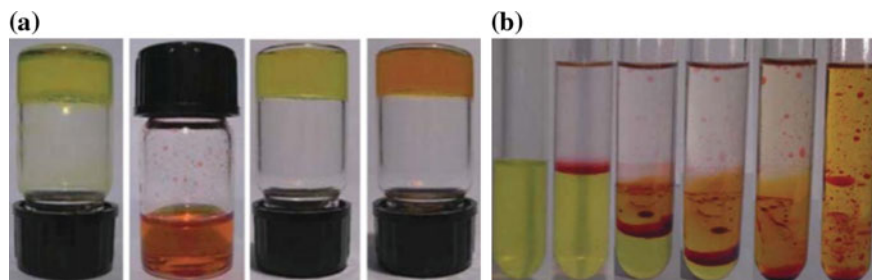


**Fig. 2.34** **a** **52**-*p*-xylene gel; addition of 10 eq. of TBAF to the hot *p*-xylene solution of **52** followed by cooling to RT; **52**-EtOH gel; reddish **52**-EtOH gel after addition of 10 eq. of  $F^-$  (from left for right). **b** Diffusion of fluoride from a concentrated *p*-xylene solution (50 equiv.) through the **52**-*p*-xylene gel. From left to right: **52**-*p*-xylene gel; immediately after addition of TBAF solution; after 2, 3 and 4 h; and overnight standing. Reprinted with the permission from Ref. [137]. Copyright 2007 Royal Society of Chemistry

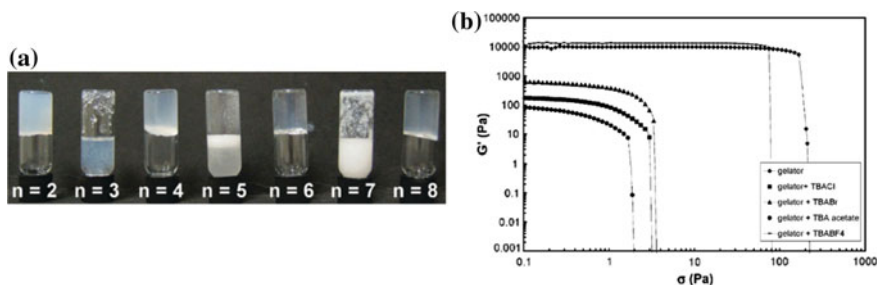


**Fig. 2.35** **a** Alternation of gel (even  $n$ ) and sol (odd  $n$ ) formation in  $\text{CHCl}_3$  by compound **53**, and **b** influence of different anions on the storage modulus ( $G'$ ) at a frequency of 1 Hz and a temperature of 20 °C. The lines are a guide for the eyes only. Reprinted with the permission from Ref. [13]. Copyright 2008 Royal Society of Chemistry

Except for low molecular organic gelators, metal-based LMWGs can also be tuned by anions stimuli. Lee and co-workers reported a metallogel formed by the bent-shaped bipyridine ligand with dendritic aliphatic appendages **54** (Scheme 2.11) complexed with silver ion through self-assembling process into supramolecular aggregates. And the secondary structure of a cationic coordination chain appears to be dependent on the size of the counteranion. With the triflate ion, these chains are dimeric rather than helical and then the units stack into hexagonally packed columns, which undergo gelation in aqueous solution. Addition of large anions such as  $\text{C}_2\text{F}_5\text{CO}_2^-$  and  $\text{C}_3\text{F}_7\text{CO}_2^-$  can lead to a gel-to-sol transitions as the ligand changes from a cisoid to transoid form, which is completely reversible (Fig. 2.36) [138].

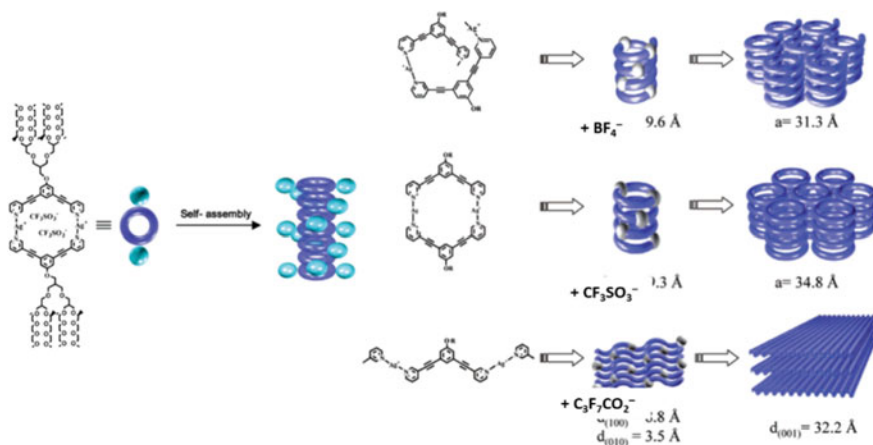


**Fig. 2.36** Schematic representation of the self-assembly of **54** with  $\text{Ag}(\text{I})$  in the presence of different counteranions into secondary structures and subsequent self-organization. Reprinted with the permission from Ref. [138]. Copyright 2004 American Chemical Society

In stimuli-responsive gels capable of interacting with cations, it is typical to design the gelators functionalized with crown ether moieties, which mainly focus on their stimuli-responsiveness, especially those based on host–guest interactions. Various kinds of crown ether moieties might interact with alkali metal cations, primary alkylammonium cations (PAA), and secondary ammonium cations etc., and further tune the gel properties through self-assembly processes. A crown-appended quaterthiophene gelator **55** (Scheme 2.11) based on unique functional and constructive properties of oligothiophenes (OT's) and stimuli-responsive behaviour of the crown ethers was reported by Shinkai and co-workers. The control of the sol-to-gel transition was realized by stimuli-responsive to specific alkali metal cations such as  $K^+$  and  $Cs^+$  with enhanced fluorescence emission due to the  $\pi$ – $\pi$  stacking interactions of the  $\pi$ -conjugated OT's. Moreover, the self-assembled fibres can have a tolerance up to 1 eq. of specific alkali metal cations, but the further increase will cause gel-to-sol transition with dissolution of the assemblies due to electrostatic repulsion between bound cations (Fig. 2.37) [139]. Smith and co-workers reported a gelator **56** (Scheme 2.11) by second (G2)-generation dendritic branches based on L-lysine building blocks with an [18] crown-6 unit. The dendritic functionalization enables gelators to assemble via intermolecular hydrogen bond interactions and consequently form gels in non-hydrogen bonding solvents. Dopamine is an important molecule because it is a neurotransmitter, associated with Parkinson's disease, Tourette's syndrome, schizophrenia and attention deficit hyperactivity disorder (ADHD). The addition of dopamine can modify the thermal stability of gels with a decrease of  $T_{gel}$  as the specific bound with crown ether moiety, and the subsequent addition of potassium ions causes release of protonated dopamine with triggering disassembly [140].

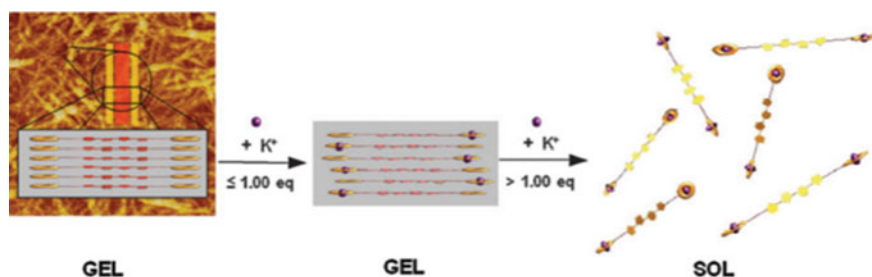


**Fig. 2.37** Schematic representation of the gel–sol phase transition upon increasing concentration of  $K^+$ . Reprinted with the permission from Ref. [139]. Copyright 2011 Royal Society of Chemistry

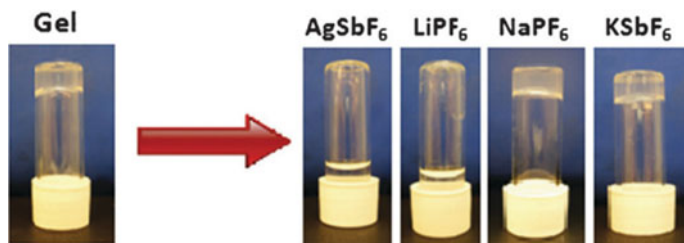


**Fig. 2.38** Response of gels of **57** in ethyl acetate to solutions of metal salts ( $\text{AgSbF}_6$ ,  $\text{LiPF}_6$ ,  $\text{NaPF}_6$  and  $\text{KSbF}_6$ ). All gels are 3 mM, salt solutions are 90 mM, except for  $\text{AgSbF}_6$  which is 30 mM. Reprinted with the permission from Ref. [141]. Copyright 2012 Royal Society of Chemistry

Besides, there some examples with other functional groups can also show stimuli-responsive to cations for tuning of gel properties, leading to gel-to-sol transition. Smith and co-workers reported the first example of the  $\text{Ag}^+$ -alkene interactions as the driving force for the gel-to-sol transitions. The ethyl acetate gel of alkene-terminated gelator **57** (Scheme 2.11) shows selective response to  $\text{Ag}^+$  or  $\text{Li}^+$  cation compared to  $\text{Na}^+$  or  $\text{K}^+$ . The  $\text{Ag}^+$ -alkene interactions play a vital role in mediating a response in soft matter systems, providing fundamental insight into the nature of this interaction and acting as a step on the way to development of heavy-metal-responsive materials (Fig. 2.38) [141]. Similarly, the amphiphilic Schiff base organogelator **58** (Scheme 2.11) was studied by Liu and co-workers with stimuli-responsiveness to metal ions. The gelator **58** can gel in DMSO, acetonitrile and toluene owing to strong  $\pi$ - $\pi$  interactions, hydrogen-bonding interactions and hydrophobic interactions. The addition of  $\text{Cu}^{2+}$  and  $\text{Mg}^{2+}$  ions maintained the gelating ability of the compound, while  $\text{Zn}^{2+}$  and  $\text{Ni}^{2+}$  ions destroyed the gel. Interestingly, the addition of copper can tune the morphology of the gel from achiral to chiral twisted nanofibres. Moreover,  $\text{Mg}^{2+}$  ions can enhance the fluorescence of the gel, and the  $\text{Mg}^{2+}$ -ion-mediated organogel showed differences in the fluorescence quenching by D- and L-tartaric acid, thus showing chiral recognition ability (Fig. 2.39) [142].

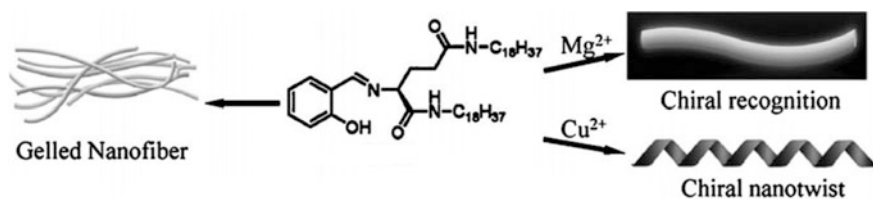


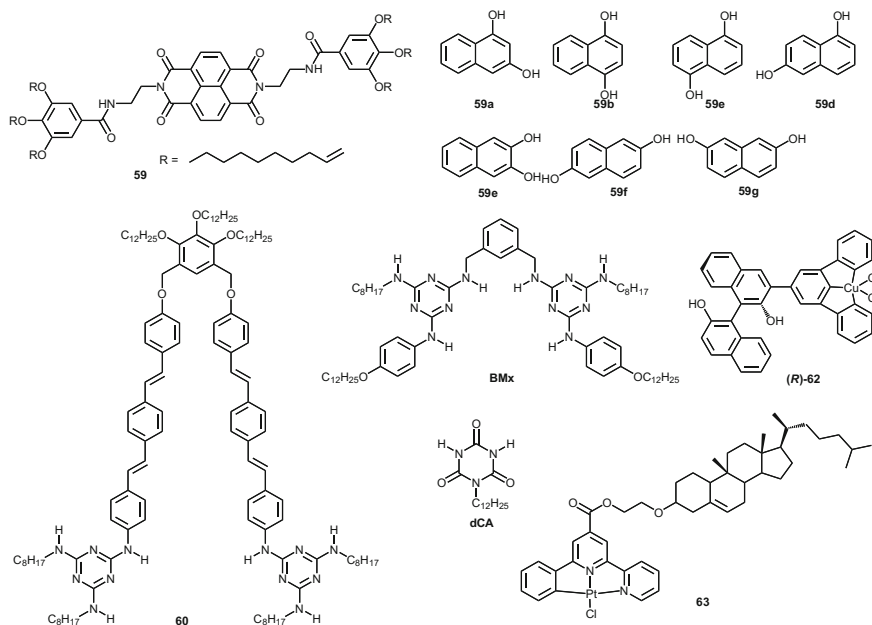
**Fig. 2.39** Structure of the amphiphilic Schiff bases **58** and their manner of self-assembly, which depended on the metal ions. Reprinted with the permission from Ref. [142]. Copyright 2012 John Wiley & Sons, Inc.

Of course, metal ions as important and convenient cations have been investigated in many studies. They have been used to construct gel systems by metallo gels or metal–organic gels, and the content will be talked about in detail in Chap. 3.

### 2.4.4 Neutral Species

Apart from charged guest such as cations or anions, the addition of neutral species may involve specific non-covalent interactions between accessible binding sites of the gelators and complementary functional groups of the small molecule, which is similar with biological protein–substrate binding. The interaction and recognition processes represent a response to physical or chemical properties of gel and guest, and the non-covalent interactions like  $\pi$ – $\pi$  stacking, H-bonding, and van der Waals forces play a pivotal role in the self-assembly processes.

Shinkai and co-workers reported one of the first example of an organogel matrix naphthalenediimide–alkoxynaphthalene derived gelator **59** (Scheme 2.12) in colorimetric detection system. Organogels shows selective recognition of the polar, hydrophilic dihydroxynaphthalenes by intercalation between naphthalenediimide moieties to form columnar  $\pi$ -stacked donor–acceptor superstructures with a combination of hydrogen bonding as driving forces. Moreover, this system can distinguish clearly several positional isomers of dihydroxynaphthalenes with the naked



**Scheme 2.12** Chemical structures of gelators **59**, **60**, **62** and **63**

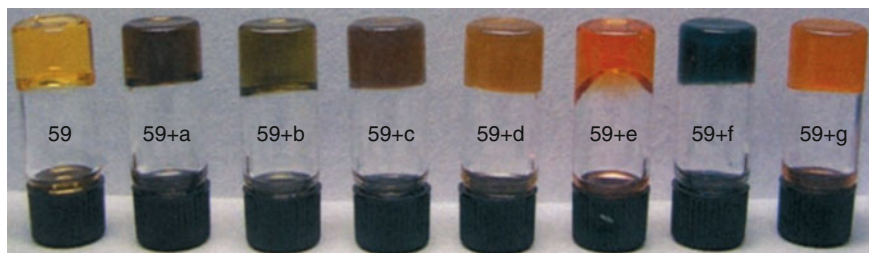


**Fig. 2.40** The photograph depicts the spontaneous colour changes of organogel **59** upon addition of positional isomers of dihydroxynaphthalene (**a–g**) (from left to right, and the first one is organogel **59**). Reprinted with the permission from Ref. [143]. Copyright 2006 John Wiley & Sons, Inc.

eye due to the selective photochromic response at a very low concentration of analytes that predominantly operates only in the gel state, as compared with the convenient sensing systems in solution state (Fig. 2.40) [143]. In addition, hydrogen-bonding-driven self-assembly recognition has been reported in other systems. Yagai and co-workers reported a related gelator **60** (Scheme 2.12) based on OPV dimer end-capped by monotopic melamine hydrogen bonding units, which can self-assemble in methylcyclohexane to form flexible fibrous nanostructures. The multiple hydrogen-bonding interactions enables a guest-induced transformation upon addition of ditopic triple hydrogen-bonding modules such as cyanurate dCA, and leads to the disassembly of the gel due to the change of morphology from flexible fibrous nanostructures into rigid nanofibres. The reversible gel-to-sol transition can be realized by addition of competing *m*-xylylene-linked bismelamine ( $BM_x$ ) (Fig. 2.41) [144].

It is well known that cyclodextrins (CDs) exhibit host-guest interactions in two ways: one is to incorporate various guest compounds into their cavities through hydrophobic interactions to form inclusion complexes in aqueous media, another is

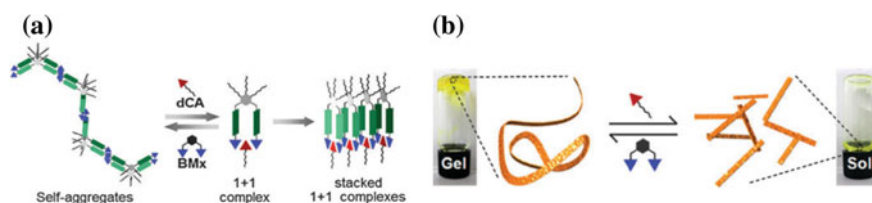


**Fig. 2.41** **a** Schematic representation of self- and coaggregation of gelator and guests. **b** Photographs of a cyclohexane gel of **60** (left) and a solution of **60** + dCA (right) with schematic representation of nanostructure changes of **60** induced by cyanurates and  $BM_x$ . Reprinted with the permission from Ref. [144]. Copyright 2009 Royal Society of Chemistry

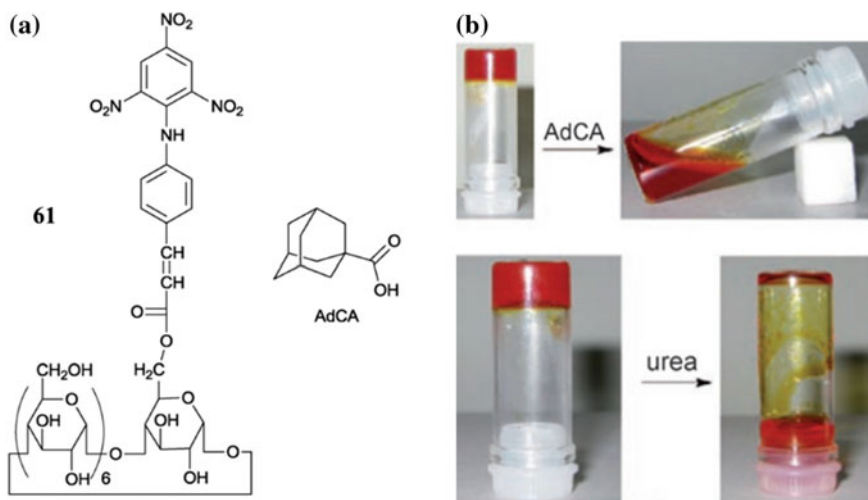
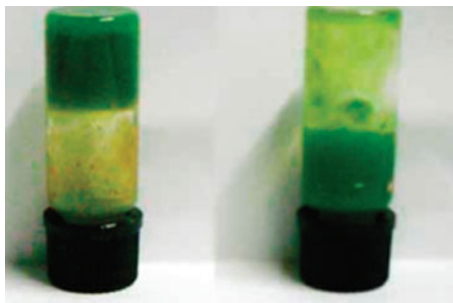


**Fig. 2.42** a Chemical structures of gelator **61** and AdCA. b The gel-to-sol transition upon addition of AdCA and urea to a solution of **61**. Reprinted with the permission from Ref. [145]. Copyright 2007 John Wiley & Sons, Inc.

to interact with hydrophilic moieties by H-bonding interactions. And the responsive cyclodextrins (CDs) hydrogels can be obtained based on the host-guest interactions.  $\beta$ -Cyclodextrin ( $\beta$ -CD) substituted with a cinnamoyl-trinitrophenyl tail gelator **61** was reported by Harada and co-workers. The 2D ROESY NMR results show that hydrogel is formed by self-assembly of the host-guest interactions of 2,4,6-trinitrophenyl (TNB) moiety in the CD cavities combined with hydrogen bonding between CD scaffolds. The addition of a competitive guest such as 1-adamantane carboxylic acid (AdCA) or urea as a denaturing reagent can lead to the gel-to-sol transitions (Fig. 2.42) [145].

Additionally, the chemical-responsive to stereoselectivity with molecular gel formation and collapsing can be applied for visual chiral recognition. Pu and co-workers reported a chiral molecular gel prepared by sonication of a BINOL-terpyridine-based Cu(II) complex **62** (Scheme 2.12) by molecular assembly based on  $\pi$ - $\pi$  interaction between the terpyridine units, and the enantioselective gel collapsing is as a new method for the visual discrimination of chiral amino alcohols. The addition of 0.1 eq. of (*S*)-phenylglycinol solution into (*R*)-**62**  $\text{CHCl}_3$  gel with subsequent 2 min sonication treatment leads to the gel collapsed, while the gel remains stable after addition of 0.1 eq. (*R*)-phenylglycinol, and additional 0.1 eq. of additive is required to cause the gel collapsed. The reverted behaviour was occurred for the gel of (*S*)-**62** with similar treatment (Fig. 2.43) [146].

**Fig. 2.43** Enantioselective responses of the gel of (*R*)-**62** toward (*R*)-phenylglycinol (left) and (*S*)-phenylglycinol (right). Reprinted with the permission from Ref. [146]. Copyright 2010 American Chemical Society



Similarly, ALS chiral pincer platinum(II) metallogelators **63** (Scheme 2.12) was prepared by Tu and co-workers. When addition of 0.1 eq. of the *S* enantiomer of bulky phosphine chiral ligands leads to the collapse of the gel, while the *R* enantiomer remains the gel stable [147].

## 2.5 Conclusions

LMWGs based on supramolecular self-assembly by non-covalent are sensitive to external stimulus, and the multiple stimulus responsive to heat, light, sound, chemicals, potentially makes supramolecular gels “smart” gels with typical variety, specificity, reversibility of the reactive behaviours. On account of these properties, the systems may be advantageous in delivering drugs, binding pollutants or catalysing reactions. In addition, an ambitious goal is that complex dynamic multi-responsive system in the cell with the development of smart gelloosomes to mimic the cell architecture such as intracellular filaments, muscle tissue and sensory receptors in the near future.

Though a range of smart gels have been investigated to date, the chemical variation, the use of co-gelators, additives or solvent mixtures may provide potential chances to adjust the physical or chemical properties of gels for a wide variety of applications. However, the design of LMWGs is mainly dependent on well-defined scaffolds and reactive groups to achieve the desired responsive characteristics in supramolecular systems, which may be limited in the development of multifarious properties of gels. By exploring a number of potential structural motifs, it's a useful scope to introduce non-gelating functional materials, such as polymers, nanoparticles, metal-organic frameworks into traditional LMWGs to evolve hybrid systems, which provide access to more varied and switchable behaviours. Additionally, the incomplete model of gel formation may limit the design of gelators. Because the

nucleation and growth processes are often sensitive to external factors such as temperature, solvent or solvent mixtures, the well-designed gelators based on the idealized and predictable supramolecular self-assembly processes may exhibit variable nano/microstructures. Moreover, in order to decrease the empiricism and serendipity by current level of understanding, it is important to provide more robust methods of gelator design, and the theoretical calculation method can predict the dominant self-assembly aggregation pathway.

## References

1. Harada A, Kobayashi R, Takashima Y, Hashidzume A, Yamaguchi H (2011) Macroscopic self-assembly through molecular recognition. *Nat Chem* 3:34
2. Park T, Zimmerman SC (2006) Formation of a miscible supramolecular polymer blend through self-assembly mediated by a quadruply hydrogen-bonded heterocomplex. *J Am Chem Soc* 128:11582
3. Shirakawa M, Fujita N, Shinkai S (2003) [60]Fullerene-motivated organogel formation in a porphyrin derivative bearing programmed hydrogen-bonding sites. *J Am Chem Soc* 125:9902
4. Dastidar P (2008) Supramolecular gelling agents: can they be designed? *Chem Soc Rev* 37:2699
5. de Jong JDD, Feringa BL (2006) In *Molecular gels, materials with self-assembled fibrillar networks*. Springer, The Netherlands
6. Puigmarti-Luis J, Laukhin V, Pérez del Pino Á, Vidal-Gancedo J, Rovira C, Laukhina E, Amabilino DB (2007) Supramolecular conducting nanowires from organogels. *Angew Chem Int Ed* 46:238
7. Yang Z, Ho P-L, Liang G, Chow KH, Wang Q, Cao Y, Guo Z, Xu B (2007) Using  $\beta$ -lactamase to trigger supramolecular hydrogelation. *J Am Chem Soc* 129:266
8. Hirst AR, Escuder B, Miravet JF, Smith DK (2008) High-tech applications of self-assembling supramolecular nanostructured gel-phase materials: from regenerative medicine to electronic devices. *Angew Chem Int Ed* 47:8002
9. Yu G, Yan X, Han C, Huang F (2013) Characterization of supramolecular gels. *Chem Soc Rev* 42:6697
10. Pal A, Dey J (2013) L-cysteine-derived ambidextrous gelators of aromatic solvents and ethanol/water mixtures. *Langmuir* 29:2120
11. Caplar V, Frkanec L, Sijakovic Vujicic N, Zinic M (2010) Positionally isomeric organic gelators: structure-gelation study, racemic versus enantiomeric gelators, and solvation effects. *Chem Eur J* 16:3066
12. Abraham S, Lan Y, Lam RS, Grahame DA, Kim JJ, Weiss RG, Rogers MA (2012) Influence of positional isomers on the macroscale and nanoscale architectures of aggregates of racemic hydroxyoctadecanoic acids in their molecular gel, dispersion, and solid states. *Langmuir* 28:4955
13. Piepenbrock MOM, Lloyd GO, Clarke N, Steed JW (2008) Gelation is crucially dependent on functional group orientation and may be tuned by anion binding. *Chem Commun* 2644
14. Nakagawa T, Amakatsu M, Munenobu K, Fujii H, Yamanaka M (2013) Effect of optical purity of C3-symmetric chiral tris-ureas on supramolecular gel formation. *Chem Lett* 42:229
15. Grahame DAS, Olason C, Lam RSH, Pedersen T, Borondics F, Abraham S, Weiss RG, Rogers MA (2011) Influence of chirality on the modes of self-assembly of 12-hydroxystearic acid in molecular gels of mineral oil. *Soft Matter* 7:7359

16. Kuroiwa K, Shibata T, Takada A, Nemoto N, Kimizuka N (2004) Heat-set gel-like networks of lipophilic Co(II) triazole complexes in organic media and their thermochromic structural transitions. *J Am Chem Soc* 126:2016
17. Peterca M, Imam MR, Ahn CH, Balagurusamy VS, Wilson DA, Rosen BM, Percec V (2011) Transfer, amplification, and inversion of helical chirality mediated by concerted interactions of C3-supramolecular dendrimers. *J Am Chem Soc* 133:2311
18. Kasha M (1963) Energy transfer mechanisms and the molecular exciton model for molecular aggregates. *Radiat Res* 20:55
19. Yamane S, Sagara Y, Kato T (2013) Steric effects on excimer formation for photoluminescent smectic liquid-crystalline materials. *Chem Commun* 49:3839
20. Das A, Molla MR, Maity B, Koley D, Ghosh S (2012) Hydrogen-bonding induced alternate stacking of donor (D) and acceptor (A) chromophores and their supramolecular switching to segregated states. *Chemistry* 18:9849
21. Bowen EJ, Sahu J (1959) The effect of temperature on fluorescence of solutions. *J Phys Chem* 63:4
22. Praveen VK, George SJ, Varghese R, Vijayakumar C, Ajayaghosh A (2006) Self-assembled  $\pi$ -nanotapes as donor scaffolds for selective and thermally gated fluorescence resonance energy transfer (FRET). *J Am Chem Soc* 128:7542
23. Zhao Z, Lam JWY, Tang BZ (2013) Self-assembly of organic luminophores with gelation-enhanced emission characteristics. *Soft Matter* 9:4564
24. Hong Y, Lam JWY, Tang BZ (2011) Aggregation-induced emission. *Chem Soc Rev* 40:5361
25. Kamikawa Y, Kato T (2007) Color-tunable fluorescent organogels: columnar self-assembly of pyrene-containing oligo(glutamic acid)s. *Langmuir* 23:274
26. Yan N, Xu Z, Diehn KK, Raghavan SR, Fang Y, Weiss RG (2013) Pyrenyl-linker-glucono gelators. Correlations of gel properties with gelator structures and characterization of solvent effects. *Langmuir* 29:793
27. Braga D, d'Agostino S, D'Amen E, Grepioni F (2011) Polymorphs from supramolecular gels: four crystal forms of the same silver(i) supergelator crystallized directly from its gels. *Chem Commun* 47:5154
28. Ruiz-Palmero C, Kennedy SR, Soriano ML, Jones CD, Valcarcel M, Steed JW (2016) Pharmaceutical crystallization with nanocellulose organogels. *Chem Commun* 52:7782
29. Cayuela A, Kennedy SR, Soriano ML, Jones CD, Valcárcel M, Steed JW (2015) Fluorescent carbon dot-molecular salt hydrogels. *Chem Sci* 6:6139
30. Foster JA, Piepenbrock Marc-Oliver M, Lloyd GO, Clarke N, Howard Judith AK, Steed JW (2010) Anion-switchable supramolecular gels for controlling pharmaceutical crystal growth. *Nat Chem* 2:1037
31. Diaz Diaz D, Kuhbeck D, Koopmans RJ (2011) Stimuli-responsive gels as reaction vessels and reusable catalysts. *Chem Soc Rev* 40:427
32. Escuder B, Rodríguez-Llansola F, Miravet JF (2010) Supramolecular gels as active media for organic reactions and catalysis. *New J Chem* 34:1044
33. Rodríguez-Llansola F, Escuder B, Miravet JF (2009) Remarkable increase in basicity associated with supramolecular gelation. *Org Biomol Chem* 7:3091
34. Quesada-Perez M, Ramos J, Forcada J, Martín-Molina A (2012) Computer simulations of thermo-sensitive microgels: quantitative comparison with experimental swelling data. *J Chem Phys* 136:244903
35. Xing B, Yu C-W, Chow K-H, Ho P-L, Fu D, Xu B (2002) Hydrophobic interaction and hydrogen bonding cooperatively confer a vancomycin hydrogel: a potential candidate for biomaterials. *J Am Chem Soc* 124:14846
36. Zhou SL, Matsumoto S, Tian HD, Yamane H, Ojida A, Kiyonaka S, Hamachi I (2005) pH-Responsive shrinkage/swelling of a supramolecular hydrogel composed of two small amphiphilic molecules. *Chemistry* 11:1130

37. Shi C, Huang Z, Kilic S, Xu J, Enick RM, Beckman EJ, Carr AJ, Melendez RE, Hamilton AD (1999) The gelation of CO<sub>2</sub>: a sustainable route to the creation of microcellular materials. *Science* 286:1540
38. Zhang M, Meng L, Cao X, Jiang M, Yi T (2012) Morphological transformation between three-dimensional gel network and spherical vesicles via sonication. *Soft Matter* 8:4494
39. Bromberg L, Temchenko M, Moeser GD, Hatton TA (2004) Thermodynamics of temperature-sensitive polyether-modified poly(acrylic acid) microgels. *Langmuir* 20:5683
40. Krieg E, Shirman E, Weissman H, Shimoni E, Wolf SG, Pinkas I, Rybtchinski B (2009) Supramolecular gel based on a perylene diimide dye: multiple stimuli responsiveness, robustness, and photofunction. *J Am Chem Soc* 131:14365
41. Komatsu H, Matsumoto S, Tamaru S-i, Kaneko K, Ikeda M, Hamachi I (2009) Supramolecular hydrogel exhibiting four basic logic gate functions to fine-tune substance release. *J Am Chem Soc* 131:5580
42. Kiyonaka S, Sugiyasu K, Shinkai S, Hamachi I (2002) First thermally responsive supramolecular polymer based on glycosylated amino acid. *J Am Chem Soc* 124:10954
43. de Loos M, Feringa BL, van Esch JH (2005) Design and application of self-assembled low molecular weight hydrogels. *Eur J Org Chem* 2005:3615
44. Tiller JC (2003) Increasing the local concentration of drugs by hydrogel formation. *Angew Chem Int Ed* 42:3072
45. Vintiloiu A, Leroux JC (2008) Organogels and their use in drug delivery—a review. *J Control Release* 125:179
46. Yagai S, Karatsu T, Kitamura A (2005) Photocontrollable self-assembly. *Chemistry* 11:4054
47. Pieroni O, Fissi A, Angelini N, Lenci F (2001) Photoresponsive polypeptides. *Acc Chem Res* 34:9
48. Tian H, Wang S (2007) Photochromic bisthiénylene as multi-function switches. *Chem Commun* 781
49. Yagai S, Kitamura A (2008) Recent advances in photoresponsive supramolecular self-assemblies. *Chem Soc Rev* 37:1520
50. Xie F, Qin L, Liu M (2016) A dual thermal and photo-switchable shrinking-swelling supramolecular peptide dendron gel. *Chem Commun* 52:930
51. Yagai S, Nakajima T, Kishikawa K, Kohmoto S, Karatsu T, Kitamura A (2005) Hierarchical organization of photoresponsive hydrogen-bonded rosettes. *J Am Chem Soc* 127:11134
52. Tamai N, Miyasaka H (2000) Ultrafast dynamics of photochromic systems. *Chem Rev* 100:1875–1890
53. Das S, Varghese S, Kumar NS (2010) Butadiene-based photoresponsive soft materials. *Langmuir* 26:1598
54. Melanie RM, Hecht S (2010) Photoswitches: from molecules to materials. *Adv Mater* 22:3348
55. Bleger D, Yu Z, Hecht S (2011) Toward optomechanics: maximizing the photodeformation of individual molecules. *Chem Commun* 47:12260
56. Murata K, Aoki M, Suzuki T, Harada T, Kawabata H, Komori T, Ohseto F, Ueda K, Shinkai S (1994) Thermal and light control of the sol-gel phase transition in cholesterol-based organic gels. Novel helical aggregation modes as detected by circular dichroism and electron microscopic observation. *J Am Chem Soc* 116:6664
57. Murata K, Aoki M, Shinkai S (1992) Sol-gel phase transition of switch-functionalized cholesterols as detected by circular dichroism. *Chem Lett* 21:739
58. Duan P, Li Y, Li L, Deng J, Liu M (2011) Multiresponsive chiroptical switch of an azobenzene-containing lipid: solvent, temperature, and photoregulated supramolecular chirality. *J Phys Chem B* 115:3322
59. Wu Y, Wu S, Tian X, Wang X, Wu W, Zou G, Zhang Q (2011) Photoinduced reversible gel–sol transitions of dicholesterol-linked azobenzene derivatives through breaking and reforming of van der Waals interactions. *Soft Matter* 7:716

60. Ran X, Wang H, Zhang P, Bai B, Zhao C, Yu Z, Li M (2011) Photo-induced fiber-vesicle morphological change in an organogel based on an azophenyl hydrazide derivative. *Soft Matter* 7:8561
61. Koehler JM, Mueller SC (1995) Frozen chemical waves in the belousov-zhabotinsky reaction. *J Phys Chem* 99:980
62. Li Y, Tanaka Toyochi (1990) Kinetics of swelling and shrinking of gels. *J Chem Phys* 92:1365
63. Xu JF, Chen YZ, Wu D, Wu LZ, Tung CH, Yang QZ (2013) Photoresponsive hydrogen-bonded supramolecular polymers based on a stiff stilbene unit. *Angew Chem Int Ed* 52:9738
64. Draper ER, Eden EG, McDonald TO, Adams DJ (2015) Spatially resolved multicomponent gels. *Nat Chem* 7:848
65. Zhu L, Li X, Zhang Q, Ma X, Li M, Zhang H, Luo Z, Agren H, Zhao Y (2013) Unimolecular photoconversion of multicolor luminescence on hierarchical self-assemblies. *J Am Chem Soc* 135:5175
66. Srivastava A, Ghorai S, Bhattacharjya A, Bhattacharya S (2005) A tetrameric sugar-based azobenzene that gels water at various pH values and in the presence of salts. *J Org Chem* 70:6574
67. Yagai S, Karatsu T, Kitamura A (2005) Melamine-barbiturate/cyanurate binary organogels possessing rigid azobenzene-tether moiety. *Langmuir* 21:11048
68. Miljanić S, Frkanec L, Meić Z, Žinić M (2005) Photoinduced gelation by stilbene oxalyl amide compounds. *Langmuir* 21:2754
69. Yagai S, Ishiwatari K, Lin X, Karatsu T, Kitamura A, Uemura S (2013) Rational design of photoresponsive supramolecular assemblies based on diarylethene. *Chem Eur J* 19:6971
70. Yarimaga O, Jaworski J, Yoon B, Kim JM (2012) Polydiacetylenes: supramolecular smart materials with a structural hierarchy for sensing, imaging and display applications. *Chem Commun* 48:2469
71. Neabo JR, Rondeau-Gagne S, Vigier-Carriere C, Morin JF (2013) Soluble conjugated one-dimensional nanowires prepared by topochemical polymerization of a butadiynes-containing star-shaped molecule in the xerogel state. *Langmuir* 29:3446
72. Aoki K, Kudo M, Tamaoki N (2004) Novel odd/even effect of alkylene chain length on the photopolymerizability of organogelators. *Org Lett* 6:4009
73. Fujita N, Sakamoto Y, Shirakawa M, Ojima M, Fujii A, Ozaki M, Shinkai S (2007) Polydiacetylene nanofibers created in low-molecular-weight gels by post modification: control of blue and red phases by the odd-even effect in alkyl chains. *J Am Chem Soc* 129:4134
74. Minkin VI (2004) Photo-, thermo-, solvato-, and electrochromic spiroheterocyclic compounds. *Chem Rev* 104:2751
75. Berkovic G, Nuclear S, Krongauz V (2000) Spiropyran and spirooxazines for memories and switches. *Chem Rev* 100:1741
76. Raymo FM, Tomasulo M (2005) Electron and energy transfer modulation with photochromic switches. *Chem Soc Rev* 34:327
77. Qiu Z, Yu H, Li J, Wang Y, Zhang Y (2009) Spiropyran-linked dipeptide forms supramolecular hydrogel with dual responses to light and to ligand-receptor interaction. *Chem Commun* 0:3342
78. Li Y, Wong KM, Tam AY, Wu L, Yam VW (2010) Thermo- and acid-responsive photochromic spironaphthoxazine-containing organogelators. *Chem Eur J* 16:8690
79. Chen Q, Feng Y, Zhang D, Zhang G, Fan Q, Sun S, Zhu D (2010) Light-triggered self-assembly of a spiropyran-functionalized dendron into nano-/micrometer-sized particles and photoresponsive organogel with switchable fluorescence. *Adv Funct Mater* 20:36

80. Irie M (2000) Diarylethenes for memories and switches. *Chem Rev* 100:1685
81. Praveen VK, George SJ, Varghese R, Vijayakumar C, Ajayaghosh A (2012) A smart gelator as a chemosensor: application to integrated logic gates in solution, gel, and film. *Chem Eur J* 18:3549
82. Foster JA, Parker RM, Belenguer AM, Kishi N, Sutton S, Abell C, Nitschke JR (2015) Differentially addressable cavities within metal-organic cage-cross-linked polymeric hydrogels. *J Am Chem Soc* 137:9722
83. de Jong JJD, Lucas LN, Kellogg RM, van Esch JH, Feringa BL (2004) Reversible optical transcription of supramolecular chirality into molecular chirality. *Science* 304:278
84. Xiao S, Zou Y, Yu M, Yi T, Zhou Y, Li F, Huang C (2007) A photochromic fluorescent switch in an organogel system with non-destructive readout ability. *Chem Commun* 4758
85. de Jong JJ, Browne WR, Walko M, Lucas LN, Barrett LJ, McGarvey JJ, van Esch JH, Feringa BL (2006) Raman scattering and FT-IR spectroscopic studies on dithienylethene switches-towards non-destructive optical readout. *Org Biomol Chem* 4:2387
86. Tian H, Yang S (2004) Recent progresses on diarylethene based photochromic switches. *Chem Soc Rev* 33:85
87. Andréasson J, Pischel U (2010) Smart molecules at work-mimicking advanced logic operations. *Chem Soc Rev* 39:174
88. Andreasson J, Pischel U, Straight SD, Moore TA, Moore AL, Gust D (2011) All-photonic multifunctional molecular logic device. *J Am Chem Soc* 133:11641
89. Cravotto G, Cintas P (2009) Molecular self-assembly and patterning induced by sound waves. The case of gelation. *Chem Soc Rev* 38:2684
90. Paulusse JM, Sijbesma RP (2006) Molecule-based rheology switching. *Angew Chem Int Ed* 45:2334
91. Gerber TP, Hout M (1998) More shock than therapy: market transition, employment, and income in Russia, 1991–1995. *Am J Sociol* 104:1
92. Sijbesma RP, Beijer FH, Brunsveld L, Folmer BJB, Hirschberg JHKK, Lange RFM, Lowe JKL, Meijer EW (1997) Reversible polymers formed from self-complementary monomers using quadruple hydrogen bonding. *Science* 278:1601
93. Wu J, Yi T, Xia Q, Zou Y, Liu F, Dong J, Shu T, Li F, Huang C (2009) Tunable gel formation by both sonication and thermal processing in a cholesterol-based self-assembly system. *Chem Eur J* 15:6234
94. Jadhav SR, Vemula PK, Kumar R, Raghavan SR, John G (2010) Sugar-derived phase-selective molecular gelators as model solidifiers for oil spills. *Angew Chem Int Ed* 49:7695
95. Mukherjee S, Mukhopadhyay B (2012) Phase selective carbohydrate gelator. *RSC Adv* 2:2270
96. Blanco E, Esquivias L, Litrán R, Piñero M, Ramírez-del-Solar M, de la Rosa-Fox N (1999) Sonogels and derived materials. *Appl Organometal Chem* 13:399
97. Bardelang D (2009) Ultrasound induced gelation: a paradigm shift. *Soft Matter* 5:1969
98. Cai X, Wu Y, Wang L, Yan N, Liu J, Fang X, Fang Y (2013) Mechano-responsive calix[4]arene-based molecular gels: agitation induced gelation and hardening. *Soft Matter* 9:5807
99. Anderson KM, Day GM, Paterson MJ, Byrne P, Clarke N, Steed JW (2008) Structure calculation of an elastic hydrogel from sonication of rigid small molecule components. *Angew Chem Int Ed* 47:1058
100. Yu X, Cao X, Chen L, Lan H, Liu B, Yi T (2012) Thixotropic and self-healing triggered reversible rheology switching in a peptide-based organogel with a cross-linked nano-ring pattern. *Soft Matter* 8:3329
101. Wang R-Y, Liu X-Y, Li J-L (2009) Engineering molecular self-assembled fibrillar networks by ultrasound. *Cryst Growth Des* 9:3286
102. Cao Y, Tang LM, Wang YJ, Zhang BY, Jia LK (2008) Influence of ultrasound treatment on assembling structures and properties of supramolecular hydrogels formed from 1,3,5-benzenetricarboxylic acid and 4-hydroxypyridine. *Chem Lett* 37:554

103. van Herpt JT, Stuart MC, Browne WR, Feringa BL (2013) Mechanically induced gel formation. *Langmuir* 29:8763
104. Yu X, Liu Q, Wu J, Zhang M, Cao X, Zhang S, Wang Q, Chen L, Yi T (2010) Sonication-triggered instantaneous gel-to-gel transformation. *Chem Eur J* 16:9099
105. Naota T, Koori H (2005) Molecules that assemble by sound: an application to the instant gelation of stable organic fluids. *J Am Chem Soc* 127:9324
106. Yaobing Wang CZ, Fu H, Li X, Sheng X, Zhao Y, Xiao D, Ma Y, Ma JS, Yao Jiannian (2008) Switch from intra- to intermolecular H-bonds by ultrasound: induced gelation and distinct nanoscale morphologies. *Langmuir* 24:7635
107. Liu K, Meng L, Mo S, Zhang M, Mao Y, Cao X, Huang C, Yi T (2013) Colour change and luminescence enhancement in a cholesterol-based terpyridyl platinum metallogel via sonication. *J Mater Chem C* 1:1753
108. Chen Q, Zhang D, Zhang G, Yang X, Feng Y, Fan Q, Zhu D (2010) Multicolor tunable emission from organogels containing tetraphenylethene, peryleneimide, and spiropyran derivatives. *Adv Funct Mater* 20:3244
109. Mahesh S, Thirumalai R, Yagai S, Kitamura A, Ajayaghosh A (2009) Role of complementary H-bonding interaction of a cyanurate in the self-assembly and gelation of melamine linked tri(p-phenyleneethynylene)s. *Chem Commun* 5984
110. Li JL, Liu XY (2010) Architecture of supramolecular soft functional materials: from understanding to micro-/nanoscale engineering. *Adv Funct Mater* 20:3196
111. Bardelang D, Zaman MB, Moudrakovski IL, Pawsey S, Margeson JC, Wang D, Wu X, Ripmeester JA, Ratcliffe CI, Yu K (2008) Interfacing supramolecular gels and quantum dots with ultrasound: smart photoluminescent dipeptide gels. *Adv Mater* 20:4517
112. Gaponik N, Wolf A, Marx R, Lesnyak V, Schilling K, Eychmüller A (2008) Three-dimensional self-assembly of thiol-capped CdTe nanocrystals: gels and aerogels as building blocks for nanotechnology. *Adv Mater* 20:4257
113. Wu J, Tian Q, Hu H, Xia Q, Zou Y, Li F, Yi T, Huang C (2009) Self-assembly of peptide-based multi-colour gels triggered by up-conversion rare earth nanoparticles. *Chem Commun* 4100
114. Brochu AB, Craig SL, Reichert WM (2011) Self-healing biomaterials. *J Biomed Mater Res A* 96:492
115. Hager MD, Greil P, Leyens C, van der Zwaag S, Schubert US (2010) Self-healing materials. *Adv Mater* 22:5424
116. Huang X, Raghavan SR, Terech P, Weiss RG (2006) Distinct kinetic pathways generate organogel networks with contrasting fractality and thixotropic properties. *J Am Chem Soc* 128:15341
117. Vemula PK, John G (2008) Crops: a green approach toward self-assembled soft materials. *Acc Chem Res* 41:769
118. Bhattacharya S, Krishnan Ghosh Y (2001) First report of phase selective gelation of oil from oil/water mixtures. Possible implications toward containing oil spills. *Chem Commun* 185
119. Abe S, Endo M, Sato M, Awano K (1996) Solid-liquid extraction of metal ions with thixotropic gels. *Anal Commun* 33:137
120. Yan J, Liu J, Lei H, Kang Y, Zhao C, Fang Y (2015) Ferrocene-containing thixotropic molecular gels: creation and a novel strategy for water purification. *J Colloid Interface Sci* 448:374
121. Carretti E, Bonini M, Dei L, Berrie BH, Angelova LV, Baglioni P, Weiss RG (2010) New frontiers in materials science for art conservation: responsive gels and beyond. *Acc Chem Res* 43:751
122. Sun K, Oh H, Emerson JF, Raghavan SR (2012) A new method for centrifugal separation of blood components: creating a rigid barrier between density-stratified layers using a UV-curable thixotropic gel. *J Mater Chem* 22:2378

123. Rodriguez-Llansola F, Escuder B, Miravet JF, Hermida-Merino D, Hamley IW, Cardin CJ, Hayes W (2010) Selective and highly efficient dye scavenging by a pH-responsive molecular hydrogelator. *Chem Commun* 46:7960
124. Miravet JF, Escuder B (2005) Pyridine-functionalised ambidextrous gelators: towards catalytic gels. *Chem Commun* 5796
125. Adams DJ, Butler MF, Frith WJ, Kirkland M, Mullen L, Sanderson P (2009) A new method for maintaining homogeneity during liquid–hydrogel transitions using low molecular weight hydrogelators. *Soft Matter* 5:1856
126. Samanta K, Ehlers M, Schmuck C (2016) Two-component self-assembly: hierarchical formation of pH-switchable supramolecular networks by  $\pi$ - $\pi$  induced aggregation of ion pairs. *Chem Eur J* 22:15242
127. Tena-Solsona M, Alonso-de Castro S, Miravet JF, Escuder B (2014) Co-assembly of tetrapeptides into complex pH-responsive molecular hydrogel networks. *J Mater Chem B* 2:6192
128. Jeppesen JO, Nielsen MB, Becher J (2004) Tetrathiafulvalene cyclophanes and cage molecules. *Chem Rev* 104:5115
129. Canevet D, Salle M, Zhang G, Zhang D, Zhu D (2009) Tetrathiafulvalene (TTF) derivatives: key building-blocks for switchable processes. *Chem Commun* 2245
130. Wang C, Zhang D, Zhu D (2005) A low-molecular-mass gelator with an electroactive tetrathiafulvalene group: tuning the gel formation by charge-transfer interaction and oxidation. *J Am Chem Soc* 127:16372
131. Wang C, Chen Q, Sun F, Zhang D, Zhang G, Huang Y, Zhao R, Zhu D (2010) Multistimuli responsive organogels based on a new gelator featuring tetrathiafulvalene and azobenzene groups: reversible tuning of the gel–sol transition by redox reactions and light irradiation. *J Am Chem Soc* 132:3092
132. Liu J, He P, Yan J, Fang X, Peng J, Liu K, Fang Y (2008) An organometallic super-gelator with multiple-stimulus responsive properties. *Adv Mater* 20:2508
133. Kawano S, Fujita N, Shinkai S (2005) Quater-, quinque-, and sexithiophene organogelators: unique thermochromism and heating-free sol-gel phase transition. *Chem Eur J* 11:4735
134. Ikeda M, Tanida T, Yoshii T, Hamachi I (2011) Rational molecular design of stimulus-responsive supramolecular hydrogels based on dipeptides. *Adv Mater* 23:2819
135. Steed JW (2010) Anion-tuned supramolecular gels: a natural evolution from urea supramolecular chemistry. *Chem Soc Rev* 39:3686
136. Yamanaka M, Nakamura T, Nakagawa T, Itagaki H (2007) Reversible sol–gel transition of a tris–urea gelator that responds to chemical stimuli. *Tetrahedron Lett* 48:8990
137. Džolić Z, Cametti M, Dalla Cort A, Mandolini L, Žinić M (2007) Fluoride-responsive organogelator based on oxalamide-derived anthraquinone. *Chem Commun* 3535
138. Kim H-J, Zin W-C, Lee M (2004) Anion-directed self-assembly of coordination polymer into tunable secondary structure. *J Am Chem Soc* 126:7009
139. Sobczuk AA, Tamarua S, Shinkai S (2011) New strategy for controlling the oligothiophene aggregation mode utilizing the gel-to-sol phase transition induced by crown-alkali metal interactions. *Chem Commun* 47:3093
140. Brignell SV, Smith DK (2007) Crown ether functionalised dendrons—controlled binding and release of dopamine in both solution and gel-phases. *New J Chem* 31:1243
141. Edwards W, Smith DK (2012) Cation-responsive silver-selective organogel-exploiting silver-alkene interactions in the gel-phase. *Chem Commun* 48:2767
142. Jin Q, Zhang L, Zhu X, Duan P, Liu M (2012) Amphiphilic Schiff base organogels: metal-ion-mediated chiral twists and chiral recognition. *Chem Eur J* 18:4916
143. Mukhopadhyay P, Iwashita Y, Shirakawa M, Kawano S, Fujita N, Shinkai S (2006) Spontaneous colorimetric sensing of the positional isomers of dihydroxynaphthalene in a 1D organogel matrix. *Angew Chem Int Ed* 45:1592
144. Tazawa T, Yagai S, Kikkawa Y, Karatsu T, Kitamura A, Ajayaghosh A (2010) A complementary guest induced morphology transition in a two-component multiple H-bonding self-assembly. *Chem Commun* 46:1076

145. Deng W, Yamaguchi H, Takashima Y, Harada A (2007) A chemical-responsive supramolecular hydrogel from modified cyclodextrins. *Angew Chem Int Ed* 46:5144
146. Chen X, Huang Z, Chen SY, Li K, Yu X-Q, Pu L (2010) Enantioselective gel collapsing: a new means of visual chiral sensing. *J Am Chem Soc* 132:7297
147. Tu T, Fang W, Bao X, Li X, Dotz KH (2011) Visual chiral recognition through enantioselective metallogel collapsing: synthesis, characterization, and application of platinum-steroid low-molecular-mass gelators. *Angew Chem Int Ed* 50:6601

## Chapter 3

# Metal–Organic Gels

**Abstract** Metal–organic coordination has been incorporated in gels. In this chapter, metal–organic gels are classified into two general catalogues according to the nature of gelators and the interactions between gelators: gelation by discrete molecules, and gelation by coordination polymers. In the section of discrete gelators, metal–organic gelators with monodentate ligands, metal–organic gelators with chelate ligands, organometallic gelators and metal–organic gelators based on tripyridine and tridentate ligands are discussed. Coordination cycles and cages have been employed as supramolecular gelators and are discussed in the second section. In the third section, coordination polymer gels are discussed including metal-carboxylate gels, metal-heterocycle polymer gels and coordination polymer gels with hybrid donors. Finally, some typical applications of metal–organic gels are discussed including gels as crystallization media, post-modification of organogels by metal ions, metal–organic gels for sorption, metal–organic gels as template and metal–organic gels as catalyst.

**Keywords** Metal–organic gels • Supramolecular gels • Discrete gelators  
Organometallic compounds • Coordination polymers • Cage compounds  
Porous materials

Metal–organic gels are classified into two general catalogues according to the nature of gelators and the interactions between gelators: gelation by discrete molecules, and gelation by coordination polymers. Metal–organic coordination bonding can be involved to form low molecular weight gelators. Discrete metal–organic gelators self-assemble to form gels through multiple non-covalent interactions such as hydrogen bonding,  $\pi$ – $\pi$  stacking, hydrophobic and other supramolecular weak interactions. Such gels may be readily reverted to the fluid state by applying external stimuli (e.g. heating) to break the supramolecular weak interactions, thus thermoreversible. Metal–organic coordination bonding is the primary force in the formation of 3D gel networks as small molecules with multiple

---

Jianyong Zhang, Xiying Feng and Peisen Liao contributed together to this chapter.

functional groups react to form dynamic covalent polymers in coordination polymer gels. Such metal–organic gels usually have infinitely extended structures, and thus cannot be redissolved upon heating and do not show thermoreversible gel–sol transitions.

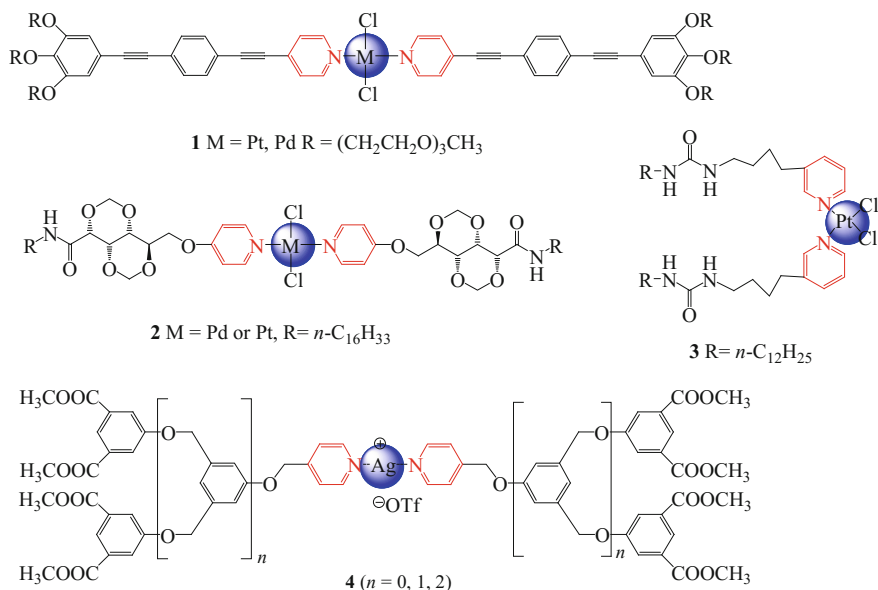
## 3.1 Discrete Gelators

### 3.1.1 Metal–Organic Gelators with Monodentate Ligands

Pyridyl ligands are widely studied. Monodentate pyridyl ligands form stable coordination compounds with Pd<sup>2+</sup>/Pt<sup>2+</sup>, which have square-planar coordination geometry. A series of gelators Pd<sup>2+</sup>/Pt<sup>2+</sup> dipyrindyl gelators have been developed with the aid of long alkyl/oligoether oxide chain or H-bonding motifs. Fernández and co-workers reported an oligophenyleneethynylene (OPE)-based amphiphilic *trans*-Pt<sup>2+</sup> compound **1**-Pt [1]. **1**-Pt (Scheme 3.1) forms supramolecular polymeric structures in aqueous and polar media driven by  $\pi$ – $\pi$  and weak C–H $\cdots$ X (X=Cl, O) hydrogen-bonding interactions involving chlorine atoms attached to the Pt<sup>II</sup> centres as well as oxygen atoms and polarized methylene groups belonging to the peripheral glycol chains. They also found that **1**-Pd self-assemble in polar media into fibre-like structures [2]. The self-assembly is governed by cooperative intra- and interstrand CH $\cdots$ O interactions between peripheral triethylene glycol chains leading to slipped  $\pi$ -stacks. Aromatic and CH $\cdots$ Cl interactions are also important. Nolte and co-workers developed *trans*-Pd<sup>2+</sup>/Pt<sup>2+</sup> compound **2** (Scheme 3.1) of gluconamide derivatives by incorporating a pyridine functionality [3]. **2**-Pd gave a gel in THF and helical ribbons were observed in the xerogel by TEM. **2**-Pt is also an effective gelator, giving fibres but without the helical twist. Steed and co-workers developed *cis*-Pt(II) complex **3** (Scheme 3.1) of urea derivative [4]. **3** is a gelator for toluene, o-xylene and others. Interfacial crystallization of cisplatin in a gel–sol biphasic system is employed to address the insolubility of the drug molecule in organic solvents, and a new *N,N*-dimethylacetamide (DMA) solvate of cisplatin has been identified.

Feng, Fan and co-workers reported three Ag<sup>+</sup> gelators **4** (Scheme 3.1) of pyridine-functionalized poly(aryl ether) dendritic ligands [5]. These gelators gelate various organic solvents. During the gelation, strong solvophobic interactions enhance aromatic  $\pi$ – $\pi$  stacking interactions of the polar pyridine moieties distinctly, which synergistically enable the formation of gels. These metallogels respond to different external stimuli, such as temperature, chemicals and shear stress, resulting in reversible gel–sol phase transitions. Moreover, these dendritic metallogel systems (Fig. 3.1) can be used as templates to in situ form and stabilize silver nanoparticles.

Rotaxanes-based  $\alpha$ -CD and coordination complexes have been employed for gelation [6]. Addition of [Pd(en)(NO<sub>3</sub>)<sub>2</sub>] (en = 1,2-ethylenediamine) to the aqueous



**Scheme 3.1** Metal-organic gelators 1–4

reaction of alkylbipyridinium **5** (Scheme 3.2) and  $\alpha$ -CD, followed by heating the solution to 60 °C, then cooling to ambient temperature forms a gel in 1 h. Complex **6** (Scheme 3.2) also forms gels under similar conditions, but the gelation products are controlled by the reaction of Pd–N coordination bond of **6**. The metallo-gel from **6** and  $\alpha$ -CD exhibits reversible sol–gel transition which was triggered by temperature and concentration. At higher concentrations, rotaxane **6**( $\alpha$ -CD)<sub>4</sub> fabricates polyrotaxane-like fibrous structures, followed by formation of nanoparticles that trap the water molecules into the gel network (Fig. 3.2).

The gelation occurred when mixing  $\text{NiCl}_2 \cdot 6\text{H}_2\text{O}$  with amines in protic solvents [7]. The amines have pK<sub>a</sub> values in the range 7.41–13.6 such as triethylamine, *N*-methyl morpholine, 1,8-diazabicycloundec-7-ene, 1,1,3,3-tetramethyl guanidine. The interactions between  $\text{NiCl}_2 \cdot 6\text{H}_2\text{O}$  and methoxide ions probably lead to the formation of *cis*-Ni(OMe)<sub>2</sub>(MeOH)<sub>4</sub>, a thermodynamically stable hexacoordinated complex. The extensive H-bonding network between free and metal-bound MeOH and free and metal-bound amines could stabilize the metal–organic gels.

An amphiphilic gelator **7** (Scheme 3.2) functionalized with a triazole fragment forms organogels in  $\text{H}_2\text{O}$ -*t*-BuOH (*v:v* 1:1) at 80 °C [8]. When  $\text{Cu}^+$  is introduced, a metallo-gel forms with a decrease in the minimum gelation concentration. PXRD exhibits that vertically piled **7** molecules repeat side-to-side horizontally, and self-assembly of gelator **7** is conducted by intermolecular hydrogen bonding between the different amide groups (Fig. 3.3). CD spectrum of Cu(I)-**7** gels shows that the coordination geometry of metal centre favours a twist into fibre orientation leading to a helical orientation. The amphiphilic Cu(I) metal–organic gel exhibits

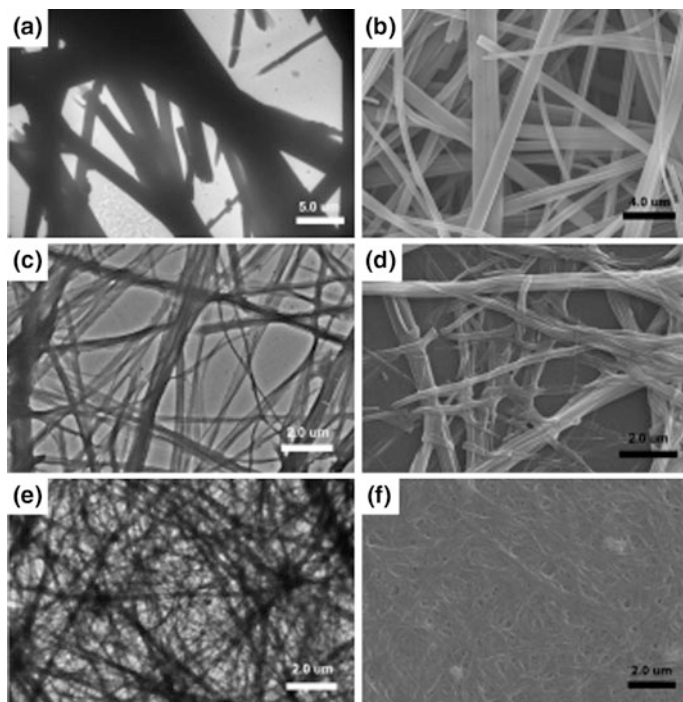
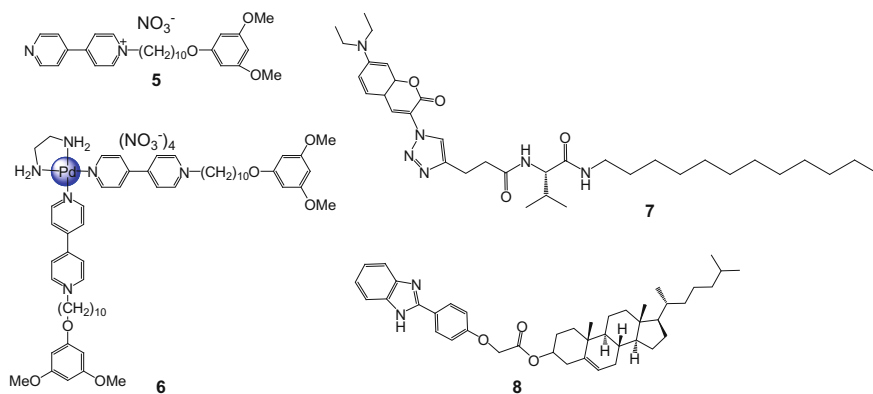


**Fig. 3.1** TEM and SEM images of the corresponding xerogels of dendritic metallogels from tetrahydrofuran, **a, b** Pyr-G0/Ag, **c, d** Pyr-G1/Ag and **e, f** Pyr-G2/Ag. Reprinted with permission from [5]. Copyright © 2014 WILEY-VCH Verlag GmbH & Co. KGaA, Weinheim



**Scheme 3.2** Molecular structures of **5–8**

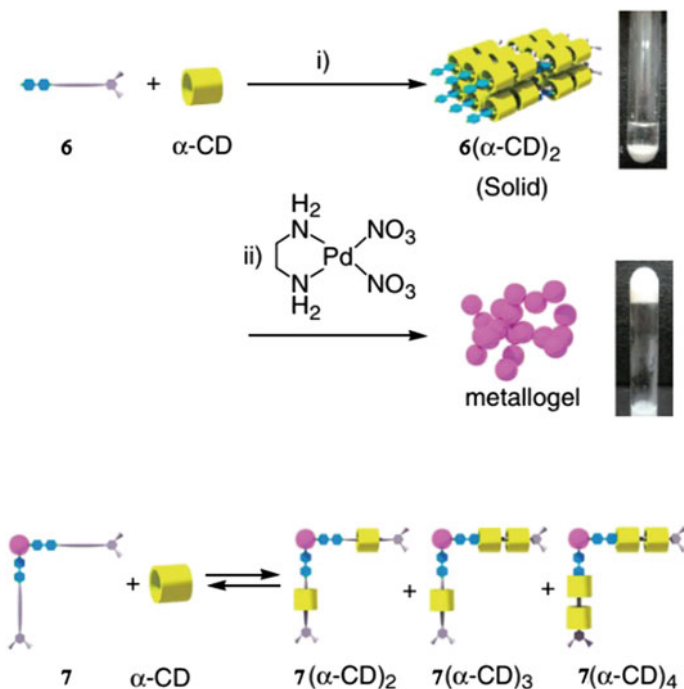


**Fig. 3.2** Formation of Pd-containing rotaxanes and gels. Reprinted with permission from [6]. Copyright © 2013 The Chemical Society of Japan

high catalytic activity towards the model “click” reaction between benzylazide and phenylacetylene, obtaining conversions of 71% in the first 3 h of reaction and in the presence of 1 mol% catalyst.

Cholesterol-appended benzimidazole **8** (Scheme 3.2) shows selective gelation ability with silver perchlorate in DMF-H<sub>2</sub>O (1:1, v/v) [9]. The gelators aggregate via  $\pi$ - $\pi$  stacking and hydrophobic interaction (Scheme 3.2). Silver ion-specific gelation highlights compound **8** as an excellent visual detector of Ag<sup>+</sup> ions over a series of other metal ions. The detection limit for Ag<sup>+</sup> was estimated to be  $4.31 \times 10^{-5}$  M in DMF-H<sub>2</sub>O. Silver-induced gel of **8** shows thermally activated ionic conductivity due to the movement of Ag<sup>+</sup> ions within the gel network (Scheme 3.3).

### 3.1.2 Metal–Organic Gelators with Chelate Ligands

8-quinolinol chelate motifs have been incorporated in metal–organic gels [10]. Shinkai and co-workers reported that a square-planar Pt(II) bis-quinolinol complex (**9**, Scheme 3.4) functionalized via amide linkages with long chains formed gels in a

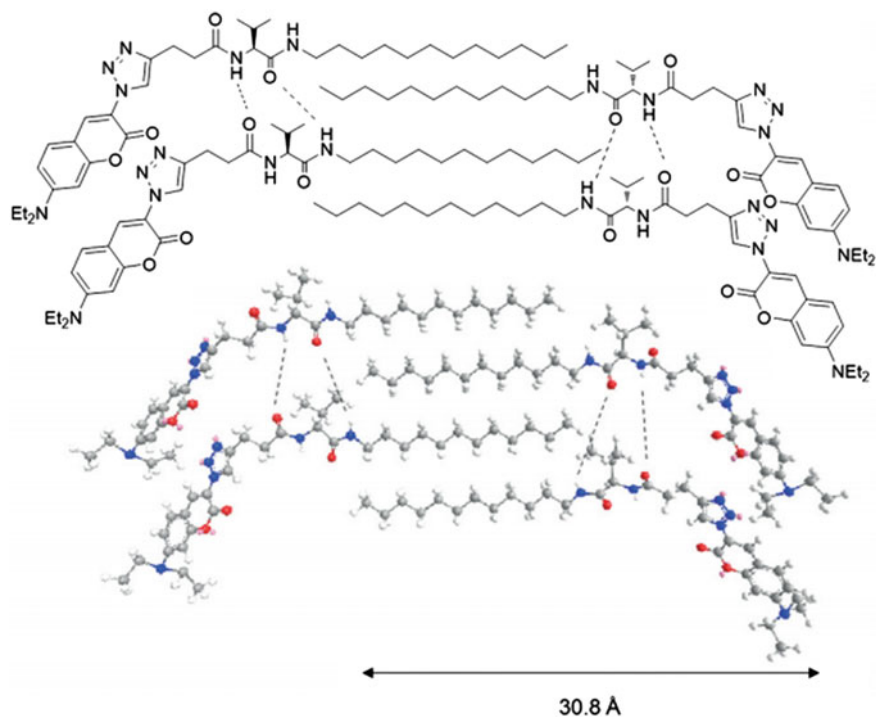


**Fig. 3.3** Proposed molecular packing for the gelator **7**. Reprinted with permission from [8]. Copyright © 2017 Wiley-VCH Verlag GmbH & Co. KGaA, Weinheim

wide range of solvents. Absorption bands were shifted to longer wavelength in the gel (orange) than in the solution (yellow) due to the columnar  $\pi$ -stacking. The gels show interesting emission behaviour. The difference in luminescence intensity in  $O_2$ -saturated conditions and in Ar-saturated conditions was less in the gels than in solutions, showing that there is indeed protection from quenching by the formation of gel filaments insulated by peripheral alkoxy groups.

Liu and co-workers reported 8-quinolinol-containing 1-glutamic lipid **10** (Scheme 3.4) and found that its derivative with  $Cu^{2+}$  ions ( $Cu(\mathbf{10})_2$ ) had powerful gelation ability in low-polar solvents [11]. PXRD exhibited that the alkyl chains of the complex gelled in an interdigitated or inclined manner. Comparing with the bilayer structure of ligand **10**, the complex showed a monolayer structure. Instead of intermolecular hydrogen-bonding interaction in **10** gels, the  $Cu^{2+}$  gels gelled by coordination interactions between the  $Cu^{2+}$  ions and the quinolinol head-groups (Fig. 3.4). Moreover, the square coordination mode of  $Cu^{2+}$  atoms could enhance the  $\pi$ - $\pi$  stacking of the quinolinol rings. A reversible gel-sol phase transition of the  $Cu^{2+}$  gels occurred after redox stimuli. Because after reduction, the central  $Cu^{2+}$  ions change into  $Cu^+$  ions which causes a decrease in  $\pi$ - $\pi$  stacking between the adjacent molecules and as a result, the gel collapses into a sol. While the oxidation



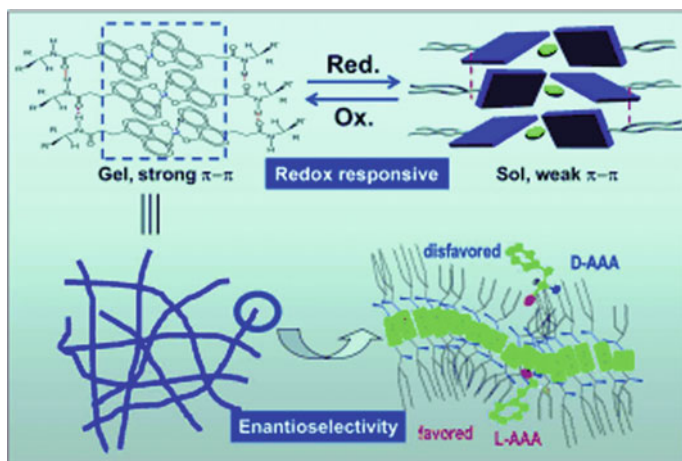


**Fig. 3.4** Reversible gel–sol transition of Cu(10)<sub>2</sub> which self-assembles into gels through coordination, hydrogen-bonding and hydrophobic interactions, as well as  $\pi$ – $\pi$  stacking, and the chiral nanostructure of gels shows enantioselective recognition towards L-aromatic amino acid. Reprinted with permission from [11]. Copyright © 2013 WILEY-VCH Verlag GmbH & Co. KGaA, Weinheim

Quinolinol-functionalized L-glutamide **10** also forms fluorescent metal–organic gels with Li<sup>+</sup>, Zn<sup>2+</sup>, and Al<sup>3+</sup> in organic solvents [12]. SEM indicates that all metal gelator molecules self-assembled into fine nanofibres in THF. From the result of XRD, **10**-Li<sup>+</sup> may form bilayers with the interdigitation of the alkyl chains, like many other L-glutamide gels do; while both of Zn(10)<sub>2</sub> and Al<sub>2</sub>(10)<sub>3</sub> gels form a layered structure by strong hydrogen bonding interaction,  $\pi$ – $\pi$  stacking of the quinolinol rings, and hydrophobic interaction from the interdigitated adjacent aliphatic alkyl tails. The Zn(10)<sub>2</sub> gel exhibits different fluorescence changes between enantiomeric (*R,R*)- and (*S,S*)-1,2-diaminocyclohexane realizing visible chiral recognition of (*S,S*)-1,2-diaminocyclohexane.

Xu and co-workers fabricated metallo-hydrogelator **11** (Scheme 3.4) of tripeptide derivative with bipyridine moiety [13]. The intermolecular aromatic–aromatic interactions of **11** from the overlapping of phenyl and/or naphthyl groups lead to the supramolecular chains. And the other amide groups and hydroxyl groups contribute to the formation of hydrogen bonds with water molecules except for the intramolecular hydrogen bonds formed by amide groups and hydroxyl groups of **11**. These interactions make sure that the supramolecular chains are able to hold a considerable amount of water, even at a quiet low molecular density. The redox change of the ruthenium metal centre of **11** resulted in a gel–sol transition. The self-assembled structure of **11** in water changed with the redox change of Ru. With the tripeptide motifs, **11** is cell compatible at a relatively high concentration, so the nanofibres of **11** are able to enter the cells (Fig. 3.5).

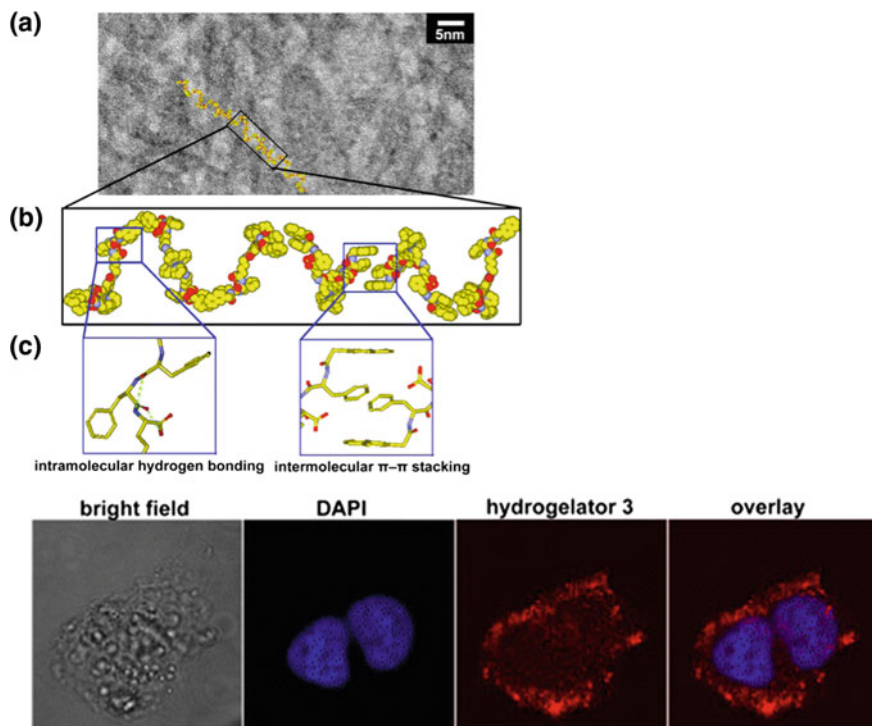


**Fig. 3.5** **a** High-resolution TEM image of the nanofibres in hydrogel of **11**, **b** a tentative molecular arrangement in the nanofibres of **11**, **c** illustrations of plausible intramolecular hydrogen bonds and intermolecular  $\pi$ - $\pi$  stacking and fluorescent images of a HeLa cell incubated with **11** (200  $\mu$ M, 24 h) (from left to right: phase-contrast image, live cell stain DAPI (blue), luminescence emission of **3** (red) and overlay image). Reprinted with permission from [13]. Copyright © 2013, American Chemical Society

Mitsumoto, Cameron and co-workers reported a heterometallic octanuclear gelator  $[\text{Fe}_4^{\text{III}}\text{Ni}_4^{\text{II}}(\text{CN})_{12}(\text{tp})_4(\mathbf{12})_4](\text{BF}_4)_4$  synthesized from a hydrophobic tetrathiafulvalene (TTF) ligand **12** (Scheme 3.4) with long-chain alkyl moieties (Fig. 3.6) [14]. The TTF moieties of **12** shows redox behaviour, with two reversible one-electron oxidation waves of cyclic voltammogram observed at  $E^{0'}$  = 0.46 and 0.78 V (vs. SCE). In the cubic moiety  $[\text{Fe}_4\text{Ni}_4(\text{CN})_{12}]^{8+}$  of the gelator, a core of four iron(III) and four nickel(II) ions are bridged by twelve cyanide ions. A red gel forms over the course of one week in 1,2-dichlorobenzene solution at room temperature. The gel shows gel-to-sol transformations at room temperature induced by both the oxidation and reduction through its interaction with redox agents, such as 2,3,5,6-tetrafluoro-7,7,8,8-tetracyanoquidimethane and decamethylferrocene.

A pyridine containing anthraquinone-based ligand forms a stable three component gel in DMSO/water in the presence of  $\text{Cu}^{2+}$  and chloride ions [15]. In this work, the factors that contributed to the formation of this gel were explored. To

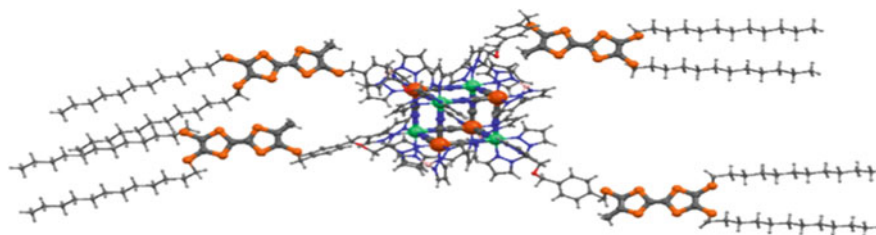
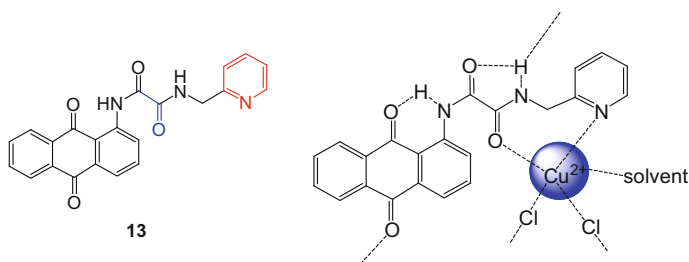


**Fig. 3.6** Proposed structure of **12**. Reprinted with permission from [14]. Copyright © 2017 Wiley-VCH Verlag GmbH & Co. KGaA, Weinheim



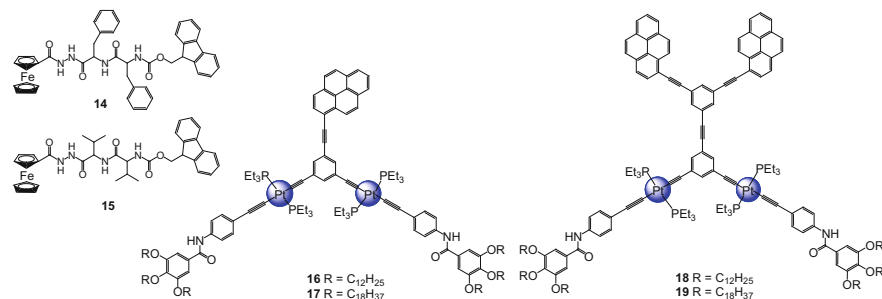
**Scheme 3.5** Proposed structure for the gelating **13**-Cu(II) complex

obtain  $\text{Cu}^{2+}$  induced metallo-gelation, the NH deprotonation must be avoided; the ligand acts in a bidentate fashion with metal coordination conducted by one oxalyl  $\text{C}(=\text{O})$  group and a pyridine ring; the stoichiometry of the final gelating species is required;  $\pi$ - $\pi$  stacking and hydrophobic interactions also play a role in gelation. In metallo-gel **13**- $\text{Cu}^{2+}$ , the  $\text{Cu}^{2+}$  ion is coordinated by the pyridyl nitrogen and an oxalamidic carbonyl in a bidentate **13**. Meanwhile, solvent molecules and chloride ions complete the coordination sphere of the  $\text{Cu}^{2+}$  ion (Scheme 3.5).

### 3.1.3 Organometallic Gelators

Various organometallic moieties have been incorporated in supramolecular gels, including chromium carbene, [16] gold *N*-heterocyclic carbene (NHC) [17], titanocene [18, 19], pincer Pd(II)/Pt(II) carbene [20–24], ferrocene [25–28] and others [29, 30].

Ferrocene acts as an organometallic sub-unit with well-known redox-active properties, showing fully reversible oxidation/reduction properties of  $\text{Fe}^{2+}$  [25]. As a redox centre ferrocene is a nonpolar compound in the neutral state and is soluble in non-polar solvents. For example, Li, Yu and co-workers reported a series of ferrocene-peptide gelators, which consist of a ferrocenyl group and a dipeptide



**Scheme 3.6** Molecular structures of **14–19**

protected by a fluorenyl-9-methoxycarbonyl (Fmoc) group at the N-terminus. Gelators **14** and **15** (Scheme 3.6) are capable of gelating various common organic solvents, such as mixed solvent-systems of alcohol and water, especially alcohols, via the intermolecular hydrogen bonds of the dipeptide segment and  $\pi$ - $\pi$  stacking of the fluorenyl moiety in the protecting group. SEM and TEM images of these metallogels showed fibrous morphologies, and the density of the fibres changed with the different solvent. Addition of  $\beta$ -CD to the gel systems led to the gel collapse because the host-guest interactions between ferrocene and  $\beta$ -CD destroyed the gel network. Moreover, changing of the redox state of ferrocene resulted in a reversible gel-sol transition (Fig. 3.7).

Yang and co-workers reported a family of ethynyl-pyrene-modified platinum-acetylide organometallic gelators (**16–19**, Scheme 3.6) which exhibit good gel formation properties in the mixed solvents of alkane and benzene via  $\pi$ - $\pi$  stacking and hydrogen bonding interaction [31]. The monoethynyl pyrene-modified complex could form stable hybrid gels with graphene through the large aromatic surface of graphene and the charge transfer interactions between the aromatic ethynyl-pyrene moiety, which was proved by the decrease of emission intensity of the hybrid metallogels at around 500 nm. Comparing with the native gel, the graphene-containing hybrid metallogel was more rigid and still maintained the entangled nanofibrillar structure.

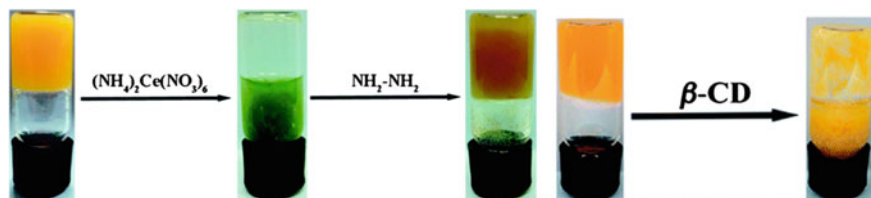
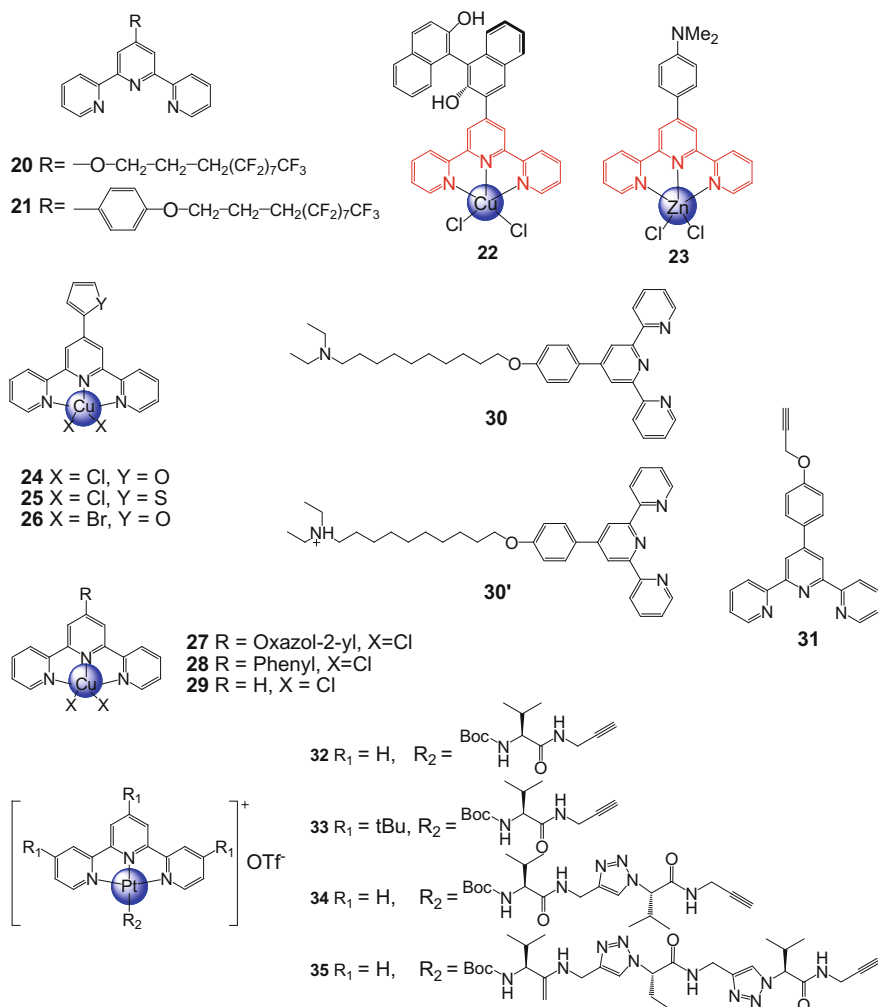


**Fig. 3.7** Photographs of the reversible gel-sol phase transition of gel **14** triggered by chemical redox and gel-sol phase transition of gel **14** triggered by two molar equivalents of  $\beta$ -CD. Adapted with permission from [25]. Copyright © 2014, Royal Society of Chemistry

### 3.1.4 Metal–Organic Gelators Based on Terpyridine and Tridentate Ligands

2,2':6',2''-Terpyridine is a widely used tridentate ligand because it can form well-defined chelate complexes. For example, divalent  $\text{Cu}^{2+}$  may form pentacoordinated  $\text{N}_3\text{Cl}_2$  terpyridine complexes. Cametti, Haukka and co-workers prepared two ligands **20** and **21** (Scheme 3.7) based on a terpyridine moiety decorated with a perfluorinated  $\text{C}_8\text{F}_{17}$  tag [32]. Both of them are able to gelate a series of d-block metal ions, such as  $\text{Zn}^{2+}$  and  $\text{Hg}^{2+}$  in the mixture of DMSO and water. All four



Scheme 3.7 Molecular structures of **20–35**

complexes (**20**-ZnCl<sub>2</sub>, **20**-HgCl<sub>2</sub>, **20**-ZnBr<sub>2</sub> and **20**-CuCl<sub>2</sub>) show pentacoordination and can be viewed as a distorted trigonal bipyramidal type ignoring the metal identity. This is influenced by the NNN chelation from the terpyridine parts and by two halide ions that complete a N<sub>3</sub>X<sub>2</sub> coordination sphere. The fluoruous chains are mainly packed by means of C–F...F–C interchain geometries. From the result of electron microscopy, the fibres of gels made with **21** are thinner than those of **20** and so are the aspect ratios. And according to the different response to the common anions, it turns out that **20** can form more stable gel systems.

Yu, Pu and co-workers reported a chiral terpyridine derivative of BINOL (1,1'-bi-2-naphthol) and its Cu<sup>2+</sup> complex (**22**, Scheme 3.7) forms a gel in CHCl<sub>3</sub> [33]. The gel shows enantioselective collapse towards amino alcohols. The gel remains stable when (*R*)-phenylglycinol was added, while the gel collapses when more than 0.06 equiv (*S*)-phenylglycinol was added. Rissanen and co-workers reported that luminescent terpyridine-Zn<sup>2+</sup> complex **23** (Scheme 3.7) form a hydrogel [34]. The complex shows an unprecedented fluorescence response (~500 fold increase) and record nanomolar sensitivity (detectable fluorescent response at 20 nM and LOD ~0.8 nM) towards pyrophosphate (PPi), biologically significant ions. The gel is used to make gel-coated paper strips for easy, low-cost detection and selective sensing of PPi in water.

Tu and co-workers developed a series of terpyridine-Cu<sup>2+</sup> gelators **24–29** (Scheme 3.7). The complexes assemble to a fibrous aggregate via metal–metal interactions and  $\pi$ - $\pi$  stacking between two side pyridine rings [35]. In alcohols, these aggregates further elongate and bind to form routine long and twisted nanofibres by hydrogen-bonding interactions between gelator and guest molecules, which lead to the gelation. When the solvent changes to water, the aforesaid fibre aggregates tend to shrink into rare metal–organic nanoparticles (NMPs). These gels exhibit thixotropic property and self-healing ability under external stress (Fig. 3.8).

The chloride ligands are easily substituted by external N-containing ligands, because of the five-coordination number of the Cu<sup>2+</sup> centre [36]. Rigid substituting

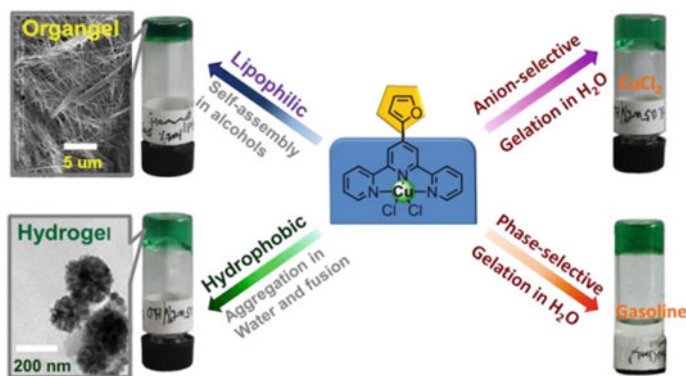


**Fig. 3.8** Terpyridine-Cu<sup>2+</sup> complexes and corresponding metal–organic gel formation. Reprinted with permission from [35]. Copyright © 2013, American Chemical Society

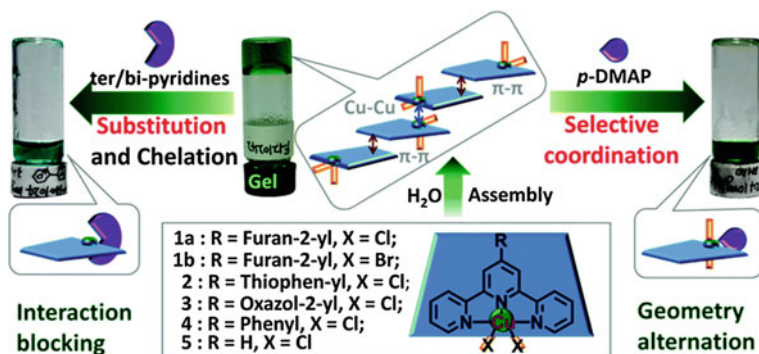


**Fig. 3.9** Control over metallo-hydrogel collapse *via* different strategies, **a** halide substitution with a bulky multidentate ligand and ligand chelation and **b** selective coordination with a mono-dentate ligand. Reprinted with permission from [37]. Copyright © 2015, Royal Society of Chemistry

chelate ligands may handicap the  $\pi$ -stacking and Cu–Cu interactions and lead to gel collapse. For example, metal–organic gels fabricated by terpyridine  $\text{Cu}^{2+}$  complex realize visual discrimination of 2,2'-bipy from its positional isomers. Gel collapse and reformation process are achieved through a reversible interaction blocking strategy using photo-reversible 2,2'-azopyridine. *Trans*-2,2'-azopyridine is a photoresponsive ligand, which could change to *cis*-2,2'-azopyridine when a photo-stimulus was applied. As a result, the gel of *trans*-2,2'-azopyridine collapses after irradiation at 320 nm. The terpyridine- $\text{Cu}^{2+}$  gels also show ability to discriminate 4-dimethylaminopyridine (p-DMAP) conveniently visually out of its positional isomers and other analogues via selective metallogel collapse [37]. 4-dimethylaminopyridine is a less-hindered monodentate ligand, and it may coordinate and change the coordination geometry of  $\text{Cu}^{2+}$  (Fig. 3.9).

Terpyridine-based ligand **30** (Scheme 3.7) is first protonized by HCl and then the resulting amphiphilic **30'** coordinates to  $\text{Cu}^{2+}$  in slightly acidic condition to form a hydrogel [38]. In **30'**- $\text{Cu}^{2+}$  gel, strong  $\pi$ - $\pi$  stacking interactions between the middle pyridine ring of terpyridine and the benzene ring of neighbouring complex lead to the formation of nanofibres. The nanofibres then twist to form a 3D network via van der Waals interactions of alkyl chains. The gel exhibits multiresponsiveness towards gel-to-sol transitions including temperature, thixotropy, and addition of alkali or sodium L-ascorbate. Additionally, the ammonium salt group on **30** can be threaded through the cavity of water-soluble pillararene **WP5** to form a host-guest complex (Fig. 3.10). And the addition of water-soluble pillar [5] arene **WP5** led to the gel-to-sol transition and turned nanofibre into vesicle at the nanoscale, for a stable host-guest complex was form after mixing **30'** and **WP5**.

Pandey and co-workers fabricated terpyridyl-based ligand **31** [39]. Compound Zn-**31** (Scheme 3.7) forms a stable gel in MeOH in the presence of HCl. Crowding does not restrict the molecule from achieving planarity, which enables **31** to serve as a gelator and aggregate via  $\pi$ - $\pi$  stacking interactions leading to the gelation because

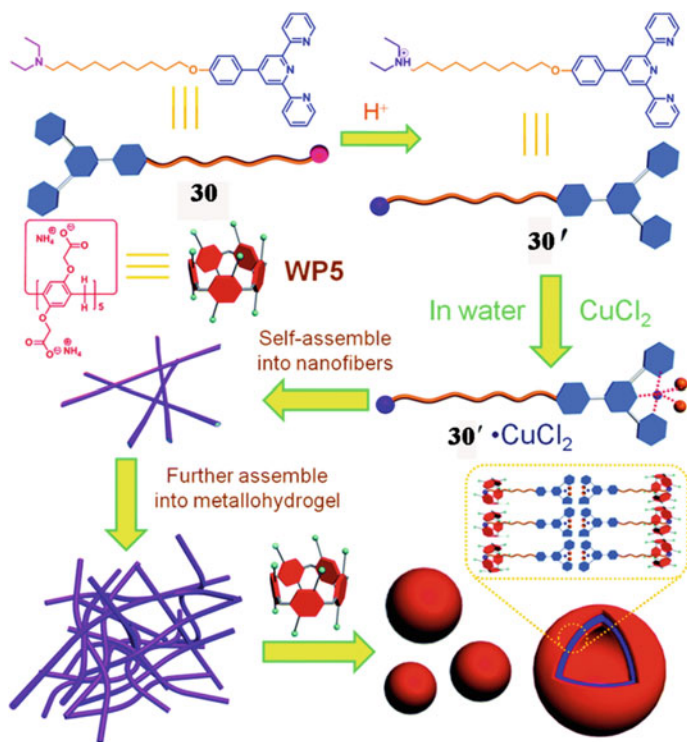
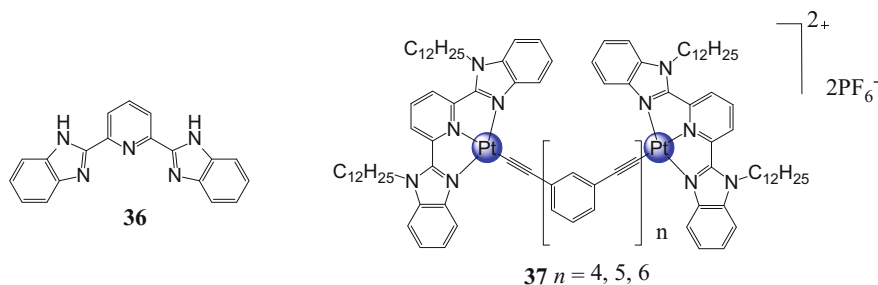


**Fig. 3.10** Chemical structures of ligands **30** and **30'** and anionic water-soluble pillar [5] arene **WP5** and cartoon representations of the gelation process and WP5-induced morphology transformation. Reprinted with permission from [38]. Copyright © 2015, Royal Society of Chemistry

of the relatively far distance from the alkyne chain of **31** to its terpyridyl part, and the small size of  $\text{Cl}^-$  compared to other anions, such as  $\text{Br}^-$ ,  $\text{HCOO}^-$ ,  $(\text{COO})_2^{2-}$ ,  $\text{SO}_4^{2-}$ ,  $\text{NO}_3^-$ . Addition of  $\text{HNO}_3$  to  $\text{Zn-31}$  resulted in a clear solution and gradually yields crystals within the gel matrix. In the crystals, two protons attach to two terminal pyridine rings to get terpyridyl moiety  $[(\mathbf{31})\text{H}_2]^{2+}$ . A nanocomposite gel is obtained for  $\text{Zn-31}$  capped with Au nanoparticles via alkynyl group. Interestingly, the nanocomposite gel exhibits superior viscoelastic properties.

Yam and co-workers designed a series of platinum(II) terpyridine complexes **32–35** (Scheme 3.7) with *L*-valine-modified alkynyl ligands. They show good capability of gel formation in MeCN [40]. Hydrogen-bonding interactions between the chiral valine moieties help the platinum<sup>2+</sup>-terpyridine parts align into a helical arrangement in the gel state and the Pt···Pt interactions,  $\pi$ - $\pi$  stacking interactions lead to the close proximity of these Pt<sup>2+</sup> terpyridine parts, then further strengthen the gel.



**Scheme 3.8** Molecular structures of **36** and **37**

Li and co-workers prepared a metal–organic gel by reacting tridentate ligand, 6-bis(2-benzimidazolyl) pyridine (**36**, Scheme 3.8) with  $\text{Cu}^{2+}$  in MeOH at 60 °C [41]. Ligand **36** provides three N-atoms in tridentate mode to coordinate with  $\text{Cu}^{2+}$ , while the imidazole imine  $-\text{NH}$  groups lead to the formation of hydrogen bonding. Both interactions of  $\pi$ – $\pi$  stacking caused by the benzene ring and halide bridging of metal centres also play a significant role in gelation. The gel is used to modify a polished GCE (glassy carbon electrode) for detection of nitrite. The oxidation peak currents of nitrite on MOG-modified GCE are linearly correlated to the logarithm values of its concentration when the concentration is about 2–150  $\mu\text{M}$ . The detection of limit is 0.86  $\mu\text{M}$  for nitrite. The good current response towards nitrite oxidation on MOG/GCE is probably due to the greater active site provided by MOG to contact with nitrite compared with the bare GCE.

Yam and co-workers designed a series of *m*-phenyleneethynylene-containing dinuclear alkynylplatinum(II) gelators **37** (Scheme 3.8) with the incorporation of a sterically undemanding,  $\pi$ -conjugated and hydrophobic 2,6-bis(*N*-dodecylbenzimidazol-2'-yl)pyridine pincer ligand which show gelation in  $\text{CH}_3\text{CN}$  [42]. Such a gelation process has been found to undergo a cooperative assembly mechanism according to the nucleation-elongation model (Fig. 3.11). UV–Vis absorption, emission, electronic microscopic, PXRD studies exhibit that intra- and/or intermolecular Pt···Pt and  $\pi$ – $\pi$  stacking interactions, which acted as directional non-covalent interactions in building up the hierarchy of the metallogel, determine the helical pitch of the stacks of the folded state. Gelator **37** ( $n = 5$ ) packs in the hexagonal array in the solid state. The luminescent and spectroscopic behaviours can be readily modulated by the metal···metal interactions, such that functional materials with rich spectroscopic behaviour can be designed.

### 3.1.5 Coordination Cages

Some coordination cages have been evolved in gelation process. The solution of the self-assembled trinuclear coordination complex  $[\text{Pd}_3(\mathbf{39})_6](\text{NO}_3)_6$  (**Pd2**)

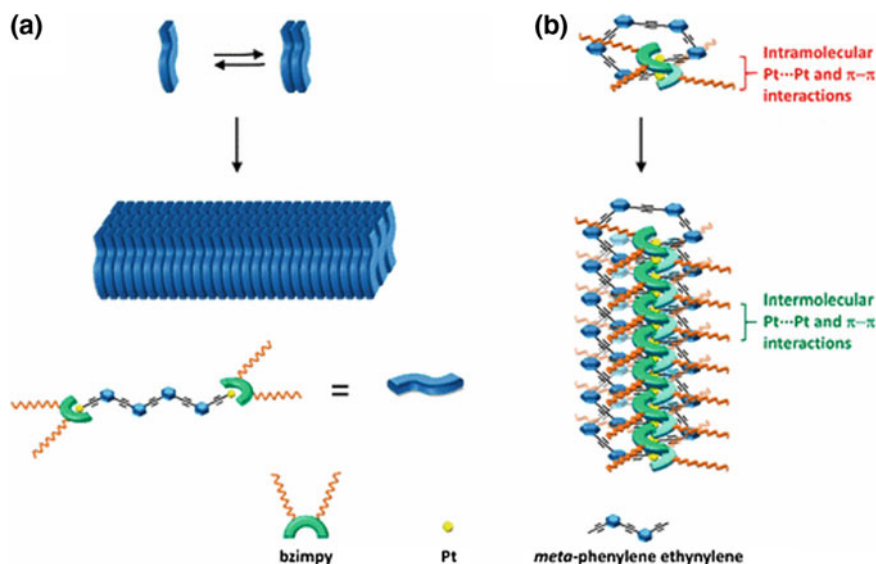
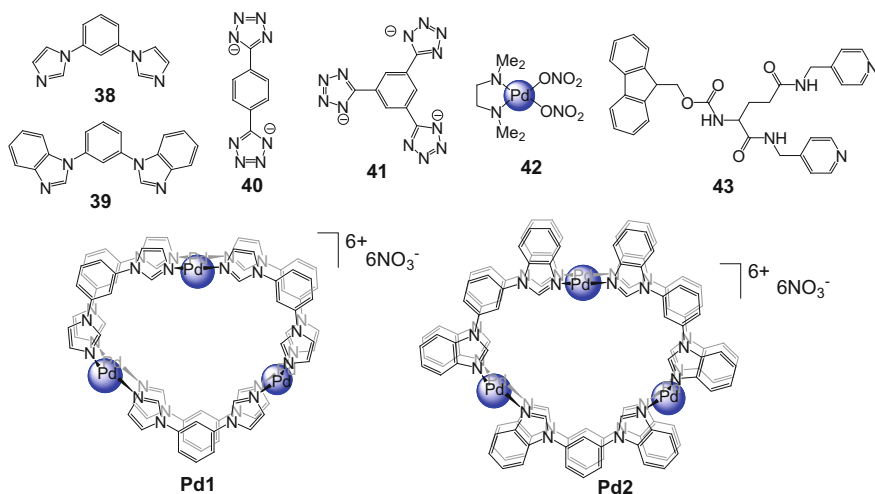


**Fig. 3.11** Schematic drawing of **a** the extended chain ribbons of **37** and its self-assembly behaviours and **b** the single-turn helix of **37** ( $n = 5$ ) and the formation of the hierarchical architecture stabilized by the Pt...Pt and  $\pi$ - $\pi$  stacking interactions. Reprinted with permission from [37]. Copyright © 2017, American Chemical Society

(Scheme 3.9) in DMSO forms a supramolecular gel, while  $[\text{Pd}_3(\mathbf{38})_6](\text{NO}_3)_6$  (**Pd1**) (Scheme 3.9) cannot because of the presence of an extra  $\pi$ -surface in the benzimidazole moiety which made it easier to self-assemble through intermolecular  $\pi$ -interactions [43]. Oxoanions like nitrate, perchlorate, triflate and tosylate are easier to gelate because they are capable to form H-bonds. The stimuli-responsive nature of the gel is triggered by halide-nitrate, DMAP- $\text{HNO}_3$  and ethylenediamine- $\text{Pd}(\text{NO}_3)_2$ .

Howlader and Mukherjee reported formation of a supramolecular  $\text{Pd}^{2+}$  gel (**G1**) upon 1:1 treatment of  $\text{H}_2(\mathbf{40})$  (Scheme 3.9) with a *cis*-blocked  $\text{Pd}^{2+}$  90 °C acceptor (**42**, Scheme 3.9) in  $\text{H}_2\text{O}$  or DMSO [44]. Post-metalation of **G1** with **42** in water or DMSO results in deprotonation of the N-H moieties and turned the gel into a highly water-soluble edge-directed tetrahedral  $(\mathbf{42})_{12}(\mathbf{40})_6$  (**T1**) cage (Fig. 3.12). For **T1** cage every vertex corner of the tetrahedron includes three  $\text{Pd}^{2+}$  acceptors connected by the nitrogens from the tetrazole moieties of the linkers to form a  $\text{Pd}_3$  triangle and **40** molecules are tied by two corners along the edges. A water-soluble chiral face-direct etrahedral cage  $(\mathbf{42})_{12}(\mathbf{41})_4$  (**T2**) is fabricated when replaced  $\text{H}_2(\mathbf{40})$  with  $\text{H}_3(\mathbf{41})$  in a 2:3 molar ratio of  $\text{H}_3(\mathbf{41})$  with **42** under the same condition. For **T2** cage every vertex corner of the tetrahedron includes three acceptors and the linker **41** is fastened by three corners along the face.

Bispyridyl-conjugated Fmoc-L-glutamate **43** (Scheme 3.9) reacts with silver salt to form gel in aqueous solution or EtOH at room temperature [45]. The self-assembly behaviour of **43** is highly dependent on the concentration of gelators



**Scheme 3.9** Molecular structures of **38–43**, **Pd1** and **Pd2**

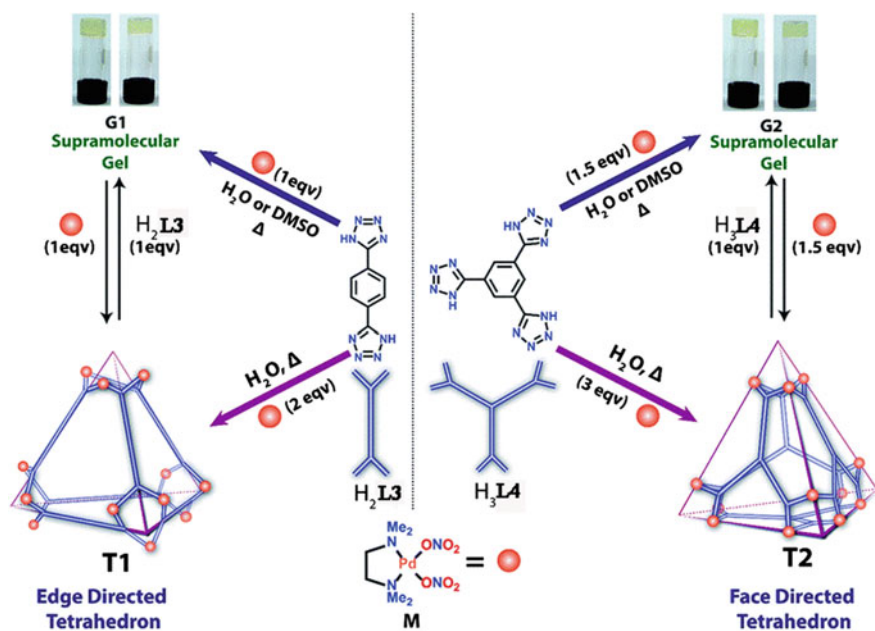


**Fig. 3.12** Schematic representation of the synthesis of metallogels and their facile conversion to 3D tetrahedral nanocages (**L3** = **40**; **L4** = **41**; **M** = **42**). Reprinted with permission from [44]. Copyright © 2016, Royal Society of Chemistry

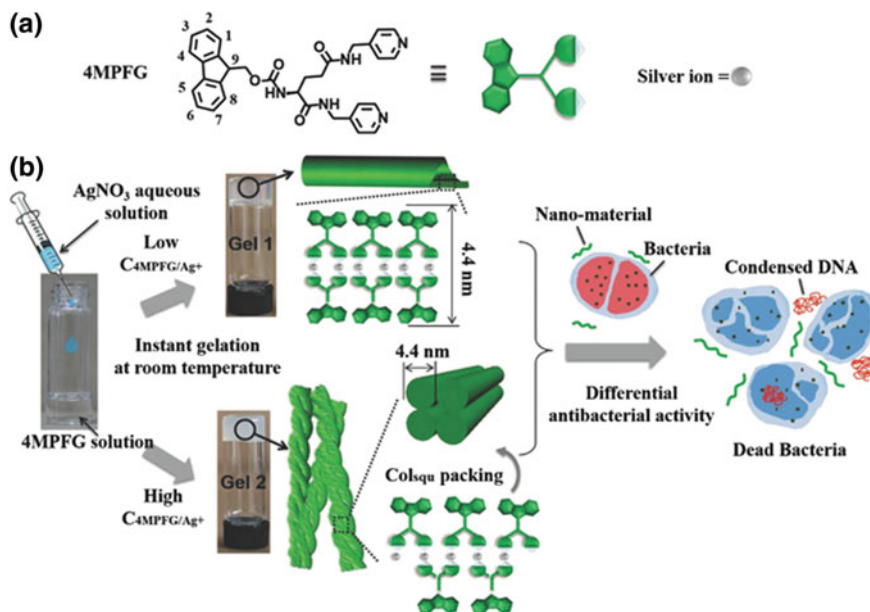


**Fig. 3.13** Schematic illustration of silver ion-induced instant gelation of **43** and their antibacterial activity. Reprinted with permission from [45] © 2015 The Authors. Published by WILEY-VCH Verlag GmbH & Co. KGaA, Weinheim

and the self-assembled nanotube (G**43**-1) and nanofibre structure (G**43**-2) can be obtained at different concentration (Fig. 3.13). When the concentration of **43** is increasing, G**43**-2 with entangled fibrillar structure is formed. In G**43**-1, two **43** molecules are bridged by two silver ions to form an oval-shaped ring, which adopts face-to-face packing due to  $\pi$ - $\pi$  stacking of fluorenyl and hydrogen bonding interactions and finally leads to nanotube structures. The major gelators of G**43**-2, linked by silver ions, form the helical coordination polymer chains. Both G**43**-1 and G**43**-2 exhibit thermally reversible sol-gel transition. The gel nanomaterials show differential antibacterial activity when they are utilized as the antibiotic agents. The antimicrobial mechanism is that the nanomaterials can destroy the membrane integrity and induce DNA condensation to finally kill the bacteria.

Huang, Stang and co-workers used hierarchical self-assembly to fabricate advanced supramolecular materials [46]. Benzo-21-crown-7 (B21C7)-functionalized 120° dipyrindyl, ligand **44** has highly directional dipyrindyl donors decorated with a benzo-21-crown-7 moiety (Fig. 3.14). **44** first self-assemble into a hexagonal metal-organic cycle when mixed with a 120° acceptor **45** driven by coordination. These discrete hexagons then form a hexagonal-cored supramolecular polymer network by cross-linking the B21C7 moieties with a bis ammonium salt **46**, through crown ether-based host/guest interactions. SEM of the xerogel shows extended and interconnected fibres. The gel shows completely reversible thermo- and cation-induced gel-sol transitions.

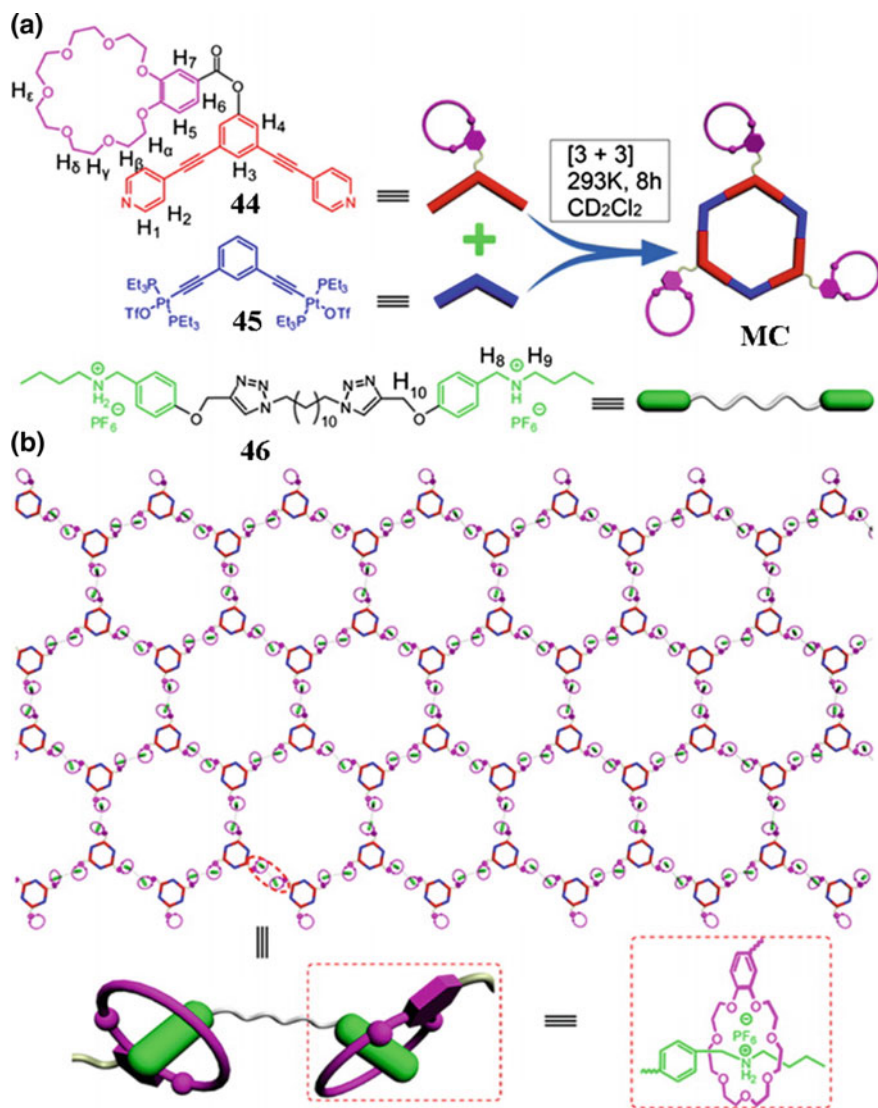


**Fig. 3.14** **a** Self-assembly of discrete metal–organic cyclic hexagon **MC** and **b** cartoon representation of the formation of a cross-linked 3D supramolecular polymeric network from self-assembly of hexagon **MC** and bis ammonium salt. Reprinted with permission from [46]. Copyright © 2014, American Chemical Society

## 3.2 Coordination Polymer Gelators

### 3.2.1 Metal-Carboxylate Gels

Various bridging carboxylate derivatives have been used to produce this class of metal-carboxylate gels in the past decade.  $\text{Fe}^{3+}$  and benzene-1,3,5-tricarboxylic acid (**H<sub>3</sub>BTC**) can be easily to form gels in alcohols in a few minutes [47]. The **Fe-BTC** gel can be readily extended to a series of gels based on trivalent metal ions (e.g.  $\text{Al}^{3+}$ ,  $\text{Cr}^{3+}$ ) and carboxylates with a bridging dicarboxylate motif [48, 49]. Metal-carboxylate gels of  $\text{Fe}^{3+}$  are easy to form at room temperature, but those of  $\text{Al}^{3+}$ ,  $\text{Cr}^{3+}$  need heating during the gelation process. Metal-rigid bridging carboxylate gels are easy to design and adjust in their structure and function, due to metal ion variability and a variety of organic ligands. This kind of materials can be used in adsorption, separation and catalysis applications and as templates.

The metal-carboxylate gels are made up of coordination polymer nanoparticles, which is different from usual fibrous networks of supramolecular gels [48, 50, 51]. Interestingly, highly porous aerogels may be obtained through sub-critical/supercritical  $\text{CO}_2(\text{l})$  drying from rigid bridging carboxylates (**BTC**, **BDC**, etc.) (Fig. 3.15). For example, **Fe-BTC** (Scheme 3.10) aerogels show high-specific surface area and hierarchical porosity (total pore volume  $5.62 \text{ cm}^3 \text{ g}^{-1}$ , BET surface area  $1618 \text{ m}^2 \text{ g}^{-1}$ ).

The microporosity of the materials may be adjusted and controlled by molecular precursors and the framework structure, while the mesoporosity is readily by the reactant concentration. For example, the microporosity of **Al-BDC** gel materials is decided by the MIL-53 MOF nanoparticles which aggregate to form the gel matrix [49]. At high reactant concentrations **Cr-BTC** materials are mainly microporous, while at lower concentrations, hierarchical porous materials with wide mesopore size distribution are obtained (Fig. 3.16) [48]. The mesopore size distribution and structure of these materials can be controlled by template. The formation

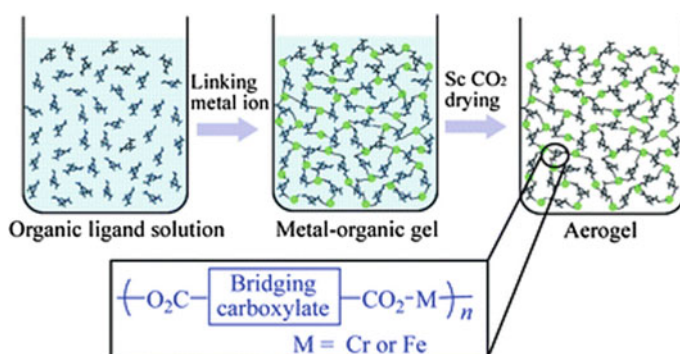
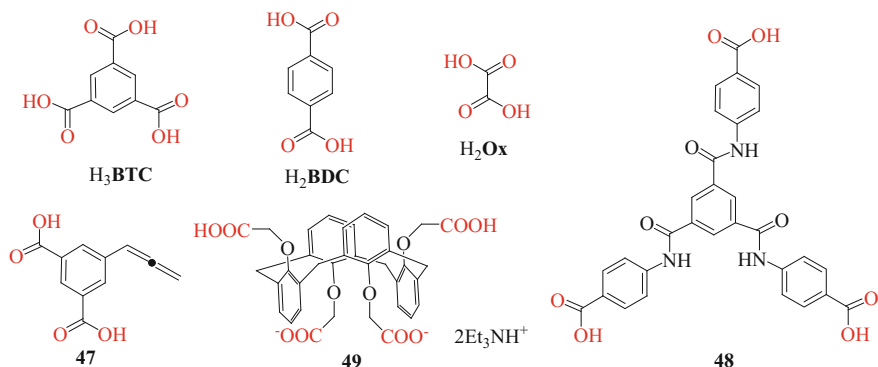


**Fig. 3.15** Schematic representation of the formation of porous metal-organic aerogel. Reprinted with permission from [48]. Copyright © 2011, Royal Society of Chemistry



**Scheme 3.10** Bridging carboxylic acid derivatives

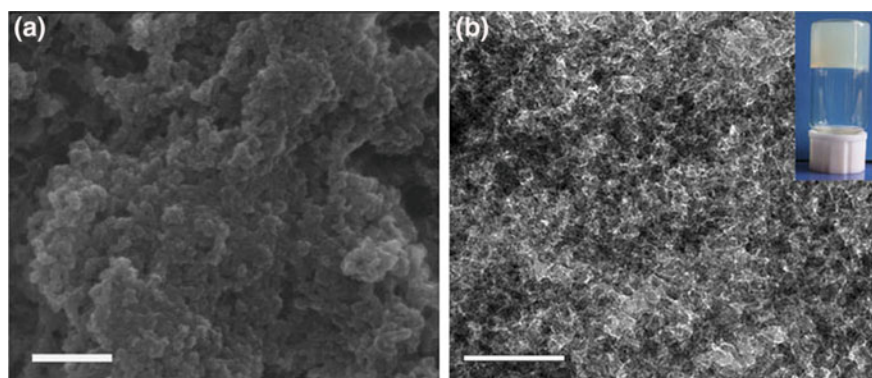


**Fig. 3.16** **a** SEM and **b** TEM of Al-BTC gel (bars represent 500 and 100 nm, respectively, the insert shows digital photograph of wet gel). Reprinted with permission from [49]. Copyright © 2013, Rights Managed by Nature Publishing Group

mechanism has been proposed for this unusual metal–organic system based on the known structure. In a metal–organic system, amorphous coordination polymers usually result in fast reaction, while crystalline metal–organic frameworks are prepared by slow assembly. The reaction is influenced by reaction conditions such as the metal-to-ligand ratio, anion, solvent and concentration used. Temperature is the most important factor for the growth of coordination polymer nanoparticles. If the concentration is appropriate, with suitable surface tension in a certain solvent, coordination polymer nanoparticles can be stabilized and further to form gel based on coordination polymer particles [52].

The above metal–organic gels formed by  $H_3BTC$  and trivalent metal ions represent a major category of metal–organic gels. It has been extended into many metal ions and carboxylic acid derivatives. Tetravalent and divalent metal ions show ability to coordinate with bridging carboxylic acids to form gel as well. For

example, metal–organic gels are obtained from  $Zr^{4+}$  and 2-aminoterephthalic acid. The gels are based on UiO-66-NH<sub>2</sub> MOF nanoparticles [52]. Cu<sup>2+</sup> gel materials are prepared from Cu(NO<sub>3</sub>)<sub>2</sub>·3H<sub>2</sub>O and H<sub>3</sub>BTC in the present of triethylamine [53]. Cu<sup>2+</sup> gel materials are also obtained via deprotonation of H<sub>3</sub>BTC by KOH. A continuous morphology evolution from granular particles to fibres exists is adjusted and controlled with a gradual decrease of the Cu/BTC molar ratio [54]. Cu<sup>2+</sup> gels are also readily obtained by simple mixing of stock solutions of Cu<sup>2+</sup> and oxalic acid at room temperature. The gel shows proton conduction of 10<sup>-3</sup>–10<sup>-4</sup> S cm<sup>-1</sup> under anhydrous conditions [55]. What's more, the Cu<sup>2+</sup>-oxalate gel shows self-healing and mouldable properties. The system displays an ability to impart self-healing properties to other gel networks lacking this capacity [56]. Stable hybrid materials form when placing in direct contact Cu<sup>2+</sup>-oxalate and DACBA pre-cut monolithic blocks prepared in DMF. This is a result of the dynamic characteristics of internal composite material and formation of interpenetrating network. The lowest gel ratio of 0.8:0.2 (DACBA/Cu gel, v/v) is necessary for the preparation of a self-healing monolithic hybrid gel based on non-healable DACBA gel (Fig. 3.17). Divalent gels have been extended to Pb<sup>2+</sup> by Burrows, Raithby, Wilson and co-workers. Reacting equimolar quantities of **47** (Scheme 3.10) with lead(II) acetate trihydrate in DMF result in gelation [57].

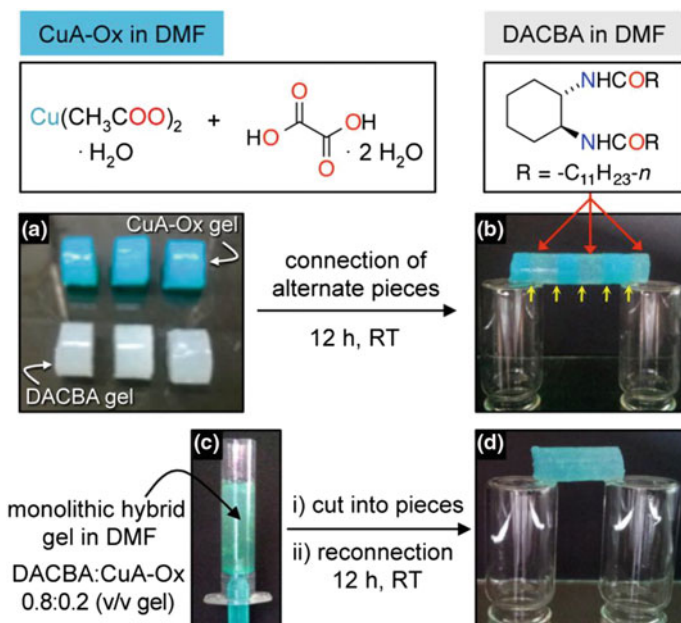


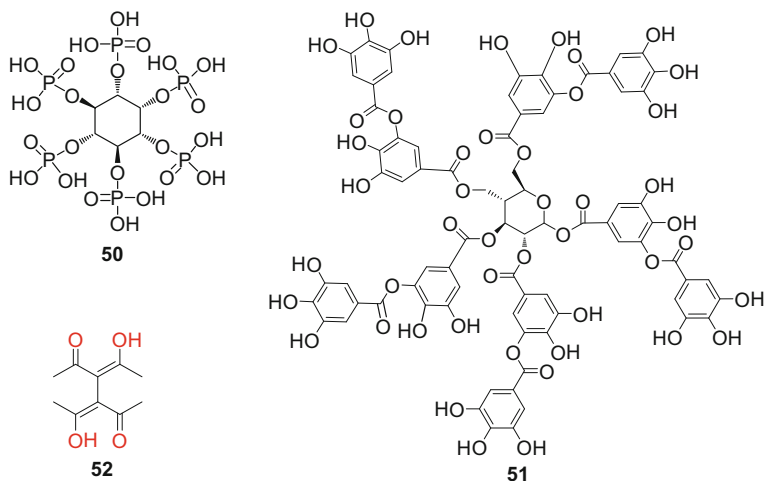
**Fig. 3.17** a, b Self-supporting monolithic bridge by reconnection of alternate block gels made of Cu<sup>2+</sup> gel and DACBA, and c, d self-supporting and self-healing hybrid (DACBA/Cu<sup>2+</sup> gel = 0.8:0.2 v/v). Reprinted with permission from [56]. Copyright © 2016, American Chemical Society

Metal-carboxylate gels may be further functionalized by modifying the ligands or metal ions. Dastidar and co-workers found that reaction of  $C_3$ -symmetric tris-amide-tris-carboxylate ligand **48** (Scheme 3.10) with various metal salts such as  $\text{Cd}(\text{NO}_3)_2$ ,  $\text{Cu}(\text{NO}_3)_2$ ,  $\text{Co}(\text{NO}_3)_2$  and  $\text{Zn}(\text{NO}_3)_2$  in pure water resulted in metallo-gels [58]. Moulton and co-workers reported that metal cluster  $\text{Mn}_{12}\text{O}_{12}(\text{AcO})_{16}(\text{H}_2\text{O})_4$  coordinates with polycarboxylate ligands to form gels [59]. Thiocalix [4] arene-based  $\text{Co}^{2+}$  gel was reported by Jung and co-workers [60]. The gel was prepared from thiocalix [4] arene derivative (**49**, Scheme 3.10) and  $\text{Co}^{2+}$  in  $\text{H}_2\text{O}$ -DMF at  $\text{pH} = 7.0$ . The gel shows selectively colour changing property in the presence of gases that yield hydrogen chloride upon hydrolysis due to the coordination geometry, which is proved by single-crystal X-ray. The red gel derived from  $\text{Co}(\text{NO}_3)_2$ , an octahedral  $\text{Co}^{2+}$  complex, changes to blue gel with a tetrahedral structure by the introducing of volatile gases containing a chlorine atom (VGCl). More detailly, the addition of VGCl results in the removal of three DMF molecules by the intermolecular hydrogen-bonding interaction between DMF and HCl and forming the tetrahedral structure meanwhile. The gel can be used as a chemoprobe for VGCl such as HCl,  $\text{SOCl}_2$ ,  $(\text{COCl})_2$  and  $\text{COCl}_2$ .

$\text{K}^+/\text{Rb}^+$  gels based on **49** (Scheme 3.10) were prepared in MeOH-water (v:v 1:1) by Lee, Park and co-workers [61]. The formation of the  $\text{K}^+/\text{Rb}^+$  metallo-gels suggests metal ion recognition based on the size effect is an important factor for the gelation because other alkali metal ions are too small (e.g.  $\text{Li}^+$ ,  $\text{Na}^+$ ) or too big (e.g.  $\text{Cs}^+$ ) to accommodate in gelator **49**. The  $\text{Rb}^+$  gel is more stable than  $\text{K}^+$  gel. The analysis of single crystals from the corresponding gels through thermal treatment indicates that each of two  $\text{K}^+$  present in the calix moiety is coordinated by two phenolic oxygen and two monodentate carboxyl oxygen atoms from different pendants in a *cis*-arrangement for **49**- $\text{K}^+$ . The association of the dipotassium(I) unit cross-links via intermolecular hydrogen bonding, generating a pseudo 3D framework. Different from **49**- $\text{K}^+$ , the connectivity pattern of **49**- $\text{Rb}^+$  is strongly associated with triply bridged additional two  $\text{Rb}^+$  ions in different calix moieties. In short, both the  $\text{K}^+$  and the  $\text{Rb}^+$  gel have an H-bonded framework, while the  $\text{Rb}^+$  gel is more stable due to extra coordination bonds.

The design principles of metal-carboxylate gels may be extended into various systems. A high proton conducting metallo-gel is synthesized by immobilizing protogenic phytic acid (**50**, Scheme 3.11) [62] using iron(III) nitrate in DMF. The gel consists of 20–40 nm nanospheres which interweave into a 3D gel network. The xerogel has a Brunauer–Emmett–Teller (BET) surface area of  $124 \text{ m}^2 \text{ g}^{-1}$  and shows high proton conductivity of  $2.4 \times 10^{-2} \text{ S cm}^{-1}$  at  $120 \text{ }^\circ\text{C}$ . Such gel materials are used as solid electrolyte in fuel cell with  $0.94 \text{ mW cm}^{-2}$  power density at 0.6 V.

A series of phenolic gels were prepared through direct gelation of **51** (Scheme 3.11) [63] and group IV metal ions. Polyphenolic compound **51** consists of five digalloyl ester groups covalently attached to a central glucose core. These metallo-gels form in different organic solvents and aqueous solutions through simple mixing at a range of molar ratios. Redox reactions between **51** and  $\text{Ti}^{4+}$  during gelation, the high oxidation state and formal charge of  $\text{Ti}^{4+}$  play a significant



**Scheme 3.11** Molecular structures of **50–52**

role in the solvent-trapping process of the gelation in addition to coordinative cross-linking, thus enabling the formation of gel networks. The gels show stable shape persistence with any change in either the shape or size when kept in air over time (up to 3 months). The gels also show high load-bearing capabilities, a weight over 70 times than their own weight. What's more, the gels exhibit self-healing properties and the fractures disappeared completely within 2 h in the fracture-recovery test. Furthermore, these gels can be engineered to exhibit optical transparency, inject ability, mould ability, shape persistence and adhesiveness. Similarly, bridging bis(acetylacetonate) ligand **52** (Scheme 3.11) reacts with trivalent metal ions ( $\text{Al}^{3+}$  and  $\text{Cr}^{3+}$ ) to form metal–organic gels composed of nanoscale metal–organic particles [64]. A multiconnecting motif readily leads to formation of a three-dimensional matrix.  $\text{N}_2$  sorption shows that the aerogels have high BET surface areas up to  $\sim 1100 \text{ m}^2 \text{ g}^{-1}$  and hierarchical porosity. The aerogels show ability to adsorb various gases ( $\text{H}_2$ ,  $\text{CO}_2$  and  $\text{CH}_4$ ) and vapours (MeOH and EtOH). Water sorption measurements reveal that the aerogels have relatively hydrophobic pore surface.

Metal-carboxylate gels have been modified for various functions. For example, the redox property of  $\text{Fe}^{3+}$  ions has been used for preparation of hybrid materials [65, 66]. A redox-active gel has been obtained by incorporate conducting polymers inside Fe-BTC (Scheme 3.10) gel. In situ incorporation of conducting polypyrrole and polythiophene moieties into the xerogel matrix is achieved and results in the formation of hybrid composite materials. Interestingly, no extraneous oxidant is needed. The in situ formation of polypyrrole and polythiophene is attributed to an oxidative polymerization reaction induced by the  $\text{Fe}^{3+}$  ions. Additionally, the photoluminescence may be changed with redox change [67]. For example, there is no luminescence for Fe-BDC (Scheme 3.10) gel. However, when small reactive

organic molecules like pyrrole, aniline and bithiophene are present in Fe-BDC gel, highly photoluminescent hybrid materials are obtained while the gelation process is unaffected. The morphology of the metal–organic gel transforms remarkably from spindle-like structure to nanofibres. The photoluminescence turn-on response is primarily attributed to the redox reaction between iron ions and the small organic molecules generating oxidized oligomers in the porous gel matrix.

The carboxylate ligands are easy to be modified to enrich the functionalized of metal-carboxylate gels. The photoresponsive chromophores have been introduced into metal-carboxylate gels [68]. Mixing the dicarboxylic acid derivative of **53** (Fig. 3.18) which contains photoresponsive DTE moiety with  $\text{Al}^{3+}$  yields a clear solution, from which a metal–organic gel is obtained upon heating at 80 °C. The xerogels are composed of nanoscale particles with an approximate 20 nm diameter, which are interconnected to form a porous gel matrix. The gel shows responsive to multiple stimuli, including light, heat, water and anions. The light responsive behaviour of the metal–organic system results from the photoisomerization property of the DTE moiety. A yellow open (O) solution converts into a yellow O-gel when heated, and it can be converted into a red closed (C) gel by UV irradiation. The red

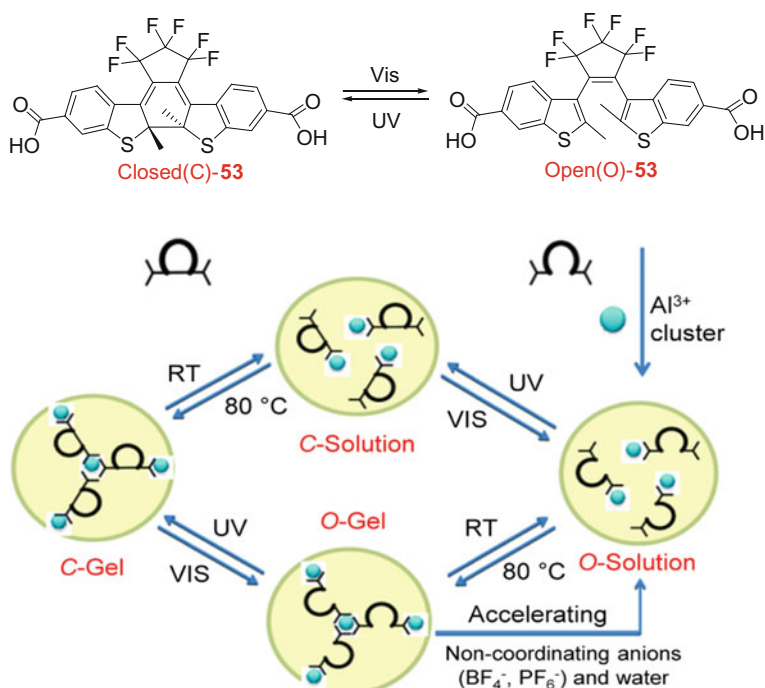


**Fig. 3.18** Reversible photoisomerization between the opened- and closed-ring forms of the photochromic dicarboxylic acid ligand **53**, and schematic representation of multiple transformations among gels and solutions in both open and closed forms. Reprinted with permission from Ref. [48]. Copyright © 2013 WILEY-VCH Verlag GmbH & Co. KGaA, Weinheim

C-gel changes into a red C-solution when kept at room temperature in the dark, and finally reverts back into the original yellow O-solution when exposed to visible light. The gelation process is affected by the addition of anions. Interestingly, addition of non-coordinating anions like  $\text{BF}_4^-$  and  $\text{PF}_6^-$  causes gel-solution transition and preventing further gelation.

Ayyappanpillai and co-workers reported that the reaction of azobenzene-4,4'-dicarboxylic acid (**54**, Fig. 3.19) and  $\text{Fe}^{3+}$  leads to immediate gelation in the presence of  $\text{NEt}_3$  in DMSO or DMF [69]. The gel of **54** contains globular seeds, which grow into two-dimensional sheets; the smaller sheets lead to a cabbage like structure, and finally result in a macroscopic flowers structure. Presynthetic photoisomerization of the precursor **54** leads to morphologically different macroscopic structures. When **54** is irradiated with UV light before the gelation, where  $\sim 37.5\%$  of the molecules are present in the cis form, another **54'** gel is obtained by mixing with  $\text{Fe}^{3+}$ . The **54'** gel shows six armed metal-organic stars which is very different from the gel of **54**. Ultraviolet light induced coordination modulation via

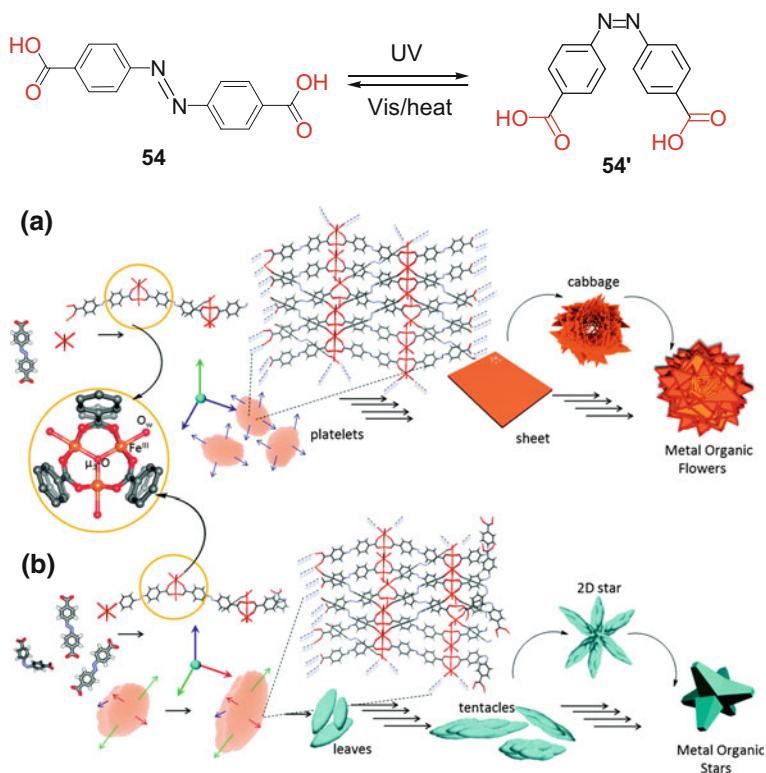
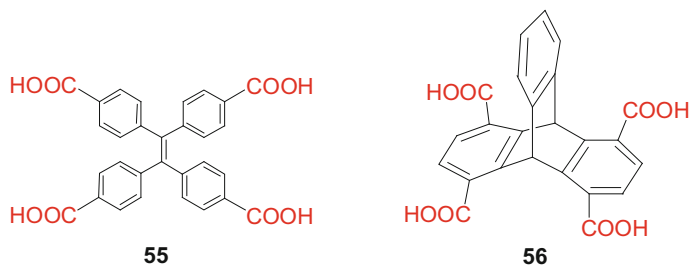


**Fig. 3.19** *Trans-cis (E-Z)* isomerization of azobenzene-4,4'-dicarboxylic acid (**54**) upon irradiation with ultraviolet (UV) and visible (Vis) light and proposed formation pathways of **a** flowers in **54** gel and **b** stars in **54'** gel. Reprinted with permission from [69]. Copyright © 2015, Royal Society of Chemistry



**Scheme 3.12** Molecular structures of **55** and **56**

photoisomerization of an azobenzene-based dicarboxylate linker **54** followed by aggregation mediated crystal growth resulted in two distinct morphological forms (flowers and stars). The two materials show subtle differences in their physical properties. The maximum amounts of  $N_2$  adsorbed at saturation pressure for **54** gel and **54'** gel are 88 and 46  $\text{mL g}^{-1}$ , and Brunauer–Emmett–Teller (BET) surface area 223 and 90  $\text{m}^2 \text{g}^{-1}$ , respectively.

Zhang and co-workers reported a gel with aggregation-induced emission (AIE) features based on tetrakis(4-carboxyphenyl)ethylene **55** (Scheme 3.12) by introducing the tetraphenylethene unit [70]. A series of trivalent metal ions ( $\text{Al}^{3+}$ ,  $\text{Cr}^{3+}$ ,  $\text{Fe}^{3+}$ ,  $\text{Ga}^{3+}$ , and  $\text{In}^{3+}$ ) induce gelation with **55** successfully. These metal–organic gels contain wormhole-like networks structure, except for In-TCPE gel with a wide fibres structure due to the structural difference at the molecular level. When the precursor concentration of **55** increases to 0.03  $\text{mol L}^{-1}$ , the resulting Al-**55** aerogel exhibits high permanent hierarchical micro- and mesoporosity with BET-specific surface area and total pore volume of 989  $\text{m}^2 \text{g}^{-1}$  and 4.23  $\text{cm}^3 \text{g}^{-1}$ , respectively. The luminescent Al-**55** gel can detect picric acid with concentration as low as 0.76 ppm in aqueous solutions.

Venkatesan, Berke and co-workers report a luminescent Al-based metal–organic gel comprising 1,4,5,8-triptycenetetracarboxylic acid **56** (Scheme 3.12) and  $\text{Al}^{3+}$  in DMF [71]. The gel exhibits highly sensitive detection towards nitro aromatic compounds particularly picric acid and shows high photostability because the initial emission intensity is recovered with a significant extent ( $\sim 75\%$  after 6 cycles) after being treated with excess picric acid and then washed by EtOH.

What's more, incorporation of lumiphore molecules with AIE property may remarkably change the luminescent property of metal–organic gels [72]. For example, trace doping (as low as 0.01 mol%) of the Zr-BDC gel materials with **55** causes a remarkable change to the luminescence properties and the gel emits blue luminescence with high quantum yield (59%). When trace of **55** (Scheme 3.12) is introduced, the Zr-BDC gels still keep the structure based on nanoscale crystalline components of UiO-66. The doped materials have BET surface areas of 1145–1280  $\text{m}^2 \text{g}^{-1}$  and total pore volumes of 0.598–0.832  $\text{cm}^3 \text{g}^{-1}$ . The limit of detection is up to  $1.05 \times 10^{-7} \text{ mol L}^{-1}$  (24 ppb) towards picric acid (Fig. 3.20).

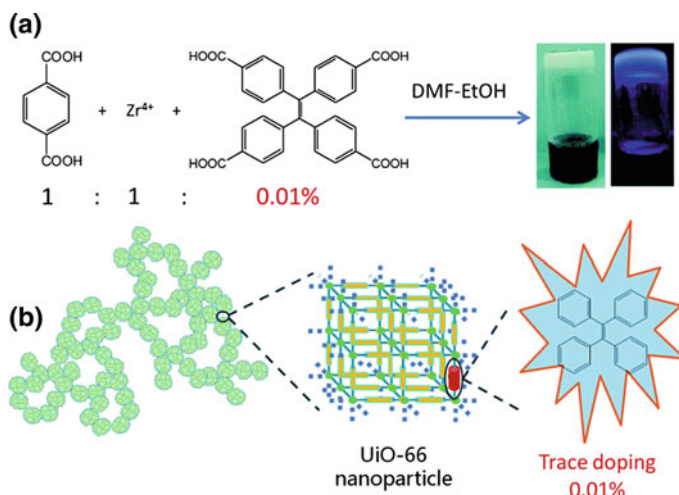


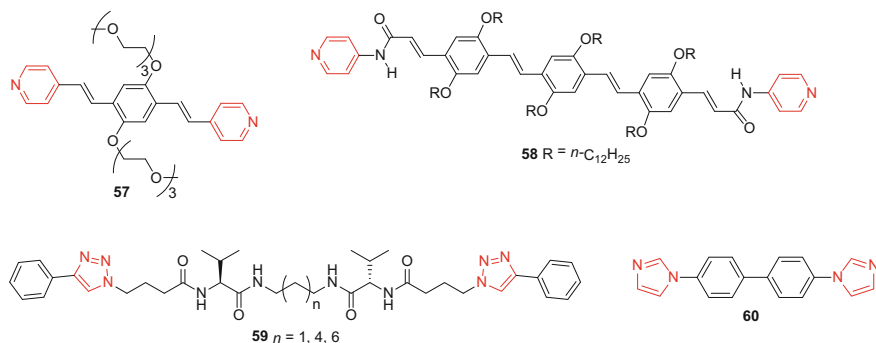
**Fig. 3.20** **a** Preparation and **b** schematic illustration for the construction of trace-doped luminescent Zr-BDC gel. Reprinted with permission from [72]. Copyright © 2017, Royal Society of Chemistry

### 3.2.2 Metal-Heterocycle Polymer Gels

Various heterocycle-based bridging ligands have been employed to develop metal-organic gels, such as pyridine, imidazole, triazole, pyrazole, tetrazole and others. These ligands are also widely used in coordination chemistry [73].

A series of bridging dipyrindyl gelators have been developed with the aid of amide/urea H-bonding motifs [74–77] or long alkyl/oligoether oxide chain [78–80]. Bhattacharya and co-workers reported that *p*-pyridyl ended oligophenylenevinylene **57** (Scheme 3.13) forms gels selectively with  $\text{Cu}^{2+}$  among a variety of transition metal cations [78]. The driving forces of gelation include metal ion coordination,  $\pi$ - $\pi$  interactions and interdigitation of the oxyethylene chains through the van der Waals interactions (Fig. 3.21). The position of the pyridyl N-atom in the molecular backbone is vital to gelation. The resulting gel is injectable and also shows multistimuli responsiveness, including thixotropy. The reversible nature of the gel-sol transition is also demonstrated using  $\text{Cu}^{2+}/\text{Cu}^+$  redox chemistry in the presence of sodium L-ascorbate and  $\text{O}_2$ . Ajayaghosh and co-workers reported an oligo (*p*-phenylenevinylene) derivative connected to pyridyl end groups through an amide linkage (**58**, Scheme 3.13) [79]. Addition of  $\text{Ag}^+$  ions to a solution of **58** facilitates the formation of a metal-organic assembly leading to gelation.

Bridging ditrizolyl gelators **59** (Scheme 3.13) with amide H-bonding motif have been developed by Escuder and co-workers [80]. **59** are able to form self-sustainable gels in alcohols and  $\text{H}_2\text{O}$ . On the other hand,  $\text{Cu}^+$  gels are prepared by heating the copper salt  $[\text{Cu}(\text{MeCN})_4]\text{PF}_6$  together with the gelator **59** in a 1:2 ratio, until complete dissolution, followed by sonication, via the  $\text{CuN}_4$  coordination



**Scheme 3.13** Molecular structures of 57–60

between Cu(I) and triazolyl and hydrogen bond. The gelator with the shortest carbon chain self-assembles in a completely amorphous pattern in comparison to those having longer carbon chains due to the carbon spacer length with different hydrogen-donor and hydrogen-acceptor atoms.

Bridging diimidazolyl ligands, 4,4'-bisimidazolylbiphenyl (**60**, Scheme 3.13), react with  $\text{Zn}(\text{OTf})_2$  in a 2:1 molecular ratio in MeOH at room temperature to get a white suspension, which under sonication undergoes complete and homogeneous liquid gelation [81]. This represents an example of ultrasound-induced switching of sheet-like coordination polymer microparticles into nanofibres capable of gelating organic solvents. The gelation is proposed to originate from a change in the coordination chemistry of  $\text{Zn}^{2+}$  ions from tetrahedral to seesaw geometry. Sonication may facilitate a break-reorganization of coordination bonds (Fig. 3.22).

Various bridging tripyridyl or polypyridyl ligands have also been developed for gelation study [82–84]. Polypyridine-based metal–organic gels utilizing  $\text{Pd}^{2+}$  complexes show interesting morphology transformation [85–87]. Tripyridine ligand **61** (Fig. 3.23) has amide hydrogen-bonding motif for holding solvent molecules, and pyridine groups for cross-linking. **61** formed gels with  $\text{Pd}(\text{COD})(\text{NO}_3)_2$  in a range of mixed organic solvents (e.g. MeOH– $\text{CHCl}_3$ ) with a range of Pd/L ratios of 1:1 ~ 4 during a shorter period of 2 min to 2 h. Morphology evolution of spherical assemblies to fibrous structures occurs in xerogels with Pd/L ratios decreasing from 1:1 to 1:4 (Fig. 3.23). The **61**- $\text{Pd}^{2+}$  gel/xerogels show catalytic activity in Suzuki–Miyaura coupling under mild conditions, and the fibrous network has higher activity than spheres as recycled catalyst.

Gels based on tetrazolyl derivatives have been investigated. **62–65** (Scheme 3.14) reacted with a DMF solution of  $\text{Pd}(\text{OAc})_2$  at a 2:1 molar ratio of tetrazolyl unit: $\text{Pd}^{2+}$  at room temperature to spontaneously yield complete and homogeneous gels [88]. The cooperative hydrogen bonding interaction of the NH group of tetrazoles played a key role in the formation of gels. The gels are self-healing and mouldable materials presumably through solvent-mediated cooperative hydrogen bond rearrangements. Gels also form by reacting **63**

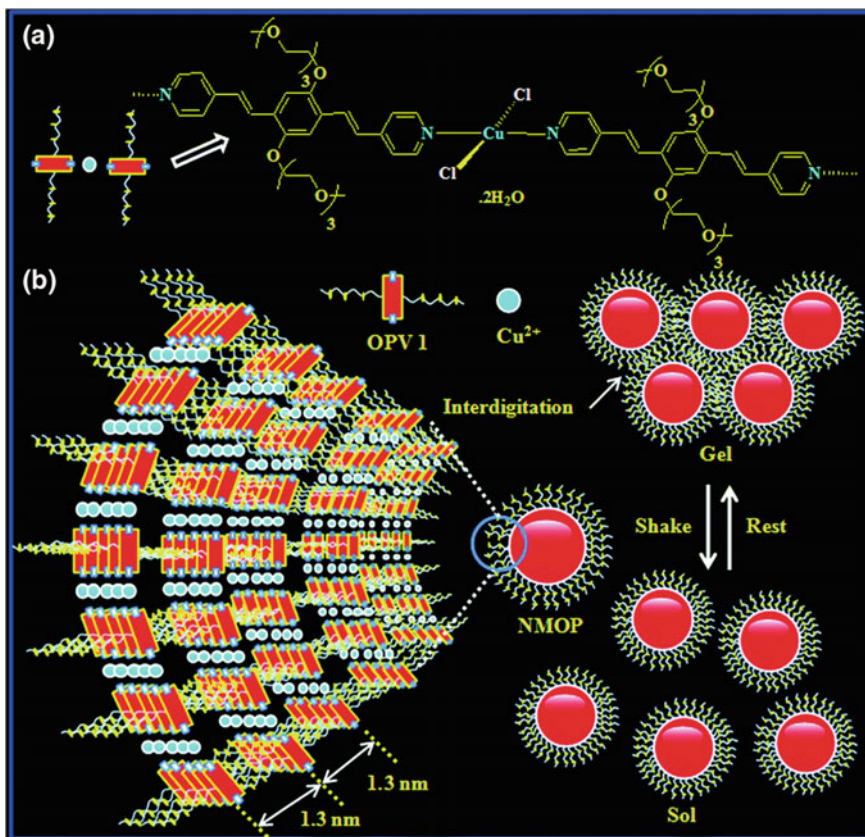


**Fig. 3.21** **a** Coordination geometry of the  $\text{Cu}^{2+}$  ion in the metallogel and **b** schematic illustration of supramolecular metallogel formation through the aggregation of individual NMOPs (the  $\text{Cl}^-$  ion coordinated to the  $\text{Cu}^{2+}$  ion was not shown in the model of NMOPs for clarity). Reprinted with permission from [78]. Copyright © 2014, Royal Society of Chemistry

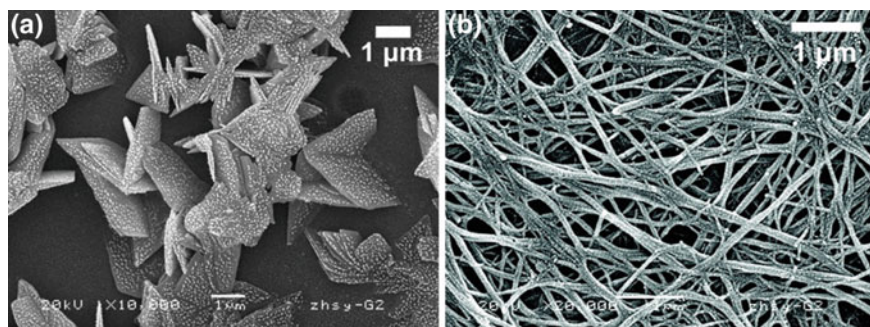


**Fig. 3.22** SEM images of **a** sheet-like microparticles of  $\{\text{Zn}(\mathbf{60})_2(\text{OTf})_2\}_n$ , and **b** the xerogel. Reprinted with permission from Ref. [81]. Copyright 2009 American Chemical Society

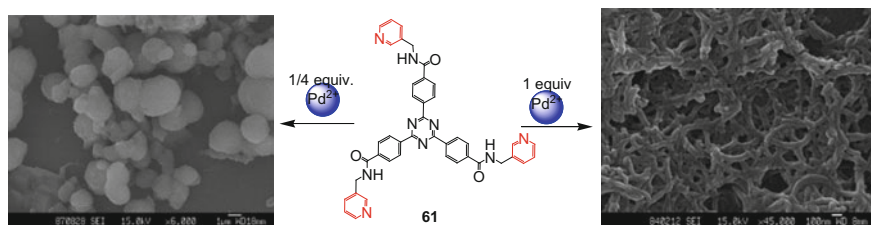
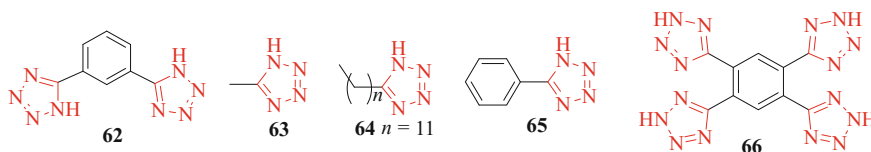


**Fig. 3.23** Morphology evolution of **61**-Pd<sup>2+</sup> gels depending on Pd/L ratio. Reprinted with permission from [86]. Copyright 2009 American Chemical Society

(Scheme 3.14) with NiCl<sub>2</sub>·6H<sub>2</sub>O or CoCl<sub>2</sub>·6H<sub>2</sub>O in DMF at room temperature [89]. Interestingly, heterometallic gels show synergistic properties using **63** with Co<sup>2+</sup> and Ni<sup>2+</sup>, showing self-healing property. Each monometallic gel formed by **63** and Co<sup>2+</sup> (**63**-Co) or Ni<sup>2+</sup> (**63**-Ni) fails to self-heal (Fig. 3.24). It suggests that the unfavourable viscoelasticity of monometallic gel is improved by doping with another appropriate metal ion. The improved macroscopic stability of **63**-Co–Ni



**Scheme 3.14** Tetrazolyl derivatives **62–66**

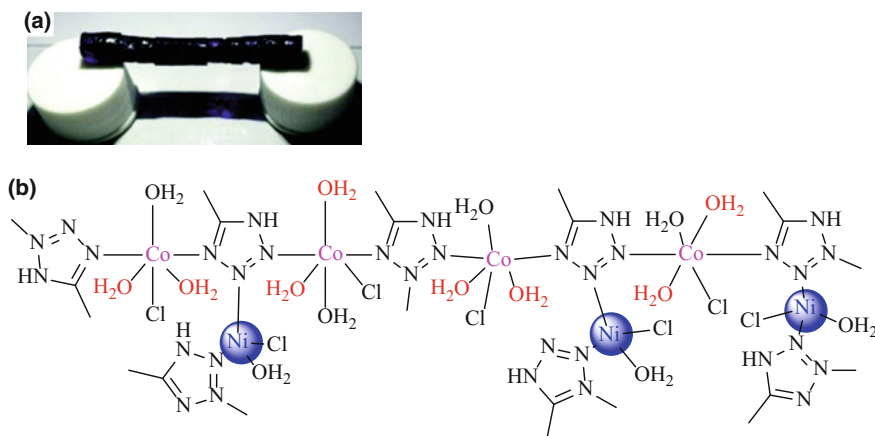
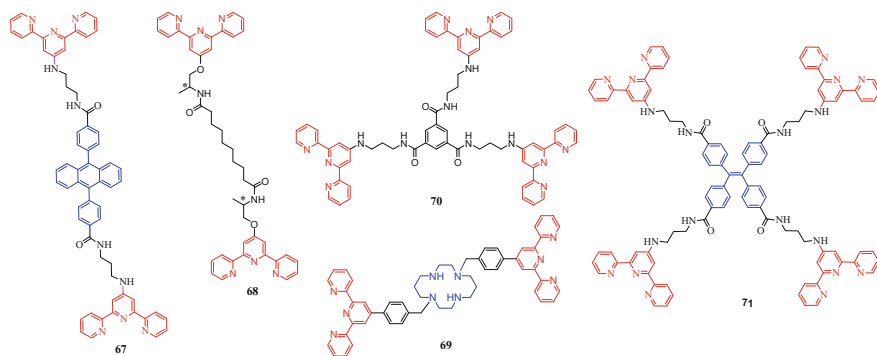


**Fig. 3.24** **a** A self-healing bridge made of heterometallic gel **63**-Co–Ni and **b** a schematic illustration of the Ni-supported network of heterometallic gel **63**-Co–Ni. Adapted with permission from [89]. Copyright © 2015, Royal Society of Chemistry



**Scheme 3.15** Terpyridyl derivatives **67–71**

should be attributed to the polymeric network supported by  $\text{Ni}^{2+}$  that preventing the disruption of the entire coordination network.

Metal–organic gels of tetrazole-appended ligand **66** (Scheme 3.14) and  $\text{Co}^{2+}$  were prepared in polar solvents by Shinkai and co-workers [90]. The gels have spherical morphology structure with 20–30 nm diameter. Powder XRD pattern reveals a crystalline structure with 2D coordination polymer structure for the freeze-dried gels. The gels show potential application as chemosensors or adsorbents for toxic gases. The **66**- $\text{CoBr}_2$  gel selectively recognizes toxic gases containing chloride atoms, such as  $\text{HCl}$ ,  $\text{SOCl}_2$ ,  $(\text{COCl})_2$  and  $\text{COCl}_2$ .

Tripodal terpyridine has been used in coordination polymeric gels as well.  $\text{Tb}^{3+}$  or  $\text{Eu}^{3+}$  ion coordinates to terpyridine-appended chiral ligand **67** (Scheme 3.15) results in green and pink emissive coordination polymer gels, respectively [91]. Control over stoichiometry of  $\text{L}:\text{Tb}^{3+}:\text{Eu}^{3+}$  leads to yellow and white light emitting bimetallic gels (Fig. 3.25).

Terpyridine-appended chiral ligand **68** (Scheme 3.15) forms luminescent gels without and with  $\text{Tb}^{3+}$  or  $\text{Eu}^{3+}$  in  $\text{H}_2\text{O}$ -DMSO (3:7 v/v) [92]. By AFM observations, these gels show well-defined right-handed helical nanofibres formed by coordination bonds (Fig. 3.26). The helical pitch lengths are strongly dependent on the concentrations of lanthanide ions. A gel can be prepared when 1 wt% of **68** was dissolved in a mixture of DMSO and various solvents such as  $\text{CH}_2\text{Cl}_2$ ,  $\text{CHCl}_3$ , toluene, ethyl acetate, MeOH, EtOH, MeCN, acetone, THF and water. The gels can be used in a water-compatible inkjet printing system to generate luminescent metallogels on A4-sized paper.

Terech and co-workers inserted a coordinating cyclam macrocycle (1,4,8,11-tetraazacyclotetradecane) as a spacer between two terminal chelating terpyridine units [93, 94]. A metal–organic gel with remarkable self-healing property is fabricated based on **69** (Scheme 3.15) through the coordination of nickel ion and nitrogen atom of terpyridine and cyclam.  $\text{Ni}^{2+}$  ion is in the centre of **69** coordinating with four N-atoms, and the network is connected by coordination

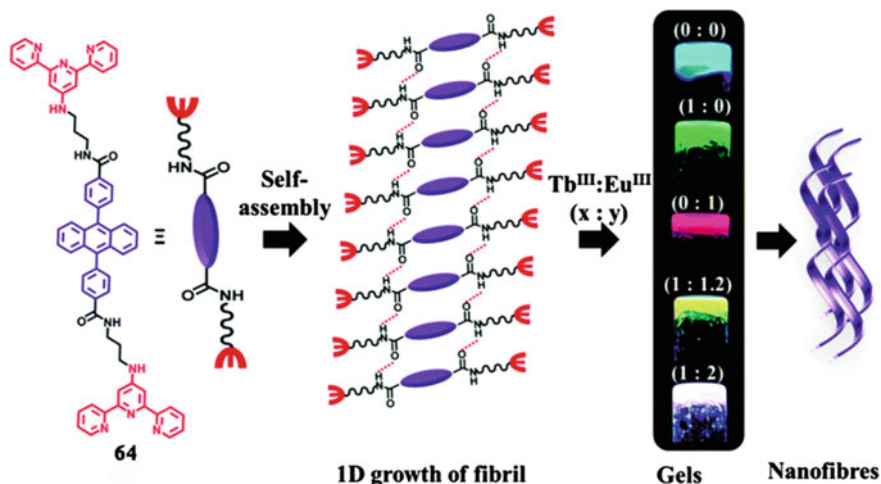


**Fig. 3.25** Schematic representation of self-assembly of **67** through H-bonding and  $\pi$ - $\pi$  stacking interactions and its coordination to  $\text{Ln}^{3+}$  forming luminescent metal-organic gels. Reprinted with permission from [91]. Copyright © 2015, Royal Society of Chemistry

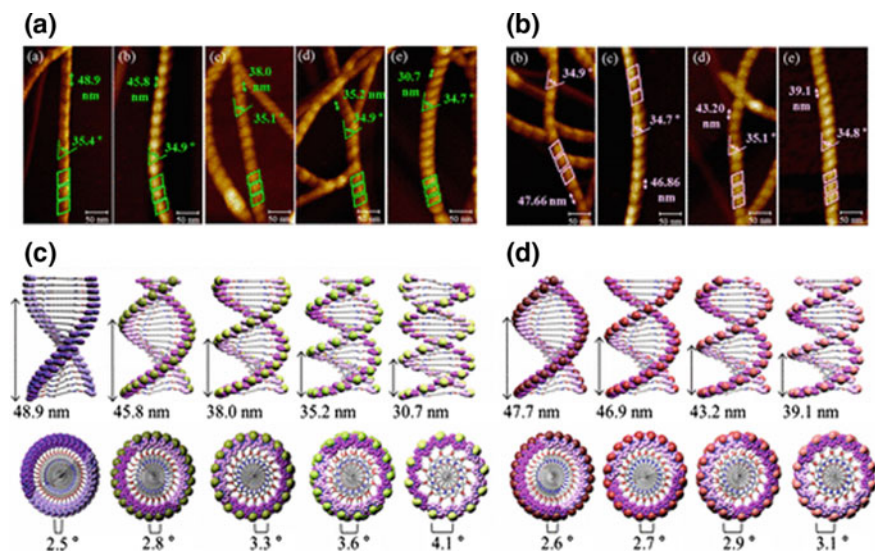


**Fig. 3.26** **a** AFM images of gel-Tb and prepared with different  $\text{Tb}^{3+}$  concentrations, **b** AFM images of gel-Eu prepared with different  $\text{Eu}^{3+}$  concentrations, and 3D models of right-handed helical structures of **c** gel-Tb and **d** gel-Eu of the internal and external helical structures (upper, helical pitch; below, the titling angle between lanthanide ion coordinated two molecules). Reprinted with permission from [92]. Copyright © 2017, American Chemical Society

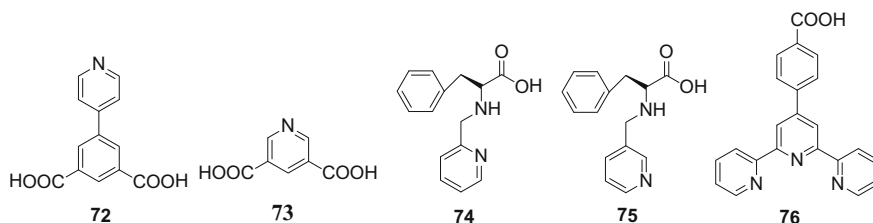
between  $\text{Ni}^{2+}$  ion and nitrogen atom of terpyridine and cyclam, thus brand stretching to form polymers structure.

The self-assembly properties of  $C_3$ -symmetric tripodal terpyridine ligand **70** (Scheme 3.15) with lanthanide ions or d-block ions were investigated by Gunnlaugsson and co-workers [95, 96]. The gelation with d-block ions, such as Fe(II), Ni(II), Cu(II), Zn(II) and Ru(III) in MeOH, was investigated by monitoring the changes in the ligand-centred absorbance and the fluorescence. **70** formed 1D helical gel in  $\text{H}_2\text{O}$ –MeOH solution itself through hydrogen bonding and  $\pi$ – $\pi$  interactions. After the addition of metal ions (M) such as Fe(II), Ni(II), Cu(II), Zn(II) and Ru(III), these gels further cross-link into 3D metallo gels. Through threefold hydrogen bonding between benzene-1,3,5-tricarboxamide core and the interaction between terpyridine and d-metal ions, the coloured or colourless gels are formed and all of them retain their fibrous nature. Only the addition of Zn(II), which has a filled d orbital, results in the formation of fluorescent gels while the other metal ions quench fluorescence of **70**.

Luminescence metal–organic gel of tetrapodal terpyridine ligand **71** (Scheme 3.15) with  $\text{Eu}^{3+}$  ions was reported by Maji and co-workers [97]. **71** reacts with  $\text{Eu}^{3+}$  (1:2 eq.) in  $\text{CHCl}_3$ –THF (v:v 1:2) to form gels with nanotubular structure. The gel shows enhanced mechanical stability along with tunable emission properties. The gel is solution-processable and made into transparent films. The gel shows matrix coordination-induced emission (MCIE) and aggregation-induced emission (AIE), which can be attributed to the combined effect of metal coordination.

### 3.2.3 Coordination Polymer Gels with Hybrid Donors

A rigid hybrid ligand with pyridine N-donor and carboxylate O-donor, 5-(pyridin-4-yl)isophthalic acid (**72**, Scheme 3.16) has been employed to develop heterometallic metal–organic gels [98]. A series of heterometallic metal–organic gels were prepared with  $\text{Pd}^{2+}$  and  $\text{M}^{n+}$  ( $\text{M}^{n+} = \text{Cr}^{3+}$ ,  $\text{Mn}^{2+}$ ,  $\text{Fe}^{3+}$ ,  $\text{Co}^{2+}$ ,  $\text{Ni}^{2+}$ ,  $\text{Cu}^{2+}$ ,  $\text{Zn}^{2+}$  and  $\text{Cd}^{2+}$ ) at the ratio L/TM/Pd = 2:2:1 in mixed solvent systems (e.g. DMF–MeOH–MeCN).  $\text{Pd}^{2+}$  ions may coordinate to the pyridine group, and  $\text{TM}^{n+}$  may



**Scheme 3.16** Molecular structures of **72**–**76**

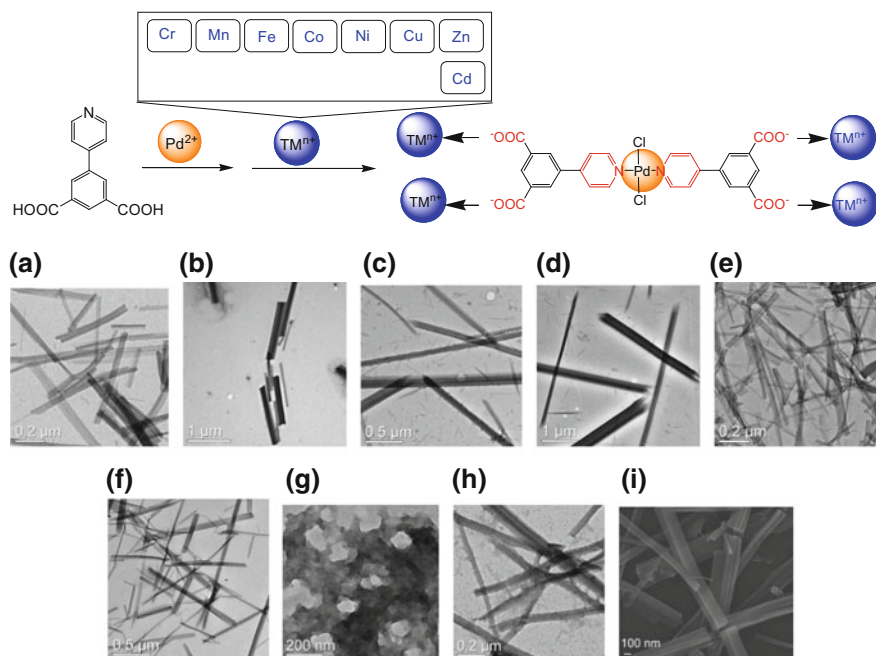


**Fig. 3.27** TEM images of **97**-based heterometallic gels: **a** PdCr(NO<sub>3</sub>)<sub>3</sub>–H<sub>2</sub>O, **b** PdMnCl<sub>2</sub>–MeOH, **c** PdCo(NO<sub>3</sub>)<sub>2</sub>–MeOH, **d** PdNi(NO<sub>3</sub>)<sub>2</sub>–MeOH, **e** PdCu(NO<sub>3</sub>)<sub>2</sub>–H<sub>2</sub>O, **f** PdZnCl<sub>2</sub>–MeOH, **g** PdFe(NO<sub>3</sub>)<sub>3</sub>–MeOH, and **h** PdFeCl<sub>3</sub>–MeOH, and SEM image of **i** PdNi(NO<sub>3</sub>)<sub>2</sub>–MeOH. Reprinted with permission from [98]. Copyright © 2011 WILEY-VCH Verlag GmbH & Co. KGaA, Weinheim

coordinate to carboxylate groups to aggregate to coordination polymers leading to gelation. The xerogels show various fibre-, rod-, and sponge-like morphologies depending on the metal ion present (Fig. 3.27). The gelation had a profound effect on the redox properties of Cu(II) ions, which changed oxidation state from +2 to +1 under ambient conditions, suggesting that gel nanofibres can stabilize Cu(I).

Pyridine-3,5-dicarboxylate **73** (Scheme 3.16) with one pyridyl-N and two carboxylic acid motifs reacts with La<sup>3+</sup> or Ce<sup>3+</sup> to form gels in DMA [99]. In contrast single crystals are obtained from the DMF solution of **73**-La and **73**-Ce showing isomorphous behaviour. Take **73**-La for example, the resulting **73**-La<sup>3+</sup> structure exhibits a 3D polymeric framework with wide hexagonal channels along the *a*-axis. The gels show multistimuli responsive property towards thermal and mechanical stimuli.

The gelling behaviour of **74** and **75** (Scheme 3.16) with pyridine and amino acid motifs was studied by Wei and co-workers [100]. The ligands show utterly different gelling abilities with Ni<sup>2+</sup> in water owing to different positions of the pyridine nitrogen atoms. The **76**-Ni gel turns out to be much easier to get than the gel **75**-Ni. The green gel **76**-Ni is more stable than the lavender metallohydrogel **74**-Ni (Fig. 3.28). The coordination mode between Ni and the gelator precursors is the key

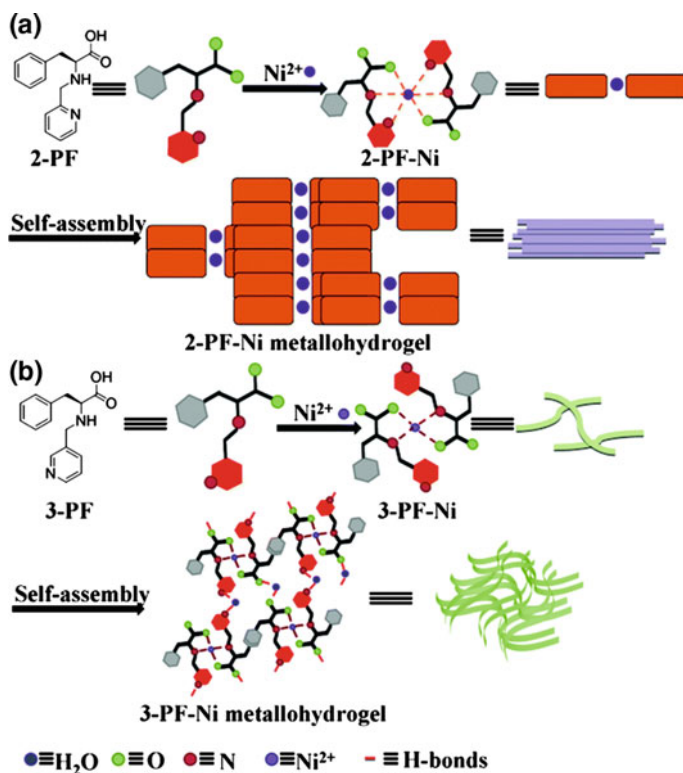
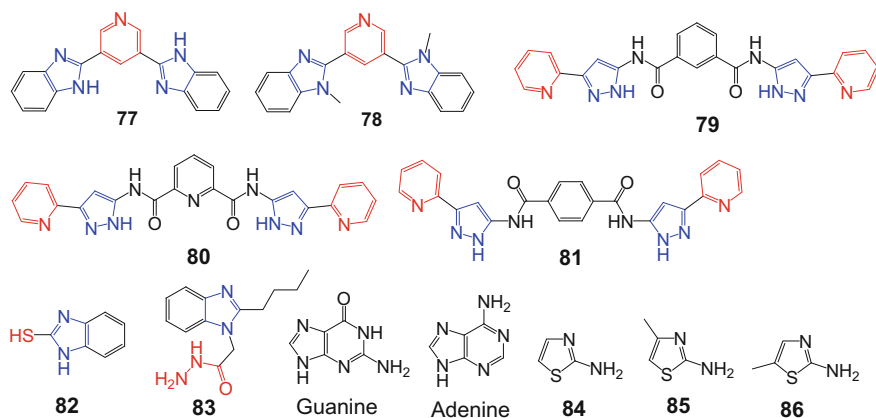


**Fig. 3.28** Schematic representations of the probable local structures for **a** **74**-Ni **b** **75**-Ni metal-organic gels. Reprinted with permission from [100]. Copyright © 2016, Royal Society of Chemistry

to determine the gelation pathway, which finally leads to the individual functional properties of gels. **74** serves as a tridentate ligand and binds  $\text{Ni}^{2+}$  to form a hexacoordination compound. **74** first self-assembles into flake-like fibres after the addition of  $\text{Ni}^{2+}$ . Then the fibres aggregate to rod-like clusters. Differently, **75** binds  $\text{Ni}^{2+}$  to form a tetra-coordination compound as a bidentate ligand by carboxyl oxygen and amino nitrogen atoms.

Metal-organic gels of **76** (Scheme 3.16) with terpyridine and carboxylic motifs were reported by Li and co-workers [101]. **76** reacts with zinc sulphate to induce gelation in the presence of  $\text{NEt}_3$ . In the gelation, **76** links two  $\text{Zn}^{2+}$  ions via monodentate carboxylate and the tridentate chelating terpyridyl to form a one-dimensional chain with the assistance of  $\text{NEt}_3$ .  $\text{Zn}^{2+}$ -**76** coordination,  $\pi$ - $\pi$  stacking between the benzene ring and  $\text{Zn} \cdots \text{Zn}$  interactions play vital roles in the gelation. The Zn gels have excellent visual recognition for anions, including  $\text{F}^-$ ,  $\text{Br}^-$ ,  $\text{I}^-$ ,  $\text{SCN}^-$ ,  $\text{N}_3^-$ ,  $\text{CO}_3^{2-}$  and  $\text{PO}_4^{3-}$ , because of the affinity of anions to  $\text{Zn}^{2+}$  ion centre in the MOGs.



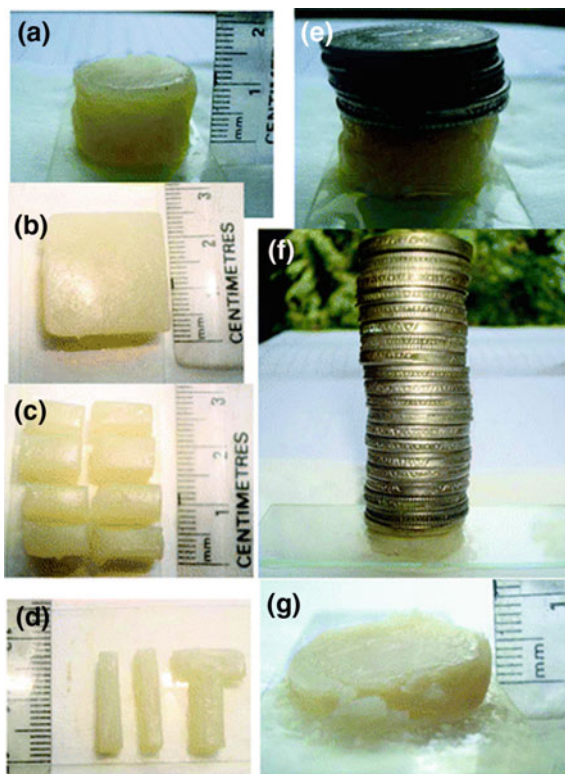
**Scheme 3.17** Molecular structures of **77–86**, guanine and adenine

Metal–organic gels of pyridyl containing bis(benzimidazole) ligand, namely pyridine-3,5-bis(benzimidazole-2-yl) (**77**, Scheme 3.17), with  $\text{Cu}^{2+}$  and  $\text{Cd}^{2+}$  metal halide salts in alcohols were developed by Biradha and co-workers [102]. The gels have typical intertwining 3D fibrous networks and are sensitive to mechanical stimuli, showing thixotropic behaviour (Fig. 3.29). Additionally, the gels have significantly high mechanical strength and exhibit self-sustainability. Pyridine-3,5-bis(1-methyl-benzimidazole-2-yl) (**78**, Scheme 3.17) also forms metal–organic gels upon reaction with  $\text{CuCl}_2$ ,  $\text{CuBr}_2$  or  $\text{CdBr}_2$  in alcoholic solutions [103]. The gels exhibit self-sustainability as well. In comparison, the gel materials of **77** are firmer than those of **78**, because **78** contains only coordinating functionality but not a hydrogen bonding donor (N–H group) group.

A series of gels of pyridine-pyrazole-based amide derivatives **79–81** (Scheme 3.17) have been investigated by Mondal and co-workers [104]. The ligands form gels in the presence of copper salt. **79** is highly selective towards copper halides only and can gelate copper halides in DMF–water (v:v 3:2), making it a good candidate for both selective cation and anion capture. The addition of  $\text{Pb}^{2+}$  and  $\text{Cd}^{2+}$  (toxic metals) to **80** results in the formation of metallogels, respectively [105]. Formation of coordination polymer, hydrogen bonding between amide moieties and  $\pi$ – $\pi$  interactions are responsible for gel formation. The metallogel formed by mixing **81** with copper triflate is highly stable towards heat, mineral acids and mechanical stress thus showing self-sustainability [106]. And the xerogels made from the metallogels of **80** and **81** are capable of absorbing the toxic dyes, which means it can remove not only toxic metals but also toxic dyes in waste water.

A metallogel have been fabricated by 2-mercaptobenzimidazole (**82**, Scheme 3.17) and copper(II) chloride in alcoholic medium, involving one-electron reduction of  $\text{Cu}^{2+}$  to  $\text{Cu}^+$  by 2-MBIm via  $\text{Cu}^+$ –ligand coordination and extensive hydrogen-bonding interactions involving the “–NH” protons (of 2-MBIm ligand) [107]. The N–H protons of **82** provide the formation of N–H...S and N–H...Cl

**Fig. 3.29** Self-sustaining behaviour of  $77\text{-CdBr}_2$  gel. Reprinted with permission from [102]. Copyright © 2012, American Chemical Society



hydrogen bonds throughout the whole structure. To operate between the **82** molecules as the molecules keep packed in the gel matrix,  $\pi$ - $\pi$  stacking interaction is also needed. In brief, these interactions make the supramolecular gel assembly. This gel exhibited stimuli-responsive behaviour towards various chemical stimuli (pH, selective metal ions and anions, selective complexing agents, etc.). The Cu(I) metal centre provides this gel with an excellent opportunity to remove Cr(VI) ions from aqueous solution effectively (Fig. 3.30). The removal capacity could reach at  $\sim 331 \text{ mg g}^{-1}$  at pH  $\sim 2.7$ .

A green-light-emitting metal-organic gel has been prepared with  $\text{Tb}^{3+}$  and hydrazide-functionalized benzimidazole ligand **83** (Scheme 3.17) [108]. Different luminescence is observed in the gel state and xerogel due to the different amount of water. In the xerogel, the luminescence of  $\text{Tb}^{3+}$  is sensitized because of the high energy transfer efficiency from **83** to  $\text{Tb}^{3+}$  in the absence of excess water. However, in the wet gel state, the luminescence of  $\text{Tb}^{3+}$  is quenched by water. The obtained quantum yields of the wet gel state and xerogel were 34.6 and 14.2%, respectively. The lower quantum yield of the xerogel is ascribed to the less efficient non-radioactive relaxation processes.

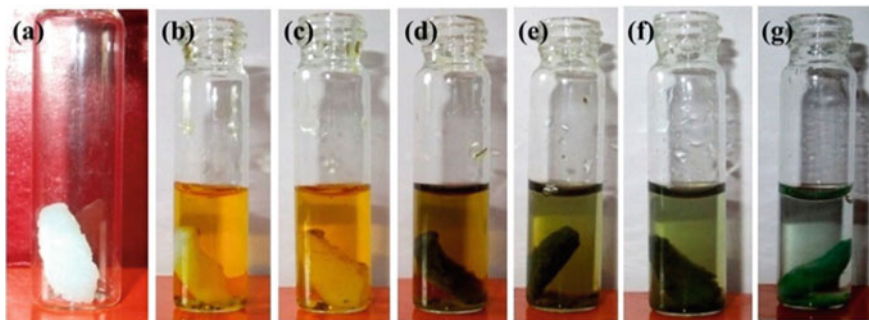


**Fig. 3.30** Successive reduction of Cr(VI) to Cr(III) **b–g** at room temperature with a small piece of the freeze-dried metal–organic gel **a** when this is incubated in an aqueous solution of  $\text{K}_2\text{Cr}_2\text{O}_7$ . Reprinted with permission from [107]. Copyright © 2014, American Chemical Society

A series of metallogels through spontaneous self-assembly of unsubstituted nucleobases with  $\text{Ag}^+$  ions were reported by Pathak, Sarma and co-workers [109]. The metallohydrogels with 3D fibrous networks are obtained by simple introduction of  $\text{Ag}^+$  to a deprotonated solution of adenine, cytosine, thymine or uracil.  $\text{Ag}^+$ -induced hydrogelation of guanine only occurs under acidic conditions. However, gelation of guanine induced by  $\text{Ag}^+$  only occurs under acidic conditions through the self-assembly of nanoscale metal–organic particles. The resulting metallogels exhibits in situ reduction of Ag salts to yield  $\text{Ag}^+$  nanoparticles decorated with the gel nanofibres, which may be used in recognition and catalysis area. The hydrogels show excellent antimicrobial properties against gram-positive and gram-negative bacteria using basic biological building units.

A class of  $\text{Hg}^{2+}$  metal–organic gels form based on aminothiazole ligands (**84–86**, Scheme 3.17) with  $\text{Hg}(\text{OAc})_2$  [110]. Suitable positioning of the methyl group in **85** on the thiazole moiety enhances the gelation behaviour because of additional participation of methyl protons in hydrogen bonding besides the thiazole ring proton. The methyl functional group plays a key role in controlling and enhancing the gelation behaviour. So **85**-Hg gel has better strength than **84**-Hg gel. **84** and **85** can remove and visually detect mercury in polluted water because mercury forms stable metallogels with them and then the resulting metallogels can be easily separated by skimming off or filtering from contaminated water. Once mercury-polluted water is treated with a 1 wt% (w/v) solution of **85** in chloroform at room temperature, a metallogel is formed at the interface. The detection limits can be as low as 0.1 ppm with visual observation in a biphasic system of  $\text{H}_2\text{O}$ – $\text{CHCl}_3$ . Both **84** and **85** are able to remove almost quantitative of  $\text{Hg}^{2+}$  ions from polluted water.

### 3.3 Applications

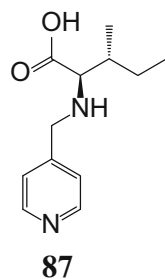
#### 3.3.1 Gels as Crystallization Media

Pyridyl functionalized L-isoleucine ligand **87** (Scheme 3.18) reacts with  $\text{Zn}^{2+}$  to induce metal–organic hydrogels at room temperature [111, 112]. The gels with  $\text{Zn}(\text{NO}_3)_2 \cdot 6\text{H}_2\text{O}$  or  $\text{Zn}(\text{ClO}_4)_2 \cdot 6\text{H}_2\text{O}$  display an interesting (opaque gel)-to-(transparent gel) transition [111]. The gel of **87** with  $\text{Zn}(\text{OAc})_2 \cdot 2\text{H}_2\text{O}$  in 1:2 stoichiometric ratio shows thermal gel-sol-gel transition when the gel was heated to  $45 \pm 1^\circ\text{C}$  and then spontaneous cooling. Meanwhile, this gel also shows remarkable self-healing properties. Moreover, it can be transformed into six different crystalline metal–organic frameworks (MOFs) by selective picking of anions (Fig. 3.31). After the gel were layered with an aqueous solution of sodium or potassium salts with different anions ( $\text{Cl}^-$ ,  $\text{Br}^-$ ,  $\text{OAc}^-$ ,  $\text{NO}_3^-$ ,  $\text{OTs}^-$ ,  $\text{N}_3^-$ ) in 1:1 stoichiometric ratio MOF crystals was observed at the interface within 2–3 days. The resulting **87**- $\text{Zn}^{2+}$  MOFs have one-dimensional chain or three-dimensional network structures.

The gel of **87** (Scheme 3.18) with  $\text{Zn}(\text{OAc})_2 \cdot 2\text{H}_2\text{O}$  has been also used to in situ synthesize cadmium sulfide (CdS) quantum dots (<10 nm in size) [113]. After the gel is doped with the precursors ( $\text{CdCl}_2$  and  $\text{Na}_2\text{S}$  aqueous solution), it shows tunable luminescence with time, owing to gradual increments in the size of CdS in the gel matrix. The luminescence colour becomes persistent if the doped gel is converted into xerogel. In addition, the CdS incubated **87** gel can easily be transformed into a CdS-loaded MOF by simple addition of chloride salt (e.g.  $\text{NaCl}$ ,  $\text{KCl}$ ,  $\text{NH}_4\text{Cl}$ ) (Fig. 3.32). These CdS embedded MOFs can be utilized as photocatalysts invisible light water-splitting reactions.

Efficient conversion of viable Fe-BTC gels into Fe-MOFs has been achieved by  $\text{PdCl}_2$ -mediated gel degradation [114]. The Fe-MOFs (two new MOFs, Fe-Pd-BTC-DEF and Fe-BTC-NMF, and a known Fe-BTC-DMF MOF) resulting from the degradation of the metallogels show different structure in the solvent (NMF, DMF or DEF) due to oxidation–reduction quality of the solvent (Fig. 3.33). The reaction was monitored on Fe-BTC-DMF gel by gas chromatography. On addition of  $\text{PdCl}_2$ , evolution of  $\text{CO}_2$  and  $\text{CO}$  along with traces of  $\text{H}_2$  was observed, so a

**Scheme 3.18** Molecular structure of **87**



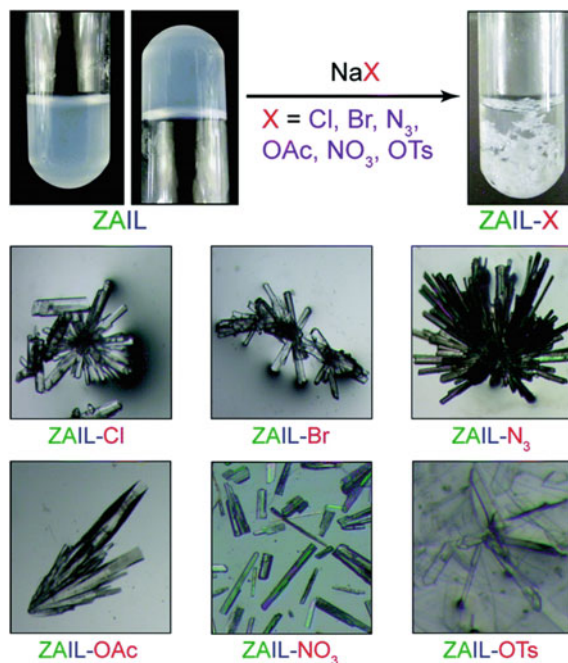


**Fig. 3.31** Synthesis of different MOFs and optical microscopy image of single crystals of MOFs. Reprinted with permission from [111]. Copyright © 2014, Royal Society of Chemistry

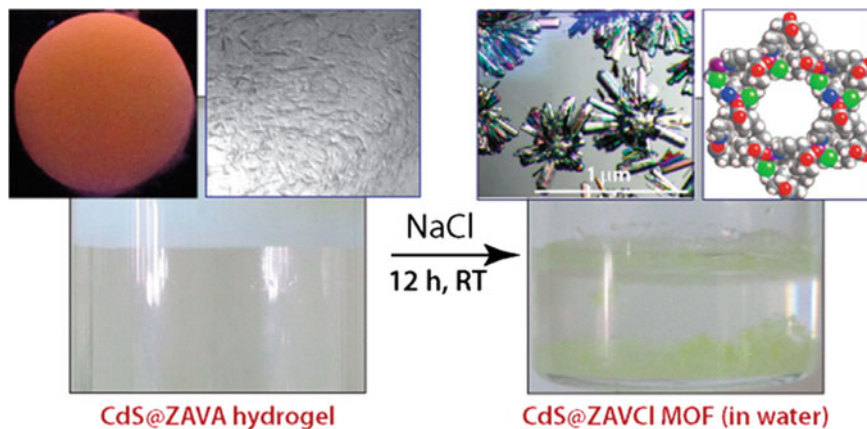


**Fig. 3.32** Room temperature transformation of CdS-loaded **87**-Zn(OAc)<sub>2</sub> gel into CdS-loaded MOF. Reprinted with permission from [113]. Copyright © 2014, American Chemical Society

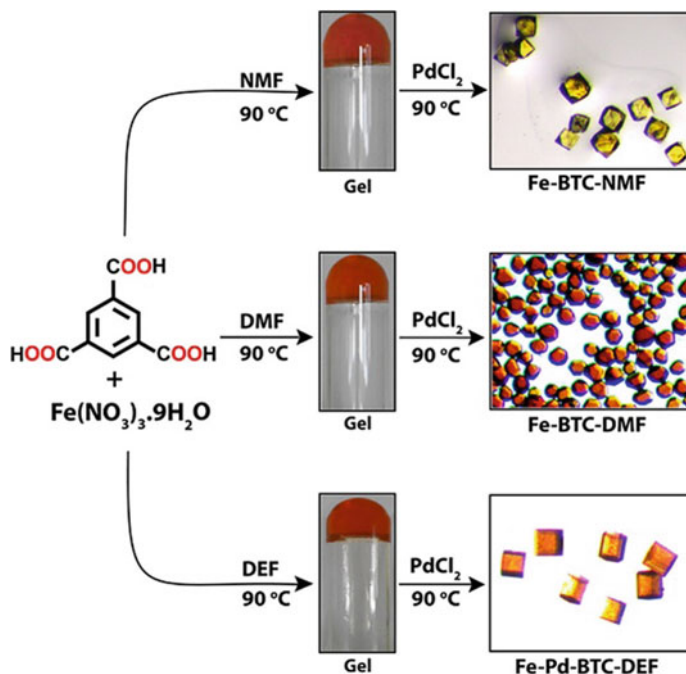


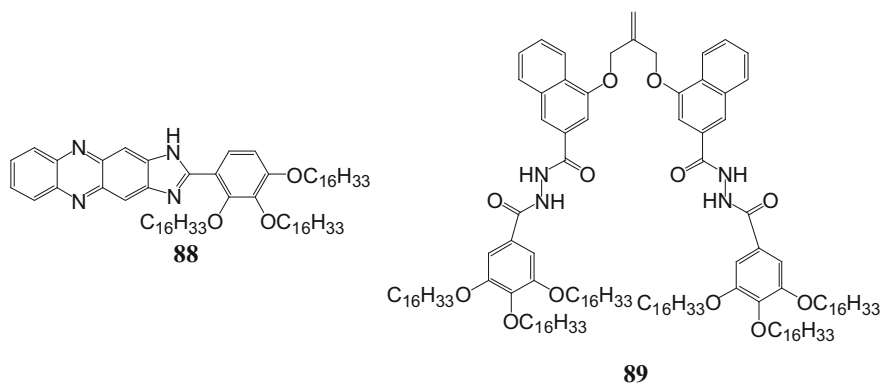
**Fig. 3.33** Schematic representation of conversion of Fe-metallogel into Fe-MOFs via  $\text{PdCl}_2$ -mediated gel degradation. Reprinted with permission from [114]. Copyright © 2014, American Chemical Society

probable mechanism is that  $\text{Pd}^{2+}$  was reduced to  $\text{Pd}^0$  by methanoic acid or DMF during the reaction, and methanoic acid was oxidized to  $\text{CO}_2$ ,  $\text{CO}$  and  $\text{H}_2$ .

The aforesaid  $\text{Zn}^{2+}$ -**76** gels can be used to synthesize Co-MOFs by  $\text{Co}^{2+}$  exchange-mediated transformation from  $\text{Zn}^{2+}$ -based gels [115]. After  $\text{CoCl}_2 \cdot 6\text{H}_2\text{O}$  solution is added to the  $\text{Zn}^{2+}$ -**76** gel and stand for 20 d, Co-MOFs crystals are gained. During the gel-to-crystal transformation,  $\text{Co}^{2+}$  occupies the site of  $\text{Zn}^{2+}$  and coordinates with **76**, leading to the formation of Co-MOFs crystal nucleus. The Co-MOFs have uniform octahedral morphology and high activity to catalyze luminol chemiluminescence without extra oxidants.

### 3.3.2 Post-modification of Organogels by Metal Ions

Subsequent introducing of metal ions in organogels may lead to gel materials with novel stimuli-responsive properties. Organogelator **88** (Scheme 3.19) with 1H-imidazo[4,5-b] phenazine moiety forms a stable and fluorescent organogel in DMF [116]. Then, the competitive coordination of  $\text{Fe}^{3+}$  with N of imidazole in the **88** gel produces a metallogel **FeG** (Fig. 3.34). The fluorescence of **88** is quenched



**Scheme 3.19** Molecular structures of **88** and **89**

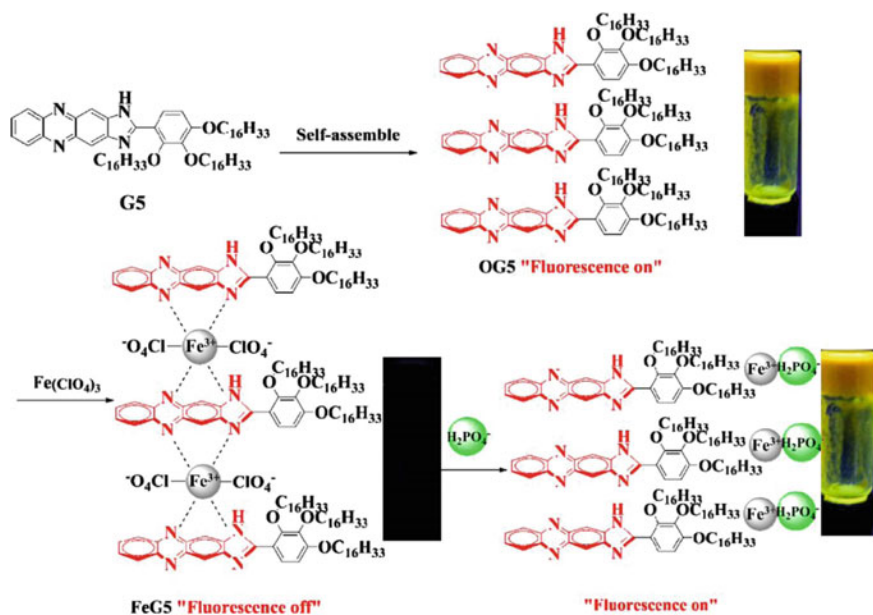


**Fig. 3.34** Proposed self-assembly and reversible stimuli-response mechanism of **88**. Reprinted with permission from [116]. Copyright © 2017 Elsevier B.V.

with the formation of **FeG**. This metallogel can sense  $\text{H}_2\text{PO}_4^-$  selectively and sensitively. The detection limit of **FeG** for  $\text{H}_2\text{PO}_4^-$  is  $1.0 \times 10^{-6} \text{ mol L}^{-1}$ . As a result, metallogel **FeG** shows potential application as a convenient and reversible  $\text{H}_2\text{PO}_4^-$  test kit.

The robust organogel of **89** (Scheme 3.19) in DMF is strong blue fluorescent. Hydrogen bonding, van der Waal forces and  $\pi$ - $\pi$  interactions between the

naphthalene moieties are responsible for the gelation [117]. Addition of  $\text{Zn}^{2+}$  produces  $\text{Zn}^{2+}$ -coordinated metallogel **89-Zn** and the fluorescence intensity of **89** gel decreases with red shift from 410 to 430 nm. In the gelation strong coordination between  $\text{Zn}^{2+}$  and both of N-atoms and O-atoms of the hydrazide groups is involved. Both **89** and **89-Zn** gels show efficient and different sensing behaviours towards  $\text{F}^-$  ion without a gel–sol transition because of the variation in self-assembling nature. During the process, **89** forms fluoride-containing organogel **89-F** with variation in colour from blue to greenish yellow via strong aggregation-induced emission (AIE) phenomenon and **89-Zn** produces fluoride-containing metallogel **89-Zn-F** with modulation in colour from blue to blue green. The binding constant and the detection limit of **89-Zn** towards  $\text{F}^-$  are about  $4.0 \times 10^6 \text{ L mol}^{-1}$  and  $1.3 \times 10^{-6} \text{ mol L}^{-1}$ .

### 3.3.3 Metal–Organic Gels for Sorption

Metal-carboxylate gels show hierarchical porosity with micro- and mesoporosity. The microporosity has been applied in gas uptake [118]. Thallapally and co-workers reported that Fe-**BTC** aerogel selectively uptakes 33 wt% ( $7.5 \text{ mmol g}^{-1}$ ) of  $\text{CO}_2$  at high pressure (30 bar), while only ca. 3.5 wt% of  $\text{CH}_4$  is taken up under similar conditions. What's more, Zhang, Su and co-workers reported that Al-**BTC**/Al-**BDC** aerogels uptakes  $\text{H}_2$  up to 1.52 wt% (the total uptake is 2.52%) without saturation at 1 bar and 77 K. The aerogels display  $\text{CO}_2$  uptakes up to 61 wt% ( $308 \text{ cm}^3 \text{ g}^{-1}$ ) without saturation at 1 bar and 195 K. The aerogels also adsorb benzene up to 86% ( $247 \text{ cm}^3 \text{ g}^{-1}$ ), *n*-hexane up to 47 wt% ( $122 \text{ cm}^3 \text{ g}^{-1}$ ) and methanol up to 96 wt% ( $672 \text{ cm}^3 \text{ g}^{-1}$ ) [49].

The mesoporosity of metal-carboxylate gels can be applied in uptake of bulky molecules. Cr-**BTC** aerogel is highly efficient in the absorption of several dyes, including methyl orange, dimethyl phthalate, and methylene blue [48]. Al-**BDC** aerogels show high adsorbing capacities of up to 633.4 and 621.3  $\text{mg g}^{-1}$  for congo red (CR) and brilliant blue R-250 (BBR-250), respectively [49]. Zou and co-workers developed heterometallic MOGs based on  $\text{Fe}^{3+}$  and  $\text{Al}^{3+}$ .  $\text{Fe}^{3+}$  and  $\text{Al}^{3+}$  at the Fe/Al ratio of 1:1 react with  $\text{H}_3\text{BTC}$  to form metal–organic gels (Fig. 3.35) [119]. The corresponding aerogel shows high surface area ( $1861 \text{ m}^2 \text{ g}^{-1}$ ) and pore volume ( $9.737 \text{ cm}^3 \text{ g}^{-1}$ ). This material shows the large uptakes of dye molecules ( $290 \text{ mg g}^{-1}$  rhodamine B and  $265 \text{ mg g}^{-1}$  methyl orange) with fast sorption kinetics. So, the hierarchical gels can be used to absorb dye molecules with high efficiency. Zou and co-workers shows that Al-**BTC** gel with sufficient metal sites and carboxyl groups has strong affinity for the toxic pollutant microcystin-LR [120]. The Al-**BTC** xerogel effectively removes microcystin-LR in water and its adsorption capacity is as high as  $6861 \mu\text{g g}^{-1}$  at an initial MC-LR concentration of 10,000 ppb. Al-**BTC** aerogel shows more adsorption capacity  $9007 \text{ mg g}^{-1}$  to MC-LR at the same conditions. It indicates that it is a good material to remove microcystin-LR from the environment.

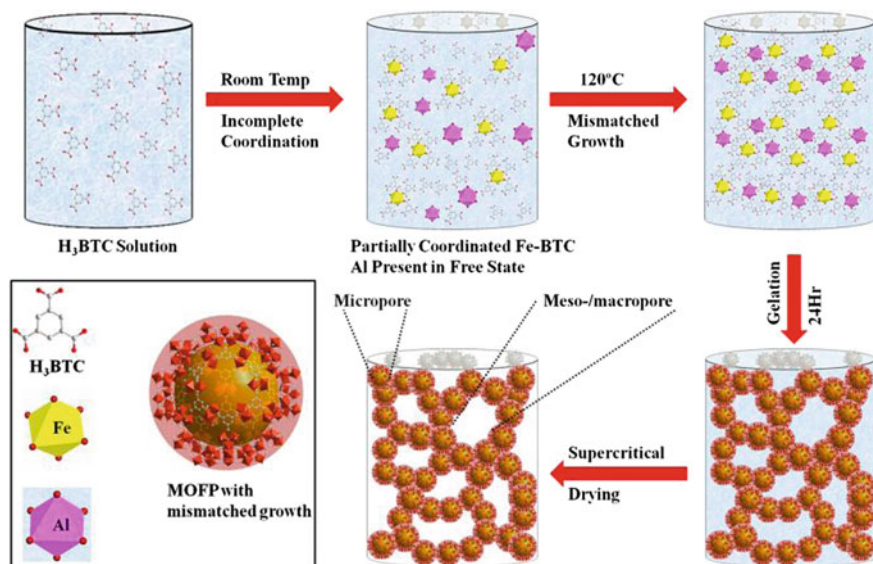


**Fig. 3.35** Heterometallic metal–organic aerogels. Reprinted with permission from [119]. Copyright © 2015, Rights Managed by Nature Publishing Group

Fe-BTC xerogel can be used as an adsorbent for arsenic removal from water [121]. Fe-BTC xerogel shows high adsorption capacity of  $57.7 \text{ mg g}^{-1}$  to  $\text{AsO}_4^{3-}$  in solution ( $\text{pH} = 4$ ) at 298 K. Kinetic studies show that the adsorption is spontaneous, the adsorption isotherms are well described with the Langmuir equation, and the kinetic data are well described by the pseudo-second-order kinetic model. Al-BTC gel provides an excellent ability to accommodate electrolyte ingredients because the sponge-like porous metal–organic skeleton can hold a considerable amount of solvent and active species of the electrolyte. It is used as quasi-solid electrolyte for dye-sensitized solar cell and shows high conversion efficiency of over 8.60% [122].

### 3.3.4 Metal–Organic Gels as Template

Metal-carboxylate gel materials are useful for templating porous materials due to their high-specific surface area and porosity. For example, Fe-BTC gel forms in the presence of methylmethacrylate, while dissolves in aqueous HCl. So it is easy to get macroporous organic polymer through Fe-BTC gel as template [47]. The Fe-BTC gel is also employed as template for synthesis of macroporous poly(glycidyl methacrylate-co-ethylene glycol dimethacrylate), which was applied in the chromatographic separation of proteins [123]. A macroporous boronate affinity monolithic column is prepared using Fe-BTC gel as a porogenic template and applied to

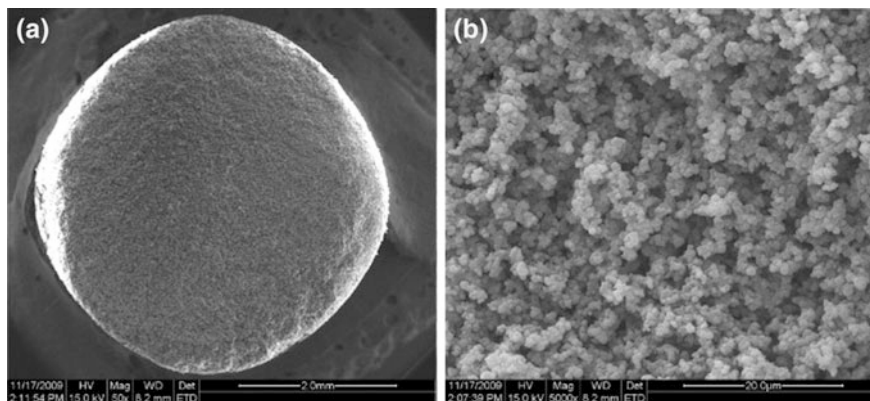


**Fig. 3.36** SEM images of macroporous boronate affinity monolithic columns at different magnifications. Reprinted with permission from [124]. Copyright © 2011 Elsevier B.V. All rights reserved

specifically capture glycoproteins, showing a higher selectivity and better dynamic binding capacity towards horseradish peroxidase and transferrin (Fig. 3.36). The resulting affinity monolithic column has been successfully employed to specifically capture transferrin from a bovine serum sample [124]. Fe-BTC gel was also employed as a porogen to prepare molecular imprinting polymer [125]. The resulting molecularly imprinted polymer has greater-specific surface areas and can be used to identify the levofloxacin in the water with high efficiency.

A gel of **90** and  $\text{AgNO}_3$  forms in the presence of *N,N'*-methylenebisacrylamide (MBA), acrylic acid (AAc) and benzoyl peroxide in THF [126]. The hybrid gel is heated at 63 °C to carry out the radical copolymerization of MBA and AAc, and the gel template is removed by excess ammonia to get P(MBA-AAc) 1D nanostructures (Fig. 3.37). The hybrid gel can also be heated at 120 °C to reduce  $\text{Ag}^+$  ions to obtain Ag nanoparticles-loaded P(MBA-AAc) nanowires. The nanowires effectively catalyze the photodegradation of methylene blue. The photodegradation of methylene blue is pH-responsive, and the rate at pH 7 is almost four times than that at pH 2.2.

Hierarchically porous carbons can be obtained through metal-organic gel templates [127]. Casted Al-BTC xerogel has hierarchical micro-meso-macro porous architectures (Fig. 3.38) with ultrahigh surface areas ( $3770 \text{ m}^2 \text{ g}^{-1}$ ), considerable hydrogen uptake (2.98 wt%) and quite large pore volume ( $2.62 \text{ cm}^3 \text{ g}^{-1}$ ). It can be used as cathode material after sulphur impregnation for lithium-sulphur battery, showing a discharge capacity of  $1240 \text{ mA h g}^{-1}$  (74% of  $1675 \text{ mA h g}^{-1}$  the theoretical value) at the 2nd cycle. Simple pyrolysis of polypyrrole-doped Al-based metal-organic gel at 800 °C produces nitrogen-doped porous carbon material (N@MOG-C) with high surface area of  $1542.6 \text{ m}^2 \text{ g}^{-1}$  and large pore volume of  $0.76 \text{ cm}^3 \text{ g}^{-1}$ . The N@MOG-C-modified electrode is able to detect  $\text{Cd}^{2+}$  ions present in concentrations of  $0.025\text{--}5 \mu\text{mol L}^{-1}$ , with a detection limit of  $2.2 \mu\text{mol L}^{-1}$  [128].

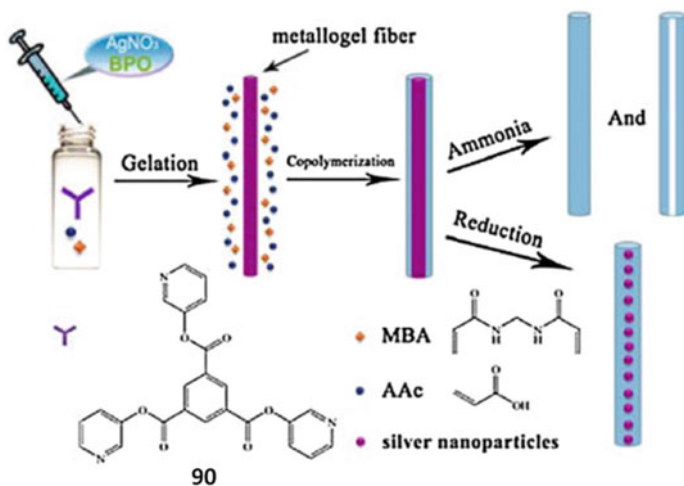


**Fig. 3.37** Illustration of the procedure for fabrication of P(MBA-AAc) 1D nanostructures and Ag NPs-loaded P(MBA-AAc) nanowires. Reprinted with permission from [126]. Copyright © 2015 Elsevier B.V. All rights reserved

### 3.3.5 Metal–Organic Gels as Catalyst

Metal–organic gels are characteristic of finite short-ranged order with periodically disordered arrangement of the building units [129–131]. When catalytically active motifs are incorporated, they have advantages such as efficient and readily accessible active centres, easy recovery, well-defined nanoscale objects (fibres), dynamic supramolecular interactions and easy modification. Metal–organic gels have been applied for various catalytic reactions with three strategies (Fig. 3.39), (a) coordination polymer gels with catalytically active centres; (b) post-modification of coordination polymer gels with catalytically active centres; (c) post-modified organogels with catalytically active centres.

The metal centres of the gel matrix may be employed as catalytically active centre. For example, The **59**-Cu<sup>+</sup> gels exhibit a high copper loading capacity and can be regarded as efficient heterogeneous catalysts for click reactions (e.g. between phenylacetylene and benzylazide) [80], and they have biodegradability and biocompatibility. The gels of Zr<sup>4+</sup> and 2-aminoterephthalic acid show activity as a heterogeneous catalyst in the chemical fixation of CO<sub>2</sub> and an excellent catalytic performance was achieved for the cycloaddition of atmospheric pressure of CO<sub>2</sub> to epoxides at 373 K [52]. The gels of dirhodium(II) are effective in the coupling reaction of CO<sub>2</sub> and epoxides as well as intramolecular C–H amination of vinyl azides [132]. The gel of Pd<sup>2+</sup> and tripodal triphosphine efficiently catalyses the Suzuki–Miyaura coupling of aryl halides and boronic acids in water [133].

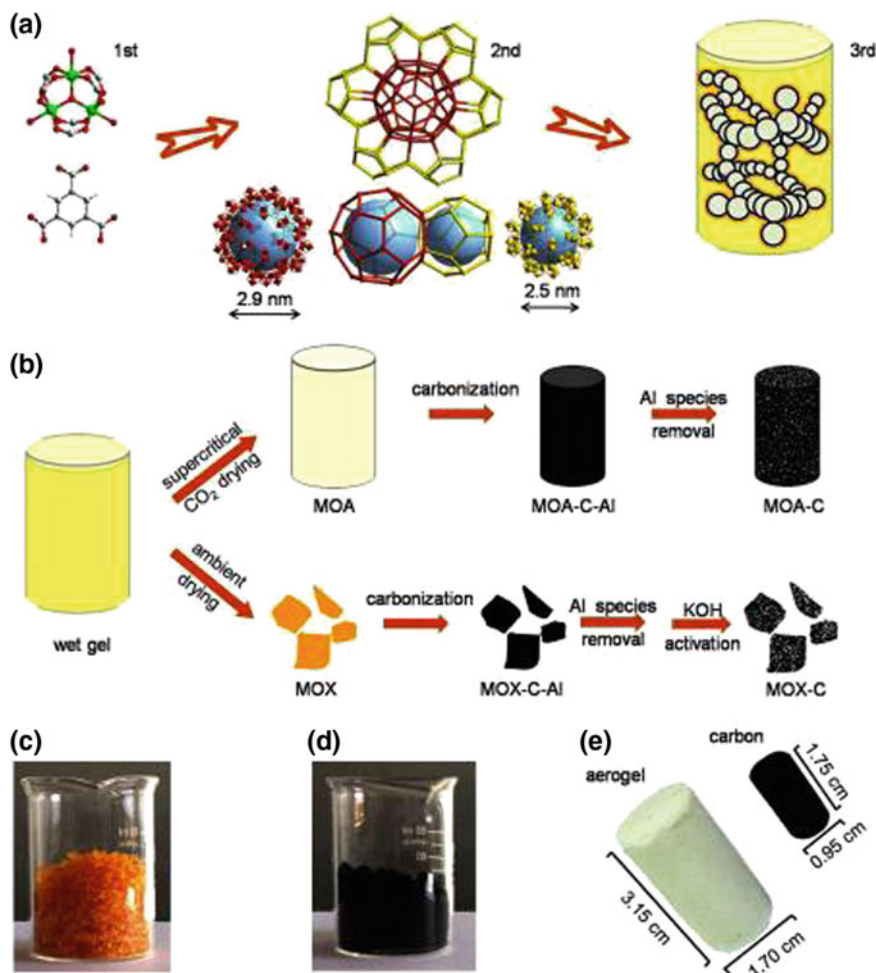


**Fig. 3.38** Fabrication of porous carbon materials from Al-based metal–organic gels. Reprinted with permission from [127]. Copyright © 2013, Rights Managed by Nature Publishing Group

Metal–organic gels may also be post-functionalized for catalysis after incorporation of catalytically active centres. For example, Fe<sup>3+</sup> gels of 5-diphenylphosphanylisophthalic acid (**91**, Scheme 3.20) are produced in alcohols or DMF [134]. Based on the hard and soft acids and bases theory, carboxyl groups in the gel are in strong binding with Fe<sup>3+</sup>, while coordination of –PPh<sub>2</sub> unit is weak. The phosphine-functionalized gel is post-modified with Pd<sup>2+</sup>, showing efficient catalytic applications in Suzuki–Miyaura cross-coupling reaction with recyclability. As a special feature of metal–organic gels, dynamic coordination bond present in metallogels can be used for post-modification. The bifunctional ligand 5-1H-benzo [d]imidazole-1,3-dicarboxylic acid **92** (Scheme 3.20) forms metal–organic gels

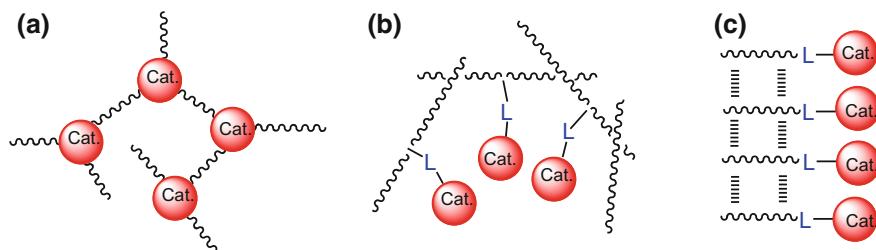
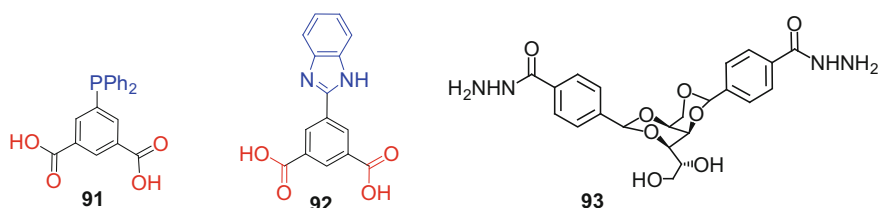


**Fig. 3.39** Schematic representation of incorporation of catalytically active centres into gel matrixes, **a** coordination polymer gels; **b** post-modification of coordination polymer gels; **c** post-modified organogels



**Scheme 3.20** Molecular structures of **91–93**

with  $\text{Fe}^{3+}$  in polar solvents [135]. The gel network is assembled by the strongly coordination between hard  $\text{Fe}^{3+}$  ion and the carboxyl groups, while  $\text{Fe}^{3+}$  coordinate to the imidazole group less strongly based on the hard and soft acids and bases theory. When  $\text{Pd}^{2+}$  is introduced, Pd–N bond may form in the gel network. The  $\text{Pd}^{2+}$ -functionalized gel exhibits significantly improved activity in Suzuki–Miyaura cross-coupling and could be recovered and reused several times.

Supramolecular organogels may be post-modified with catalytically active centres for catalytic applications. Smith and co-workers reported that gelator **93** (Scheme 3.20) forms a pH-stable hydrogel by a simple heat–cool cycle [136]. The hydrogel shows preferential uptake of precious heavy metals (gold/silver salts) from metal-ion mixtures. Reduction in situ of the ions results in Au or Ag nanoparticles with high loading on the gel nanofibres. The conductive hybrid materials can be used to modify electrode surfaces. Cyclic voltammetry of the modified electrode shows a large reductive current at potentials more negative than  $-0.2$  V versus SCE, which is attributed to Au-catalyzed  $\text{O}_2$  reduction.

## References

1. Rest C, Mayoral MJ, Fucke K, Schellheimer J, Stepanenko V, Fernández G (2014) Self-assembly and (hydro)gelation triggered by cooperative  $\pi$ - $\pi$  and unconventional C-H...X hydrogen bonding interactions. *Angew Chem Int Ed* 53:700-705
2. Rest C, Martin A, Stepanenko V, Allampally NK, Schmidt D, Fernández G (2014) Multiple CH...O interactions involving glycol chains as driving force for the self-assembly of amphiphilic Pd(II) complexes. *Chem Commun* 50:13366-13369
3. Hafkamp RJH, Kokke BPA, Danke IM, Geurts HPM, Rowan AE, Feiters MC, Nolte RJM (1997) Organogel formation and molecular imprinting by functionalized gluconamides and their metal complexes. *Chem Commun* 545
4. Dawn A, Andrew KS, Yufit DS, Hong Y, Reddy JP, Jones CD, Aguilar JA, Steed JW (2015) Supramolecular gel control of cisplatin crystallization: identification of a new solvate form using a cisplatin-mimetic gelator. *Cryst Growth Des* 15:4591-4599
5. Liu Z, Feng Y, Zhao Z, Yan Z, He Y, Luo X, Liu C, Fan Q (2014) A new class of dendritic metallogels with multiple stimuli-responsiveness and as templates for the in situ synthesis of silver nanoparticles. *Chem Eur J* 20:533-541
6. Taira T, Suzuki Y, Osakada K (2013) Metallohydrogel formed from amphiphilic Pd complex and  $\alpha$ -cyclodextrin: control of its sol-gel transition. *Chem Lett* 42:1062-1064
7. Dey S, Datta D, Chakraborty K, Nandi S, Anoop A, Pathak T (2013) A coordination-assisted general approach to nickel-based nanometallogels. *RSC Adv* 3:9163-9166
8. Araujo M, Escuder B (2017) Transient catalytic activity of a triazole-based gelator regulated by molecular gel assembly/disassembly. *Chem Select* 2:854-862
9. Ghosh K, Panja S, Bhattacharya S (2017) Visual sensing of  $\text{Ag}^+$  ions through gelation of cholesterol-appended benzimidazole and associated ion conducting behaviour. *Chem Select* 2:959-966
10. Shirakawa M, Fujita N, Tani T, Kaneko K, Shinkai S (2005) Organogel of an 8-quinolinol platinum(II) chelate derivative and its efficient phosphorescence emission effected by inhibition of dioxygen quenching. *Chem Commun* 4149
11. Miao W, Zhang L, Wang X, Cao H, Jin Q, Liu M (2013) A dual-functional metallogel of amphiphilic Copper(II) quinolinol: redox responsiveness and enantioselectivity. *Chem Eur J* 19:3029-3036
12. Miao W, Zhang L, Wang X, Qin L, Liu M (2013) Gelation-induced visible supramolecular chiral recognition by fluorescent metal complexes of quinolinol-glutamide. *Langmuir* 29:5435-5442
13. Zhang Y, Zhang B, Kuang Y, Gao Y, Shi J, Zhang X, Xu B (2013) A redox responsive, fluorescent supramolecular metallohydrogel consists of nanofibers with single-molecule width. *J Am Chem Soc* 135:5008-5011
14. Mitsumoto K, Cameron JM, Wei R, Nishikawa H, Shiga T, Nihei M, Newton GN, Oshio H (2017) A multi-redox responsive cyanometalate-based metallogel. *Chem Eur J* 23:1502-1506
15. Cametti M, Cetina M, Džolić Z (2015) Cu(II)-specific metallogel formation by an amido-anthraquinone-pyridyloxalamide ligand in DMSO-water. *Dalton Trans* 44:7223-7229
16. Bühler G, Feiters MC, Nolte RJM, Dötz KH (2003) A metal-carbene carbohydrate amphiphile as a low-molecular-mass organometallic gelator. *Angew Chem Int Ed* 42:2494-2497
17. Hsu THT, Naidu JJ, Yang BJ, Jang MY, Lin IJB (2012) Self-assembly of silver(I) and gold (I) N-heterocyclic carbene complexes in solid state, mesophase, and solution. *Inorg Chem* 51:98-108
18. Klawonn T, Gansäuer A, Winkler I, Lauterbach T, Franke D, Nolte RJM, Feiters MC, Börner H, Hentschel J, Dötz KN (2007) A tailored organometallic gelator with enhanced amphiphilic character and structural diversity of gelation. *Chem Commun* 1894
19. Gansäuer A, Winkler I, Klawonn T, Nolte RJM, Feiters MC, Börner HG, Hentschel J, Dötz KH (2009) Novel organometallic gelators with enhanced amphiphilic character: structure-property correlations, principles for design, and diversity of gelation. *Organometallics* 28:1377

20. Tu T, Assenmacher W, Peterlik H, Weisbarth R, Nieger M, Dötz KH (2007) An air-stable organometallic low-molecular-mass gelator: synthesis, aggregation, and catalytic application of a palladium pincer complex. *Angew Chem Int Ed* 46:6368
21. Tu T, Bao X, Assenmacher W, Peterlik H, Daniels J, Dötz KH (2009) Efficient air-stable organometallic low-molecular-mass gelators for ionic liquids: synthesis, aggregation and application of pyridine-bridged bis(benzimidazolylidene)-palladium complexes. *Chem Eur J* 15:1853
22. Ogata K, Sasano D, Yokoi T, Isozaki K, Yoshida R, Takenaka T, Seike H, Ogawa T, Kurata H, Yasuda N, Takaya H, Nakamura M (2013) Synthesis and self-assembly of NCN-pincer Pd-complex-bound norvalines. *Chem Eur J* 19:12356–12375
23. Tu T, Fang W, Bao X, Li X, Dötz KH (2011) Visual chiral recognition through enantioselective metallogel collapsing: synthesis, characterization, and application of platinum-steroid low-molecular-mass gelators. *Angew Chem Int Ed* 50:6601
24. Afrasiabi R, Kraatz H (2015) Rational design and application of a redox-active, photoresponsive, discrete metallogelator. *Chem Eur J* 21:7695–7700
25. He T, Li K, Wang N, Liao Y, Wang X, Yu X (2014) A ferrocene-based multiple-stimuli responsive organometallogel. *Soft Matter* 10:3755–3761
26. Liu J, He P, Yan J, Fang X, Peng J, Liu K, Fang Y (2008) An organometallic super-gelator with multiple-stimulus responsive properties. *Adv Mater* 20:2508
27. Liu J, Yan J, Yuan X, Liu K, Peng J, Fang Y (2008) A novel low-molecular-mass gelator with a redox active ferrocenyl group: tuning gel formation by oxidation. *J Colloid Interface Sci* 318:397
28. Sahoo P, Kumar DK, Trivedi DR, Dastidar P (2008) An easy access to an organometallic low molecular weight gelator: a crystal engineering approach. *Tetrahedron Lett* 49:3052
29. Yadav YJ, Heinrich B, Luca GD, Talarico AM, Mastropietro TF, Ghedini M, Donnio B, Szerb EI (2013) Chromonic-like physical luminescent gels formed by ionic octahedral Iridium(III) complexes in diluted water solutions. *Adv Optical Mater* 1:844–854
30. Siu SKL, Po C, Yim KC, Au VKM, Yam VWW (2015) Synthesis, characterization and spectroscopic studies of luminescent l-valine modified alkynyl-based cyclometalated gold (iii) complexes with gelation properties driven by  $\pi$ - $\pi$  stacking, hydrogen bonding and hydrophobic-hydrophobic interactions. *Cryst Eng Comm* 17:8153–8162
31. Wu NW, Zhang J, Xu XD, Yang HB (2014) Design and preparation of ethynyl-pyrene modified platinum-acetylidogelators and their application in dispersion of graphene. *Chem Commun* 50:10269–10272
32. Tatikonda R, Bhowmik S, Rissane K, Haukka M, Cametti M (2016) Metallogel formation in aqueous DMSO by perfluoroalkyl decorated terpyridine ligands. *Dalton Trans* 45:12756–12762
33. Chen X, Huang Z, Chen SY, Li K, Yu XQ, Pu L (2010) Enantioselective gel collapsing: a new means of visual chiral sensing. *J Am Chem Soc* 132:7297–7299
34. Bhowmik S, Ghosh BN, Marjomäki V, Rissanen K (2014) Nanomolar pyrophosphate detection in water and in a self-assembled hydrogel of a dimple terpyridine-Zn<sup>2+</sup> complex. *J Am Chem Soc* 136:5543–5546
35. Fang W, Sun Z, Tu T (2013) Novel supramolecular thixotropic metallohydrogels consisting of rare metal-organic nanoparticles: synthesis, characterization, and mechanism of aggregation. *J Phys Chem C* 117:25185–25194
36. Fang W, Liu X, Lu Z, Tao T (2014) Photoresponsive metallo-hydrogels based on visual discrimination of the positional isomers through selective thixotropic gel collapse. *Chem Commun* 50:3313–3316
37. Fang W, Liu C, Chen J, Lu Z, Li ZM, Bao X, Tu T (2015) The electronic effects of ligands on metal-coordination geometry: a key role in the visual discrimination of dimethylaminopyridine and its application towards chemo-switch. *Chem Commun* 51(20):4267–4270

38. Jie K, Zhou Y, Shi B, Yao Y (2015) A Cu<sup>2+</sup> specific metallohydrogel: preparation, multi-responsiveness and pillar[5]arene-induced morphology transformation. *Chem Commun* 51:8461–8464
39. Biswas A, Dubey M, Mukhopadhyay S, Kumar A, Pandey DS (2016) Anion triggered metallohydrogels: demetalation and crystal growth inside the gel matrix and improvement in viscoelastic properties using Au-NPs. *Soft Matter* 12:2997–3003
40. Po C, Ke Z, Tam AYY, Chow HF, Yam VWW (2013) A Platinum(II) terpyridine metallohydrogel with an L-valine-modified alkynyl ligand: interplay of Pt...Pt,  $\pi$ - $\pi$  and hydrogen-bonding interactions. *Chem Eur J* 19:15735–15744
41. Peng Z, Yuan D, Jiang Z, Li Y (2017) Novel metal-organic gels of bis (benzimidazole)-based ligands with copper(II) for electrochemical selectively sensing of nitrite. *Electrochim Acta* 238:1–8
42. Chan MHY, Ng M, Leung SYL, Wai HL, Yam VWW (2017) Synthesis of luminescent Platinum(II) 2,6-bis(N-dodecylbenzimidazol-2'-yl) pyridine foldamers and their supramolecular assembly and metallohydrogel formation. *J Am Chem Soc* 139:8639–8645
43. Ganta S, Chand DK (2015) Nanoscale metallohydrogel via self-assembly of self-assembled trinuclear coordination rings: multi-stimuli-responsive soft materials. *Dalton Trans* 44:15181–15188
44. Howlader P, Mukherjee PS (2016) Face and edge directed self-assembly of Pd 12 tetrahedral nano-cages and their self-sorting. *Chem Sci* 7:5893–5899
45. Qin L, Wang P, Guo Y, Chen C, Liu M (2015) Self-assembled soft nanomaterials via Silver (I)-coordination: nanotube, nanofiber, and remarkably enhanced antibacterial effect. *Adv Sci* 2(11):1500134
46. Yan X, Cook TR, Pollock JB, Wei P, Zhang Y, Yu Y, Huang F, Stang PJ (2014) Responsive supramolecular polymer metallohydrogel constructed by orthogonal coordination-driven self-assembly and host/guest interactions. *J Am Chem Soc* 136:4460–4463
47. Wei Q, James SL (2005) A metal-organic gel used as a template for a porous organic polymer. *Chem Commun* 1555–1556
48. Xiang S, Li L, Zhang J, Tan X, Cui H, Shi J, Hu Y, Chen L, Su C, James SL (2012) Porous organic-inorganic hybrid aerogels based on Cr<sup>3+</sup>/Fe<sup>3+</sup> and rigid bridging carboxylates. *J Mater Chem* 22:1862–1867
49. Li L, Xiang S, Cao S, Zhang J, Ouyang G, Chen L, Su C (2013) A synthetic route to ultralight hierarchically micro/mesoporous Al(III)-carboxylate metal-organic aerogels. *Nat Commun* 4:1774
50. Lohe MR, Rose M, Kaskel S (2009) Metal-organic framework (MOF) aerogels with high micro- and macroporosity. *Chem Commun* 6056–6058
51. Rose M, Weber D, Lotsch BV, Kremer RK, Goddard R, Palkovits R (2013) Biogenic metal-organic frameworks: 2,5-furandicarboxylic acid as versatile building block. *Microporous Mesoporous Mater* 18:217–221
52. Liu L, Zhang J, Fang H, Chen L, Su C (2016) Metal-organic gel material based on UiO-66-NH<sub>2</sub> nanoparticles for improved adsorption and conversion of CO<sub>2</sub>. *Chem Asian J* 11:2278–2283
53. Chaudhari AK, Han I, Tan JC (2015) Multifunctional supramolecular hybrid materials constructed from hierarchical self-ordering of in situ generated metal-organic framework (MOF) nanoparticles. *Adv Mater* 27:4438–4446
54. Liao P, Fang H, Zhang J, Hu Y, Chen L, Su C (2017) Transforming HKUST-1 metal-organic frameworks into gels-stimuli-responsiveness and morphology evolution. *Eur J Inorg Chem* 19:2580–2584
55. Saha S, Schön EM, Cativiela C, Díaz DD, Banerjee R (2013) Proton-conducting supramolecular metallohydrogels from the lowest molecular weight assembler ligand: a quote for simplicity. *Chem Eur J* 19:9562–9568
56. Feldner T, Häring M, Saha S, Esquena J, Banerjee R, Díaz DD (2016) Supramolecular metallohydrogel that imparts self-healing properties to other gel networks. *Chem Mater* 28:3210–3217

57. Knichal JV, Gee WJ, Burrows AD, Raithby PR, Wilson CC (2015) A new small molecule gelator and 3D framework ligator of lead(II). *Cryst Eng Comm* 17:8139–8145
58. Banerjee S, Adarsh NN, Dastidar P (2012) A crystal engineering rationale in designing a Cd<sup>II</sup> coordination polymer based metallogel derived from a C<sub>3</sub> symmetric tris-amide-tris-carboxylate ligand. *Soft Matter* 8:7623–7629
59. Luisi BS, Rowland KD, Moulton B (2007) Coordination polymer gels: synthesis, structure and mechanical properties of amorphous coordination polymers. *Chem Commun* 2802
60. Kim KY, Park S, Jung SH, Lee SS, Park KM, Shinkai S, Jung JH (2014) Geometric change of a thiocalix [4] are nesupramolecular gel with volatile gases and its chromogenic detection for rapid analysis. *Inorga Chem* 53:3004–3011
61. Hwang D, Lee E, Jung JH, Lee SS, Park KM (2013) Formation of calix[4]arene-based supramolecular gels triggered by K<sup>+</sup> and Rb<sup>+</sup>: exemplification of a structure-property relationship. *Cryst Growth Des* 13:4177–4180
62. Aiyappa HB, Saha S, Wadge P, Banerjee R, Kurungot S (2015) Fe(III) phytate metallogel as a prototype anhydrous, intermediate temperature proton conductor. *Chem Sci* 6:603–607
63. Rahim M, Björnalm M, Suma T, Faria M, Ju Y, Kempe K, Caruso F (2016) Metal-phenolic supramolecular gelation. *Angew Chem Int Ed* 55:13803–13807
64. Yang Q, Tan X, Wang S, Zhang J, Chen L, Zhang JP, Su CY (2014) Porous organic-inorganic hybrid aerogels based on bridging acetylacetonate. *Microporous and Mesoporous Mater* 187:108–113
65. Dhara B, Ballav N (2013) In situ generation of conducting polymer in a redoxactive metal-organic gel. *RSC Adv* 3:4909–4913
66. Dhara B, Sappati S, Singh SK, Kurungot S, Ghosh P, Ballav N (2016) Coordination polymers of Fe(III) and Al(III) ions with TCA ligand: distinctive fluorescence, CO<sub>2</sub> uptake, redox-activity and oxygen evolution reaction. *Dalton Trans* 45:6901–6908
67. Dhara B, Patra PP, Jha PK, Jadhav VS, Pavan Kumar GV, Ballav N (2014) Redox-induced photoluminescence of metal-organic coordination polymer gel. *J Phys Chem C* 118:19287–19293
68. Wei SC, Pan M, Li K, Wang S, Zhang J, Su CY (2014) A multistimuli-responsive photochromic metal-organic gel. *Adv Mater* 26:2072–2077
69. Mukhopadhyay RD, Praveen VK, Hazra A, Maji TK, Ajayaghosh A (2015) Light driven mesoscale assembly of a coordination polymeric gelator into flowers and stars with distinct properties. *Chem Sci* 6:6583–6591
70. Li H, Zhu Y, Zhang J, Chi Z, Chen L, Su CY (2013) Luminescent metal-organic gels with tetraphenylethylene moieties: porosity and aggregation-induced emission. *RSC Adv* 3:16340–16344
71. Barman S, Garg JA, Blacque O, Venkatesan K, Berke H (2012) Triptycene based luminescent metal-organic gels for chemosensing. *Chem Commun* 48:11127–11129
72. Feng X, Zeng L, Zou D, Zhang Z, Zhong G, Peng S, Zhang J (2017) Trace-doped metal-organic gels with remarkably enhanced luminescence. *RSC Adv* 7:37194–37199
73. Eicher T, Hauptmann S, Speicher A (2012) The chemistry of heterocycles. Wiley-VCH Verlag GmbH & Co., KGaA, Weinheim
74. Kim HJ, Lee JH, Lee M (2005) Stimuli-responsive gels from reversible coordination polymers. *Angew Chem Int Ed* 44:5810–5814
75. Adarsh NN, Dastidar P (2010) A new series of Zn<sup>II</sup> coordination polymer based metallogels derived from bis-pyridyl-bis-amide ligands: a crystal engineering approach. *Cryst Growth Des* 11:328–336
76. Lee H, Lee JH, Kang S, Lee JY, John G, Jung JH (2011) Pyridine-based coordination polymeric hydrogel with Cu<sup>2+</sup> ion and its encapsulation of a hydrophobic molecule. *Chem Commun* 47:2937–2939
77. Paul M, Adarsh NN, Dastidar P (2012) Cu<sup>II</sup> coordination polymers capable of gelation and selective SO<sub>4</sub><sup>2-</sup> separation. *Cryst Growth Des* 12:4135–4143

78. Bhattacharjee S, Bhattacharya S (2014) Pyridylenevinylene based  $\text{Cu}^{2+}$ -specific, injectable metallo(hydro)gel: thixotropy and nanoscale metal-organic particles. *Chem Commun* 50:11690–11693
79. Kartha KK, Praveen VK, Babu SS, Cherumukkil S, Ajayaghosh A (2015) Pyridyl-amides as a multimode self-assembly driver for the design of a stimuli-responsive  $\pi$ -gelator. *Chem Asian J* 10:2250–2256
80. Araújo M, Díaz-Oltra S, Escuder B (2016) Triazolyl-based molecular gels as ligands for autocatalytic “Click” reactions. *Chem Eur J* 22:8676–8684
81. Zhang S, Yang S, Lan J, Tang Y, Xue Y, You J (2009) Ultrasound-induced switching of sheetlike coordination polymer microparticles to nanofibers capable of gelating solvents. *J Am Chem Soc* 131:1689–1691
82. Lee HH, Jung SH, Park S, Park KM, Jung JH (2013) A metal-organic framework gel with  $\text{Cd}^{2+}$  derived from only coordination bonds without intermolecular interactions and its catalytic ability. *New J Chem* 37:2330–2335
83. Roy S, Katiyar AK, Mondal SP, Ray SK, Biradha K (2014) Multifunctional white-light-emitting metal-organic gels with a sensing ability of nitrobenzene. *ACS Appl Mater Interfaces* 6:11493–11501
84. Hamilton TD, Bučar DK, Baltrusaitis J, Flanagan DR, Li Y, Ghorai S, MacGillivray LR (2011) Thixotropic hydrogel derived from a product of an organic solid-state synthesis: properties and densities of metal-organic nanoparticles. *J Am Chem Soc* 133:3365–3371
85. Xing B, Choi MF, Xu B (2002) Design of coordination polymer gels as stable catalytic systems. *Chem Eur J* 8:5028–5032
86. Liu YR, He L, Zhang J, Wang X, Su CY (2009) Evolution of spherical assemblies to fibrous networked Pd(II) metallogels from a pyridine-based tripodal ligand and their catalytic property. *Chem Mater* 21:557–563
87. Liao Y, He L, Huang J, Zhang J, Zhuang L, Shen H, Su CY (2010) Magnetite nanoparticle-supported coordination polymer nanofibers: synthesis and catalytic application in suzuki-miyaura coupling. *ACS Appl Mater Inter* 2:2333–2338
88. Yan L, Gou S, Ye Z, Zhang S, Ma L (2014) Self-healing and moldable material with the deformation recovery ability from self-assembled supramolecular metallogels. *Chem Commun* 50:12847–12850
89. Yan L, Shen L, Lv M, Yu W, Chen J, Wang S, Ye Z (2015) Self-healing supramolecular heterometallic gels based on the synergistic effect of the constituent metal ions. *Chem Commun* 51:17627–17629
90. Lee H, Jung SH, Han WS, Moon JH, Kang S, Lee JY, Shinkai S (2011) A Chromo-fluorogenic tetrazole-based  $\text{CoBr}_2$  coordination polymer gel as a highly sensitive and selective chemosensor for volatile gases containing chloride. *Chem Eur J* 17:2823–2827
91. Sutar P, Suresh VM, Maji TK (2015) Tunable emission in lanthanide coordination polymer gels based on a rationally designed blue emissive gelator. *Chem Commun* 51:9876–9879
92. Kim C, Kim KY, Lee JH, Ahn J, Sakurai K, Lee SS, Jung JH (2017) Chiral supramolecular gels with lanthanide ions: correlation between luminescence and helical pitch. *ACS Appl Mater Inter* 9:3799–3807
93. Terech P, Yan M, Maréchal M, Royal G, Galvez J, Velu SK (2013) Characterization of strain recovery and “self-healing” in a self-assembled metallo-gel. *Phys Chem Chem Phys* 15:7338–7344
94. Gasnier A, Royal G, Terech P (2009) Metallo-supramolecular gels based on a multitopic cyclam bis-terpyridine platform. *Langmuir* 25:8751–8762
95. Kotova O, Daly R, dos Santos CM, Kruger PE, Boland JJ, Gunlaugsson T (2015) Cross-linking the fibers of supramolecular gels formed from a tripodal terpyridine derived ligand with d-block metal ions. *Inorg Chem* 54:7735–7741
96. Kotova O, Daly R, dos Santos CM, Boese M, Kruger PE, Boland JJ, Gunlaugsson T (2012) Europium-directed self-assembly of a luminescent supramolecular gel from a tripodal terpyridine-based ligand. *Angew Chem Int Ed* 51:7208–7212

97. Suresh VM, De A, Maji TK (2015) High aspect ratio, processable coordination polymer gel nanotubes based on an AIE-active LMWG with tunable emission. *Chem Commun* 51:14678–14681
98. Zhang J, Chen S, Xiang S, Huang J, Chen L, Su CY (2011) Heterometallic coordination polymer gels based on a rigid, bifunctional ligand. *Chem Eur J* 17:2369–2372
99. Nandi G, Titi HM, Thakuria R, Goldberg I (2014) Solvent dependent formation of metallogels and single-crystal MOFs by La(III) and Ce(III) connectors and 3,5-pyridinedicarboxylate. *Cryst Growth Des* 14:2714–2719
100. Wang X, He T, Yang L, Wu H, Yin J, Shen R, Wei C (2016) Designing isomeric gel precursors to identify the gelation pathway for nickel-selective metallohydrogels. *Dalton Trans* 45:18438–18442
101. Xiao B, Zhang Q, Huang C, Li Y (2015) Luminescent Zn(II)-terpyridine metal-organic gel for visual recognition of anions. *RSC Adv* 5:2857–2860
102. Samai S, Biradha K (2012) Chemical and mechano responsive metal-organic gels of bis (benzimidazole)-based ligands with Cd(II) and Cu(II) halide salts: self sustainability and gas and dye sorptions. *Chem Mater* 24:1165–1173
103. Dey A, Mandal SK, Biradha K (2013) Metal-organic gels and coordination networks of pyridine-3,5-bis(1-methyl-benzimidazole-2-yl) and metal halides: self sustainability, mechano, chemical responsiveness and gas and dye sorptions. *Cryst Eng Comm* 15:9769–9778
104. Sengupta S, Mondal R (2013) Elusive nanoscale metal-organic-particle-supported metallo-gel formation using a nonconventional chelating pyridine-pyrazole-based bis-amide ligand. *Chem Eur J* 19:5537–5541
105. Sengupta S, Mondal R (2014) A novel gel-based approach to wastewater treatment-unique one-shot solution to potentially toxic metal and dye removal problems. *J Mater Chem A* 2:16373–16377
106. Sengupta S, Mondal R (2016) A novel low molecular weight supergelator showing an excellent gas adsorption, dye adsorption, self-sustaining and chemosensing properties in the gel state. *RSC Adv* 6:14009–14015
107. Sarkar S, Dutta S, Bairi P, Pal T (2014) Redox-responsive copper(I) metallogel: a metal-organic hybrid sorbent for reductive removal of chromium(VI) from aqueous solution. *Langmuir* 30:7833–7841
108. Ma X, Yu D, Tang N, Wu J (2014) Tb<sup>3+</sup>-containing supramolecular hydrogels: luminescence properties and reversible sol-gel transitions induced by external stimuli. *Dalton Trans* 43:9856–9859
109. Sharma B, Mahata A, Mandani S, Sarma TK, Pathak B (2016) Coordination polymer hydrogels through Ag(I)-mediated spontaneous self-assembly of unsubstituted nucleobases and their antimicrobial activity. *RSC Adv* 6:62968–62973
110. Yadav P, Ballabh A (2014) Room temperature metallogelation for a simple series of aminothiazole ligands with potential applications in identifying and scavenging mercury ions. *RSC Adv* 4:563–566
111. Saha S, Bachl J, Kundu T, Diaz DD, Banerjee R (2014) Dissolvable metallohydrogels for controlled release: evidence of a kinetic supramolecular gel phase intermediate. *Chem Commun* 50:7032–7035
112. Suwendu K, Sushil K, Saibal B, David DD, Subhrashis B, Kumar V, Rahul B (2017) Interplaying anions in a supramolecular metallohydrogel to form metal organic frameworks. *Chem Commun* 53:3705–3708
113. Saha S, Das G, Thote J, Banerjee R (2014) Photocatalytic metal-organic framework from CdS quantum dot incubated luminescent metallohydrogel. *J Am Chem Soc* 136:14845–14851
114. Aiyappa HB, Saha S, Garai B, Thote J, Kurungot S, Banerjee R (2014) A distinctive PdCl<sub>2</sub>-mediated transformation of Fe-based metallogels into metal-organic frameworks. *Cryst Growth Des* 14:3434–3437

115. Tang XQ, Xiao BW, Li CM, Wang DM, Huang CZ, Li YF (2017) Co-metal-organic-frameworks with pure uniform crystal morphology prepared via  $\text{Co}^{2+}$  exchange-mediated transformation from Zn-metallogels for luminol catalyzed chemiluminescence. *Spectrochim Acta A Mol Biomol Spectrosc* 175:11–16
116. Lin Q, Zheng F, Lu T, Liu J, Li H, Wei T, Yao H, Zhang Y (2017) A novel imidazophenazine-based metallogel act as reversible  $\text{H}_2\text{PO}_4^-$  sensor and rewritable fluorescent display material. *Sens Actuators B: Chem* 251:250–255
117. Mehdi H, Pang H, Gong W, Dhinakaran MK, Wajahat A, Kuang X, Ning G (2016) A novel smart supramolecular organic gelator exhibiting dual-channel responsive sensing behaviours towards fluoride ion via gel-gel states. *Org Bio Chem* 14:5956–5964
118. Nune SK, Thallapally PK, McGrail BP (2010) Metal organic gels (MOGs): a new class of sorbents for  $\text{CO}_2$  separation applications. *J Mater Chem* 20:7623–7625
119. Mahmood A, Xia W, Mahmood N, Wang Q, Zou R (2015) Hierarchical heteroaggregation of binary metal-organic gels with tunable porosity and mixed valence metal sites for removal of dyes in water. *Sci Rep* 5:10556
120. Xia W, Zhang X, Xu L, Wang Y, Lin J, Zou R (2013) Facile and economical synthesis of metal-organic framework MIL-100(Al) gels for high efficiency removal of microcystin-LR. *RSC Adv* 3:11007–11013
121. Zhu B, Yu X, Jia Y, Peng F, Sun B, Zhang M, Luo T, Liu J, Huang X (2012) Iron and 1,3,5-Benzenetricarboxylic metal-organic coordination polymers prepared by solvothermal method and their application in efficient As(V) removal from aqueous solutions. *J Phys Chem C* 116:8601–8607
122. Fan J, Li L, Rao H, Yang Q, Zhang J, Chen H, Chen L, Kuang D, Su C (2014) Novel metal-organic gel based electrolyte for efficient quasi-solid-state dye-sensitized solar cells. *J Mater Chem A* 2:15406–15413
123. Yan J, Yang G, Wang H, Chen Y (2007) Macroporous polymer monoliths fabricated by using a metal-organic coordination gel template. *Chem Commun* 4614–4616
124. Yang F, Lin Z, He X, Chen L, Zhang Y (2011) Synthesis and application of a macroporous boronate affinity monolithic column using a metal-organic gel as a progenic template for the specific capture of glycoproteins. *J Chromatogr A* 1218:9194–9201
125. Ma L, Tang L, Li R, Huang Y, Liu Z (2015) Water-compatible molecularly imprinted polymers prepared using metal-organic gel as porogen. *RSC Adv* 5:84601–84609
126. Wen X, Tang L (2015) One-dimensional copolymer nanostructures loaded with silver nanoparticles fabricated via metallogel template copolymerization and their pH dependent photocatalytic degradation of methylene blue. *J Mol Catal A: Chem* 399:86–96
127. Xia W, Qiu B, Xia D, Zou R (2013) Facile preparation of hierarchically porous carbons from metal-organic gels and their application in energy storage. *Sci Rep* 3:1935
128. Cui L, Wu J, Ju H (2014) Nitrogen-doped porous carbon derived from metal-organic gel for electrochemical analysis of heavy-metal ion. *ACS Appl Mater Interfaces* 6:16210–16216
129. Zhang J, James SL (2011) Chapter 5 supramolecular gel catalyst: bridging homogeneous and heterogeneous catalysis, in homogeneous catalysts: types, reactions and applications (Editor: Poehler AC). Nova Science Publishers, Inc., New York
130. Díaz DD, Kühbeck D, Koopmans RJ (2011) Stimuli-responsive gels as reaction vessels and reusable catalysts. *Chem Soc Rev* 40:427–448
131. Escuder B, Rodríguez-Llansola F, Miravet JF (2010) Supramolecular gels as active media for organic reactions and catalysis. *New J Chem* 34:1044–1054
132. Zhu B, Liu G, Chen L, Qiu L, Chen L, Zhang J, Zhang L, Barboiu M, Si R, Su C (2016) Metal-organic aerogels based on dinuclear rhodium paddle-wheel units: design, synthesis and catalysis. *Inorg Chem Front* 3:702–710
133. Yamada YM, Maeda Y, Uozumi Y (2006) Novel 3D coordination palladium-network complex: a recyclable catalyst for Suzuki-Miyaura reaction. *Org Lett* 8:4259–4262

134. Zhang J, Wang X, He L, Chen L, Su C, James SL (2009) Metal-organic gels as functional supports for catalysis. *New J Chem* 33:1070–1075
135. Huang J, He L, Zhang J, Chen L, Su C (2010) Dynamic functionalised metallogel: an approach to immobilised catalysis with improved activity. *J Mol Catal A Chem* 317:97–103
136. Okesola BO, Suravaram SK, Parkin A, Smith DK (2016) Selective extraction and in situ reduction of precious metal salts from model waste to generate hybrid gels with embedded electrocatalytic nanoparticles. *Angew Chem Int Ed* 55:183–187

## Chapter 4

# Dynamic Covalent Gels

**Abstract** Various dynamic covalent bonds have been studied in the area of supramolecular gels, such as imine/acylhydrazone formation, boronic ester formation, disulphide formation and anthracene dimerization. Two catalogues of dynamic covalent gels are discussed in this chapter, namely gelation by discrete molecules and gelation by dynamic covalent polymers. Discrete gelators include imine/acylhydrazone gels, borate gels, anthracene-based gels and gels based on dynamic covalent cycles and cages. In the section of dynamic covalent polymer gels, imine gels and calix[4]arene-derived acylhydrazone gels are discussed in detail.

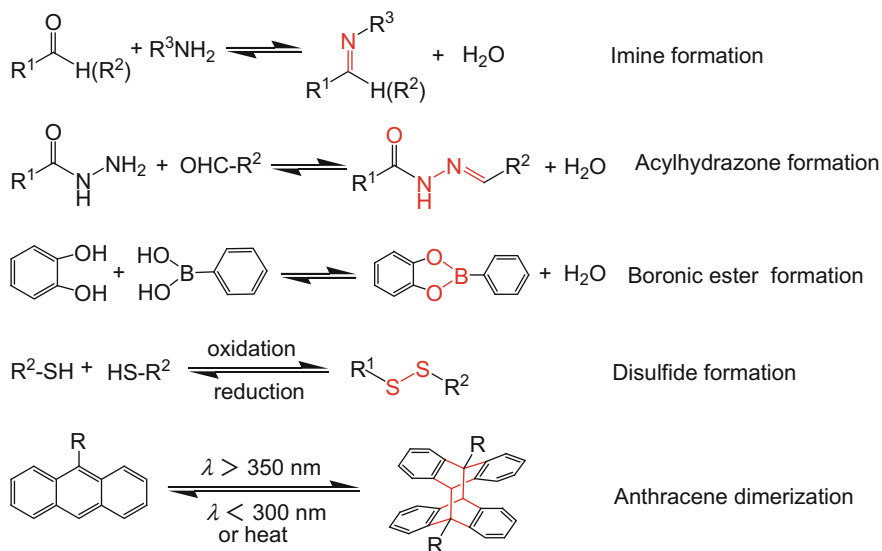
**Keywords** Dynamic covalent chemistry • Supramolecular gels  
Imine • Acylhydrazone • Cage compounds

Dynamic covalent chemistry, first introduced by Lehn, studies the formation of reversible covalent bonds under thermodynamic control [1]. The development of dynamic covalent chemistry has opened up new opportunities for the design and fabrication of supramolecular gels [2–4]. Compared with non-covalently bonded molecular systems, the formation of dynamic covalent bonds between gelators can potentially enhance the toughness and stability of resulting gels. To date, a number of dynamic covalent bonds have been studied in the area of supramolecular gels [5]. The functionalization of gelators with bond-forming groups allows control over the backbone structures of gel networks. The dynamic reactions that have been applied for gels include formation of imines, hydrazones, acylhydrazones, Diels–Alder cycloaddition, boronic esters, disulfides and so on (Scheme 4.1). Catalysts are often needed in order to access the reversibility of these bonds such as acid, base and redox agents.

Condensations of amino and carbonyl groups to give C=N compounds (imines or hydrazones) are one of the frequently used dynamic covalent reactions [6, 7]. The imine bond is formed by the reversible condensation between a primary amine

---

Jianyong Zhang, Haobin Fang and Xiyong Feng contributed together to this chapter.



**Scheme 4.1** Typical reversible dynamic covalent reactions

and an aldehyde or ketone. This kind of reaction is also called Schiff base condensation reaction and it is acid catalyzed. Imine bonding has good stability under neutral or basic conditions. In general, imine gels are based on equilibrium-controlled reactions like imine formation, hydrolysis (imine reverts back to its amine and carbonyl precursors on addition of  $\text{H}_2\text{O}$  or acid), exchange (the original R groups next to  $\text{C}=\text{N}$  may be exchanged by another groups), metathesis (two imines undergo a reaction in which their R groups are exchanged with each other). Imines are good ligands for metal ions, and imines with ortho-hydroxy substituents in the aromatic ring or pyridine have been widely studied for metal complexation.  $\text{C}=\text{N}$  derivatives of aldehydes and ketones formed by hydrazines and acylhydrazines are called hydrazones and acylhydrazones, respectively.

Formation of boronic ester has also been used in the formation of supramolecular gels. Reversible condensation reactions between boronic acid and 1,2-diols (catechol) form five-membered cyclic boronic esters. This reaction is easier to happen at high pH. Oxidation of thiols forms disulfide bond which is stable under neutral and acidic conditions, but dynamic under reductive or basic conditions in the presence of thiolates. The formation of disulfide is promoted by various oxidants such as air, and the exchange can be triggered by a catalytic amount of reductant such as dithiothreitol. Another dynamic covalent reaction is anthracene dimerization. Anthracene and its derivatives dimerize when irradiated at wavelengths above 350 nm, and the dimers dissociate upon exposure to light of less than 300 nm or heating.

In this chapter, dynamic covalent gels are classified into two general catalogues according to the nature of gelators and the interactions between gelators: gelation by discrete molecules and gelation by dynamic covalent polymers.

## 4.1 Discrete Gelators

Dynamic covalent bonding can be involved to form low molecular weight gelators, and discrete gelators self-assemble to form gels through multiple non-covalent interactions such as hydrogen bonding,  $\pi$ - $\pi$  stacking, hydrophobic and other supramolecular weak interactions. In such gels, supramolecular weak interactions may be readily broken by applying external stimuli (e.g. heating), and thus the gels are thermoreversible.

### 4.1.1 Imine/Acylhydrazone Gels

Based on imine chemistry, reversible and pH-responsive self-assembly systems have been developed. Hao and co-workers reported that the morphology transformation of imine assemblies may be controlled [8]. The amine group of 11-aminoundecanoic acid reacts with the aldehyde group of benzaldehyde or 1-naphthaldehyde by imine bond in alkaline conditions to form a small organic building block accompanied by the morphological transformation from vesicles to fibres (Fig. 4.1). When pH is lowered to a neutral value, the imine bonds can be

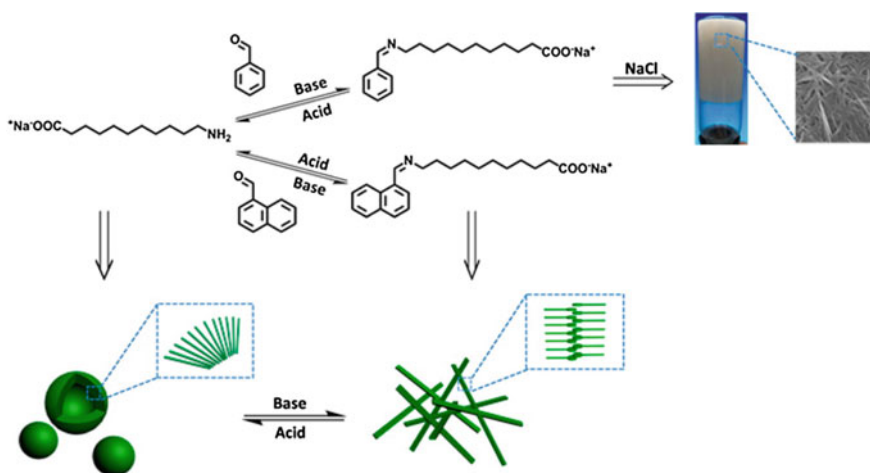
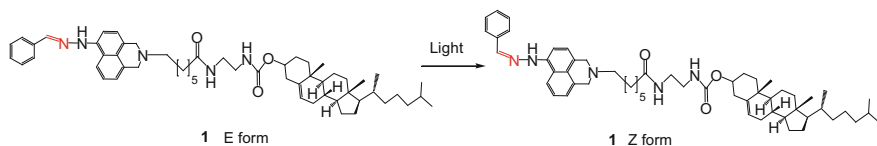


**Fig. 4.1** Reversibly controlled amphiphiles based on imine bonding. Adapted with permission from [8]. Copyright (2016) American Chemical Society



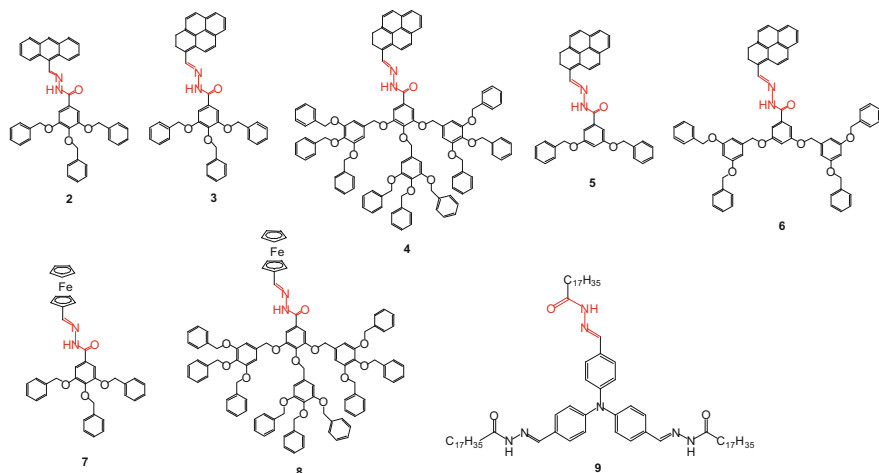
**Scheme 4.2** Trans to cis transformation of **1**

hydrolyzed, leading to the dissociation of fibres and appearance of spherical aggregates. The transformation is reversible as fibres appeared again when pH is changed back to alkaline value. In addition, a gel forms from the fiber solution at pH 12.8 after NaCl is added which is capable of greatly enhancing the nanofiber density and cross-linking. The gel collapses after pH is changed to 7.4 due to the breakage of imine bond and reforms when the pH changed back to 12.8.

Introduction of functional groups via formation of imine bonding expands the functionality of the resultant gel materials. For example, Yu, Pang and co-workers reported a novel fluorescent cholesterol-appended organogelator **1** comprised of imine bond (Scheme 4.2) [9]. This naphthalimide-based derivative undergoes trans to cis transformation both in solution and gel state by light irradiation accompanied by dramatic colour, fluorescence intensity and emission colour changes, indicating the photochromic property of **1**. Both the gels in E-isomeric and Z-isomeric form selectively respond to fluoride anion among tested anions. The cis and trans forms of C=N bond had great impact on the push–pull effect of internal charge transfer (ICT) process (caused by the electron-donating amine and the electron-withdrawing imide) of 4-amino-naphthalimide unit. The isomers expressed different fluorescence signal outputs and binding mechanisms towards fluoride anions. The E-isomeric form first bonds with  $F^-$  via hydrogen bonding interaction between acidified  $-NH$  and  $F^-$ ; then proton transfer from  $-NH$  to  $F^-$  happens in the presence of excess  $F^-$ . However, for the Z-isomer only hydrogen bonding interaction exists with  $F^-$  without proton transfer. Beside the above functions, the organogel also responds to ultrasound and heating stimuli, thus endowing the organogel with multi-stimuli responsive properties.

Compared with imine, the additional H-bonding of amide group in acylhydrazone is one of the important factors to gel formation. So reversible gel–sol transition is possible in the presence of chemical or physical stimulus which can destroy the H-bonding. These responsive gels show potential applications in various fields such as sensor devices.

Dendrimers and dendrons are important gelators because their self-replicating structure provides a suitable structural scaffold for multiple intermolecular interactions, leading to effective gelation and efficient sensing. Prasad and co-workers designed a series of poly(aryl ether)dendrons with an anthracene or pyrene chromophore **2–6** through an acylhydrazone linkage (Scheme 4.3) [10]. Poly(aryl ether) dendron compound **2** with an anthracene chromophore shows efficient gelation property in a variety of solvents such as  $CHCl_3$ , toluene,  $CHCl_3$ -methanol and THF-water. Dendron molecules of **2** assemble through H-bonding and  $\pi$ - $\pi$



**Scheme 4.3** Chemical structures of gelators 2–9

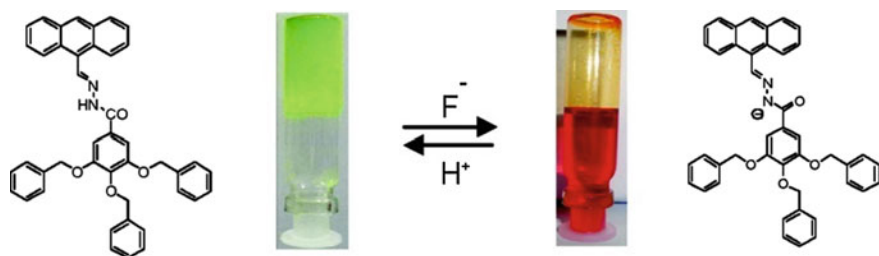


**Fig. 4.2** Poly(aryl ether)dendrons with anthracene group to detection F<sup>-</sup>. Adapted with permission from [10]. Copyright (2011) American Chemical Society

interactions into one-dimensional extended assemblies, followed by the intertwining of the chains together to form the resulting fibre. The gel of **2** was used to detect F<sup>-</sup>. After addition of F<sup>-</sup>, the NH groups perhaps undergo a deprotonation reaction resulting in a gel–sol conversion and colour change from deep yellow to bright red. The gel can reform after addition of water (Fig. 4.2).

Poly(aryl ether) dendron compounds with a pyrene chromophore **3–6** have also been developed for fluorescent gels [11]. Morphology and size can be controlled by concentration and solvent polarity. All the compounds exhibit fibrillar-type assembly in single solvents, while fine-tuning of the medium polarity results in the formation of spherical morphology. The initially formed nano-sphere assembly at concentrations below  $1 \times 10^{-5} \text{ mol L}^{-1}$  can further combine to generate twins, triplets or even multiplets when the concentrations increase by an order of magnitude ( $1 \times 10^{-4} \text{ mol L}^{-1}$ ), leading to the microspheres (Fig. 4.3). The gels are also sensitive to F<sup>-</sup>, resulting in the sol–gel transition with a colour change from

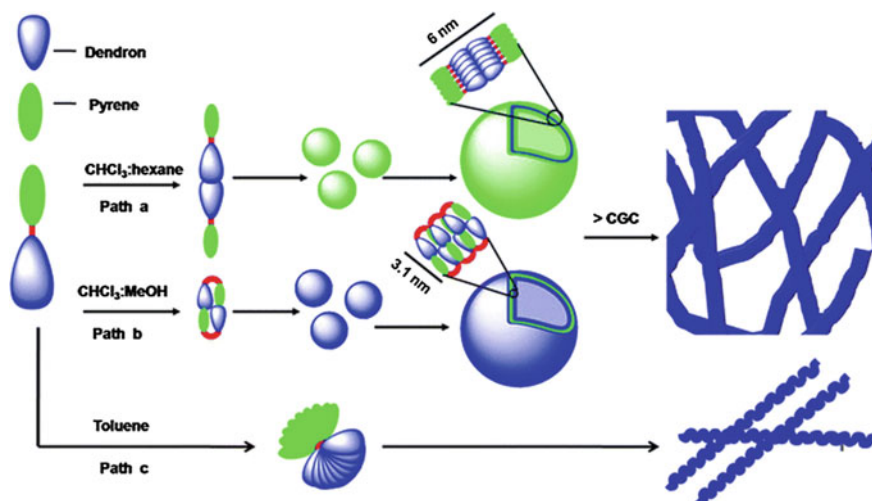


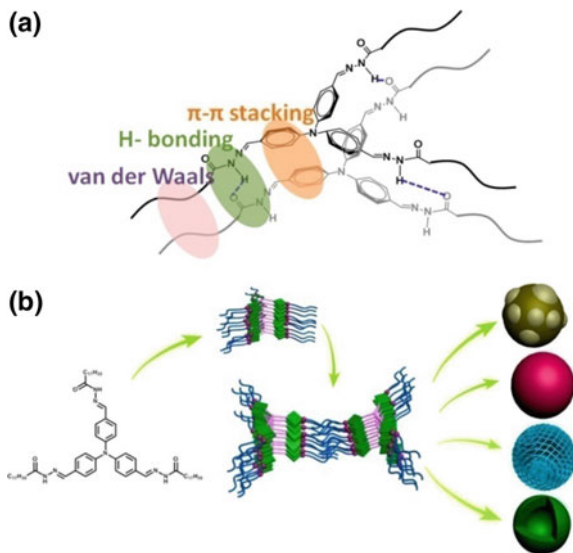
**Fig. 4.3** Scheme representation of different types of self-assembly of dendrons to form a gel. Adapted with permission from [11]. Copyright © The Royal Society of Chemistry 2012

yellow to red and reform after addition of water. Importantly, the gel system exhibits quite unconventional solvent effects on emission wavelength, which is attributed to the controlled formation of “excimer” and “exciplex” from the pyrene moiety in the self-assembly. For example, the gel formed in CHCl<sub>3</sub>–MeOH mixture has a broad structureless band at around 445 nm, associated by a bright-blue emission, while a broad structureless bright-green emission at around 525 nm is observed from the gel in a relatively non-polar solvent (CHCl<sub>3</sub>–hexane mixture). In comparison the emission of the gel in toluene is about 470 nm. The acylhydrazone spacer group is likely to be exposed to a solvent medium, and the appended benzyl rings as well as pyrene groups could “fold back” due to hydrophobic interactions in polar solvents, while it have primarily  $\pi$ – $\pi$  stacking interaction between pyrene moieties during the self-assembly of the dendron derivatives in less polar solvents.

Ghosh, Prasad and co-workers reported acylhydrazone gelators **7** and **8** based on a poly(aryl ether) dendron with a ferrocene unit (Scheme 4.3) [12]. The driving factors of gelation include intermolecular hydrogen bonding involving the acyl hydrazone spacer unit, and  $\pi$ – $\pi$  stacking interactions between poly(aryl ether) dendrons and cyclopentadienyl rings. The gels respond to multiple external stimuli such as heat, redox potential and toxic metal ion (Pb<sup>2+</sup>). These gels show specific response to Pb<sup>2+</sup> ions triggering the gel–sol transition at concentrations close to ppb level of the analyte. The plausible binding mode of Pb<sup>2+</sup> is via the oxygen atom of acylhydrazone loop and the nitrogen atom of imine group.

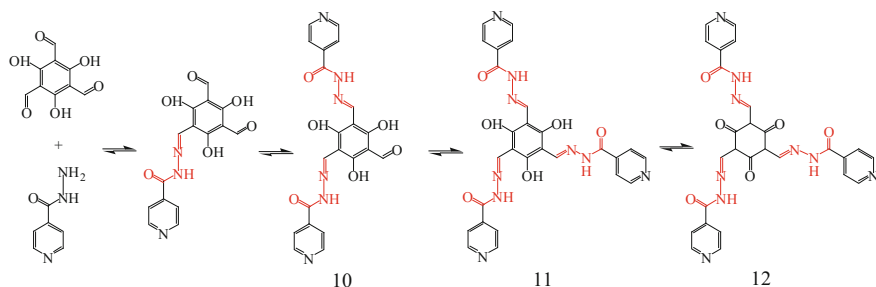
Zhang, Liu and co-workers designed triangular acylhydrazone amphiphile **9** (Scheme 4.3) [13]. **9** has three long alkyl chains in the periphery of the aromatic triangular core connected via acylhydrazone or imine bonding. The triangular structure provides more acting sites in the self-assembly process, and the

**Fig. 4.4** **a** Packing of **9** molecules with H-bonding,  $\pi$ - $\pi$  stacking and van der Waals interactions and **b** illustration of the packing of **9** molecules into various structures. Adapted with permission from [13]. Copyright (2014) American Chemical Society



hydrophobic tails endow the aggregates with enhanced stability. **9** forms various nano/microstructures in different solvents. The transparent solution or suspension with microspheres, flower like and hollow spheres form in polar solvents, while organogels with microporous structures form in nonpolar solvents. Besides  $\pi$ - $\pi$  stacking between the aromatic core and van der Waals interactions between the alkyl chains, hydrogen bonding between the acylhydrazone moieties plays an important role in promoting the formation of various organized structures (Fig. 4.4). The gel formed by **9** is thermoreversible and stable for weeks at room temperature. Compared with solution, the fluorescence intensity of gels enhanced remarkably due to the restriction of collision between fluorophore by  $\pi$ - $\pi$  stacking and hydrogen bonding. Moreover, the hollow sphere structure formed in THF can be used to encapsulate and release Rhodamine B. Rhodamine B is encapsulated within their interiors under neutral conditions and released under an acidic condition due to the breakage of imine bond.

Acylhydrazone derivative containing phenol moieties usually has two different types of tautomers, keto and enol forms, which allow pathway selectivity in the formation of hydrogelators and lead to a range of hydrogel materials with different properties. Lloyd and co-workers showed that different reaction conditions lead to different supramolecular gels based on trimethylphloroglucinol and isoniazid [3]. The acylhydrazone bond formation between trimethylphenyltriphenol and isoniazid gives discotic compounds. Changing the reaction conditions leads to three distinct gels of **10**-**12** (Scheme 4.4). (1) Mix trimethylphenyltriphenol with isoniazid at pH 8 and raise the pH to 9.5-12 by NaOH, which gives **12** gel. This gel is keto form and thermodynamically stable. (2) Mix trimethylphenyltriphenol with isoniazid at pH 8 and leave in solution for several hours before lowering the pH by glucono- $\delta$ -lactone, which gives **11** gel. This gel is enol form and less stable than **12**.

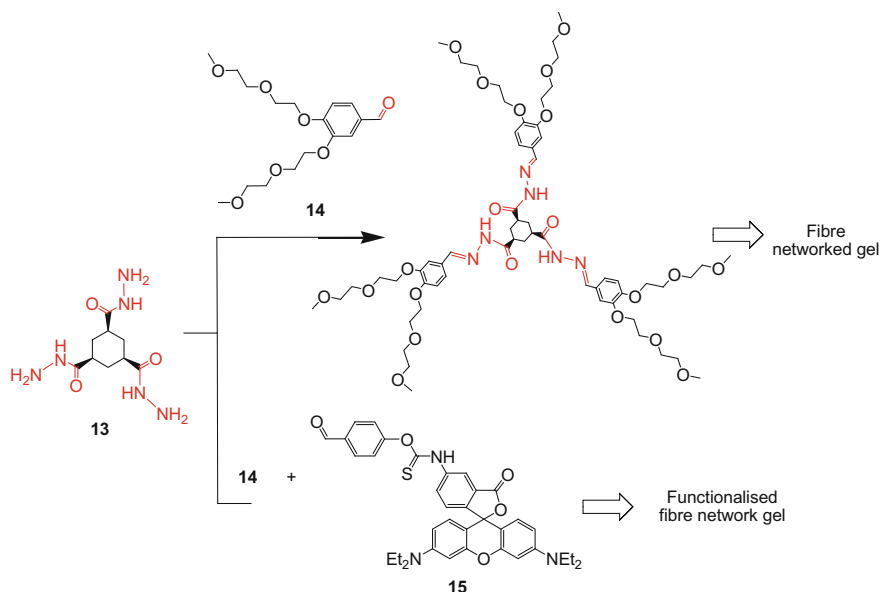


**Scheme 4.4** Various acylhydrazone derivatives assembled from trimethylphloroglucinol and isoniazid

(3) Mix trimethylphenyltriphenol with isoniazid at pH 8 and immediately lower the pH by glucono- $\delta$ -lactone at room temperature, which gives **10** gel. This gel is an intermediate during the reaction.

Esch, Eelkema and co-workers showed a supramolecular hydrogel formed by hydrazone formation between hydrazide **13** and aldehyde **14** under ambient conditions (Scheme 4.5) [4]. The rate of hydrazone formation can be increased through the use of catalysts such as aniline or acid, reducing gelation times from hours to minutes. Upon reaching a critical minimum concentration, the hydrazone gelator self-assembles into fibres, which in due course form a gel network capable of retaining water. The higher rate of hydrazone formation leads to an increased formation of defects in the gel fibre, thereby resulting in branching of the fibres, which subsequently strengthens the gel. Introduction of functional groups expands the functionality of these hydrazone gels. The same group showed that covalently functionalizing the network with a variety of fluorescent probes and integrating reactive groups in the hydrogel network allow for further modification of the gel fibres. For instance, they replaced a small part of **13** with aldehyde-derived fluorophores such as rhodamine (**15**) (Scheme 4.5). Small percentages of other aldehyde derivatives can be incorporated into the gel network without hindering the gelation [14]. Various fluorescent probes with different excitation wavelengths can be used in this strategy, which increases the flexibility with respect to future applications such as scaffolds for 3D cell culturing. They also expanded the functional precursors by synthesising aldehyde derivatives with reactive groups, allowing for modification of the fibre network, either through the formation of permanent covalent bonds via click chemistry, or by non-covalent interactions with biomolecules (Fig. 4.5). The gel system can be modified on demand without hindering gel formation, enabling potential applications in the area of smart materials and chemical biology.

Guanosine hydrazide-based supramolecular hydrogels based on reversible hydrazone bonding were developed by Lehn and co-workers (Scheme 4.6) [15]. The G-quartets **17** formed by reversible acylhydrazone bonds with various aldehydes through dynamic decoration. Among the tested aldehydes, 1-formyl furan-3-sulfonic



**Scheme 4.5** Catalytic formation of trishydrazone hydrogelator and functionalization

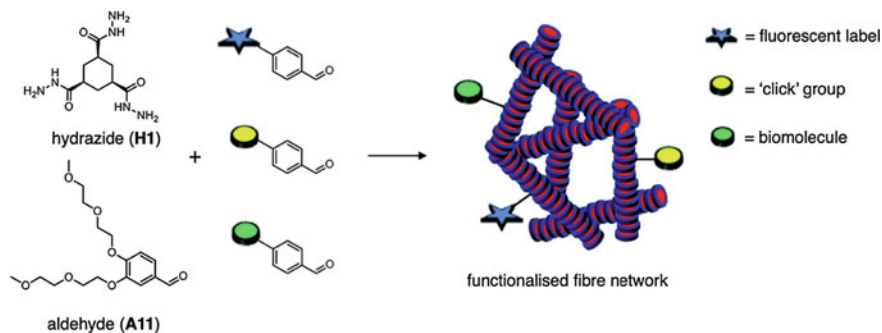
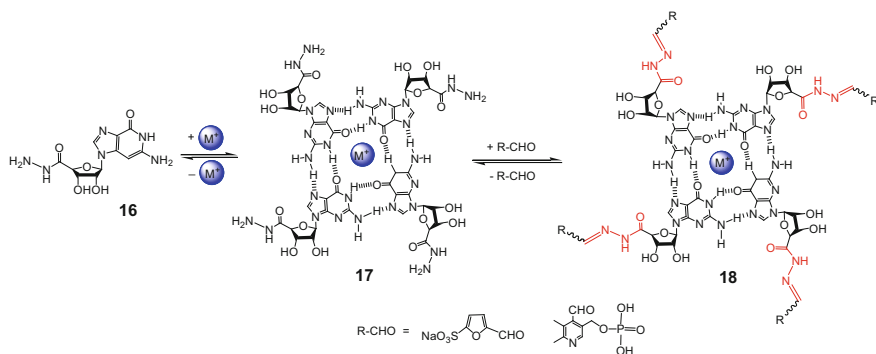


**Fig. 4.5** Concept of functionalized gel fibre network formation via partial replacement of the original aldehyde (**A11** = **14**) by a functionalized aldehyde creating a gel with tailored functionalities. Adapted with permission from [14]. Copyright © The Royal Society of Chemistry 2016

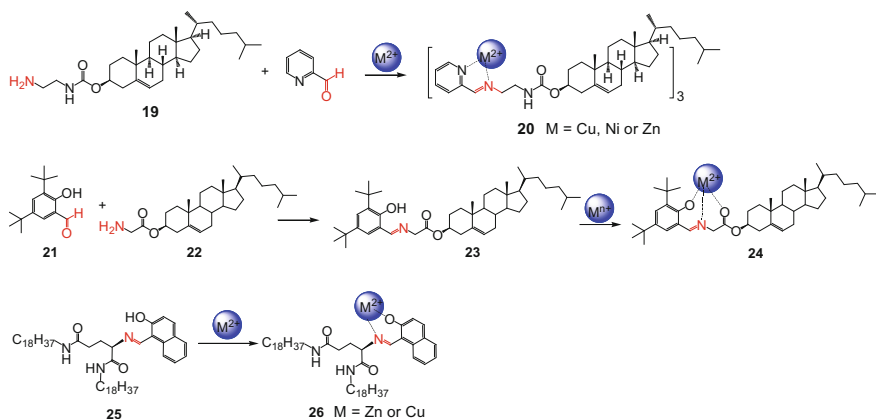
acid or pyridoxal-5-phosphate reacts with **16** to produce gels of the acylhydrazone quartet derivatives **18**. The gelation process results from a multilevel self-assembly based on the cation-templated self-assembly of quartets of guanosine acylhydrazone derivatives. This represents an example of gelation-driven self-organization with component selection and amplification in dynamic hydrogels based on G-quartet formation and reversible dynamic covalent bonding.



**Scheme 4.6** Reversible decoration of G-quartet assembly **17** of guanosine hydrazide **16** via hydrazone formation with aldehydes

### 4.1.2 Imine/Acylhydrazone Gels and Metal Ions

The properties of imine gels can be readily controlled and tuneable by metal ions considering imines are good ligands for metal ions. Bunzen and co-workers synthesized in situ imine metallogelators with cholesterol groups **20** from steroidal amine **19**, 2-pyridinecarboxaldehyde and metal ions ( $\text{Cu}^{2+}$ ,  $\text{Ni}^{2+}$ ,  $\text{Zn}^{2+}$ ) in a 3:3:1 ratio (Scheme 4.7) [16]. The resulting gelator molecules contain three cholesterol groups because the selected metal ions are hexacoordinate with octahedral coordination geometry. The precursor molecules spontaneously self-assemble around template metal ions via simultaneous imine and coordination bond formation. Compounds **20** induce gels in various alcohols at room temperature. The gels are multi-responsive and are also sensitive to stoichiometry, thermal and chemical stimuli.



**Scheme 4.7** Formation of imine metallogelators **19**, **24** and **26**

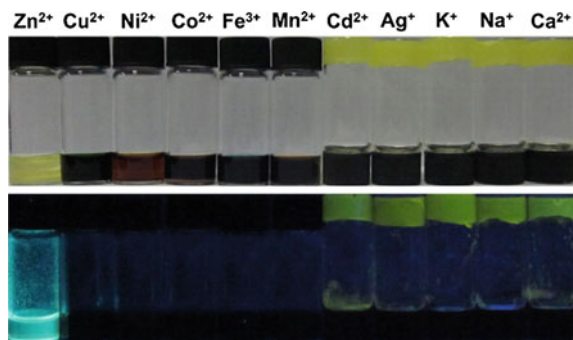


**Fig. 4.6** Color changes (up) and fluorescent changes (bottom, under 365 nm light) of **23** gel in EtOH to various metal ions (5 equiv.). Adapted with permission from [17]. Copyright © 2013 Elsevier B.V.

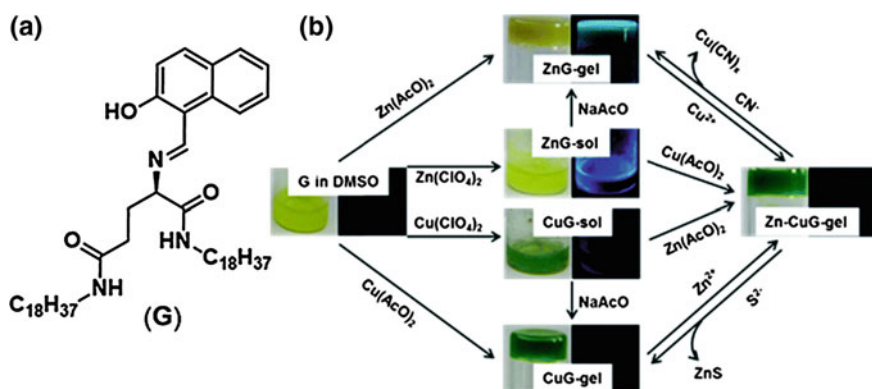


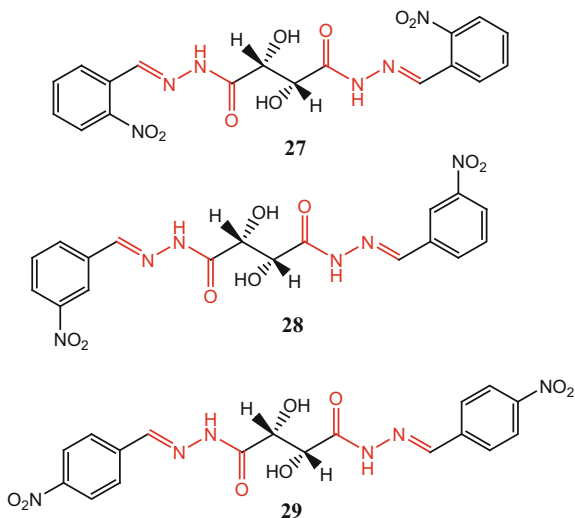
**Fig. 4.7** The gel of **25** (**G**) and metal–organic gels **ZnG**, **CuG** and **Zn–CuG** (for **ZnG**,  $25:\text{Zn}^{2+} = 1:1$ ; for **CuG**,  $25:\text{Cu}^{2+} = 1:1$ ; for **Zn–CuG**,  $25:\text{Cu}^{2+}:\text{Zn}^{2+} = 1:1:1$ ) treated with different ions. Adapted with permission from [18]. Copyright © The Royal Society of Chemistry 2016

Another example of incorporating imine bonding into metal-assisted gelation was investigated by Jiang and co-workers [17]. An ALS-type imine gelator **23** (ALS gelators are comprised of an aromatic functional group coupled with a steroidal moiety through a flexible linker) is synthesized beforehand from cholesterol 2-aminoacetate (**22**) and 3,5-di-tert-butyl-2-hydroxybenzaldehyde (**21**) (Scheme 4.7). Imine compound **23** efficiently gelate various organic solvents. Nanofibres with 30–100 nm width are responsible for the gelation. The gel shows thermochromism due to the enol–keto tautomerism. Metal ions binding affects the gelation process. In a range of metal ions, the gel shows selective dual-responsive property to  $\text{Zn}^{2+}$  through a gel–sol transition and a change in fluorescent turn-on (Fig. 4.6). The gel also shows a two-channel response to  $\text{F}^-$  by sol–gel transition and colour changes because **23** is a strong H-bonding acceptor.

Chen, Yin and co-workers reported another example of metal-assisted gelation [18]. Metal–organic gels (**26-ZnG** and **CuG**) were prepared from **25** and  $\text{Zn}^{2+}/\text{Cu}^{2+}$  in DMSO (Scheme 4.7). For **ZnG** and **CuG**, metal coordination results in the destruction of intramolecular hydrogen bonding in **25** and the formation of naphtholate, these metal ions coordinated with nitrogen and oxygen atoms in the hydroxy and imine group, respectively, with 1:1 stoichiometry. In addition,  $\text{Cu}^{2+}$  can competitively coordinate with **25** in **ZnG** and release  $\text{Zn}^{2+}$ , which result in the fluorescence quenching and colour change of **ZnG**. The resulting **Zn–CuG** can fluorescently detect  $\text{CN}^-$  with specific selectivity over  $\text{S}^{2-}$  and Cys. This property enables **Zn–CuG** to act as a  $\text{Cu}^{2+}$  and  $\text{CN}^-$  controlled “OFF–ON–OFF” fluorescent switch. The mechanism is that  $\text{CN}^-$  could competitively bound to  $\text{Cu}^{2+}$  to form stable  $[\text{Cu}(\text{CN})_x]^{n-}$  species after the addition of  $\text{CN}^-$  into **Zn–CuG**, while  $\text{Zn}^{2+}$  again coordinated with **25** (Fig. 4.7). Then upon addition of  $\text{Cu}^{2+}$  into the above mixture containing **ZnG** and  $[\text{Cu}(\text{CN})_x]^{n-}$  species, the fluorescence of the system is quenched, which is attributed to recoordination of  $\text{Cu}^{2+}$  with **25**.

Dubey and co-workers reported three chiral imine structural isomers (**27–29**), which are A– $\pi$ –D–chiral–D– $\pi$ –A-type molecules with an enantiopure chiral flexible core (Scheme 4.8) [19]. **29**+ $\text{Li}^+$ , **27**+ $\text{Li}^+$  and **27**+ $\text{Na}^+$  form metalgels, respectively. Alkali metal ions in these systems trigger intramolecular charge transfer and play a vital role in gelation.  $^1\text{H}$  NMR titration studies exhibit that the involvement of aldimine protons  $\text{Li}^+$  interaction with  $-\text{NO}_2$  and deprotonated oxo groups positioned at the chiral centre play a significant role in gelation. Upon removal of the triggering alkali metal ions with help of [16] crown-6, the gels deteriorate and produce colourless solutions (Fig. 4.8). The gel of  $\text{Na}^+$  exhibits twisted fibre morphology while  $\text{Li}^+$  gives merely long-range fibres.

**Scheme 4.8** Molecular structures of **27–29**



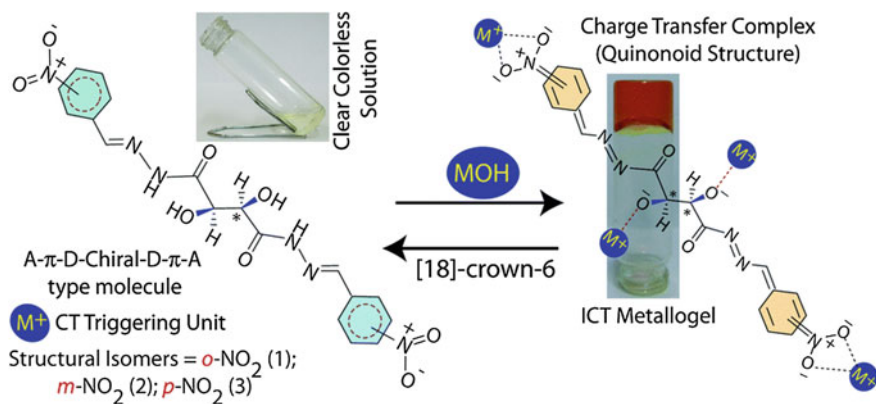
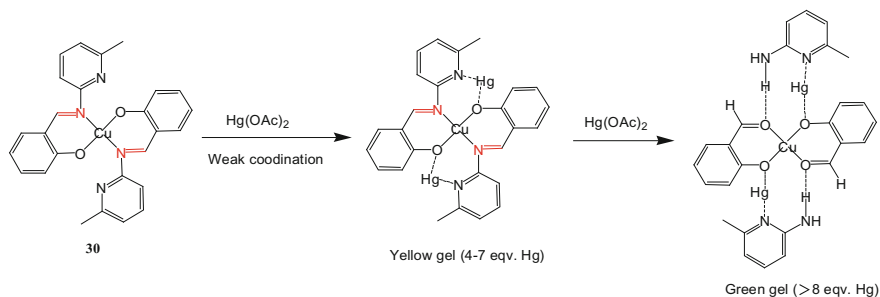


**Fig. 4.8** Chiral imine structural isomers and general scheme for the reaction involved in intramolecular charge transfer gel formation. Adapted with permission from [19]. Copyright © The Royal Society of Chemistry 2016

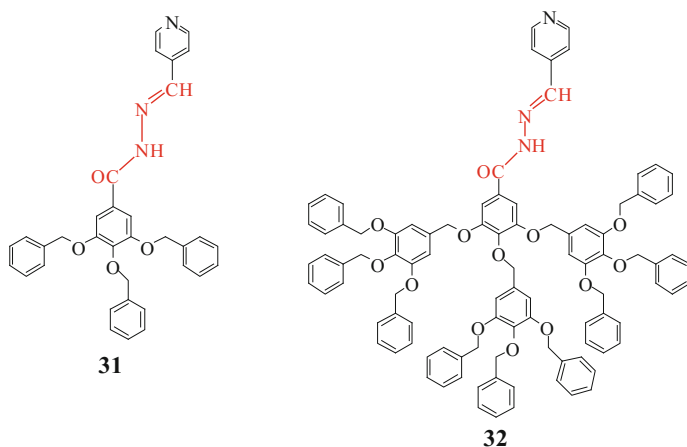
Pratihari and co-workers reported Cu<sup>II</sup>-imine complex **30**, in which tunable access of a vacant coordination site for a guest metal via stereoelectronic modulation of a substituent is possible (Scheme 4.9) [20]. **30** is thus utilized as a metallo-ligand for the formation of a heterobimetallic Cu<sup>2+</sup>/Hg<sup>2+</sup> gel in MeOH. The gelation property of **30** is dependent upon Hg<sup>2+</sup> content. Initially, a yellow gel was obtained by adding 4–7 equiv. Hg<sup>2+</sup> and it transforms into a green gel with addition of a higher equivalent (>8 equiv.) of Hg(OAc)<sub>2</sub>. The as-synthesized heterobimetallic Cu<sup>2+</sup>/Hg<sup>2+</sup> gel shows an excellent ability as a reusable material for the adsorption of various cationic as well as anionic dyes.

Prasad and co-workers showed that poly(aryl ether) dendron derivative **31** with pyridine units attached by an acylhydrazone linkage is an efficient gelator with Ag<sup>+</sup> and Cu<sup>2+</sup> ions in THF (Scheme 4.10) [21]. The resulting lamellar metallogel is assembled through hydrogen bonding between dendron monomers and pyridine-metal ion coordination. In contrast, compound **32** showed partial gel formation due to steric hindrance, which prevented effective coordination with the metal ions and intramolecular hydrogen bonding. Silver ions in the Ag<sup>+</sup> gel of **31** can be reduced in situ leading to the formation of silver nanoparticles without any external reducing agent/UV light irradiation. In this process, the gels played roles of both reducing agents and good host systems for stabilizing silver nanoparticles.

Some dynamic covalent gels' formation does not need to be assisted by metal ions, but these gels show stimuli-responsive property towards metal ions and may find potential applications in various fields. Qi, Zhang and co-workers reported a series of bimetal-acylhydrazone supramolecular gel based on **33** for sensing (Scheme 4.11) [22]. **33** was synthesized by the condensation of 1-naphthaldehyde and 3,4,5-tris(hexadecyloxy)benzohydrazide, and **33** showed excellent gelation ability in various solvents, and among these solvents, **33** showed the lowest critical gelation concentrations and the highest gel-sol transition temperature  $T_{gel}$  in EtOH. Hydrogen



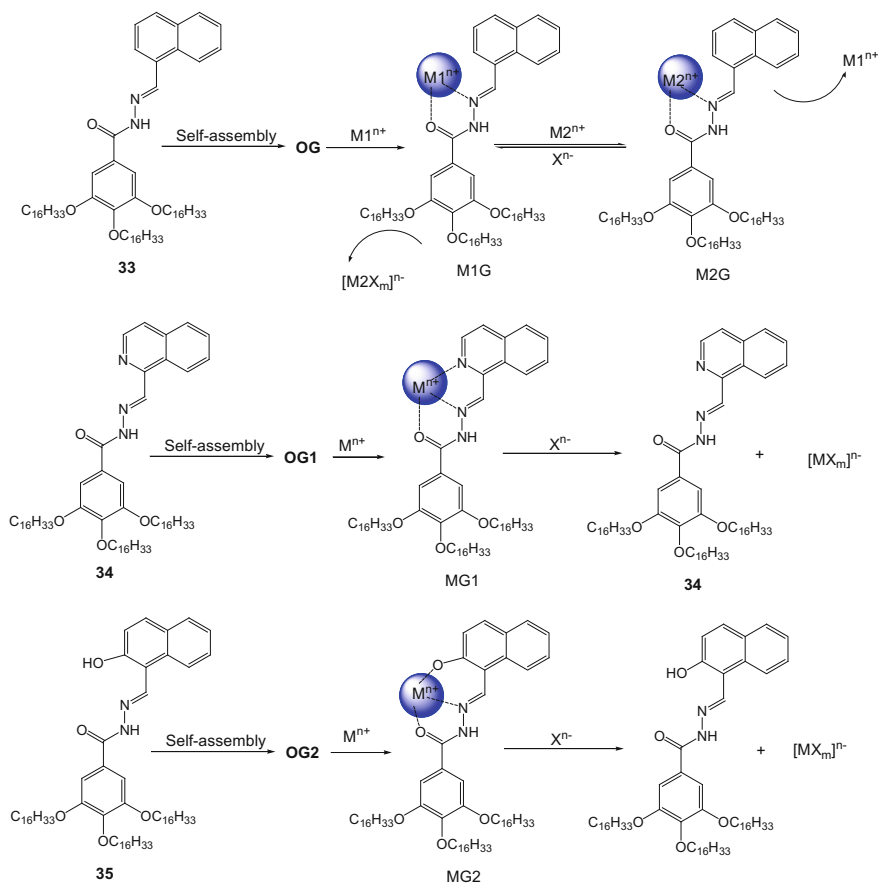
**Scheme 4.9** Proposed structures of the yellow and green gels of **30** and their transformation



**Scheme 4.10** Pyridine-functionalized dendron derivatives **31** and **32**

bonding and  $\pi$ - $\pi$  stacking as well as van der Waals force between alkyl chains are responsive for the gelation. The organogel of **33** shows the ability to be coordinated by  $\text{Ca}^{2+}$  and formed metallogel **CaG**, accompanied by strong AIE (Fig. 4.9). The addition of  $\text{Cu}^{2+}$  to **CaG** forms  $\text{Ca}^{2+}/\text{Cu}^{2+}$ -based metallogel (**CaCuG**) due to the stronger coordination ability of  $\text{Cu}^{2+}$  with **33** gel, resulting in quenching of the fluorescence. The fluorescence may be restored after the addition of  $\text{CN}^-$  because  $\text{CN}^-$  binds to  $\text{Cu}^{2+}$  while  $\text{Ca}^{2+}$  coordinates with **33** gel again. The result showed that the “OFF-ON” fluorescent switch is controlled by  $\text{Cu}^{2+}$  and  $\text{CN}^-$ .

After addition of 1 equiv.  $\text{Mg}^{2+}$  to **33** gel,  $\text{Mg}^{2+}$  was coordinated with the nitrogen and oxygen atoms on acylhydrazone group, resulting in the formation of **MgG** gel with blue fluorescence [23]. Then addition of 2 equiv.  $\text{Co}^{2+}$  into **MgG** forms  $\text{Co}^{2+}/\text{Mg}^{2+}$ -based metallogel **MgCoG** with quenched fluorescence because  $\text{Co}^{2+}$  replaces  $\text{Mg}^{2+}$  due to the stronger coordination ability with **G**. Moreover, the fluorescence could turn back after the addition of  $\text{Cl}^-$  because  $\text{Cl}^-$  binds to  $\text{Co}^{2+}$  and  $\text{Mg}^{2+}$  coordinated with **33** again. The process is reversible so that the system



**Scheme 4.11** Stimuli responsive mechanism for bimetal-acylhydrazone gels

may be used for an erasable secret documentation medium. The **CaG** gel showed “OFF–ON” fluorescent switch controlled by  $\text{Fe}^{3+}/\text{H}_2\text{PO}_4^-$  [24] and  $\text{Cd}^{2+}/\text{I}^-$  [25], respectively, as well. Acylhydrazone gels were further explored to be adjusted by more metal ions and anion-responsive [26]. Stable gel of **34** forms in DMF, which shows brilliant blue AIE (Scheme 4.11). Addition of metal ions such as  $\text{Cr}^{3+}$ ,  $\text{Fe}^{3+}$ ,  $\text{Cu}^{2+}$ ,  $\text{Hg}^{2+}$  to **34** gel results in non-fluorescent gels (**CrG1**, **FeG1**, **CuG1**, **HgG1**), while addition of  $\text{Zn}^{2+}$  leads to a yellow fluorescent gel (**ZnG1**). Interestingly, different metallogels sense different anions with high fluorescent selectivity and sensitivity ( $\text{CN}^-$  with **CuG1** and **FeG1**,  $\text{SCN}^-$  with **HgG1** and  $\text{S}^{2-}$  with **CrG1**) (Fig. 4.10). The gel films act as convenient reversible anions detection test kits and erasable security display materials.

A multi-functionalized acylhydrazone gelator **35** by introducing a coordination site,  $-\text{OH}$ , has been reported (Scheme 4.11) [27]. The gel of **35** shows ability to sense fourteen kinds of important ions with high selectivity and sensitivity in

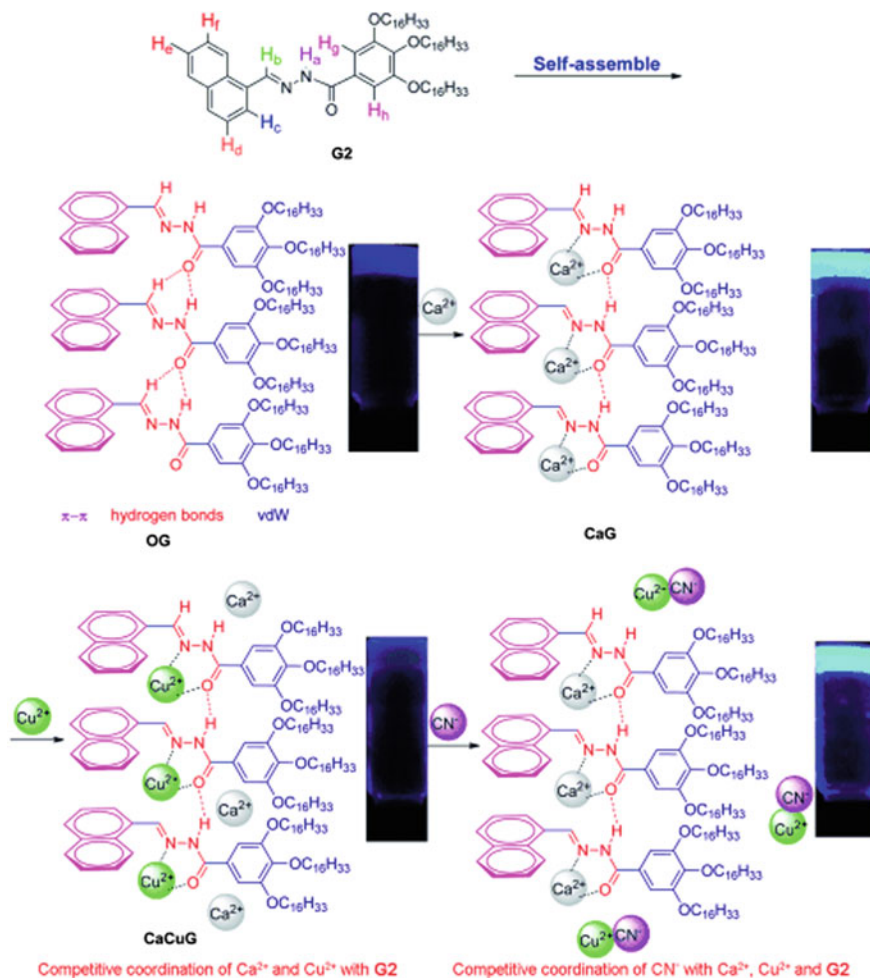


**Fig. 4.9** Proposed self-assembly of **33** (**G2**), **CaG**, **CaCuG** and its stimuli-responsive mechanism. Adapted with permission from [22]. Copyright © 2014 John Wiley and Sons

aqueous solution (Fig. 4.11). According to their test, upon the addition of 0.5 equiv. of Cu<sup>2+</sup>, Ba<sup>2+</sup>, Fe<sup>3+</sup>, Cr<sup>3+</sup>, Ru<sup>3+</sup>, Eu<sup>3+</sup> or Tb<sup>3+</sup> to **35** gel, the AIE of **35** was quenched and the corresponding no fluorescence metallo gel (**MG2**) formed; while addition of 0.5 equiv. of Ca<sup>2+</sup>, Al<sup>3+</sup>, La<sup>3+</sup>, Y<sup>3+</sup> and so on induces the AIE of **G2** with obvious shifts. What's more, the **MG2** metallo gels sense various anions. **CuG2**, **CrG2**, **BaG2**, **EuG2**, **TbG2** and **CuG2** show selective fluorescence "turn-on" towards SCN<sup>-</sup>, S<sup>2-</sup>, F<sup>-</sup> and OH<sup>-</sup>, respectively, while **FeG2**, **AlG2** and **LaG2** selectively sense HSO<sub>4</sub><sup>-</sup> and OH<sup>-</sup>, respectively. This gel system, a twenty-two member sensor array, is based on only one synthesized receptor and accurately controlled by various competitive binding interactions.

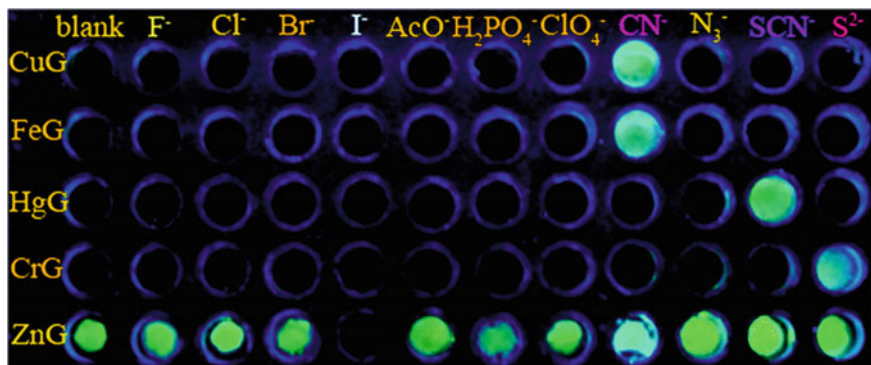


**Fig. 4.10** Fluorescence responses of the **34** gel-based sensor array in the presence of 1 equiv. of various anions. Adapted with permission from [26]. Copyright © The Royal Society of Chemistry 2015

### 4.1.3 Borate Gels

Borate formation has been used in dimerization of the guanosine gelators to form hydrogels typically involving  $G_4 \cdot M^+$  quartets. Davis and co-workers studied the formation of a hydrogel by adding 0.5 equiv of  $KB(OH)_4$  into the guanosine (**36**) (Scheme 4.12) [28]. The nucleoside's 2',3'-diol reacts with borate to form anionic guanosine-borate (GB) diesters, and they further self-assemble to form a structure containing stacked  $G_4$  quartets.  $B(OH)_4^-$ , together with  $K^+$ , is crucial for gelation.  $K^+$  stabilizes the  $G_4$  quartets and allows the hydrogel to stay intact;  $B(OH)_4^-$  cooperates with  $K^+$  to template self-assembly of **36** to give a robust, non-covalent hydrogel that remains intact indefinitely in salt water. The hydrogel is diagnostic of  $G_4$  quartets that are stacked in both head-to-tail and head-to-head orientations. GB gel absorbs methylene blue with high selectivity due to electrostatic interactions of the cationic dye with the anionic borates and stacking interactions with the  $G_4$  quartets.

Among the gels of various metal borate salt ( $Li^+$ ,  $Na^+$ ,  $Rb^+$ ,  $Cs^+$ ) with  $KB(OH)_4$ ,  $G_4K^+$  hydrogel is the strongest, self-supporting hydrogel with elastic moduli  $>10$  kPa [29]. The structure involves the formation of borate dimers and  $G_4K^+$  quartets by **36** and  $KB(OH)_4$ . Stacking of the  $G_4K^+$  quartets into nanowires via hydrogen bonding and  $\pi$ - $\pi$  stacking gives a hydrogel. Additionally when thioflavin T (ThT **6**) is incorporated, the fluorescent intensity of the  $G_4M^+$  gels is different. ThT **6** has been used as a selective indicator for G-quadruplex DNA and displays a strong enhancement in fluorescence upon binding to G-quadruplex DNA. The fluorescence is cation dependent. The highest fluorescence is seen for the  $K^+$  GB hydrogel, suggesting it has the largest number of  $G_4$ -quartets.

They further studied a  $G_4$ -quartet-based hydrogel formed by 5'-deoxy-5'-iodoguanosine (**37**) (Scheme 4.12) [30]. **37** undergoes in situ cyclization to give 5'-deoxy-N3,5'-cycloguanosine (**38**). The cyclization is temperature sensitive and

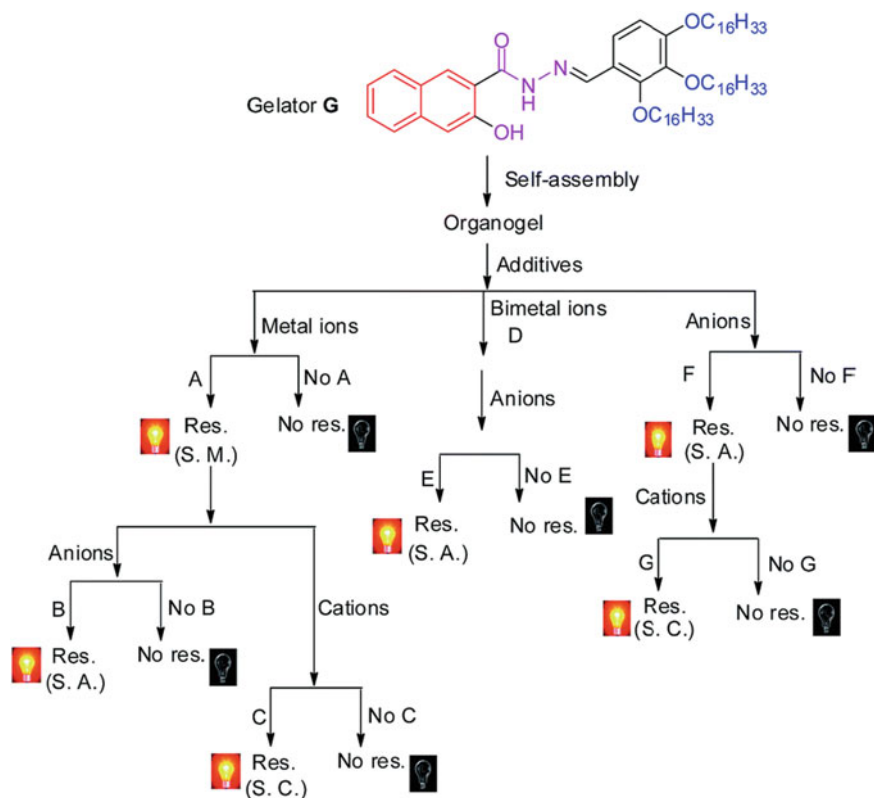
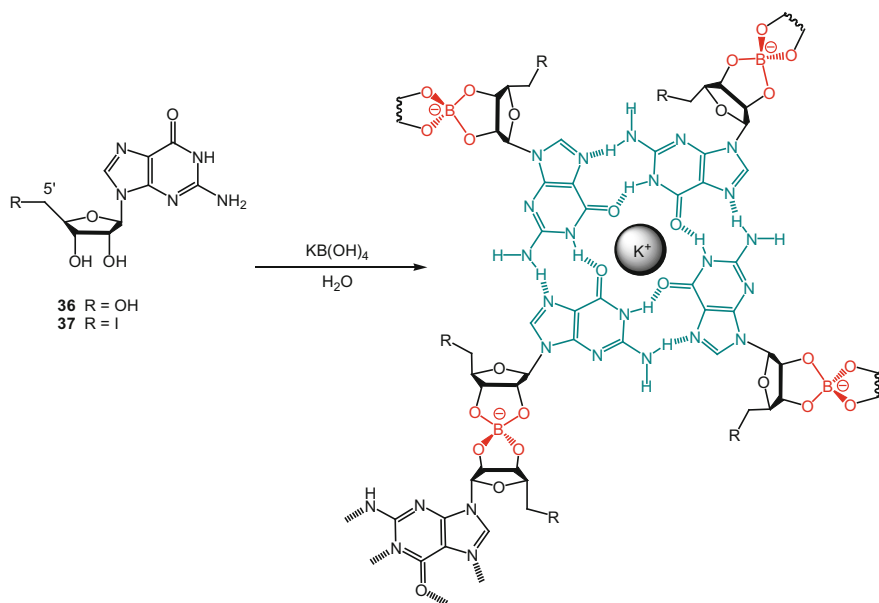


**Fig. 4.11** Competitive binding interactions of the gel of **35** (**G**), (A) metal ions competitively coordinate with the gelator; (B) anions competitively coordinate with the metal ions or gelator; (C) competitive coordination between different metal ions and the gelator; (D) bimetal ions competitively coordinate with the gelator; (E) anions competitively coordinate with the bimetal ions; (F) anions competitively binding with the gelator; (G) cations competitively coordinate with the anions or gelators. Res. or res., Response; S. A., Sensing for anions; S. C., Sensing for cations; S. M., Sensing for metal ions. Adapted with permission from [27]. Copyright © The Royal Society of Chemistry 2016

continues to occur after gel formation. The hydrogel of **37** displays a self-destruction because the content of the cyclization product (**38**) in the gel is increasing when raising the temperature. **38** cannot form a stable G<sub>4</sub>-quartet due to lacking of a N1 H-binding site, and the hydrogel is destroyed at 37 °C (Fig. 4.12). So the hydrogel can release pre-incorporated antiviral drugs (acyclovir or ganciclovir (guanine analogues)) efficiently at 37 °C.

Sadler and co-workers incorporated a photoactivatable dopamine-conjugated platinum(IV) anticancer complex into G-quadruplex G<sub>4</sub>K<sup>+</sup> borate hydrogels by using borate ester linkages (**40**) (Scheme 4.13) [31]. The molar ratio of **39** relative to guanosine hydrate is crucial for gel formation. When 1 mol equiv. of **39** was used, there is no gelation, because the presence of **39** functional group on the four



**Scheme 4.12** Formation of G<sub>4</sub>-K<sup>+</sup> hydrogel from **36** or **37**

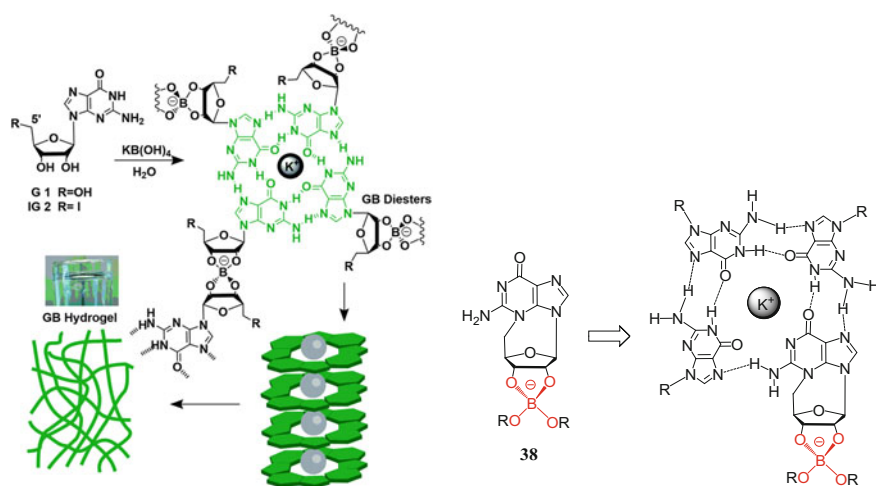
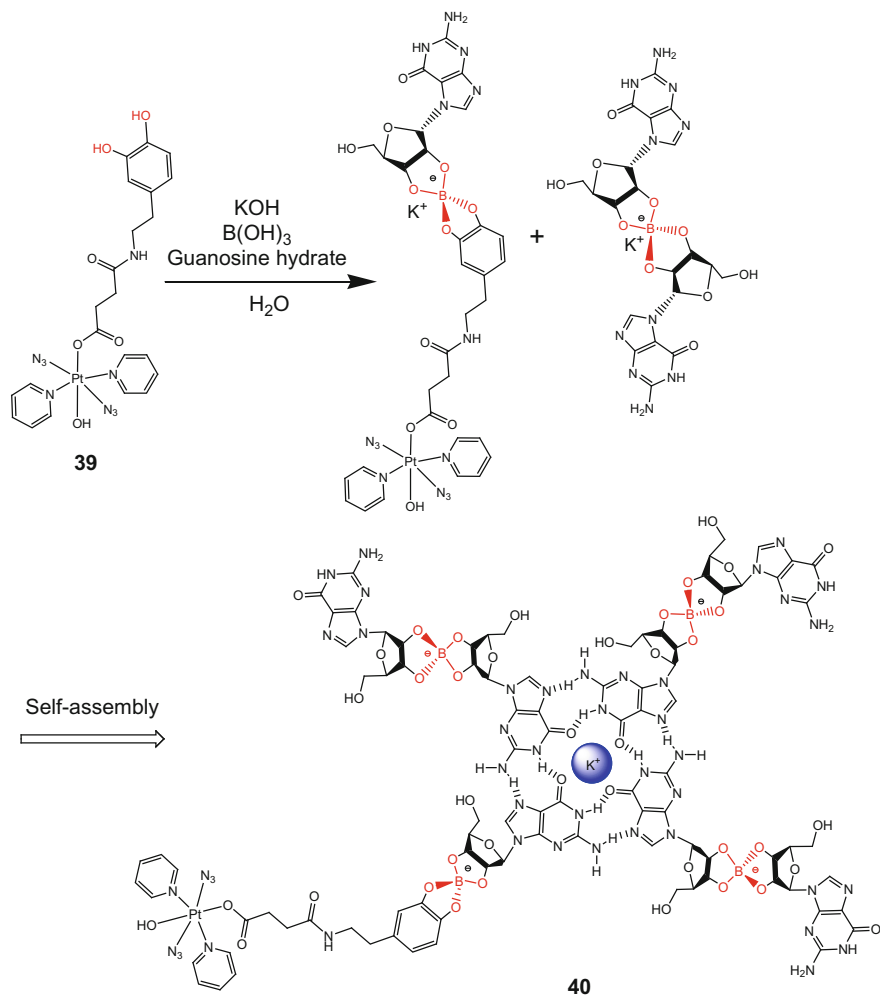


**Fig. 4.12** A hydrogel is made when **36** or **37** reacts with KB(OH)<sub>4</sub> to form GB esters that self-assemble into G<sub>4</sub>-wires stabilized by K<sup>+</sup>, and the wires entangle to give a fibrous network, and for in situ formation of **38** destroys the hydrogel network due to lacking of N1 H-bonding donor, which cannot form stable G<sub>4</sub>-quartets. Adapted with permission from [30]. Copyright © The Royal Society of Chemistry 2016



**Scheme 4.13** Synthesis of Pt-G<sub>4</sub>K<sup>+</sup>B **40** hydrogel

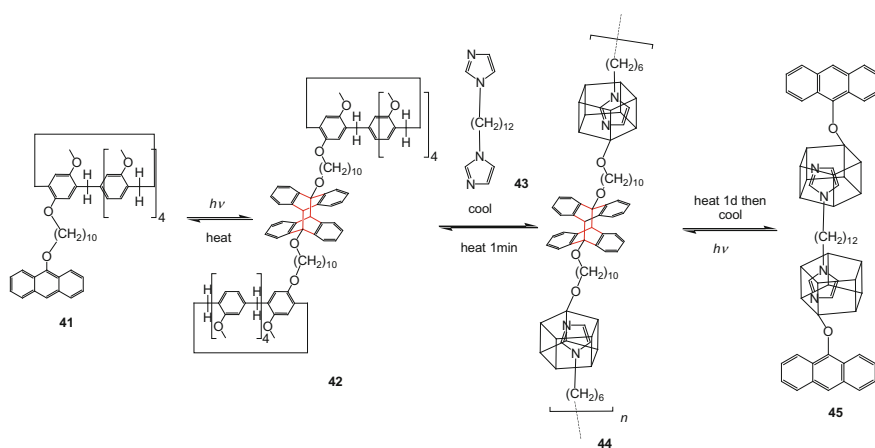
arms of the G-quartet may cause steric disruption to the stacking of G-quartets. Reducing the molar ratio of **39** to 0.1 mol equiv. results in gelation. **39** shows photocytotoxicity against cisplatin-resistant A2780C, human ovarian cancer cells, with a photocytotoxic index <2, whereas **39** hydrogel exhibits more potent photocytotoxicity with a photocytotoxic index >5. Both Pt-DA and **39** hydrogels are nontoxic towards normal cells. **39** hydrogel shows a great photocytotoxicity selectivity factor (ratio of the activity between normal and cancer cells, >18). Such high potency and selectivity provide a strong basis for development of gel materials as photochemotherapeutic agents, with potential for localized immunogenic treatment of cancers.

### 4.1.4 Conversions Between Anthracene and Its Dimer

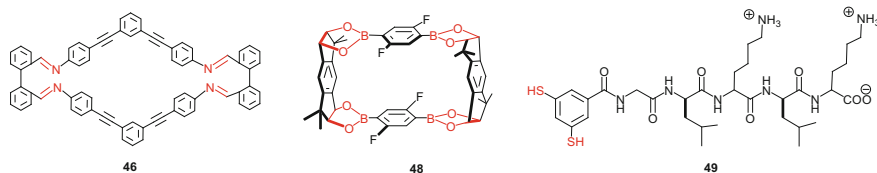
Dynamic covalent bonds based on anthracene dimerization have been introduced into supramolecular polymers built on host–guest interactions between pillar [5] arene and imidazole by Yang and co-workers (Scheme 4.14) [32]. Photochemical control of anthracene dimerization, together with thermal control of host–guest interactions and dissociation of anthracene dimers, is employed to construct double-dynamic polymers. A viscous solution of anthracene dimer **42** forms upon irradiation of anthracene-terminated supramolecular monomers **41** under UV ( $\lambda > 360$  nm). The 2:1 host–guest complex **45** formed spontaneously upon mixing solutions of **42** and **43**. Gel **44** forms not only by mixing an equimolar solution of **42** and **43** in 1,2-dichloroethane-cyclohexane (1:6 v:v) but also irradiating **45** under UV ( $\lambda > 360$  nm). Heating the gel at 333–353 K leads to its depolymerization by dissociation of either the host–guest complexes alone or the complexes and the anthracene dimers, depending on the extent of heating. These processes are reversible.

### 4.1.5 Dynamic Covalent Cycles and Cages

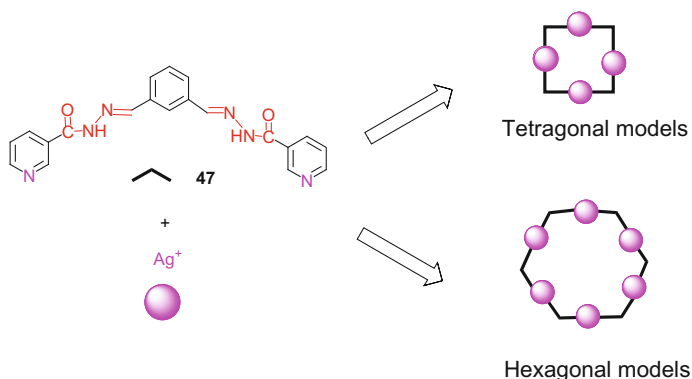
Dynamic covalent chemistry can be used to form molecular cages which have been the hot research for the unique structure and various applications [33–37] in molecular recognition [38], chemical sensing [39], catalysis [40] or gas separation [41] and storage [42]. It is an efficient strategy to access covalently linked cage molecules.



**Scheme 4.14** Dual-mode response of the gel **44**



**Scheme 4.15** Molecular structures of **46**, **48** and **49**



**Scheme 4.16** Tetragonal and hexagonal assemblies of **47** and  $\text{Ag}^+$

Osakada and co-workers synthesized an imine macrocyclic compound **46** with rhomboid molecular shape (Scheme 4.15) [43]. Ultrasound irradiation of the suspension of macrocycle **46** in organic solvent (e.g.  $\text{CH}_2\text{Cl}_2$ ) gives an opaque gel. The xerogel of **46** shows ordered fibrous structure due to linear aggregation of the molecules via  $\pi$ - $\pi$  and  $\text{CH}$ - $\pi$  interactions. According to PXRD data, the one-dimensional aggregates may have a columnar arrangement.

Xue and co-workers reported that bis(pyridine acylhydrazone) ligands **47** induced metal-organic gels with  $\text{Ag}^+$  in several pure or mixed solvents (Scheme 4.16) [44].  $^1\text{H}$  NMR and FT-IR demonstrate coordination interaction between  $\text{Ag}^+$  and nitrogen atom of the pyridine ring of the ligand, and hydrogen bonding contributes to the gelation. The result of PXRD exhibits that **47** gel in DMF packs with mixed tetragonal and hexagonal models. Particularly, the gel possesses a smart and fully reversible thixotropic property. The same gel sample can be switched reversibly (gel-sol-gel) for at least 10 cycles, which makes this gel an excellent fatigue-resistant material.

Iwasawa and co-workers reported a reversible borate gel realized by utilizing macrocyclic boronic esters **48** as gelator (Scheme 4.15) [45]. The formation of borate gel from **48** is induced by guest molecule such as toluene or azulene. A white gel forms immediately by adding 1,3-diaminopropane (2 equiv.) to a suspension of **48**-toluene in MeOH-toluene (2:1) at room temperature. A complex mixture of

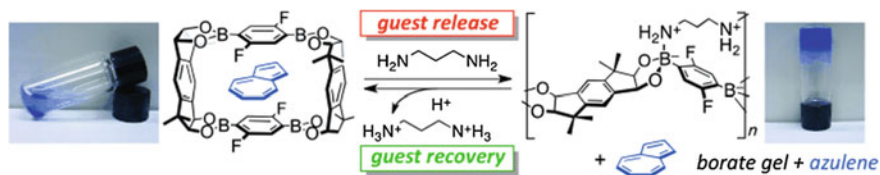


**Fig. 4.13** Release and recovery of the guest molecule during the reversible borate gel formation of **48**-azulene with 1,3-diaminopropane in MeOH-THF. Adapted with permission from [30]. Copyright © 2013 John Wiley and Sons

oligomeric boronic esters is **48** is present in the gel. That is, the role of diamine not only simply links the initial macrocyclic boronic ester **48** with its structure retained but also induces the conversion of **48** to oligomeric boronic esters and then cross-links them. This gel exhibited thermo-, base- and acid-responsive properties owing to the reversible nature of the borate bond. Moreover, it is used for the release and recovery of an equimolar amount of guest molecule such as azulene (Fig. 4.13). A blue gel is obtained when suspension of **48**-azulene is treated with 2 molar amounts of 1,3-diaminopropane in MeOH-THF (4:1) at room temperature. Azulene is released from the host molecule at this state. When the gel is treated with aqueous HCl at room temperature, the gel turns back to the suspension and the released azulene is efficiently recovered as **48**-azulene. Similar phenomenon can be seen when using naphthalene or benzothiophene as guest molecule.

Otto and co-workers reported that dithiol **49** equipped with a short peptide forms hexameric macrocycles upon oxidizing and agitation by shaking (Scheme 4.15) [46]. The hexameric macrocycles self-assemble to form fibres as a free-flowing aqueous solution. Subsequent photoirradiation of the solution induces hemolytic cleavage of disulphides and results in disulphide exchange, which rearranges the disulphide bonds without affecting the global structure of the fibres and forms a hydrogel (Fig. 4.14). The gelation is achieved by conversion of the hexameric macrocycles into polymers from fibrous stacks. This shows that the self-assembled structures are stabilized in a process akin to covalent capture. The hydrogel can be reduced by adding 10 equiv. of dithiothreitol, resulting in the quantitative recovery of building block **49**. So the peptide-derived hydrogels are not only photoresponsive but also redox responsive.

## 4.2 Dynamic Covalent Polymer Gelators

Dynamic covalent bonding can also be involved to form dynamic covalent polymers from small molecules with multiple functional groups leading to the formation of 3D gel networks. Dynamic covalent polymer is linked by the monomers with at least two reactive functional groups which can form dynamic covalent bonds. When these bridging precursors react in solution to form dynamic covalent polymers



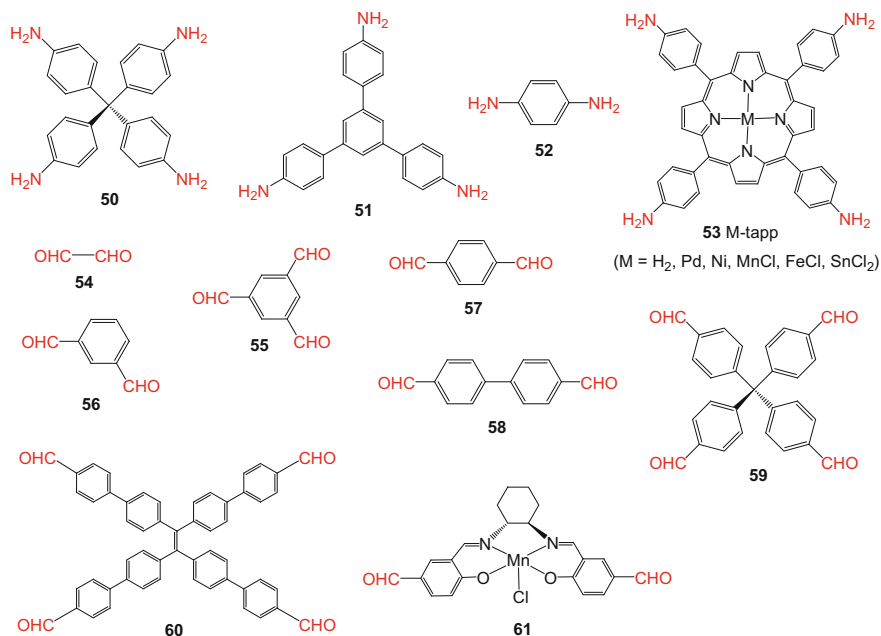
gelation. Such gels are often relatively stable and do not show thermoreversible gel–sol transitions due to the polymeric nature.

### 4.2.1 Imine Gels

A series of gels based on imine chemistry were reported by Zhang and co-workers (Scheme 4.17) [2, 47–49]. The imine gels are synthesized by polycondensation of bridging amines (**50–53**) and aldehydes (**54–61**). The corresponding aerogels are obtained by subcritical CO<sub>2</sub>(l) drying. These imine aerogels consist of three-dimensional networks of interconnected nanometer-sized particles. Bridging amine and bridging aldehyde polymerize to yield microporous nanoparticles. Then the nanoparticles aggregate to form meso- and macropores. Finally, a 3D matrix is formed to trap the solvent (Fig. 4.15). The effects of building blocks, precursor concentration and solvent have been investigated on the porosity of the aerogels. The porosity of the aerogel is controlled by the structural features of precursors, precursor concentration and reaction solvent. Among these aerogels, the aerogel synthesized by **50** and **54** (**50–54** aerogel) in H<sub>2</sub>O exhibited highest BET surface areas up to 1021 m<sup>2</sup> g<sup>-1</sup>. Imine bonds and residual amino groups decorate the pore channels so that the aerogel possesses CO<sub>2</sub> uptake of 1.5 mmol g<sup>-1</sup> at 298 K and 1.0 bar with the isosteric heat of 38.1 kJ mol<sup>-1</sup> and displays high CO<sub>2</sub>/N<sub>2</sub> selectivity up to 70.9, which is derived from the ideal adsorbed solution theory, thus it has potential for capture and recovery of CO<sub>2</sub>. This aerogel shows a good capacity for the uptake of aromatic molecules from aqueous solutions due to its aromatic network and hierarchically porous structure. The aerogel also has great performance in enrichment of large molecule PAHs/OCPs as the coating adsorbent in solid-phase microextraction (SPME) fibres.

The gas sorption properties of the imine aerogels are readily modulated. A series of metalloporphyrin (M-tapp, **53**) imine aerogels show sponge-like porous networked structures consisting of interconnected nanoparticles with hierarchical porosity, high-specific surface areas (up to 719 m<sup>2</sup> g<sup>-1</sup>) and large pore volumes (up to 2.60 cm<sup>3</sup> g<sup>-1</sup>) [48]. The H<sub>2</sub>tapp-**59** aerogel prepared from H<sub>2</sub>tapp and **59** showed good adsorption ability for both aromatic benzene and polar methanol at saturated vapour pressure and room temperature. Among the investigated M-tapp imine aerogels, Pd-tapp-**59** prepared from Pd-tapp and **59** is the best to increase the CO<sub>2</sub> adsorption and shows improved adsorption capacities for H<sub>2</sub> and C<sub>2</sub>H<sub>4</sub>.

Various functional moieties such as tetraphenylethene (TPE) have been incorporated in these imine gels, and it widely expands their application in various fields. The **50–60** gel synthesized from **50** and 1,1,2,2-tetrakis-(4-formyl-(1,10-biphenyl)) ethane (**60**) shows high hierarchical porosity and remarkable aggregation-induced emission enhancement [2]. Introducing the TPE luminescent units is a modular approach towards functional gels with novel sensing properties, and **60** is used for the construction of light-emitting materials due to its AIE characteristics. The gel exhibited a response towards electron deficient nitroaromatic compounds and



**Scheme 4.17** A series of bridging amines (50–53) and aldehydes (54–61)

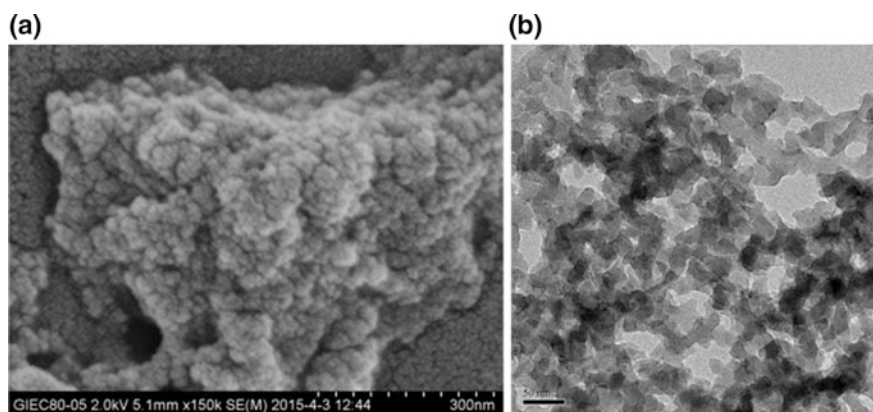


**Fig. 4.15** a SEM and b TEM micrographs of the 50–54 aerogel (bars represent 300 and 50 nm, respectively). Reproduced with permission from [47]. Copyright © The Royal Society of Chemistry 2015

among all the tested compounds, 2,4,6-trinitrophenol (PA) showed the most efficient quenching behaviour attributed to energy transfer from photo-excited  $\pi$ -electron-rich TPE to ground-state electron deficient PA.

Mn-salen catalytically active moiety has been incorporated into dynamic covalent imine gel via the reaction of a chiral Mn-salen dialdehyde unit **61** with a tetraamine linker (**50**) [49]. This Mn-salen imine gel is a good catalyst for asymmetric kinetic resolution of secondary alcohols. Moreover, the imine gel can be coated onto a functionalized capillary and displayed improved catalytic ability. After changing the  $-OH$  on the wall of fused-silica capillary to  $NH_2$ , the gel is readily immobilized on the fused-silica capillary reactor via in situ gelation (Fig. 4.16). The assembled microfluidic gel reactor is proven effective for the enantioselective kinetic resolution of secondary alcohols, giving good conversions and enantiomeric excess (ee) within shorter reaction time (15 min) compared to the batch process and can be reused at least eight times without loss of activity or enantioselectivity (Scheme 4.18).

Metalloporphyrin imine gel Pd-tapp-**50** is also supported on the inner surface of a functionalized capillary and used to assemble catalytic gel capillary reactor [48]. It achieves similar yields in a much shorter time in Suzuki–Miyaura cross-coupling of 4-bromoanisole and phenylboronic acid compared to the batch processes.

### 4.2.2 Calix[4]Arene-Derived Acylhydrazone Gels

Jaworski, Jung and co-workers reported dynamic covalent polymer gels based on acylhydrazone bonding [50]. The gels are prepared from calix[4]arene derivative **62** bearing four hydrazide groups and diphenyl terephthalate-derivative **63** bearing two aldehyde groups in DMSO via hydrazone linkage and non-covalent assembly like H-bond on hydrogen-bonding sites (Scheme 4.19). This calix[4]arene-derivative gels show ductile and high tensile strength. Reversible sol–gel transition suggests that the resulting gel consists of discrete multimeric gelator species rather than extended polymer structure. Interestingly, the mechanical and ductile properties of the gels can be controlled by catalytic HCl. The tensile strength of the gel formed without HCl approaches over 40 MPa. The most remarkable aspect of this study is the mechanical property of the hydrogel. After the solvent DMSO was exchanged with water, the resulting hydrogel showed 7000- to 100,000-fold enhanced mechanical properties. The hydrazone reaction produces  $-OH$  groups under non-acidic conditions or with addition of water, offering enhanced intermolecular hydrogen-bonding interactions and thus increased elastic properties (Fig. 4.17). This represents an interesting moulding method from small molecules to retain the gel shape after processing. The gel also shows good ionic conductivities as gel electrolytes.

Acylhydrazone gels have been developed based on calix[4]arene derivative **62** and photosensitive stilbene derivative **64** (Scheme 4.19) [51]. Calixarene-derived networks can provide robust supramolecular gels, and introducing a photoreactive stilbene moiety makes it possible that its aggregation state is tuned by heating and UV exposure. [2+2] cycloaddition of stilbene moieties occurred for stilbene H-aggregates after UV exposure result in the effect of their fluorescence by

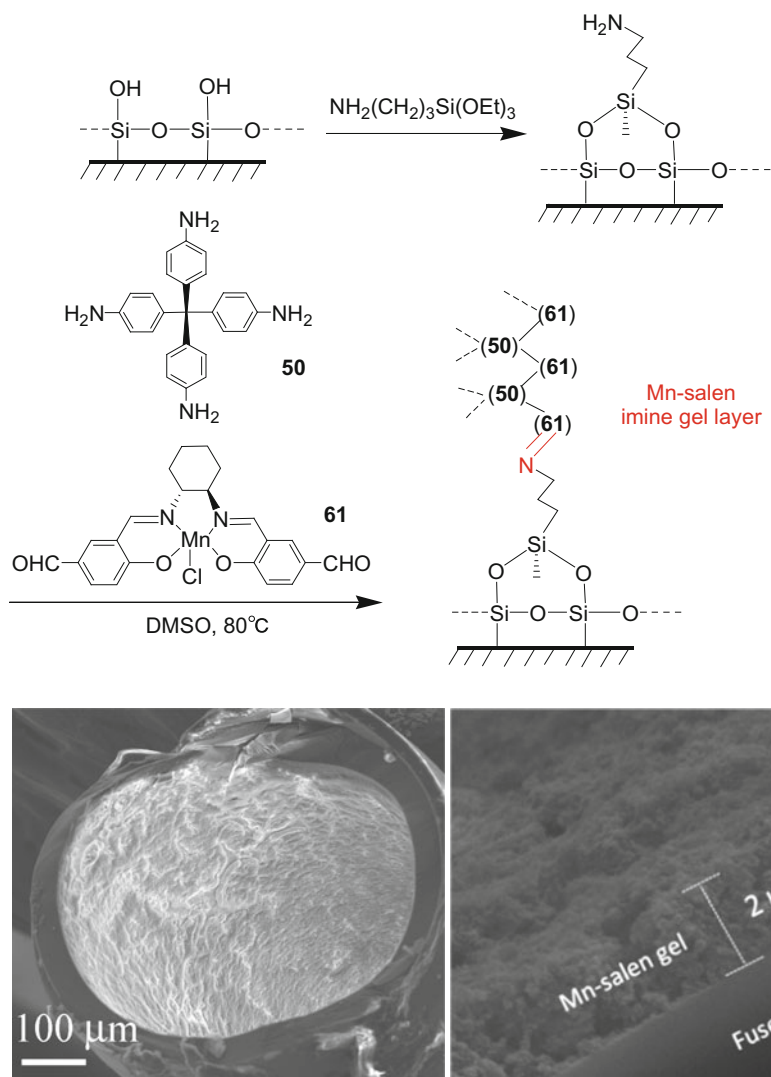
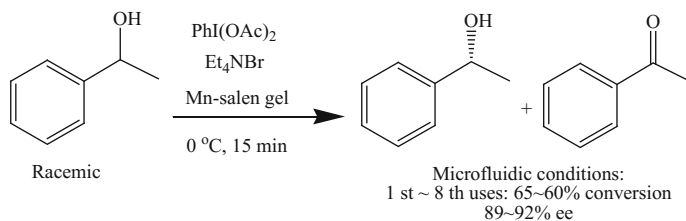
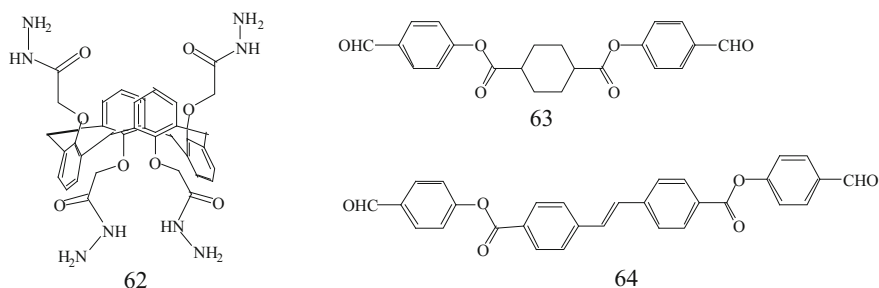


**Fig. 4.16** Schematic representation of coating of Mn-salen imine gel on the wall of fused-silica capillary, and SEM images of a cross section of the capillary coated with Mn-salen gel prepared from **50** and **61** with about  $2\ \mu\text{m}$  thickness. Reproduced with permission from [49]. Copyright © The Royal Society of Chemistry 2015

providing a strong green fluorescence emission. The proportion of H- and J-aggregations modes within supramolecular gels controlled by the temperature determines the mechanical and the fluorescent properties (Fig. 4.18). By increasing temperature, partial H-aggregates change to J-aggregate modes due to enhanced movement of encapsulated solvent molecules in the gel, leading to green



**Scheme 4.18** Enantioselective kinetic resolution of secondary alcohols catalyzed by Mn-salen gel prepared from **50** and **61**



**Scheme 4.19** Molecular structures of **62–64**

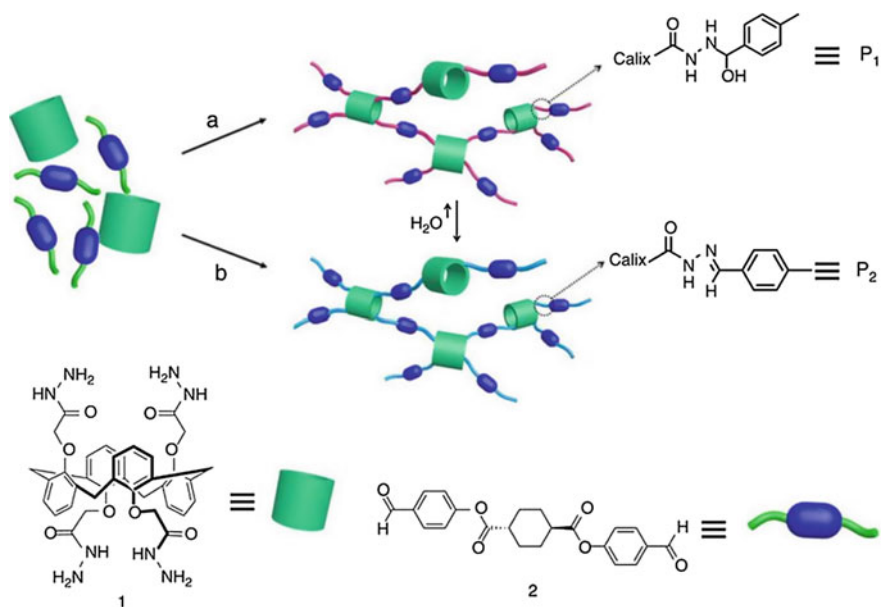


**Fig. 4.17** Schematic representation of calix[4]arene-based gel formation by acylhydrazone bonding. Reproduced with permission from [50]. Copyright © 2015 Macmillan Publishers Limited

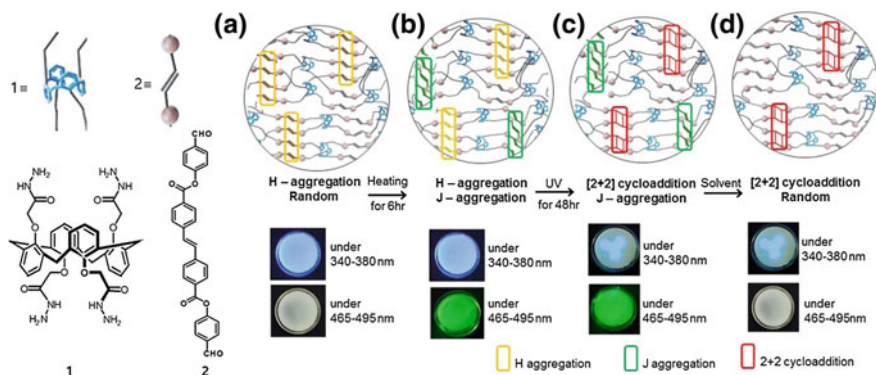


**Fig. 4.18** Schematic representation of proposed network structures: **a** before and **b** after heating, **c** after UV irradiation, and **d** after immersion in DMSO with the blue emission observed from exposure to band-pass filtered light of 340–380 nm and the green emission taken in response to band-pass filtered light of 465–495 nm. Adapted with permission from [51]. Copyright (2017) American Chemical Society

fluorescence under 465–495 nm light, while the mainly original blue fluorescence remained under 340–380 nm light. On the other hand, the mechanical properties can be controlled by UV irradiation and heating. Increasing UV irradiation time of the gel enhances the viscoelasticity and stiffness in the range from  $\sim 100$  to 450 kPa (Young's modulus). Heating the gel increases its storage and loss moduli values nearly 2.2-fold.

## References

1. Lehn J-M (2007) From supramolecular chemistry towards constitutional dynamic chemistry and adaptive chemistry. *Chem Soc Rev* 36:151–160
2. Luo W, Zhu Y, Zhang J, He J, Chi Z, Miller PW, Chen L, Su C-Y (2014) A dynamic covalent imine gel as a luminescent sensor. *Chem Commun* 50:11942–11945
3. Foster JS, Źurek JM, Almeida NMS, Hendriksen WE, le Sage VAA, Lakshminarayanan V, Thompson AL, Banerjee R, Eelkema R, Mulvana H, Paterson MJ, van Esch JH, Lloyd GO (2015) Gelation landscape engineering using a multi-reaction supramolecular hydrogelator system. *J Am Chem Soc* 137:14236–14239
4. Boekhoven J, Poolman JM, Maity C, Li F, van der Mee L, Minkenberg CB, Mendes E, van EschJan H, Eelkema R (2013) Catalytic control over supramolecular gel formation. *Nat Chem* 5:433–437
5. Li J, Carnall JMA, Stuart MCA, Otto S (2011) Hydrogel formation upon photoinduced covalent capture of macrocycle stacks from dynamic combinatorial libraries. *Angew Chem Int Ed* 50:8384–8386
6. Belowicha ME, Stoddart JF (2012) Dynamic imine chemistry. *Chem Soc Rev* 41:2003–2024
7. Zhang JY, Zeng LH, Feng J (2017) Dynamic covalent gels assembled from small molecules: from discrete gelators to dynamic covalent polymers. *Chin Chem Lett* 28:168–183

8. Wang Y-J, Xing P-Y, Li S-Y, Ma M-F, Yang M-M, Zhang Y-M, Wang B, Hao A-Y (2016) Facile stimuli-responsive transformation of vesicle to nanofiber to supramolecular gel via  $\omega$ -amino acid-based dynamic covalent chemistry. *Langmuir* 32:10705–10711
9. Yu X-D, Xie D-Y, Li Y-J, Geng L-J, Ren J-J, Wang T, Pang X-L (2017) Photochromic property of naphthalimide derivative: selective and visual  $F^-$  recognition by NSS isomers both in solution and in a self-assembly gel. *Sens Actuators B* 251:828–835
10. Rajamalli P, Prasad E (2011) Low molecular weight fluorescent organogel for fluoride ion detection. *Org Lett* 13:3714–3717
11. Rajamalli P, Prasad E (2012) Non-amphiphilic pyrene cored poly(aryl ether) dendron based gels: tunable morphology, unusual solvent effects on the emission and fluoride ion detection by the self-assembled superstructures. *Soft Matter* 8:8896–8903
12. Lakshmi NV, Mandal D, Ghosh S, Prasad E (2014) Multi-stimuli-responsive organometallic gels based on ferrocene-linked poly(aryl ether) dendrons: reversible redox switching and  $Pb^{2+}$ -Ion Sensing. *Chem Eur J* 20:9002–9011
13. Lv K, Zhang L, Liu M-H (2014) Self-assembly of triangular amphiphiles into diverse nano/microstructures and release behavior of the hollow sphere. *Langmuir* 30:9295–9302
14. Poolman JM, Maity C, Boekhoven J, van der Mee L, le Sage VAA, Groenewold GJM, van Kasteren SI, Versluis F, van Esch JH, Eelkema R (2016) A toolbox for controlling the properties and functionalisation of hydrazone-based supramolecular hydrogels. *J Mater Chem B* 4:852–858
15. Sreenivasachary N, Lehn J-M (2005) Gelation-driven component selection in the generation of constitutional dynamic hydrogels based on guanine-quartet formation. *Proc Natl Acad Sci U S A* 102:5938–5943
16. Bunzen H, Nonappa Kalenius E, Hietala S, Kolehmainen E (2013) Subcomponent self-assembly: a quick way to new metallogels. *Chem Eur J* 19:12978–12981
17. Zang L-B, Shang H-X, Wei D-Y, Jiang S-M (2013) A multi-stimuli-responsive organogel based on salicylidene Schiff base. *Sens Actuators B* 185:389–397
18. Sun J-G, Liu Y-C, Jin L-Y, Chen T, Yin B-Z (2016) Coordination-induced gelation of an L-glutamic acid Schiff base derivative: the anion effect and cyanide-specific selectivity. *Chem Commun* 52:768–771
19. Dixit MK, Pandey VK, Dubey M (2016) Alkali base triggered intramolecular charge transfer metallogels based on symmetrical A- $\pi$ -D-chiral-D- $\pi$ -A type ligands. *Soft Matter* 12:3622–3630
20. Sarmah K, Pandit G, Das AB, Sarma B, Pratihar S (2017) Steric environment triggered self-healing  $Cu^{II}/Hg^{II}$  bimetallic gel with old  $Cu^{II}$ -Schiff Base complex as a new metalloligand. *Cryst Growth Des* 17:368–380
21. Rajamalli P, Malakar P, Atta S, Prasad E (2014) Metal induced gelation from pyridine cored poly(aryl ether) dendrons with in situ synthesis and stabilization of hybrid hydrogel composites. *Chem Commun* 50:11023–11025
22. Lin Q, Sun B, Yang Q-P, Fu Y-P, Zhu X, Wei T-B, Zhang Y-M (2014) Double metal ions competitively control the guest-sensing process: a facile approach to stimuli-responsive supramolecular gels. *Chem Eur J* 20:11457–11462
23. Lin Q, Yang Q-P, Sun B, Fu Y-P, Zhu X, Wei T-B, Zhang Y-M (2014) Rewritable security display material and  $Cl^-$  sensor: based on a bimetal competitive coordination controlled supramolecular gel. *Mater Lett* 137:444–446
24. Lin Q, Sun B, Yang Q-P, Fu Y-P, Zhu X, Zhang Y-M, Wei T-B (2014) A novel strategy for the design of smart supramolecular gels: controlling stimuli-response properties through competitive coordination of two different metal ions. *Chem Commun* 50:10669–10671
25. Lin Q, Yang Q-P, Sun B, Fu Y-P, Zhu X, Wei T-B, Zhang Y-M (2014) Competitive coordination control of the AIE and micro states of supramolecular gel: an efficient approach for reversible dual-channel stimuli-response materials. *Soft Matter* 10:8427–8432
26. Lin Q, Lu T-T, Zhu X, Sun B, Yang Q-P, Wei T-B, Zhang Y-M (2015) A novel supramolecular metallogel-based high-resolution anion sensor array. *Chem Commun* 51:1635–1638

27. Lin Q, Lu T-T, Zhu X, Wei T-B, Li H, Zhang Y-M (2016) Rationally introduce multi-competitive binding interactions in supramolecular gels: a simple and efficient approach to develop multi-analyte sensor array. *Chem Sci* 7:5341–5346
28. Peters GM, Skala LP, Plank TN, Hyman BJ, Reddy GNM, Marsh A, Brown SP, Davis JT (2014) A G4 K<sup>+</sup> hydrogel stabilized by an anion. *J Am Chem Soc* 136:12596–12599
29. Peters GM, Skala LP, Plank TN, Oh H, Reddy GNM, Marsh A, Brown SP, Raghavan SR, Davis JT (2015) G4-quartet M<sup>+</sup> borate hydrogels. *J Am Chem Soc* 137:5819–5827
30. Plank TN, Davis JT (2016) A G4 K<sup>+</sup> hydrogel that self-destructs. *Chem Commun* 52:5037–5040
31. Venkatesh V, Mishra NK, Romero-Canelon I, Vernooij RR, Shi H-Y, Coverdale JPC, Habtemariam A, Verma S, Sadler PJ (2017) Supramolecular photoactivatable anticancer hydrogels. *J Am Chem Soc* 139:5656–5659
32. Xu J-F, Chen Y-Z, Wu L-Z, Tung C-H, Yang Q-Z (2013) Dynamic covalent bond based on reversible photo [4+4] cycloaddition of anthracene for construction of double-dynamic polymers. *Org Lett* 15:6148–6151
33. Jin Y-H, Wang Q, Taynton P, Zhang W (2014) Dynamic covalent chemistry approaches toward macrocycles, molecular cages, and polymers. *Acc Chem Res* 47:1575–1586
34. Jin Y, Jin A, McCaffrey R, Long H, Zhang W (2012) Design strategies for shape-persistent covalent organic polyhedrons (COPs) through imine condensation/metathesis. *J Org Chem* 77:7392–7400
35. Hasell T, Little MA, Chong S-Y, Schmidtman M, Briggs EM, Santolini V, Jelfs KE, Cooper AI (2017) Chirality as a tool for function in porous organic cages. *Nanoscale* 9:6783–6790
36. Jin Y, Zhu Y, Zhang W (2013) Development of organic porous materials through schiff-base chemistry. *Cryst Eng Comm* 15:1484–1499
37. Hasell T, Cooper AI (2016) Porous organic cages: soluble, modular and molecular pores. *Nat Rev Mater* 1:16053
38. Śolomek T, Powers-Riggs NE, Wu Y-L, Young RM, Krzyaniak MD, Horwitz NE, Wasielewski MR (2017) Electron hopping and charge separation within a naphthalene-1,4,5,8-bis(dicarboximide) chiral covalent organic cage. *J Am Chem Soc* 139:3348–3351
39. Akine S, Miyashita M, Nabeshima T (2017) A metallo-molecular cage that can close the apertures with coordination bonds. *J Am Chem Soc* 139:4631–4634
40. Chen H-Y, Gou M, Wang J-B (2017) De novo endo-functionalized organic cages as cooperative multi-hydrogen-bond-donating catalysts. *Chem Commun* 53:3524–3526
41. Hasell T, Miklitz M, Stephenson A, Little MA, Chong SY, Clowes R, Chen L-J, Holden D, Tribello GA, Jelfs KE, Cooper AI (2016) Porous organic cages for sulfur hexafluoride separation. *J Am Chem Soc* 138:1653–1659
42. Zhang G, Presly O, White F, Oppel IM, Mastalerz M (2014) A permanent mesoporous organic cage with an exceptionally high surface area. *Angew Chem Int Ed* 53:1516–1520
43. Ide T, Takeuchi D, Osakada K (2012) Columnar self-assembly of rhomboid macrocyclic molecules via step-like intermolecular interaction. *Crystal Formation Gelation Chem Commun* 48:278–280
44. Xue M, Lu Y-C, Sun O-O, Liu K-Q, Liu Z, Sun P (2015) Ag (I)-coordinated supramolecular metallogels based on schiff base ligands: structural characterization and reversible thixotropic property. *Cryst Growth Des* 15:5360–5367
45. Ito S, Takata H, Ono K, Iwasawa N (2013) Release and recovery of guest molecules during the reversible borate gel formation of guest-included macrocyclic boronic esters. *Angew Chem Int Ed* 52:11045–11048
46. Li J-W, Carnall JMA, Stuart MCA, Otto S (2011) Hydrogel formation upon photoinduced covalent capture of macrocycle stacks from dynamic combinatorial libraries. *Angew Chem* 123:8534–8536

47. Zhang J-Y, Liu L-P, Liu H-L, Lin M-J, Li S-Y, Ouyang G-F, Chen L-P, Su C-Y (2015) Highly porous aerogels based on imine chemistry: syntheses and sorption properties. *J Mater Chem A* 3:10990–10998
48. Zeng L-H, Liao P-S, Liu H-L, Liu L-P, Liang Z-W, Zhang J-Y, Chen L-P, Su C-Y (2016) Impregnation of metal ions into porphyrin-based imine gels to modulate guest uptake and to assemble a catalytic microfluidic reactor. *J Mater Chem A* 4:8328–8336
49. Liu H-L, Feng J, Zhang J-Y, Miller PW, Chen L-P, Su C-Y (2015) A catalytic chiral gel microfluidic reactor assembled via dynamic covalent chemistry. *Chem Sci* 6:2292–2296
50. Lee J-H, Park J, Park J-W, Ahn H-J, Jaworski J, Jung J-H (2015) Supramolecular gels with high strength by tuning of calix[4]arene-derived networks. *Nat Commun* 6:6650–6658
51. Lee J-H, Jung S-H, Lee S-S, Kwon K-Y, Sakurai K, Jaworski J, Jung J-H (2017) Ultraviolet patterned calixarene-derived supramolecular gels and films with spatially resolved mechanical and fluorescent properties. *ACS Nano* 11:4155–4164

# Chapter 5

## Polymer Gels

**Abstract** The cross-linking of long-chain polymeric gelators has been shown to be an effective driving force for the formation of polymer gels. In this chapter, various polymer gels are discussed according to the interaction species of the cross-linking between the gelators. The interactions include hydrogen bonding, metal–organic coordination and dynamic covalent bonding. Prior to discussing these interactions, several traditional polymer gels are introduced such as silicone-based gels and polymer hydrogels. The thermodynamic aspects relating to the swelling of polymer gels upon exposure to a liquid are described in detail. By analysing the macroscopic degree of swelling of a polymer gel, the microscopic cross-linking between polymer chains can be probed quantitatively. The formation of the polymer gels driven by different interactions is presented by illustrating the correlation between the properties and driving forces. Following the gel systems comprising individual interaction species, strategies to combine polymer and low molecular weight gels are presented. The emerging hybrid materials are promising to integrate the advantages of both polymer and low molecular weight gels.

**Keywords** Polymer gels · Cross-linking · Swelling · Hydrogen bonding  
Metal–organic coordination · Dynamic covalent bonding · Hybrid gels

### 5.1 Introduction to Polymer Gels

Polymer gels are three-dimensional (3D) molecular networks formed by the light cross-linking of long-chain polymeric gelators. Within the 3D networks, liquids such as water and organic solvents are encapsulated. Similar to low molecular weight gelators, the cross-linking of polymeric gelators can also be achieved via either non-covalent or covalent interactions. Compared with non-covalently cross-linked polymers, 3D molecular networks with covalent cross-linking are relatively robust and, however, sometimes less responsive to external stimuli.

---

Ya Hu and Jianyong Zhang contributed together to this chapter.

To program the properties of polymer gels, several factors can be tuned including polymer backbones, liquid species, polymer–liquid interactions, addition of extra additives and liquid loading.

Most of the gels we come into contact in everyday life or apply in high-tech areas are made of polymers, such as materials for uses in contact lenses [1], robotics [2], tissue surrogates [3], sensing [4] and battlefield health care [5]. According to the nature of swelling agent in liquid phases, polymer gels can also be broadly categorized into two sub-classes: hydrogels and organogels [6]. Hydrogels are made of three-dimensional cross-linked polymer chains, which absorb water rather than dispersing or dissolving. For organogels, the swelling agents for polymer networks are organic solutions. Commonly, the liquid phases of gels are made of more than 95% (by weight) of water content or organic solutions [7–9]. In the following part of this section, several key aspects of the formation of polymer gels are discussed in detail.

### 5.1.1 Cross-Linking of Polymer Chains

Cross-linking between polymer chains or between segments of the same chain plays a pivotal role in determining the formation of polymer gels. Figure 5.1 is a schematic illustration showing the interchain cross-linking and entanglements between polymer chains. In Fig. 5.1a, the entanglement of uncross-linked polymer chains is presented. The good affinity of the polymer chains with organic solvents or water often results in the formation of a uniform solution. Microscopically, the solution is composed of polymer chains, each one of which is surrounded by organic solvent or water molecules. The viscosity of the polymer solution is usually significantly larger than that of the solvent. If the polymer chains or different segments within the same chain are cross-linked via varying interactions, a strongly linked molecular assembly is established (Fig. 5.1b). The bonding strength of the cross-linkers ranges from strong covalent bonds to weak non-covalent interactions such as

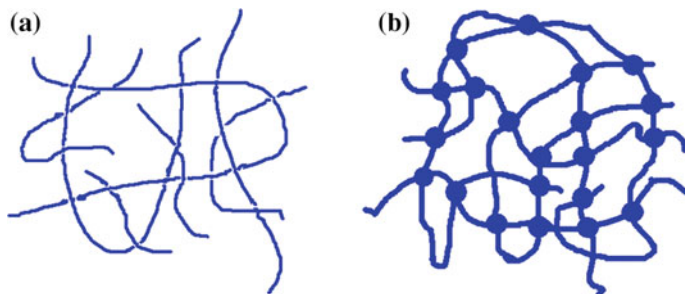


**Fig. 5.1** Schematic illustrations of **a** uncross-linked polymer chains, **b** cross-linked polymer networks. The blue knots correspond to cross-linkers between polymer gelators

hydrogen bonding. Due to these cross-linked knots, the polymer chains are still bonded, instead of being separated, while they are in contact with water or other organic solvents. Meanwhile, the surrounding water or organic solvent molecules may enter the space within the molecular assembly leading to the swelling of the molecular network. The polymer species and density of cross-linking knots play a key role in determining the mechanical properties of polymer gels. In most cases, the elasticity and mechanical strength of a polymer gel increase with the density of cross-linked knots.

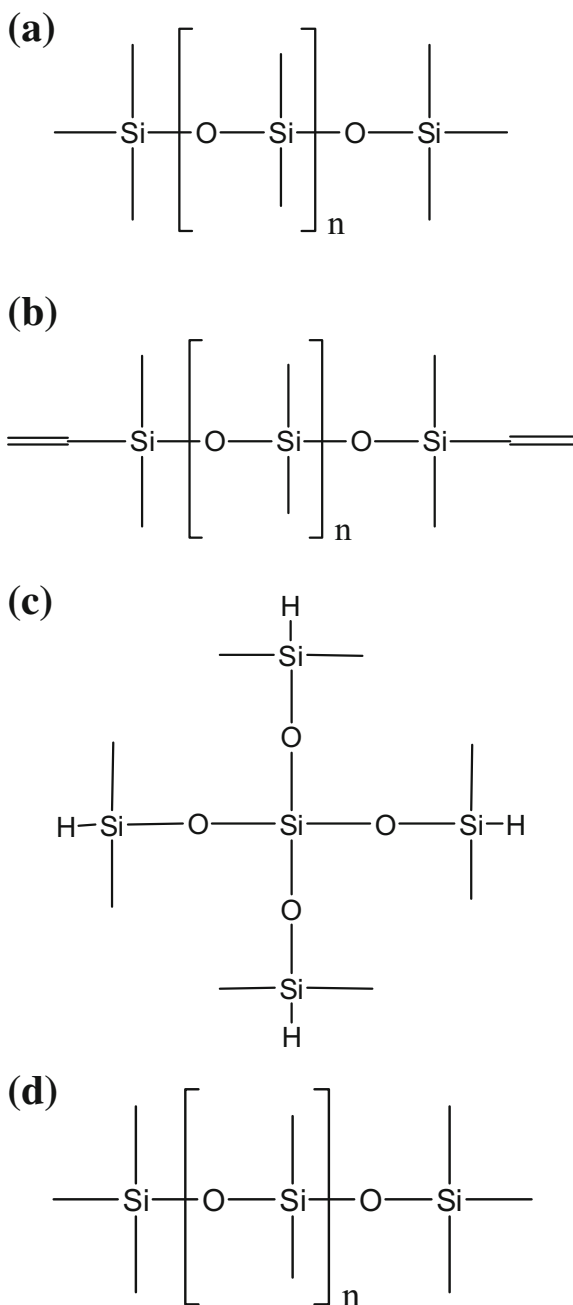
### 5.1.2 Traditional Polymer Gels

Polymer gels are conventionally prepared via permanent cross-linking of high molecular weight polymer chains. Among various species of polymer gels, silicone-based gels and hydrogels have been most intensively studied materials [10–12].

Silicones, also referred to as polysiloxanes, are commonly used polymers with applications in lubricants, thermal and electrical insulation, adhesives and sealants. The chemical composition of silicones consists of long backbone chains with alternating silicon and oxygen atoms ( $\cdots\text{Si-O-Si-O-Si-O}\cdots$ ). The most commonly used siloxane is linear silicone polydimethylsiloxane (PDMS), which is a silicone oil (Fig. 5.2a). By varying the chain lengths, side groups and cross-linking of the  $-\text{Si-O}-$  backbones, silicone oils can be converted into gel-phase materials. Figure 5.2b–d presents PDMS backbones functionalized with different chemical groups such as non-reactive methyl groups and reactive methyl groups. This versatility of the  $-\text{Si-O}-$  backbones leads to an abundant range of silicone-based gel materials.

Polymer hydrogels are a class of polymer gels that have a wide range of biomedical uses. Instead of dissolving in water, hydrogels swell due to the encapsulation of water within the 3D network made of cross-linked polymer chains. Dating back to the late 1950s, Wichterle and Lim from the Prague Institute of Chemical Technology developed the first hydrophilic gels for biological applications using copolymers of ethylene dimethacrylate and 2-hydroxyethyl methacrylate [13]. On the basis of these hydrogels, the first soft contact lenses made of polyacrylamide were introduced in the 1970s [14]. The 3D networks composed of cross-linked polyacrylamide chains can absorb water forming hydrogels. By weight, the hydrogels used for soft contact lenses contain water ranging from approximately 38–79% [15]. The water incorporated in the hydrogels results in the softness and flexibility of the contact lenses. Also, oxygen in the air is allowed to pass through the water content of the hydrogels ensuring a healthy environment for human eyes. However, the mechanical stability and clarity of vision related to the soft contact lenses may be decreased with the increase in the percentage of water content within the hydrogels.

**Fig. 5.2** Chemical structures of silicone-based gel components. **a** PDMS, **b** m-PDMS. Non-reactive methyl-terminated PDMS, **c** tetrafunctional silane as cross-linking molecules, **d** V-PDMS. Reactive vinyl-terminated PDMS



The development of hydrogels for soft contact lenses has stimulated extensive interest to study smart polymer hydrogels that are responsive to external stimuli such as light [16], electric field [17], pH [18] and temperature [19]. Traditional pathways to synthesize hydrogels include cross-linking copolymerization and cross-linking of hydrophilic polymer precursors. These methods achieve easy preparation of hydrogels but do not help achieve exact control over chain length, sequence or three-dimensional structure of hydrogels. To date, the exploration of new methods to design and synthesize smart hydrogels has always been an attractive research topic. Scientists have made efforts to synthesize hydrogels or gelation building blocks by using genetic engineering methods. In addition, a large number of associative building blocks have been designed for the self-assembly of hydrogel structures. The research goal is to achieve a rational design of hydrogels that can respond to external stimuli rapidly by adopting a combination of these methods.

Stimuli-responsive hydrogels have been formed from numerous molecular building blocks. The performance of hydrogels has been found to be closely related to the molecular arrangement of polymer components. Typical polymer components include triblock and diblock copolymers [20]. Triblock copolymers can be self-assembled into stimuli-sensitive hydrogels by protein engineering [21]. Diblock copolymers composed of polyoxyethylene and polyoxybutylene can also be used for hydrogel materials at high polymer concentrations [22].

Apart from bulk hydrogels, hybrid materials combining hydrogel and solid surfaces have also attracted extensive research interests [23, 24]. Zhao and co-workers demonstrated a range of hybrid systems composed of hydrogel and non-porous surfaces [25]. In this reported work, the solid surfaces of glass, silicon wafer, titanium, aluminium and mica ceramic were first functionalized with 3-(trimethoxysilyl) propyl methacrylate. Subsequently, the long chain polymer network of polyacrylamide or polyethylene glycol diacrylate was covalently cross-linked to the silanes. This design enhances the interaction between the resulting hydrogel layers and underlying surfaces. The tough bonding was mainly due to the high values of the intrinsic adhesion and the excellent mechanical properties of the bulk hydrogels. The hybrid hydrogel-surface systems can open up new opportunities to prepare hydrogel-based electronic and microfluidic systems.

## 5.2 Fundamental Aspects

### 5.2.1 Concepts

Depending on the nature of cross-linking between polymer chains, polymer gels can be categorized into two groups: chemical gels and physical gels. Chemical gels include the cross-linking of polymer chains via chemical reactions such as radical vinyl polymerization and stepwise polycondensation. In contrast to chemical gels,

physical gels are formed via cooperative intermolecular interactions including hydrogen bonding, metal–organic coordination, van der Waals interactions and electrostatic interactions. In some cases, the entanglement of long polymer chains at high concentrations also contributes to the structural stabilization of physical gels.

In addition to the nature of cross-linking, polymer gels can also be classified according to whether the polymer chains are biological or synthetic molecules. Biology-oriented polymer gels, also referred to as biogels, are obtained from natural polymers with animal, plant and algal origins such as protein and polysaccharide. Examples of these natural polymers include collagen, agarose, carrageenan, starch, cellulose, pectin, chitosan, cellulose, alginic acid and hyaluronic acid derivatives. The nature-inspired biogels exhibit advantages in particular, the ability to mimic biological transport processes [26, 27]. Physically cross-linked biogels can often undergo reversible sol–gel transitions in response to thermal or chemical factors. Synthetic hydrophilic polymers are common components for artificial hydrogels. Acrylics, including acrylic acid, acrylamide and maleic anhydride polymers and copolymers, are typical hydrophilic polymers for synthetic hydrogels. Other examples include amine-functional polymers (such as allylamine, ethyleneimine and oxazoline) and other polymers containing amine groups in their main chains or side chains.

### ***5.2.2 Mechanical Properties***

Polymer gels are soft materials with a hybrid structure consisting of three-dimensional polymer networks and a large amount of liquids. As a result of this unique bi-phase structure, the gels can be treated as solids macroscopically while as polymer solutions microscopically. Therefore, the chemical reactivity, the material permeability of liquids and the self-standing ability of solids also exhibit duality. The mechanical properties of polymer gels are an important aspect to consider when designing and synthesizing functional gel materials. In order to be used in real-world applications, polymer gels are required to be mechanically robust. The commonly encountered parameters used to characterize the mechanical robustness of polymer gels include Young's modulus [28], tensile or compressive fracture [29], fracture energy [30] and viscoelastic properties [31].

### ***5.2.3 Swelling and Shrinking Properties***

Swelling is a concept describing the dynamic volume change of polymer gels on immersion in liquids. Upon exposure to a solvent, a cross-linked polymer network is commonly observed to swell rather than dissolving completely. Due to the absorption of the solvent molecules by the network, the total volume of the polymer

gel increases. The degree of the increase in gel volume depends on the cross-linking of the polymer chains and the polymer–solvent interaction.

The network junctions within a polymer gel swollen in a solvent are moved away from each other by the solvent molecules. With the movement of the network junctions, a stress is experienced by the polymer chains attached to the junctions. This force is caused by the free energy of mixing trying to dilute the polymer solution. In the meantime, the polymer chains also tend to return to its random relaxed state with a higher entropy value. Thus, an elastic retractive force in opposition to the elongation of polymer chains is generated. When the relaxed state reaches an equilibrium with the strained one, the diffusion of the solvent molecules from the free solution to the polymer network stops. At this equilibrium state, the chemical potential of the solvent in the polymer network is equal to that in the free solution.

For a given gel system comprising polymer chains and solvent molecules, the swelling degree at the equilibrium state often decreases with the increase of the number of cross-linking junctions. An increased degree of cross-linking leads to reduced chain lengths between adjacent junctions and therefore the decreased extension of the polymer chains.

In practice, the microscopic degree of cross-linking within a polymer gel network can be probed by the degree of swelling in a good solvent. In a typical swelling experiment, the change in mass or volume for a swollen polymer gel is measured at a specific temperature. The experimentally measured mass or volume swelling ratio can be used for the qualitative examination of the level of cross-linking. At a high level of analysis, a quantitative calculation of the cross-link density can be conducted by using theoretical methods. Flory–Rehner theory is a classical method used for the analysis of cross-linking within a polymer according to the result of a swelling experiment [32]. According to the Flory–Rehner theory, the average molecular weight between cross-links  $M_c$  is related to the degree of swelling of a polymer network at its equilibrium state. In terms of thermodynamics, a polymer gel can be characterized as an elastic solution. Therefore, the thermodynamics of polymer solutions can be extended to calculate free energy changes in gel systems. As the swelling of polymer gels is accompanied with visible deformation, the calculation of entropy values is more complicated in comparison to solution systems.

When placed in a good solvent, the free energy change  $\Delta G$  associated with the swelling of a polymer gel can be written as:

$$\Delta G = \Delta G_m + \Delta G_e \quad (5.1)$$

In Eq. (5.1),  $\Delta G_m$  is the free energy resulting from the mixing of the polymer network and solvent, and  $\Delta G_e$  is the free energy caused by the elastic expansion of the polymer network. The physical processes associated with  $\Delta G_m$   $\Delta G_e$  are presented in Fig. 5.3. When ions are included, the energy contribution from ions should also be considered.

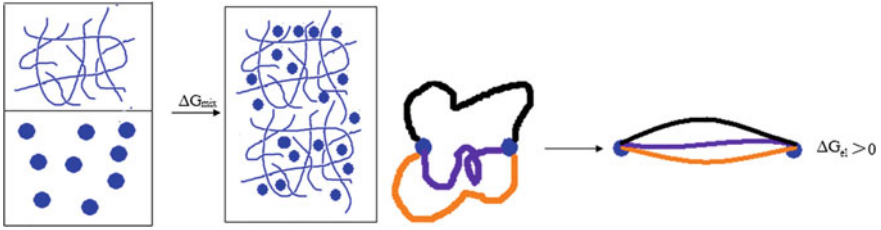


**Fig. 5.3** Schematic illustration showing the physical processes associated with  $\Delta G_m$  and  $\Delta G_e$

Regarding neutral polymer network,  $\Delta G_m$  can be calculated as:

$$\Delta G_m = \Delta H_m - T\Delta S_m \quad (5.2)$$

In Eq. (5.2),  $\Delta H_m$  and  $\Delta S_m$  are enthalpy and entropy values upon mixing, respectively.  $\Delta S_m$  represents the entropy change when mixing  $n_1$  solvent molecules and  $n_2$  polymer chains forming a homogeneous solution. In contrast to low molecular weight gelators, a significant difference in physical dimension exists between the solvent and solute molecules in a polymer gel system. Therefore, the influence of the conformation and configuration of polymer chains on entropy should not be neglected. Flory lattice model has been widely used for the interpretation of  $\Delta S_m$  which can be simplified into the following equation:

$$\Delta S_m = -k_B [n_1 \ln(1 - \varphi) + n_2 \ln \varphi] \quad (5.3)$$

In this equation,  $k_B$  is the Boltzmann constant, and  $\varphi$  is the volume fraction of solute molecules.

Apart from the mixing entropy, Flory lattice model also describes the enthalpy change associated with the mixing of solvent and polymer chains. Essentially, the mixing event can be understood as the replacement of the solvent–solvent and chain–chain homogeneous contact with solvent–chain heterogeneous contact. When considering the contact replacement, a parameter,  $\varepsilon$ , is introduced to indicate the change in contact (mixing) energy.

$$\varepsilon = \mu_{12} - \frac{\mu_{11} + \mu_{12}}{2} \quad (5.4)$$

In Eq. (5.4),  $\varepsilon$  is the enthalpy change associated with the formation of 1 solvent–chain contact pair from 1/2 solvent–solvent and 1/2 solvent–chain contact. The subscripts 1 and 2 correspond to solvent and solute molecules, respectively. When considering a polymer solution, the mixing of solvent and solute molecules can be illustrated using the following reaction formula:



For Eq. (5.5),  $A$  is the solvent molecule and  $B$  is the solute molecule. The change in internal energy associated with the mixing reaction formula (5.5) is  $2\varepsilon$ .

If the number of solvent–chain contact pairs is  $p$  in a molecular system, the change in total contact energy can be calculated as  $p\varepsilon$ .  $p = zn_1\vartheta$ , where  $z$  is the coordination number,  $n_1$  is number of solvent molecules, and  $\vartheta$  is volume fraction of polymer molecules. Therefore, the enthalpy upon mixing,  $\Delta H_m$ , is derived as:

$$\Delta H_m = p\varepsilon = zn_1\vartheta\varepsilon = k_B T n_1 \vartheta \chi_1 \quad (5.6)$$

In Eq. (5.6),  $\chi_1$ , which is the polymer–solvent interaction parameter (also called the Flory–Huggins interaction parameter), is defined as:

$$\chi_1 = \frac{z\varepsilon}{k_B T} \quad (5.7)$$

$\chi_1$  measures the interaction energy of mixing of polymer chains with solvent molecules.

As a result,  $\Delta G_m$  introduced in Eq. (5.1) can be evaluated with Eqs. (5.6) and (5.7) yielding:

$$\Delta G_m = k_B T [n_1 \ln(1 - \vartheta) + n_2 \ln \vartheta + \chi_1 n_1 \vartheta] \quad (5.8)$$

According to Eq. (5.1), the other contribution to  $\Delta G$  is  $\Delta G_e$ , the elastic free energy associated with expansion of the polymer network. This elastic component of the free energy has a correlation with the change in entropy as the polymer network is undergoing deformation and can therefore be written as:

$$\Delta G_e = -T\Delta S_e \quad (5.9)$$

In Eq. (5.9),  $\Delta S_e$  represents the elastic entropy change.

To describe the deformation of a polymer network quantitatively, a linear deformation factor,  $\alpha$ , is introduced.

$$\alpha = \frac{L}{L_0} \quad (5.10)$$

In Eq. (5.10),  $L_0$  and  $L$  are the lengths of the polymer network along a certain direction before and after undergoing deformation, respectively. At the beginning of the elastic expansion,  $L_0 = L$ , thus, the defined deformation factor,  $\alpha = 1$ , at this moment.

The change in elastic entropy,  $\Delta S_e$ , is contributed by two sub-components:

$$\Delta S_e = \Delta S_1 + \Delta S_2 \quad (5.11)$$

In Eq. (5.11),  $\Delta S_1$  is the entropy change of uncross-linked polymer chains, and  $\Delta S_2$  is correlated with the entropy change caused by the formation of a cross-linked chain pair.

### 5.3 Nature of Cross-Linking Leading to the Formation of Polymer Gels

The arrangement and interactions between polymer components are key factors to determine the performance of gel materials. The predesigned interactive groups in gelator molecules enable direct connections between the gelators via non-covalent or dynamic covalent interactions. The dynamic feature of these bonding schemes often results in the dynamic properties of polymer gels such as self-healing, and responsive or adaptive to external environments.

#### 5.3.1 *Hydrogen-Bonded Polymer Gels*

Hydrogen bonding is an electromagnetic attractive interaction between hydrogen bond donor and acceptor atoms. A typical hydrogen bond donor consists of a hydrogen atom attached to an electronegative atom, therefore forming a dipole in which the hydrogen atom is slightly positively charged. In contrast, an atom as a hydrogen bond acceptor is highly electron withdrawing, for example, nitrogen, oxygen or fluorine. Cross-linker bonded by reversible hydrogen bonding can potentially enable supramolecular polymer gels with dynamic properties, such as stimuli-responsiveness, self-healing and post-synthesis processability.

In the research area of hydrogen-bonded gels, an important sub-division is the design of polymer networks with sufficient mechanical toughness. Tough synthetic polymer gels, particularly hydrogels, are good candidates for biomedical applications. Examples include scaffolds for tissue engineering [24], optical and fluidic actuators [33] and carriers for drug delivery [34]. The formation of highly tough polymer gels can be achieved by tuning the molecular structure of building blocks. Among the polymer backbones used for gel preparation, poly(ethylene glycol) (PEG) shows hydrophilicity and melting behaviour under physiologically relevant temperatures [35]. Guo and co-workers have prepared a PEG-based polymer gel containing ureidopyrimidinone (UPy) moieties within the backbone (Fig. 5.4a) [36]. As shown in the inset of Fig. 5.4b, a fourfold hydrogen-bonding dimer is formed between two complementary UPy moieties. Driven by this strong interaction between polymer chains, the polymers first organize into a dry semicrystalline morphology. Upon water encapsulation, the bulk PEG-based polymer networks are converted into a supramolecular hydrogel. Experimental results on the mechanical properties show that the hydrogel exhibits significant strength recovery even at a

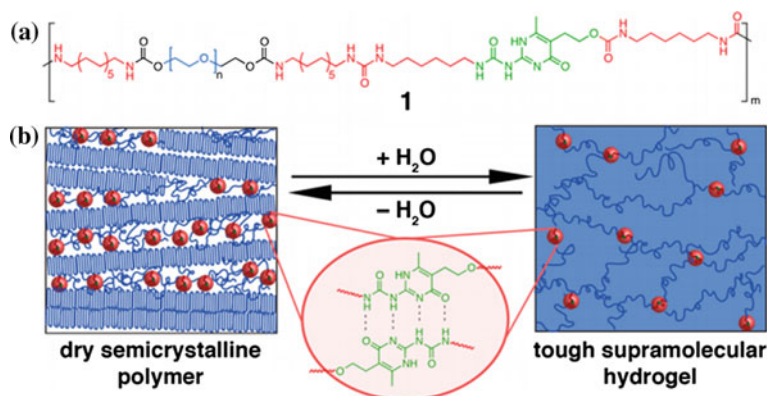


**Fig. 5.4** **a** Molecular structure of PEG-based copolymer chain containing UPy moieties, **b** schematic illustration showing the reversible transition from a dry semicrystalline polymer network into a tough hydrogel driven by hydrogen bonding between complementary UPy moieties upon water encapsulation. Adapted with permission from Ref. [36]. Copyright 2014 American Chemical Society

deformation as large as 300%. The development of this UPy-PEG hybrid gel plays a key step towards utilizing polymer gels in lithium-ion battery and biomedical devices.

The toughness and stability of most polymer gels are often strengthened by combining more than one supramolecular cross-linking modes within a single gel system [37]. To date, a variety of synthetic polymers have been developed for the formation of polymer gels linked by multiple non-covalent bonding [38, 39]. The synthetic polymers (e.g. PEG, polyglycerol (PG) and poly(hydroxyethyl methacrylate (PHEMA)) exhibit advantages over natural biopolymer gels, since these synthetic ones show more structural uniformness from batch to batch. As shown in Fig. 5.5, Hackelbusch and co-workers presented a polymer gel network based on a polyglycerol backbone. The linear polyglycerol chains are biocompatible and can be synthetically functionalized with cyanurate, diaminotriazine and terpyridine moieties. Hydrogels were formed under mild aqueous conditions through the hydrogen bonding between cyanurate and diaminotriazine, and the coordination interactions between terpyridine and iron(II) ions. Due to the stability of the non-covalent bonds, the resulting hydrogels can remain stable in water for several weeks. The mechanical performance of hydrogels can be tuned by manipulating the interactions between polymer chains. This interaction manipulation is achieved through adding de-cross-linking agents. The added acetic acid disrupts the hydrogen bonds within a few hours while maintaining the terpyridine-iron(II) coordination bonds. In contrast, the mixture of EDTA and H<sub>2</sub>O<sub>2</sub> disrupts the coordination bonds instead of the hydrogen bonding. Compared to acetic acid and EDTA/H<sub>2</sub>O<sub>2</sub>, sulphuric acid is a stronger de-cross-linking agent leading to the degradation of the entire gel networks. This agent-controlled approach enables the transition from the

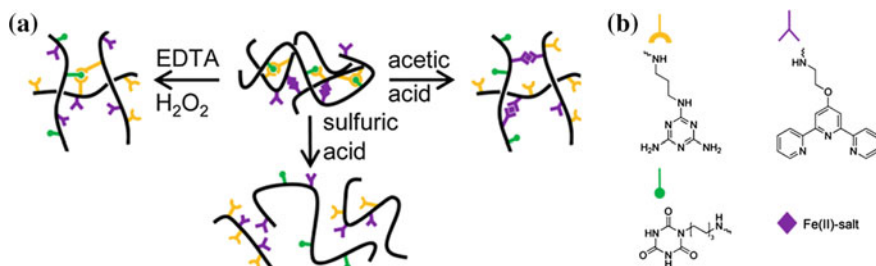


**Fig. 5.5** **a** Schematic illustration of the formation and decomposition of polyglycerol-based hydrogels cross-linked by hydrogen bonding and/or metal–ligand coordination, **b** chemical structures of pendant functional groups within the polymer chains as non-covalent bonding sites. Adapted with permission from Ref. [38]. Copyright 2014 American Chemical Society

mechanical strong hydrogel stabilized by both hydrogen bonding and metal–organic coordination into partially bonded gels or fully de-cross-linked solutions.

In addition to the formation of polymer gels from a single chain species, the blending of two molecular building blocks can also build up supramolecular gels [40–42]. In the fabrication scheme to bi-component gels, one building block acts as a bridging strand while the other one functions as a cross-linker [43]. These gels usually exhibit insufficient mechanical strength, because of a large amount of solvents encapsulated within the molecule networks. In order to use the bi-component gels for practical applications, efforts have been made to enhance the mechanical strength of the gel networks. Noro and co-workers have prepared a gel using two polymer components including carboxyl-terminated telechelic poly(ethyl acrylate) (PEA-(COOH)<sub>2</sub>) and poly(ethyleneimine) (PEI) (Fig. 5.6) [44]. Following dissolving the polymer components in a mixture of THF and MeOH, the mixed solutions were dried at 50 °C under vacuum conditions. The driving force to the gelation was revealed to be the hydrogen bonding between the carboxylic acid groups of PEA-(COOH)<sub>2</sub> and the amine of PEI by using Fourier transform infrared

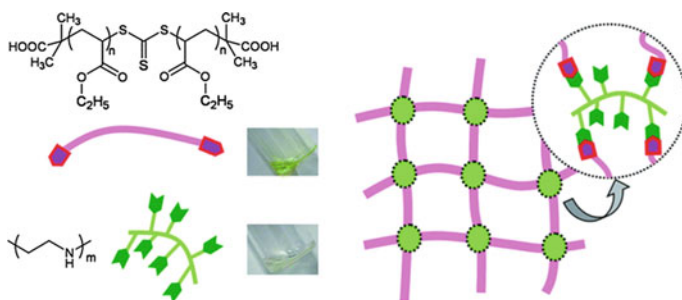


**Fig. 5.6** Schematic illustration of gel preparation by using PEA-(COOH)<sub>2</sub> and PEI as a bridging strand and a cross-linker, respectively. Reproduced from Ref. [44] with permission from The Royal Society of Chemistry

spectroscopy (FT-IR) technique. By varying the molecular ratio between PEI and PEA-(COOH)<sub>2</sub>, homogeneous hybrid gels could be formed. The driving force consists of two competitive interactions including attractive hydrogen bonding and repulsive interactions induced by phase separation. The gel preparation procedure was further extended to other similar molecular systems. When replacing PEA-(COOH)<sub>2</sub> with commercial carboxyl-terminated telechelic polydimethylsiloxane (PDMS-(COOH)<sub>2</sub>), polymer gels could also be formed at a high molecular ratio of PEI.

### 5.3.2 Metal–Organic Coordination Polymer Gels

Based on metal–organic coordination interactions, multidimensional polymer networks may be formed to yield gel phases. The binding strength of metal–organic coordinated linkages ranges from strong bonds to weak interactions. The polymer gels coordinated by weak metal–organic interactions can exhibit reversible physical properties and demonstrate an assembly–disassembly equilibrium in response to environmental stimuli including heat, shaking and sonication [45]. The dynamic feature of weak coordination gel systems enables these materials to have potential applications in drug delivery, chemical catalysis, fluorescence and sensing. The structures and functionalities of polymer metallogels can be finely adjusted by judicious choice of the metal ions, rational design of the binding sites and conformation of polymeric organic ligands [6].

Metal–ligand coordination has been found to play a crucial role in controlling the adhesion, self-assembly, toughness and hardness of biological materials [46]. Inspired by the structure and property of the natural products, biomimetic polymer metallogel systems have been explored by materials scientists. Harrington and co-workers elucidated the peculiar catecholato-iron metallopolymeric structures as underlying mechanical supports for the load-bearing network in byssus cuticles [47]. On this basis of this work, Holten-Andersen and co-workers developed a pH-responsive polymer gel cross-linked by the coordination between catechol derivatives and Fe<sup>3+</sup> ions [48]. Figure 5.7a shows the pH-dependent formation of catechol-Fe<sup>3+</sup> coordinated complexes with varying stoichiometry. At basic pH (pH > 7), the deprotonation of the catechol hydroxyl is favoured; however, the solubility of Fe<sup>3+</sup> is decreased. In order to solve this problem, mussels offer a good solution to prevent Fe<sup>3+</sup> from precipitating under basic conditions. As presented in Fig. 5.7b, Fe<sup>3+</sup> was first bounded to mono-PEG-dopa<sub>4</sub> under acidic conditions (pH ≤ 5). When increasing pH to approximately 8 by releasing in seawater, the cuticle materials cross-linked to multi-Fe<sup>3+</sup>-dopa coordinated networks. In experiments, a dopa-functionalized polyethylene glycol polymer (PEG-dopa<sub>4</sub>) was used as a gelator (Fig. 5.7c). By adopting the mussel-inspired preparation scheme, the cross-linking between PEG-dopa<sub>4</sub> and Fe<sup>3+</sup> could be realized by increasing pH while maintaining Fe<sup>3+</sup> solubility (Fig. 5.7d). The formation of gel phases started

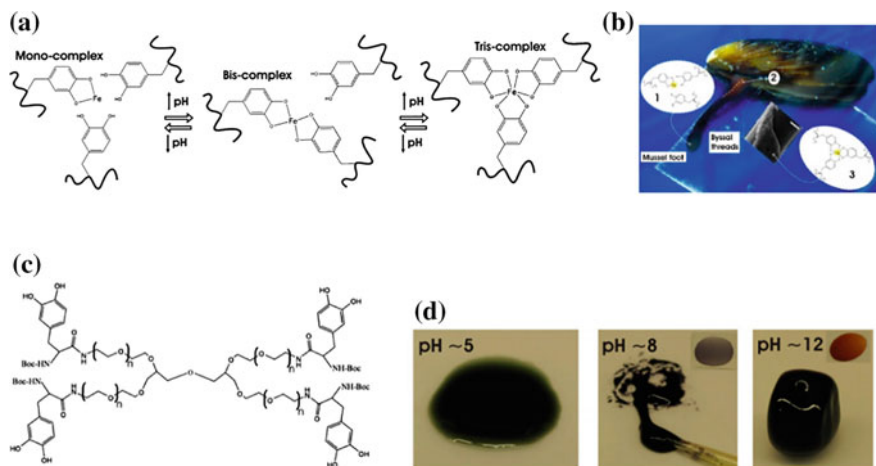


**Fig. 5.7** **a** pH-dependent coordination between catechol derivatives and  $\text{Fe}^{3+}$  ions, **b** illustration of dopa- $\text{Fe}^{3+}$  cross-linking inspired by mussel, **c** chemical structure of the dopa-functionalized polyethylene glycol polymer (PEG-dopa<sub>4</sub>) used for gelation, **d** gelation of the concentrated solution containing PEG-dopa<sub>4</sub> and  $\text{FeCl}_3$  under various pH conditions. Adapted with permission from Ref. [48]. Copyright 2011 National Academy of Sciences

from a basic pH of approximately 8. At a pH of 12, a  $\text{Fe}^{3+}$ -PEG-dopa<sub>4</sub> coordinated elastomeric polymer gel forms.

Compared with gel systems based on other non-covalent bonding, metal–organic coordinated polymer gels exhibit higher structural and functional versatility due to the incorporation of metal ions. The incorporation of metal ions, in particular transition metals, may influence the assembly modes and functional properties of the resulting gels [49, 50]. Dubey and co-workers have investigated the  $\text{Zn}^{2+}$ -induced conformational change of an L-tyrosine derived organic ligand upon gelation via metal–organic coordination [51]. As a result of the conformational change of the ligand, J-aggregated helical fibrous structures with enhanced fluorescence can be formed. The underlying reason for the fluorescence enhancement is proved to be the  $\pi$ - $\pi$  stacking interactions between phenolic rings. Xu and co-workers have developed a  $\text{Ag}^+$ -containing polymer gel based on an anhydride derivative [52]. Figure 5.8a presents the formation of poly(methyl vinyl ether-*alt*-mono-sodium maleate) PVM/Na-MA (PVM/MA, poly(methyl vinyl ether-*alt*-maleic anhydride)) by the reaction of PVM/MA with NaOH, and the synthesis of the  $\text{Ag}^+$  hydrogel. As shown in Fig. 5.8b, the cation component of the silver hydrogel in light yellow can be exchanged irreversibly with copper ions following a stirring of the hydrogel in a  $\text{Cu}(\text{NO}_3)_2$  solution. In addition to the cation exchange reactions, the silver hydrogel exhibits effective antibacterial activity against *E. coli*, *P. aeruginosa* and *S. epidermidis*. Further experiments prove that the antibacterial activity is mainly due to the release of  $\text{Ag}^+$  ions from the hydrogel.



**Fig. 5.8** **a** Chemical reactions for the formation of a Ag(I) hydrogel based on a polymaleic anhydride derivative, **b** photographs showing the exchange of the silver centres with copper by stirring the Ag(I) hydrogel in a  $\text{Cu}(\text{NO}_3)_2$  solution. Reproduced from Ref. [52] with permission from The Royal Society of Chemistry

The structural and functional versatility of metal–organic coordinated polymer gels can be further increased by integrating hydrogen-bonding interactions in the molecular networks. Efforts have been made by Nair and co-workers to functionalize the side chains of polymer backbones with both hydrogen bonding and metal coordination sites [37]. The reversible cross-linking between the polymer chains is realized by adding small molecules as linking agents (Fig. 5.9a). By tuning the molecular species added for the cross-linking, the interactions between the polymer chains can be manipulated as either one or two of the hydrogen bonding and metal–organic coordination. In this study, the functional groups for the formation of hydrogen bonding are cyanuric acid and 2,4-diaminotriazine derivatives (Fig. 5.9b). The metal–organic interactions are based on the coordination bonds between bispyridine and palladated SCS pincer derivatives.

An emerging area in the field of metal–organic coordinated polymer gels is the cross-linking of polymer gelators using metal–organic cages (MOCs). The MOCs-linked gels, abbreviated as polyMOC gels, contain predesigned polymer gelators bearing suitable cage forming functional moieties [53]. As a result of metal–ligand interactions, the MOCs are embedded within the gel networks leading to improvements in mechanical properties and porosity. In some cases, the polymer gels cross-linked by MOCs can also act as a platform for research on new functional materials.

Nitschke and co-workers reported an example of polymer hydrogels cross-linked through self-assembled MOCs [54]. As shown in Fig. 5.10a, a series of MOCs could be synthesized by mixing polyethyleneglycol derivatives functionalized with

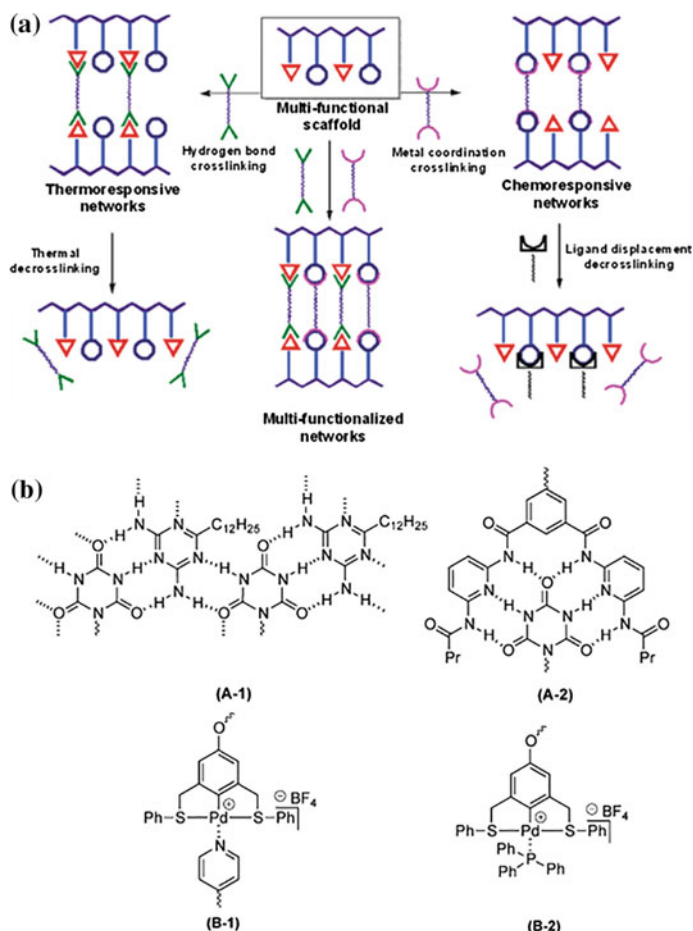


**Fig. 5.9** a Schematic illustration of polymer backbones with side chains functionalized with both hydrogen bonding and metal coordination sites, b chemical structures of the molecular motifs used for the study conducted by Nair and co-workers. Adapted with permission from Ref. [37]. Copyright 2011 American Chemical Society

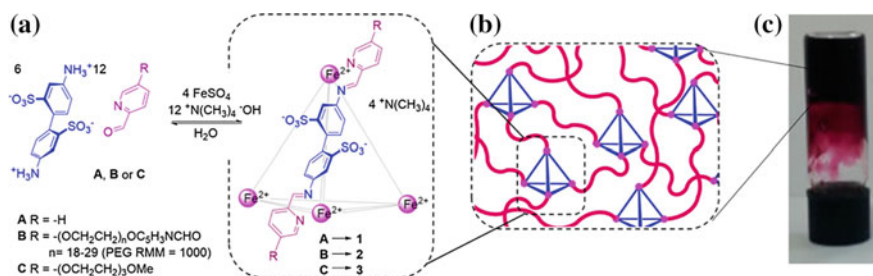


**Fig. 5.10** a Chemical reaction for the sub-components of the MOCs, b schematic illustration of MOCs embedded within the polymer network, c photograph of the MOCs-linked polymer gel. Adapted with permission from Ref. [54]. Copyright 2015 American Chemical Society

5-fluoro-2-formylpyridine, 4,4'-diaminobiphenyl-2,2'-disulfonic acid, tetramethylammonium hydroxide and an aqueous solution of iron(II) sulphate heptahydrate. The polymer network cross-linked by tetrahedral-shaped MOCs (Fig. 5.10b) has the ability to absorb water giving rise to the formation of a purple gel (Fig. 5.10c). Following the gel preparation, guest encapsulation and release studies were conducted to show the different behaviours of molecules within cage cavities and gel pores. For these investigations, furan was chosen as a competing guest against benzene and anisole. Results from adsorption experiments monitored by UV-Vis spectroscopy showed that the cages are only occupied by benzene in the absence of furan. While in the presence of furan, the benzene within the cages was released and subsequently replaced by furan partially. Therefore, the cage cavities and gel pores could be accessed selectively upon exposure to different external stimuli. This study has paved the way for further investigations on the design of cage-containing polymer gels for the controllable encapsulation of technically important guest molecules such as drugs, pesticides and fragrances.

Johnson and co-workers have increased the average number of bridges connecting network junctions by developing highly branched polymer gels linked with stable MOCs [53]. As shown in Fig. 5.11a, the polyMOCs exhibit tunable cavity-containing junctions and an enhanced network branch functionality compared with conventional metal-organic gels where point junctions are generated. Due to the increase in the network branch functionality, the resulting polymer gels connected with MOCs are expected to show an increase in elastic modulus. Two polyethylene glycol (PEG) derivatives terminated with bis-*para*-pyridyl (PL1) and bis-*meta*-pyridyl (PL2) groups were designed for the formation of MOC junctions, respectively (Fig. 5.11b, c). Upon mixing with Pd<sup>2+</sup> ions, the formation of coordinated M<sub>12</sub>L<sub>24</sub> cages and M<sub>2</sub>L<sub>4</sub> paddlewheels could be activated by thermal annealing. Resulting from the formation of cage junctions, the gelation of two polyMOC gel species (gel-1 and gel-2 in Fig. 5.11a) could be initiated as illustrated by <sup>1</sup>H magic-angle spinning (MAS) nuclear magnetic resonance (NMR), small-angle neutron scattering (SANS) and molecular dynamic simulation techniques. Using oscillatory rheometry, the mechanical properties of gel-1 and gels-2 show close correlation with their network structures. As compared to gel-2, gel-1 based on M<sub>12</sub>L<sub>24</sub> cages has a higher average number of bridges connecting network junctions and exhibits large shear moduli. The large number of elastically inactive loop defects within gel-1 could be replaced with functional ligands without altering the shear modulus of the gels. While not applicable to such ligand substitution, gel-2 demonstrates a self-healing behaviour possibly related with the dynamic feature of M<sub>2</sub>L<sub>4</sub> junctions.

Thereafter, Johnson and co-workers further extended their efforts to apply rigid MOCs as junctions for block copolymer (BCP) self-assembly [55]. The integration of MOCs with BCP self-assembly produces a new class of hybrid materials, namely block co-polyMOCs (BCPMOCs). Figure 5.12a shows the chemical structure of the molecular ligand synthesized for the preparation of BCPMOCs, poly(methylmethacrylate)-*block*-poly(*n*-butyl acrylate) (PMMA-PBA). As each PMMA-PBA contains two pyridyl groups at its chain end, these ligands form star polymers

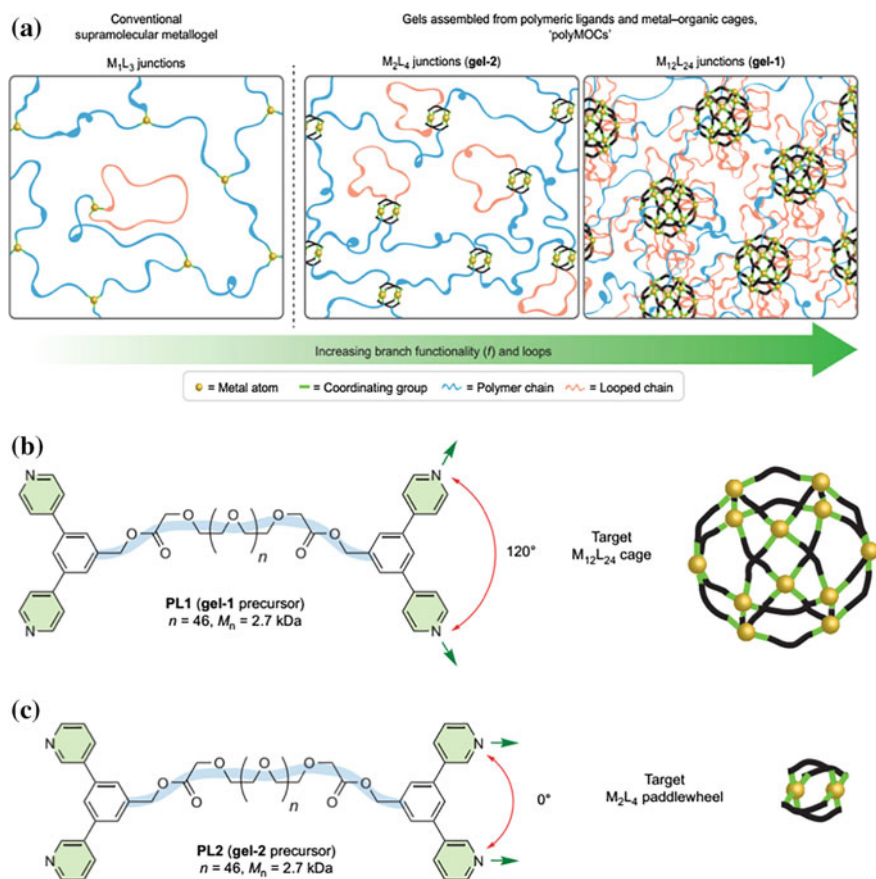


**Fig. 5.11** **a** Schematic illustrations of a conventional coordination metallogel and supramolecular polymer gels connected with  $M_2L_4$  and  $M_{12}L_{24}$  MOCs, **b** chemical structure of a bis-*para*-pyridine-terminated polyethylene glycol chain and schematic illustration of the  $M_{12}L_{24}$  cage self-assembled from the polymeric ligand and  $Pd^{2+}$ , **c** chemical structure of a bis-*meta*-pyridine-terminated polyethylene glycol chain and schematic illustration of the  $M_2L_4$  paddlewheel self-assembled from the polymeric ligand and  $Pd^{2+}$ . Reproduced with permission from Ref. [53]. Copyright 2015 Nature Publishing Group

containing a Fujita's sphere  $M_{12}L_{24}$  MOC ( $\sim 3.5$  nm) in the presence of  $Pd^{2+}$  (schematic in Fig. 5.12a). The BCPMOCs derived from the  $M_{12}L_{24}$  MOC have microphase-separated structures. The microphase separation was further characterized using small-angle X-ray scattering (SAXS) technique. Figure 5.12b shows the scattering signals for a  $PMMA_{8k}$ - $PBA_{27k}$  sample (the subscripts denote average molecule weights). For linear BCPs without metal (blue curve), a single Bragg reflection peak is observed proving the presence of phase-separated structures with a  $d$ -spacing. In the presence of metal (purple curve), higher order scattering peaks are detected in the SAXS spectrum. The  $q$  ratios for the scattering pattern of the

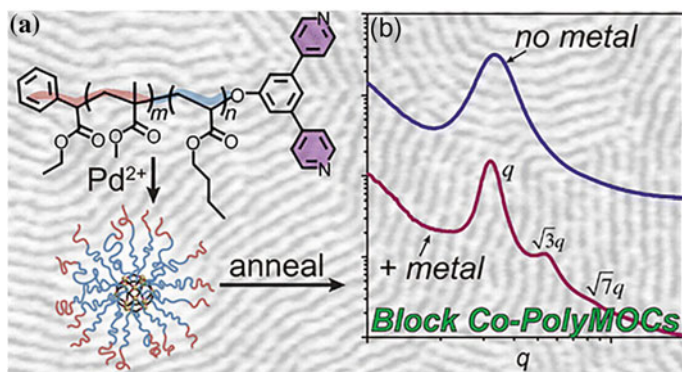


**Fig. 5.12** **a** Schematic illustration for the formation of BCPMOCs and **b** small-angle X-ray scattering of co-polyMOC with and without metals. Adapted with permission from Ref. [55]. Copyright 2016 American Chemical Society

PMMA<sub>8k</sub>-PBA<sub>27k</sub> containing the Fujita-sphere M<sub>12</sub>L<sub>24</sub> sphere are  $q_1:q_2:q_3 = 1:\sqrt{3}:\sqrt{7}$ , which suggests the presence of a hexagonally packed cylinder phase. This presence of this phase can be further resolved using atomic phase microscopy (AFM) phase imaging technique.

### 5.3.3 Polymer Gels Based on Dynamic Covalent Chemistry

In addition to non-covalent bonding, reversible covalent bonds with dynamic properties have also been used as linkages for the formation of 3D networks in polymer gels. Similarly, the gel networks based on dynamic covalent chemistry exhibit a dynamic equilibrium via the dissociation and recombination of covalent bonds (Fig. 5.13) [56]. Therefore, the cross-linked polymer networks often exhibit the mechanical robustness of chemical gels as well as the stimuli-responsiveness of physical gels. One prominent property exhibited by chemical gels based on

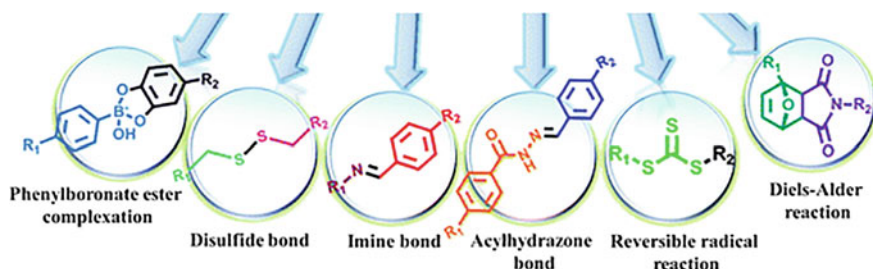


**Fig. 5.13** Chemical structures of dynamic covalent bonding schemes used for the formation of polymer gel. Reproduced from Ref. [56] with permission from The Royal Society of Chemistry

dynamic covalent chemistry is their self-healing ability upon undergoing damage. For the formation of dynamic covalent bonding, the target polymer chains are commonly designed to bear specific functional groups as reactive sites for cross-linking. To date, several dynamic covalent reaction schemes have been applied in polymer gel fabrication including Schiff base condensation [57], acyl-hydrazone bond formation [58], Diels–Alder cycloadditions [59], disulfide exchange [60], reversible radical reaction [61] and boronic acid condensation [62].

Imine bonding is an exemplary dynamic covalent linkage used for the cross-linking of polymer networks. In this reaction scheme, the polymer gelators should be functionalized with amine and aldehyde groups in order to construct imine-based polymer gels. As shown in Fig. 5.14, the betnzaldehyde groups of telechelic poly(ethylene glycol) (PEG) chain react with the amine groups on chitosan backbone to produce PEG-chitosan hydrogels [63]. The resulting hydrogels demonstrate self-healing ability due to the reversible transition of the imine linkages between the polymer chains. In addition to self-healing, the PEG-chitosan hydrogels have also been observed to responsive to a range of chemical and biological stimuli including pH, vitamin B6 derivatives, amino acids and enzymes. More interestingly, the PEG-chitosan hydrogels have the potential to be disposed in a controllable way as the chitosan component can be digested by biological enzymes. The biomedical applications of the hydrogels have been tested by studying the encapsulation and release of small molecules from the disposable hydrogel networks.

Imine-based self-healing gels have also been developed by using polyisobutylene (PIB) polymer as a molecular backbone [64]. The self-healing gels are obtained from side-chain primary amine leucine pendant diblock copolymers of polyisobutylene (PIB) ((P(H<sub>2</sub>N-Leu-HEMA)-*b*-PIB)) in the presence of PIB-based dialdehyde functionalized cross-linker (HOC-PIB-CHO) in 1,4-dioxane through imine bond formation (Fig. 5.15). Due to the forming–breaking equilibrium of imine bonding, the resulting polymer gels demonstrate a reversible transition between solution and gel phases. The reversible sol–gel transition can be

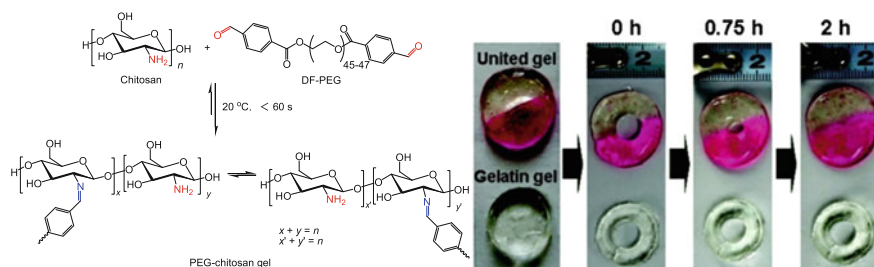


**Fig. 5.14** Comparison of an imine-bonded PEG-chitosan gel and a conventional gelatin hydrogel, highlighting the self-healing process between two different coloured semicircle hydrogels (the red one is stained by rhodamine B) and the hole punched in the middle of the united gel. Adapted with permission from [63]. Copyright 2010 American Chemical Society

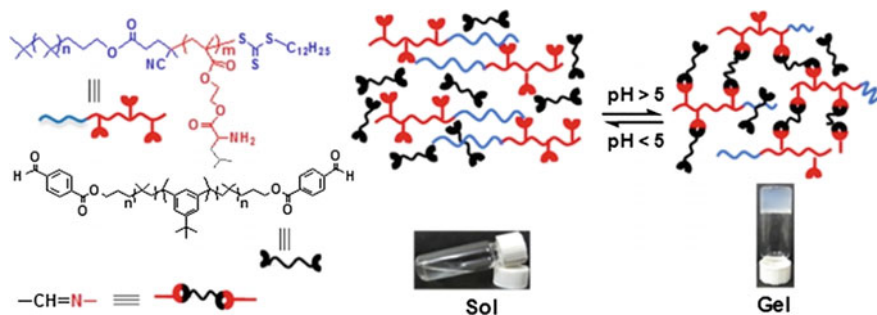


**Fig. 5.15** Schematic representation of a polymer gel synthesized from PIB-b-P(NH<sub>2</sub>-Leu-HEMA) and HOC-PIB-CHO via imine bonding in 1,4-dioxane at room temperature and responsiveness towards pH. Reproduced with permission from Ref. [64]. Copyright 2015 American Chemical Society

maintained for several cycles by adjusting the pH of the liquid medium composed of hydrochloric acid (HCl) and triethylamine (Et<sub>3</sub>N) triggers. Moreover, the mechanical strength of the dynamic gels was observed to increase when increasing the [NH<sub>2</sub>]/[CHO] ratio from 0.3 to 0.5 to 1, which is associated with the increase in imine links between polymer chains. The PIB-based polymer gels have a wide range of biomedical applications due to the biological compatibility of the PIB segments and amino acid groups.

Apart from imine bonding, acylhydrazone bonding has also been successfully employed to form a macroscopic hybrid consisting of both organogel and hydrogel [65]. As shown in Fig. 5.16, the hydrogel and the organogel are first synthesized via condensation reactions of two polymeric poly(ethylene glycol) (PEG) gelators in water and anisole, respectively. Two polymer chain species, denoted as A2 and B3 in Fig. 5.16, are terminated by acylhydrazine and aldehyde groups. Due to the condensation reaction between acylhydrazine and aldehyde, polymer networks are formed driven by the resulting dynamic acylhydrazone bonds. As a result of the reversible acylhydrazone bonds, a macroscopic organohydrogel hybrid can be formed by connecting the hydrogel and organogel pieces along the interfaces by rapid adhesion.

Boronic ester bonding has been used to cross-link polymer chains for the generation of polymer gels [66]. Examples include dynamic covalent gels reported by Xu and co-workers, where the gelation is initiated by activating condensation reactions of *N,N*-dimethylacrylamide-4-((4-vinylbenzyloxy)carbonyl)phenylboronic acid copolymer (poly(VPB-co-DMA)) and poly(2,2-bis(hydroxymethyl)butyl acrylate) (PHBA) with phenylboronic acid and 1,3-diols moieties in DMF, respectively (Fig. 5.17) [67]. A reversible sol–gel phase transition can be achieved for this poly (VPB-co-DMA)-PHBA gel by adjusting pH of the system due to the dynamic feature of the reversible boronic ester formation. Phenylboronate-salicylhydroxamate hydrogels can also be prepared from two water-soluble linear polymers containing either phenylboronic acid or salicylhydroxamic acid pendant groups synthesized

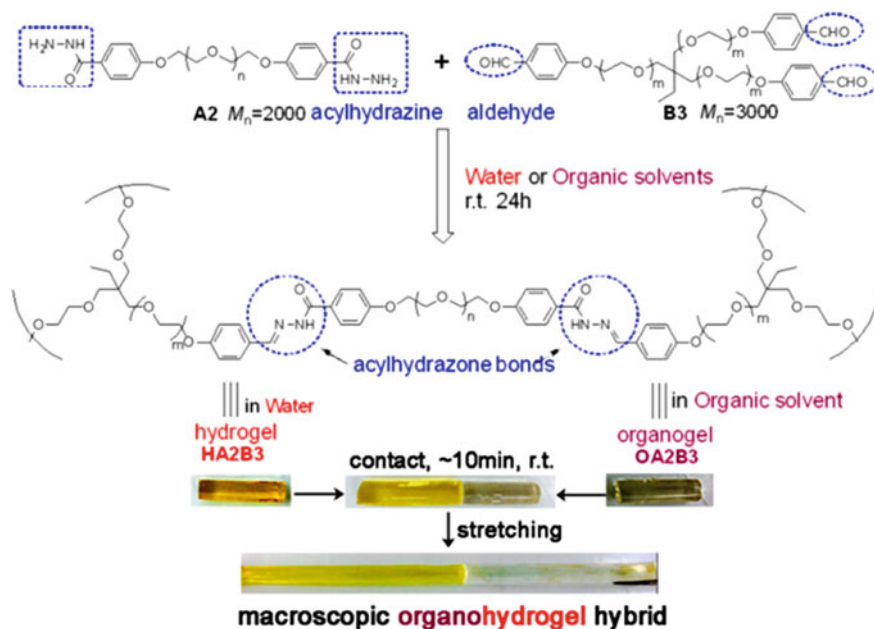


**Fig. 5.16** Formation of a macroscopic hybrid of organogel and hydrogel via acylhydrazone bonding. Reproduced with permission from Ref. [65]. Copyright 2015 American Chemical Society

with different 2-hydroxypropylmethacrylamide (HPMA) or acrylic acid (AA) polymer backbones (two degrees of substitution for each polymer are  $x = 90$  mol% or 95 mol%) [62]. The phenylboronic acid and salicylhydroxamic acid moieties react in aqueous solution at physiological pH to form boronic ester bonds and generate a cross-linked polymer hydrogel. The viscoelastic behaviour of the gel shows a dependence on the pH of the aqueous medium. Under neutral pH conditions, the cross-linked polymer forms a brittle, elastic hydrogel because the boronic ester equilibrium is shifted to the bound state. At mildly acidic pH conditions, however, a deformable semisolid is formed because the equilibrium is shifted to an unbound state. Reversible cross-links allow these boronic ester-based gels to restructure dynamically and self-heal after undergoing mechanical disruption.

The use of thiol groups for reversible cross-linking of polymers to produce polymeric networks has been reported by Chujo and co-workers [68]. A redox-reversible hydrogel based on thiol-modified poly(*N*-acetylmethacrylamide) is formed by exploiting the reversible interconversion between disulfide groups and thiols. The linear poly(*N*-acetylmethacrylamide) polymer with thiol pendant groups is soluble in water, and the resulting solution can be changed into a hydrogel upon oxidation. The cleavage of the disulfide cross-linking by reduction causes an increase in the degree of swelling.

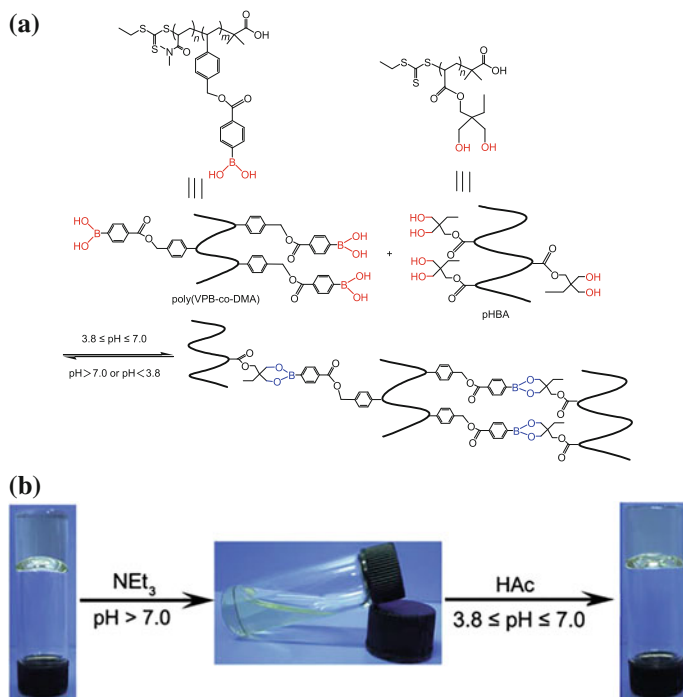


**Fig. 5.17** **a** Chemical reaction for the formation of dynamic covalent phenylboronic acid-diol ester bonding and **b** photograph showing the pH-dependent sol-gel phase transition of poly (VPB-co-DMA)-PHBA polymer gel cross-linked by the boronic ester bonding. Adapted with permission from [67]. Copyright 2011 Elsevier Ltd.

Based on the thermal equilibrium of Diels–Alder reaction, a polyoxazoline-based gel was designed by Saegusa and co-workers (Fig. 5.18) [69]. The gelation is attributed to the Diels–Alder reaction between furan-modified poly (*N*-acetyleneimine) (PAEI) and maleimide-modified PAEI in MeOH. The reversible interconversion between the polyoxazoline gel and the linear polymer precursor solution can be manipulated by changing the heating temperature. A thermally reversible transition from the polymer gel into the solution state can be achieved upon heating the molecular system.

Based on Diels–Alder reaction, a controlled release system of poly(ethylene) glycol (PEG) hydrogel has been developed by Bowman and co-workers [70]. The hydrogel is constructed via thiol–Michael addition reactions between multifunctional maleimide and thiol PEG macromers. The reaction is performed in an off-stoichiometric ratio to create excess unreacted maleimide tethering sites in the polymer network. Due to the existence of excess unreacted maleimide groups, several molecular species, such as small pharmaceutical molecules and peptides, can be covalently tethered to the network via Diels–Alder reactions. Subsequently, the molecules attached to the hydrogel networks can be released by shifting the

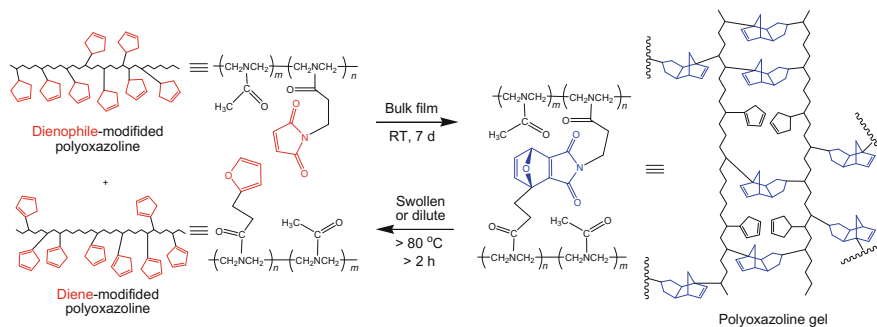


**Fig. 5.18** Schematic illustration for the formation of a polyoxazoline gel based on gelation by the Diels–Alder reaction

position of the Diels–Alder equilibrium to the reformation of furan and maleimide. As the equilibrium of the Diels–Alder reactions is dependent on temperature, the release rate of bound moieties from the hydrogel is also thermally controlled. Elevated temperatures favour the retro-Diels–Alder reaction and therefore increase the rate and quantity of molecules released from the hydrogel networks.

A large number of dynamic covalent cross-linked gels involving radical species have been developed [71–74]. Exemplary work includes the polymer gel developed by Su and co-workers in which dynamic covalent C–O bonds based on alkoxyamine functional groups are involved in the side chains (Fig. 5.19) [71]. As adducts of styryl radicals and 2,2,6,6-tetramethylpiperidine 1-oxyl, alkoxyamine functional groups undergo reversible covalent cross-linking to produce gel networks. Chemical equilibrium between the alkoxyamines and radicals as dormant and active species, respectively, is reached over 60 °C. The radical reaction of alkoxyamine functional groups is tolerant of water, organic solvents and many functional groups rendering wide applicability of the polymer reaction. The hydrophilic polymers with radically exchangeable alkoxyamine units are prepared by copolymerization of 2-(dimethylamino)ethyl methacrylate and methacrylic esters and subsequent protonation of dimethylaminoethyl groups. Heating the polymers in water at 100 °C in closed system leads to gelation. The cross-linking of the alkoxyamine-containing polymers via the radical exchange reaction is the main reason for the gelation. Following the cross-linking reaction, the gel network can be de-cross-linked by heating with an excess amount of alkoxyamines. The de-cross-linking of the polymer gel is initiated by the radical exchange reaction between the cross-linked polymer chains and the added alkoxyamines.

Figure 5.20 illustrates dynamic covalent gels produced through the radical exchange reaction of diarylbibenzofuranone (DABBF) units [72]. The polymer cross-linked by DABBF units is prepared by the polyaddition of DABBF and a toluene-2,4-diisocyanate-terminated poly(propylene glycol) ( $M_n = 2400$ ). The cross-linked polymer is de-cross-linked in DMF in air at room temperature by adding an excessive amount of DABBF. After 24 h, a THF-soluble high molecular weight component of linear polymers and/or cross-linked oligomers is obtained.

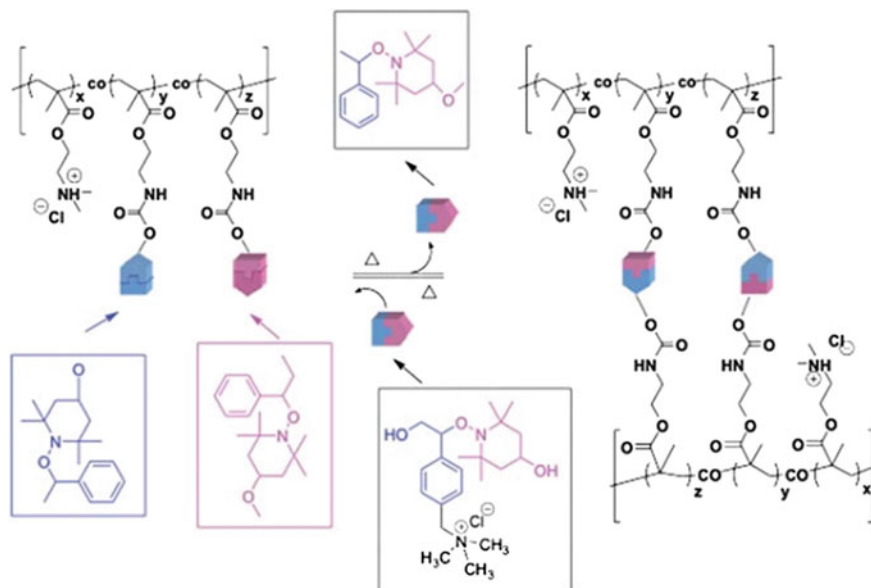


**Fig. 5.19** Cross-linking and de-cross-linking reactions of water-soluble dynamic covalent polymers via radical exchange reaction of alkoxyamine units. Reproduced from Ref. [71] with permission from The Royal Society of Chemistry

Interestingly, the cross-linked polymer gel in DMF shows self-healing property under ambient conditions (in air at room temperature). Moreover, the self-healing property of the polymer is not influenced by the freshness of the surfaces since the dynamic cross-linking reaction is tolerant of humidity and air.

Polymer gels based on the dynamic covalent cross-linking of trithiocarbonate (TTC) units have been developed [73, 74]. Dynamic exchange reactions of TTC units can be triggered via homolysis of C-S bonds either by UV irradiation or by radical generators including a thermal initiator or a copper(I) catalyst. Matyjaszewski and co-workers have reported the re-organization of poly(methyl methacrylate) (PMMA) gels containing trithiocarbonate (TTC) units along the main polymer chains in the presence of radicals [73]. Reshuffling of the cross-linked network yields a remarkable change in the degree of swelling (up to 300% increase). Moreover, the gel is proposed to undergo reprocessing and/or self-repairing as indicated by the fusion of the gels from discrete pieces into a single one. The radical reshuffling of the TTC units is triggered when the cross-linked polymers are swollen in either a good solvent or a non-solvent medium and then exposed to UV light [74]. The degree of swelling and network size in toluene increases in the presence of good solvents, whereas they decrease in non-solvents. The swelling degree in toluene prior to the UV irradiation is 650%; after exposing to UV light in THF, the value increases with the reaction time and reaches up to 1440% after 60 min. However, the degree of swelling in methanol decreases from 650% (before UV) to 500% after UV irradiation after 60 min.

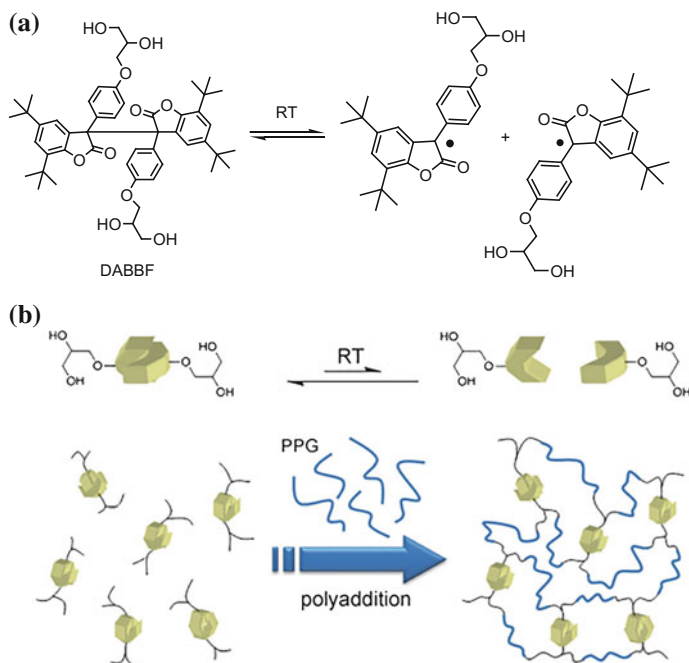


**Fig. 5.20** Dynamic covalent reaction between diarylbibenzofuranone (DABBF) and polymers cross-linked by DABBF units. Adapted with permission from Ref. [72]. Copyright 2012 Wiley-VCH Verlag GmbH & Co. KGaA, Weinheim

### 5.3.4 Hybrid Polymer and Low Molecular Weight Gels

An emerging area of studying gel materials is the combination of polymers and LMWGs [75]. One strategy to bridge the gap between polymer and low molecular weight gels is to polymerize low molecular weight gelators (LMWGs) directly. The first reported work on the polymerization of LMWGs following self-assembly was conducted by Feringa and co-workers [76]. The motivation of this work was to enhance the mechanical stability of organogels formed by the self-assembly of small organic compounds. As shown in Fig. 5.21a, a methacrylate derivative of *trans*-1,2-bis(3-methylureido)cyclohexane (MUC) was designed as a LMWG. Upon cooling down to room temperature, MUC molecules were observed to form optically transparent gels. A variety of organic solvents were tested to be effective for the gelation of MUC including tetralin, benzene, 1,2-dichloroethane, butyl acetate and cyclohexane. As illustrated in Fig. 5.21b, the supramolecular MUC gels driven by hydrogen bonding consists of interdigitated straight thin fibres with diameters reaching down to 50 nm. Subsequently, a photoinitiator, 2,2-dimethoxy-2-phenylacetophenone was added into the gelation system. When irradiated with a 200 W high-pressure Hg lamp, a fully photopolymerized MUC gel was confirmed

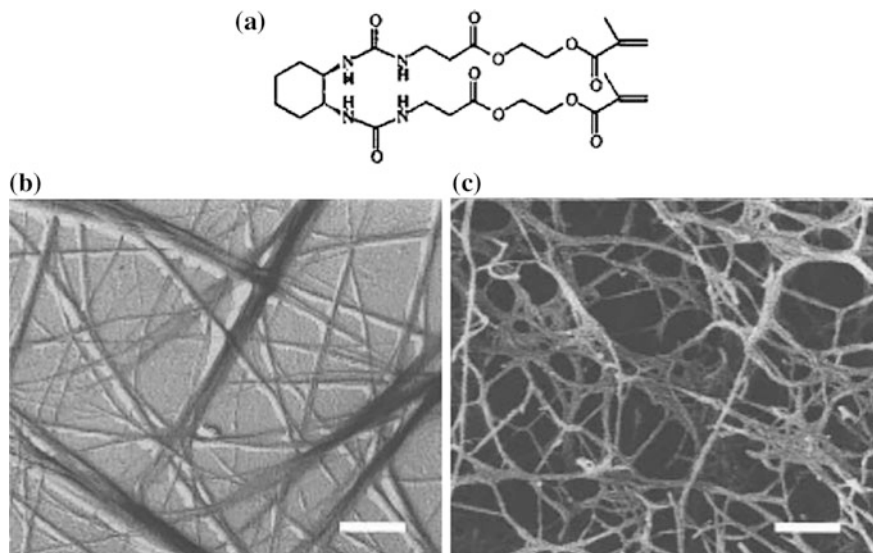


**Fig. 5.21** **a** Chemical structure of a methacrylate derivatives of *trans*-1,2-bis(3-methylureido)cyclohexane (MUC), **b** TEM image of a butyl acetate gel of the compound before polymerization (scale bar = 1000 nm), **c** SEM image of a benzene gel of the compound after irradiation for 1 h (scale bar = 400 nm). Adapted with permission from Ref. [76]. Copyright 1997 American Chemical Society

to form in 2 h monitored by  $^1\text{H}$  NMR technique. The SEM image in Fig. 5.21c demonstrates the highly cross-linked morphology of the polymerized MUC gel. Compared with the molecular network prior to polymerization, a smaller diameter of approximately 25 nm could be achieved for the thinnest fibres within the three-dimensional network (Fig. 5.21c). The increased degree of cross-linking arising from the polymerization was explained as the primary reason for the enhanced macroscopic stability of the MUC gel with covalent linkages.

Further to the radical polymerization between methyl methacrylate moieties, gelators functionalized with other reactive groups have been designed and implemented. Examples of reaction sites include acrylate [77], conjugated diacetylene units [78, 79], alkene [80], alkyne and azide [81] and triethoxysilane end groups [82].

Figure 5.22a shows a diacetylene derivative designed and synthesized by Weiss and co-workers [78]. When the diacetylene units are properly aligned, the derivatives can undergo 1,4-addition reactions forming a polymerized network (Fig. 5.22b). Prior to UV irradiation, the gelation performance of the diacetylene derivative was examined in silicone oil. A milky white gel was observed to form (Sample 1 shown in Fig. 5.22c). The gel was stabilized by both the hydrogen bonding between the amide hydrogen and carbonyl groups and the hydrophobic interactions of long alkyl chains. Upon irradiation in silicone oil at room temperature for 10 min, the colour of the gel turned from milky white to blue (Sample 2 shown in Fig. 5.22c). The realization

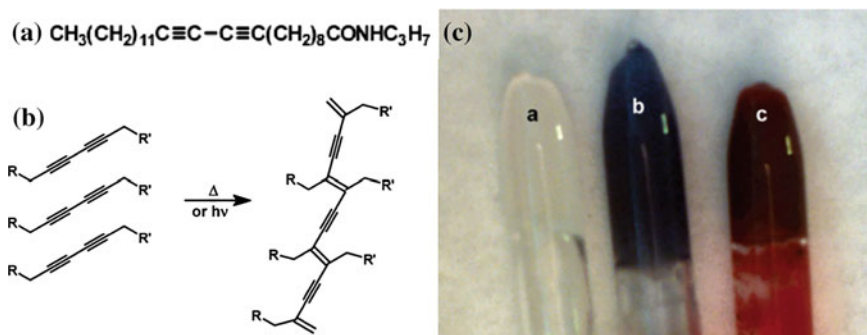


**Fig. 5.22** **a** Chemical structure of a diacetylene derivative used for photopolymerization-induced gelation, **b** 1,4-addition reaction between diacetylenes when aligning appropriately and **c** silicone oil gel of the diacetylene derivative (2 wt%) (From left to right: Sample 1: without irradiation. Sample 2: after irradiation for 10 min. Sample 3: after heating the irradiated gel at 70 °C for 3 min.). Adapted with permission from Ref. [78]. Copyright 2003 American Chemical Society

of the UV polymerization was inferred to be associated with the distance between the diacetylene units within the fibres of the gel. The packing arrangement of the molecular network was suggested to allow the diacetylene units be placed within the critical distance required for polymerization. After undergoing a heating process at 70 °C for 3 min, the polymerized gel turned from blue to red irreversibly (Sample 3 shown in Fig. 5.22c). The gel phase of the irradiated gel formed by the diacetylene could be retained upon heating to 70 °C. Further absorption spectroscopy studies revealed that the heating after irradiation could lead to changes in polydiacetylene conformations or varying contributions to resonance. The results presented in this work demonstrate the possibility to turn supramolecular systems into polymerized gel networks using LMWGs with covalent reaction sites. This strategy opens upon opportunities to construct polymer gels from simple organic compounds and control their gelation with a high precision.

Finn and co-workers developed a method to convert LMWGs into covalently cross-linked polymer gels using a “click” chemistry scheme [81]. The concept of “click chemistry” was introduced by Sharpless to describe reactions that are modular, wide in scope, give very high yields, be stereospecific and generate only inoffensive by-products [83]. Among various click reactions, copper-catalyzed azide–alkyne cycloaddition reactions are well-known for their highly accelerated rate. When introduced into organic gelators, the polyvalent network formed by a undecylamide-based *trans*-1,2-diaminocyclohexane could be cross-linked covalently via alkyne–azide reactions (Fig. 5.23). This method exhibits several advantages over much of the previous studies on the polymerization of LMWGs. For the two pieces of work described at the beginning of the section, a template for polymerization is set prior to initiating chemical gelation in order to convert non-covalent supramolecular assemblies into polymer networks. In comparison, the method of using click reactions achieves this conversion while maintaining the

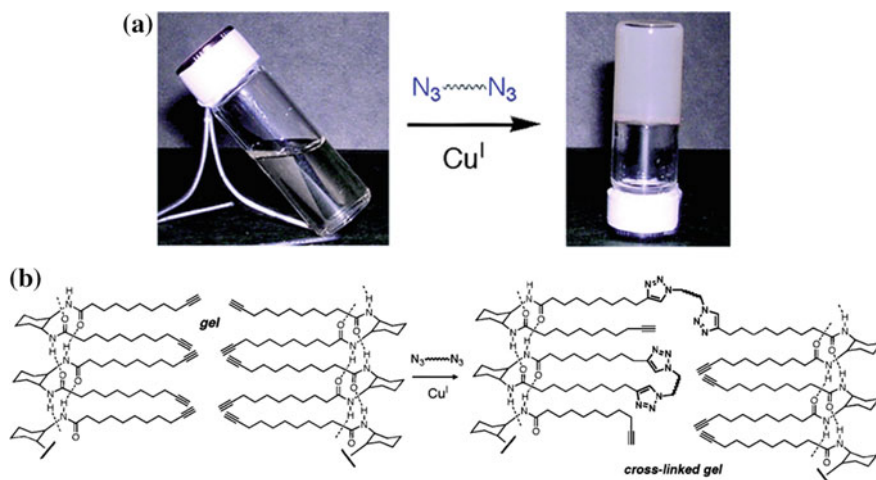


**Fig. 5.23** **a** Photographs presenting the solution of an alkyne-based gelator and the resulting polymer gel after undergoing a copper(I)-catalyzed azide–alkyne cycloaddition reaction, **b** chemical equation behind the transition shown in (a). Adapted with permission from Ref. [81]. Copyright 2006 American Chemical Society

structural order and thermo-reversibility of the gels. As a result of this, the properties of the gels can be modified rationally using the connectivity from click reactions. Overall, this method of cross-linking a wide three-dimensional network has the potential capability to tune molecular structure and composition of the resulting polymer gels with a significantly high precision.

Another area of studying the combination of low molecular weight and polymer gels is to mix LMWGs and polymer gelators prior to gelation. Each of the two types of gelators is able to form gels independently. A number of the hybrid gels have been developed to enhance the mechanical stability of gel materials formed by small molecules while improving the thermo-reversibility of polymer gels [84]. This area is still largely unexploited and requires further work to rationalize the factors controlling the gelation process.

As a hydrogel for environmental applications, the hybrid gel system developed by Yang and co-workers has the potential uses for the removal of dye molecules in water [85]. A LMWG, Fmoc-3-(2-naphthyl)-D-alanine (Fig. 5.24a), could form a clear hydrogel on its own. As shown in the SEM image in Fig. 5.24b, the low molecular weight supramolecular gel consists of thin fibres with approximately 100 nm in width. This hydrogel could be incorporated into agarose hydrogels; the morphology of which is presented in Fig. 5.24c. The two types of gels were combined by mixing both of the two gelators prior to initiating gelation via a heating–cooling process. The morphology of the hybrid gel is similar to that of the low molecular weight gel (Fig. 5.24d). Compared with the monocomponent gels, the hybrid gel exhibits higher resistance against external forces, and thus higher mechanical strength. Methyl violet is a model compound for the test of organic

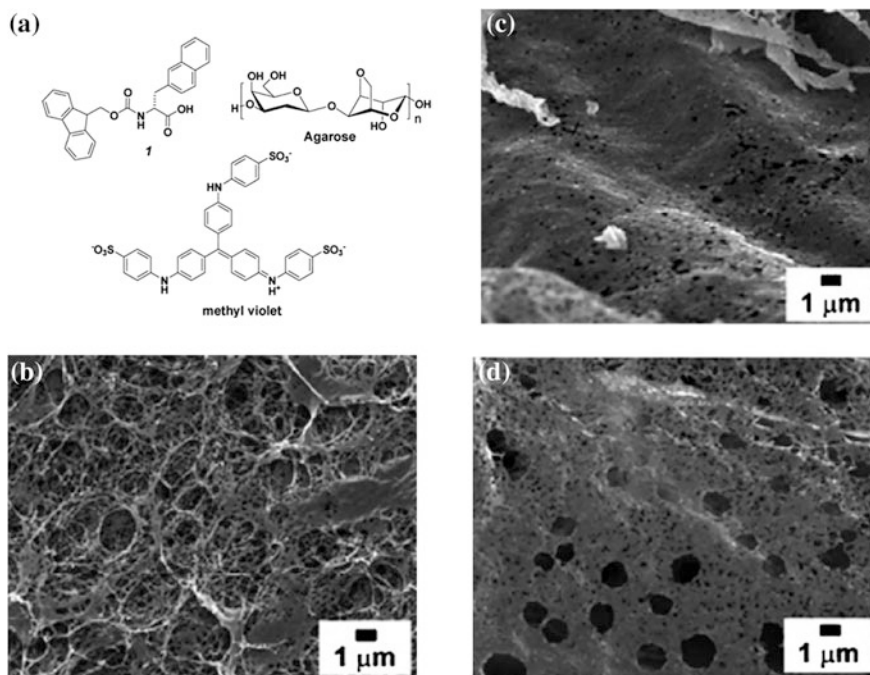


**Fig. 5.24** a Chemical structures of Fmoc-3-(2-naphthyl)-D-alanine, agarose and methyl violet. b–d SEM image of the morphological structures of the hydrogels formed by Fmoc-3-(2-naphthyl)-D-alanine (0.8 wt%), agarose (0.8 wt%) and the mixture of the two components. Adapted with permission from Ref. [85]. Copyright 2010 Elsevier B.V.

pollutant removal in industrial wastewater. Both the low molecular weight and hybrid gels demonstrate the capability to remove methyl violet from aqueous solution. In comparison, the hybrid gel shows no change in its physical appearance following the adsorption of a large amount of methyl violet while the low molecular weight gel collapses into precipitates. The superior capability for the removal of dye molecules suggests that hybrid gel systems consisting of both LMWGs and polymer gelators are promising smart materials for the capture of target molecules.

The agarose polymer gelator can be also be combined with other LMWGs including 1,3:2,4-dibenzylidene-D-sorbitol-p,p'-dicarboxylic acid (DBS-CO<sub>2</sub>H) reported by Smith and co-workers (Fig. 5.25) [86]. The investigations on the hybrid hydrogel were focused on the dynamic behaviour of the self-assembly process and the responsive character towards pH variations. An identification of the mixture of agarose and DBS-CO<sub>2</sub>H nanostructures was achieved using SEM. Results from circular dichroism (CD) spectroscopy showed the presence of chiral nanostructures formed by DBS-CO<sub>2</sub>H. The concentration of agarose was suggested to have an impact on the kinetics of the assembly process. Specifically, the agarose could decrease the initial kinetics of nanofibre nucleation and assembly at a low concentration while the effect became reduced at a high concentration applied for NMR

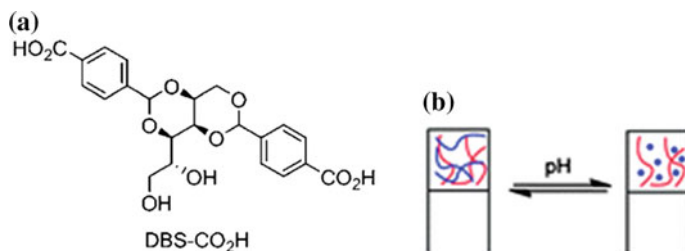


**Fig. 5.25** **a** Chemical structure of 1,3:2,4-dibenzylidene-D-sorbitol-*p,p'*-dicarboxylic acid (DBS-CO<sub>2</sub>H), **b** schematic illustration of the pH responsive property of the hybrid hydrogen combining both DBS-CO<sub>2</sub>H and agarose. Reproduced from Ref. [86] with permission from The Royal Society of Chemistry

tests. In addition to the concentration effect, the self-assembled DBS-CO<sub>2</sub>H nanofibres showed responsiveness towards pH values within the robust hybrid gel matrix supported by the agarose polymer gel.

As an extension of the study described above, Smith and co-workers have used a synthetic, covalently cross-linked polymer gelator, poly(ethylene glycol) dimethacrylate (PEGDM, Fig. 5.26a) to form hybrid gels with DBS-CO<sub>2</sub>H [87]. Poly(ethylene glycol) can form a gelator network via covalent cross-linking induced by UV photopolymerization of PEG acrylates. The hybrid gels were prepared by adding DBS-CO<sub>2</sub>H into a PEGDM solution followed by UV curing procedures. Due to the photoresponsive property of PEGDM, different regions within the hybrid hydrogel can be spatially patterned. As shown in Fig. 5.26b, a Y-shaped region is created in the middle of the gel within the mould by applying a Y-shaped mask over the top of the mixture of PEGDM and DBS-CO<sub>2</sub>H when being cured under UV light. The Y-shaped hybrid region is comprised of both DBS-CO<sub>2</sub>H and PEGDM gel networks. Compared with the non-hybrid regions, the hybrid gels are more transparent and less easily deformed (Fig. 5.26c). The mechanical robustness of the hybrid gel could be improved significantly as proved by the intact removal of the Y-shaped region (Fig. 5.26d).

The application of polymer and low molecular weight gels has been extended to the field of tissue engineering. Feng and co-workers used self-assembling materials to form stable and stiff hydrogels via sol-gel transitions [88]. The elastic modulus of the hydrogel formed by C<sub>2</sub>-phenyl-derived gelator was increased significantly after being combined with a calcium ion cross-linked alginate network. The enhanced mechanical properties of the bi-component hybrid hydrogel allow the promotion of cell adhesion and spreading.

In addition to tissue engineering, a hybrid hydrogel containing Fmoc-diphenylalanine (Fmoc-FF) peptides and konjac glucomannan (KGM) has been developed for uses in drug delivery [89]. Fmoc-peptide-based hydrogels are known to be an important *in vivo* biomedical material while being limited by the instability in buffer solutions. The limitation of the Fmoc-peptide hydrogels can be overcome by preparing a hybrid gel via the self-assembly of Fmoc-FF peptide in a KGM

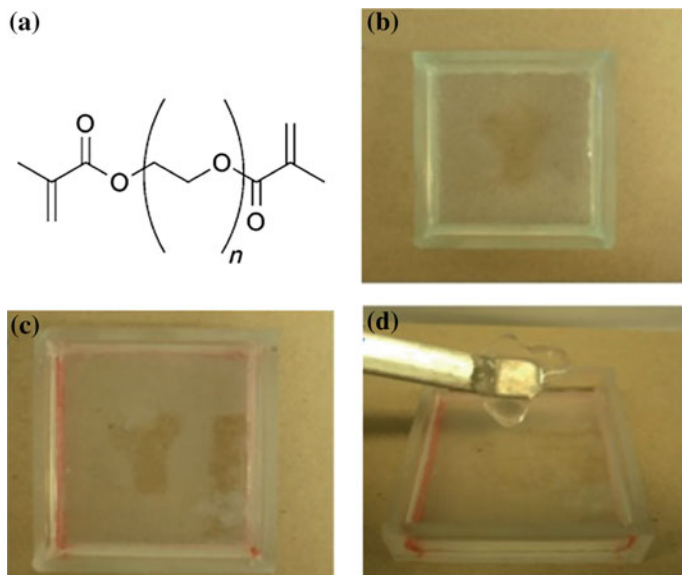


**Fig. 5.26** **a** Chemical structure of the polymer gelator, PEGDM, **b** patterned multi-domain gel consisting of Y-shaped hybrid region (more transparent) and non-hybrid network region (less transparent), **c** easy deformation of the non-hybrid region and **d** intact removal of the Y-shaped hybrid region. Adapted with permission from Ref. [87]. Copyright 2012 Wiley-VCH Verlag GmbH & Co. KGaA, Weinheim

solution. The drug release performance of the hybrid gel was characterized thoroughly including its pH responsibility, overall integrity and crystallization processes. Measurements were conducted to study the *in vitro* docetaxel release from the hybrid gel. The experimental results proved that the release rate was mainly associated with the concentration of KGM, ageing time and the concentration of  $\beta$ -mannanase added into the gel system. A fine control over these parameters can lead to a sustained docetaxel release from the peptide–polysaccharide hybrid hydrogel.

The formation of hybrid gels has been proven as an effective approach to developing novel materials where the properties of low molecular weight and polymer gelators are combined in a single structure. The properties of the two types of gel networks are not only combined simply, but also, in some cases, are entirely new. The properties of either of the components may be surpassed by those of the resulting hybrid gel materials. A large amount of further work is required to fully understand the growth mechanism of the hybrid molecular networks and gel materials with potential high-tech applications.

## References

1. Kim H-J, Zhang K, Moore L, Ho D (2014) Diamond nanogel-embedded contact lenses mediate lysozyme-dependent therapeutic release. *ACS Nano* 8(3):2998–3005. <https://doi.org/10.1021/nn5002968>
2. Laschi C, Cianchetti M (2014) Soft robotics: new perspectives for robot bodyware and control. *Front Bioeng Biotechnol* 2:3. <https://doi.org/10.3389/fbioe.2014.00003>
3. Sun Y, Jensen H, Petersen NJ, Larsen SW, Østergaard J (2017) Phase separation of in situ forming poly(lactide-co-glycolide acid) implants investigated using a hydrogel-based subcutaneous tissue surrogate and UV-vis imaging. *J Pharm Biomed Anal* 145:682–691. <https://doi.org/10.1016/j.jpba.2017.07.056>
4. Bai W, Spivak DA (2014) A double-imprinted diffraction-grating sensor based on a virus-responsive super-aptamer hydrogel derived from an impure extract. *Angew Chem* 126(8):2127–2130. <https://doi.org/10.1002/ange.201309462>
5. Mrozek RA, Sliozberg YR, Andzelm JW, Lenhart JL (2015) Polymer gels for defense applications. In: Barthelat F, Korach C, Zavattieri P, Prorok BC, Grande-Allen KJ (eds) *Mechanics of biological systems and materials. Proceedings of the 2014 annual conference on experimental and applied mechanics*, vol 7. Springer International Publishing, Cham, pp 47–51. [https://doi.org/10.1007/978-3-319-06974-6\\_7](https://doi.org/10.1007/978-3-319-06974-6_7)
6. Sutar P, Maji TK (2016) Coordination polymer gels: soft metal-organic supramolecular materials and versatile applications. *Chem Commun* 52(52):8055–8074. <https://doi.org/10.1039/C6CC01955B>
7. Wang R, Geiger C, Chen L, Swanson B, Whitten DG (2000) Direct observation of sol-gel conversion: the role of the solvent in organogel formation. *J Am Chem Soc* 122(10):2399–2400. <https://doi.org/10.1021/ja993991t>
8. Shi C, Huang Z, Kilic S, Xu J, Enick RM, Beckman EJ, Carr AJ, Melendez RE, Hamilton AD (1999) The gelation of CO<sub>2</sub>: a sustainable route to the creation of microcellular materials. *Science* 286(5444):1540–1543. <https://doi.org/10.1126/science.286.5444.1540>
9. Jung JH, Ono Y, Shinkai S (2000) Sol-gel polycondensation of tetraethoxysilane in a cholesterol-based organogel system results in chiral spiral silica. *Angew Chem Int Ed* 39(10):1862–1865
10. van den Berg O, Nguyen L-TT, Teixeira RFA, Goethals F, Özdilek C, Berghmans S, Du Prez FE (2014) Low modulus dry silicone-gel materials by photoinduced thiol-ene chemistry. *Macromolecules* 47(4):1292–1300. <https://doi.org/10.1021/ma402564a>
11. Forbes CJ, McCoy CF, Murphy DJ, Woolfson AD, Moore JP, Evans A, Shattock RJ, Malcolm RK (2014) Modified silicone elastomer vaginal gels for sustained release of antiretroviral HIV microbicides. *J Pharm Sci* 103(5):1422–1432. <https://doi.org/10.1002/jps.23913>
12. Bin Imran A, Esaki K, Gotoh H, Seki T, Ito K, Sakai Y, Takeoka Y (2014) Extremely stretchable thermosensitive hydrogels by introducing slide-ring polyrotaxane cross-linkers and ionic groups into the polymer network. *Nat Commun* 5:5124. <https://doi.org/10.1038/ncomms6124>
13. Wichterle O, Lim D (1960) Hydrophilic gels for biological use. *Nature* 185(4706):117–118
14. Lloyd AW, Faragher RGA, Denyer SP (2001) Ocular biomaterials and implants. *Biomaterials* 22(8):769–785. [https://doi.org/10.1016/S0142-9612\(00\)00237-4](https://doi.org/10.1016/S0142-9612(00)00237-4)
15. Nicolson PC, Vogt J (2001) Soft contact lens polymers: an evolution. *Biomaterials* 22(24):3273–3283. [https://doi.org/10.1016/S0142-9612\(01\)00165-X](https://doi.org/10.1016/S0142-9612(01)00165-X)
16. Suzuki A, Tanaka T (1990) Phase transition in polymer gels induced by visible light. *Nature* 346(6282):345–347
17. Kwon IC, Bae YH, Kim SW (1991) Electrically credible polymer gel for controlled release of drugs. *Nature* 354(6351):291–293

18. Lowman AM, Morishita M, Kajita M, Nagai T, Peppas NA (1999) Oral delivery of insulin using pH-responsive complexation gels. *J Pharm Sci* 88(9):933–937. <https://doi.org/10.1021/js980337n>
19. Wang C, Stewart RJ, Kopeček J (1999) Hybrid hydrogels assembled from synthetic polymers and coiled-coil protein domains. *Nature* 397(6718):417–420
20. Tsitsilianis C, Iliopoulos I, Ducoiret G (2000) An associative polyelectrolyte end-capped with short polystyrene chains. *Synth Rheological Behav Macromol* 33(8):2936–2943. <https://doi.org/10.1021/ma991410e>
21. Petka WA, Harden JL, McGrath KP, Wirtz D, Tirrell DA (1998) Reversible hydrogels from self-assembling artificial proteins. *Science* 281(5375):389–392. <https://doi.org/10.1126/science.281.5375.389>
22. Hamley IW, Daniel C, Mingvanish W, Mai S-M, Booth C, Messe L, Ryan AJ (2000) From hard spheres to soft spheres: the effect of copolymer composition on the structure of micellar cubic phases formed by diblock copolymers in aqueous solution. *Langmuir* 16(6):2508–2514. <https://doi.org/10.1021/la991035j>
23. Peppas NA, Hilt JZ, Khademhosseini A, Langer R (2006) Hydrogels in biology and medicine: from molecular principles to bionanotechnology. *Adv Mater* 18(11):1345–1360. <https://doi.org/10.1002/adma.200501612>
24. Lee KY, Mooney DJ (2001) Hydrogels for tissue engineering. *Chem Rev* 101(7):1869–1880. <https://doi.org/10.1021/cr000108x>
25. Yuk H, Zhang T, Lin S, Parada GA, Zhao X (2016) Tough bonding of hydrogels to diverse non-porous surfaces. *Nat Mater* 15(2):190–196. <https://doi.org/10.1038/nmat4463>
26. Wang X, Chen Y, Xue L, Pothayee N, Zhang R, Riffle JS, Reineke TM, Madsen LA (2014) Diffusion of drug delivery nanoparticles into biogels using time-resolved micromri. *J Phys Chem Lett* 5(21):3825–3830. <https://doi.org/10.1021/jz501929u>
27. Leocmach M, Nespoulous M, Manneville S, Gibaud T (2015) Hierarchical wrinkling in a confined permeable biogel. *Sci Adv* 1(9). <https://doi.org/10.1126/sciadv.1500608>
28. Mahaffy RE, Shih CK, MacKintosh FC, Käs J (2000) Scanning probe-based frequency-dependent microrheology of polymer gels and biological cells. *Phys Rev Lett* 85(4):880–883
29. Nakayama A, Kakugo A, Gong JP, Osada Y, Takai M, Erata T, Kawano S (2004) High mechanical strength double-network hydrogel with bacterial cellulose. *Adv Func Mater* 14(11):1124–1128. <https://doi.org/10.1002/adfm.200305197>
30. Tanaka Y, Kuwabara R, Na Y-H, Kurokawa T, Gong JP, Osada Y (2005) Determination of fracture energy of high strength double network hydrogels. *J Phys Chem B* 109(23):11559–11562. <https://doi.org/10.1021/jp0500790>
31. Yang J, Han C-R, Duan J-F, Xu F, Sun R-C (2013) Mechanical and viscoelastic properties of cellulose nanocrystals reinforced poly(ethylene glycol) nanocomposite hydrogels. *ACS Appl Mater Interfaces* 5(8):3199–3207. <https://doi.org/10.1021/am4001997>
32. Flory PJ (1953) Principles of polymer chemistry. Cornell University Press, Ithaca, New York
33. Dong L, Agarwal AK, Beebe DJ, Jiang H (2006) Adaptive liquid microlenses activated by stimuli-responsive hydrogels. *Nature* 442(7102):551–554
34. Qiu Y, Park K (2001) Environment-sensitive hydrogels for drug delivery. *Adv Drug Deliv Rev* 53(3):321–339. [https://doi.org/10.1016/S0169-409X\(01\)00203-4](https://doi.org/10.1016/S0169-409X(01)00203-4)
35. Li J, Liu T, Xia S, Pan Y, Zheng Z, Ding X, Peng Y (2011) A versatile approach to achieve quintuple-shape memory effect by semi-interpenetrating polymer networks containing broadened glass transition and crystalline segments. *J Mater Chem* 21(33):12213–12217. <https://doi.org/10.1039/C1JM12496J>
36. Guo M, Pitet LM, Wyss HM, Vos M, Dankers PYW, Meijer EW (2014) Tough stimuli-responsive supramolecular hydrogels with hydrogen-bonding network junctions. *J Am Chem Soc* 136(19):6969–6977. <https://doi.org/10.1021/ja500205v>
37. Nair KP, Breedveld V, Weck M (2011) Multiresponsive reversible polymer networks based on hydrogen bonding and metal coordination. *Macromolecules* 44(9):3346–3357. <https://doi.org/10.1021/ma102462y>

38. Hackelbusch S, Rossow T, Becker H, Seiffert S (2014) Multiresponsive polymer hydrogels by orthogonal supramolecular chain cross-linking. *Macromolecules* 47(12):4028–4036. <https://doi.org/10.1021/ma5008573>
39. Ji X, Jie K, Zimmerman SC, Huang F (2015) A double supramolecular crosslinked polymer gel exhibiting macroscale expansion and contraction behavior and multistimuli responsiveness. *Polym Chem* 6(11):1912–1917. <https://doi.org/10.1039/C4PY01715C>
40. Wang Q, Mynar JL, Yoshida M, Lee E, Lee M, Okuro K, Kinbara K, Aida T (2010) High-water-content mouldable hydrogels by mixing clay and a dendritic molecular binder. *Nature* 463(7279):339–343
41. Partridge KS, Smith DK, Dykes GM, McGrail PT (2001) Supramolecular dendritic two-component gel. *Chem Commun* 4:319–320. <https://doi.org/10.1039/B009672P>
42. Ge Z, Hu J, Huang F, Liu S (2009) Responsive supramolecular gels constructed by crown ether based molecular recognition. *Angew Chem* 121(10):1830–1834. <https://doi.org/10.1002/ange.200805712>
43. Noro A, Matsushita Y, Lodge TP (2009) Gelation mechanism of thermoreversible supramacromolecular ion gels via hydrogen bonding. *Macromolecules* 42(15):5802–5810. <https://doi.org/10.1021/ma900820g>
44. Noro A, Hayashi M, Ohshika A, Matsushita Y (2011) Simple preparation of supramolecular polymer gels via hydrogen bonding by blending two liquid polymers. *Soft Matter* 7(5):1667–1670. <https://doi.org/10.1039/C0SM01334J>
45. Jung JH, Lee JH, Silverman JR, John G (2013) Coordination polymer gels with important environmental and biological applications. *Chem Soc Rev* 42(3):924–936. <https://doi.org/10.1039/C2CS35407A>
46. Rubin DJ, Miserez A, Waite JH (2010) Diverse strategies of protein sclerotization in marine invertebrates. *Adv Insect Physiol* 38:75–133. [https://doi.org/10.1016/S0065-2806\(10\)38003-9](https://doi.org/10.1016/S0065-2806(10)38003-9)
47. Harrington MJ, Masic A, Holten-Andersen N, Waite JH, Fratzl P (2010) Iron-clad fibers: a metal-based biological strategy for hard flexible coatings. *Science* 328(5975):216–220. <https://doi.org/10.1126/science.1181044>
48. Holten-Andersen N, Harrington MJ, Birkedal H, Lee BP, Messersmith PB, Lee KYC, Waite JH (2011) pH-induced metal-ligand cross-links inspired by mussel yield self-healing polymer networks with near-covalent elastic moduli. *Proc Natl Acad Sci USA* 108(7):2651–2655. <https://doi.org/10.1073/pnas.1015862108>
49. Piepenbrock M-OM, Lloyd GO, Clarke N, Steed JW (2010) Metal- and anion-binding supramolecular gels. *Chem Rev* 110(4):1960–2004. <https://doi.org/10.1021/cr9003067>
50. Zhang J, Su C-Y (2013) Metal-organic gels: from discrete metallogelators to coordination polymer networks. *Coord Chem Rev* 257:1373–1408. <https://doi.org/10.1016/j.ccr.2013.01.005>
51. Dubey M, Kumar A, Pandey DS (2014) Homochiral coordination polymeric gel: Zn<sup>2+</sup>-induced conformational changes leading to J-aggregated helical fibres formation. *Chem Commun* 50(14):1675–1677. <https://doi.org/10.1039/C3CC47359G>
52. Xu F, Padhy H, Al-Dossary M, Zhang G, Behzad AR, Stingl U, Rothenberger A (2014) Synthesis and properties of the metallo-supramolecular polymer hydrogel poly[methyl vinyl ether-alt-mono-sodium maleate] AgNO<sub>3</sub>: Ag<sup>+</sup>/Cu<sup>2+</sup> ion exchange and effective antibacterial activity. *J Mater Chem B* 2(37):6406–6411. <https://doi.org/10.1039/C4TB00611A>
53. Zhukhovitskiy AV, Zhong M, Keeler EG, Michaelis VK, Sun JEP, Hore MJA, Pochan DJ, Griffin RG, Willard AP, Johnson JA (2016) Highly branched and loop-rich gels via formation of metal-organic cages linked by polymers. *Nat Chem* 8(1):33–41. <https://doi.org/10.1038/nchem.2390>
54. Foster JA, Parker RM, Belonguer AM, Kishi N, Sutton S, Abell C, Nitschke JR (2015) Differentially addressable cavities within metal-organic cage-cross-linked polymeric hydrogels. *J Am Chem Soc* 137(30):9722–9729. <https://doi.org/10.1021/jacs.5b05507>
55. Wang Y, Zhong M, Park JV, Zhukhovitskiy AV, Shi W, Johnson JA (2016) Block co-polyMOCs by stepwise self-assembly. *J Am Chem Soc* 138(33):10708–10715. <https://doi.org/10.1021/jacs.6b06712>

56. Wei Z, Yang JH, Zhou J, Xu F, Zrinyi M, Dussault PH, Osada Y, Chen YM (2014) Self-healing gels based on constitutional dynamic chemistry and their potential applications. *Chem Soc Rev* 43(23):8114–8131. <https://doi.org/10.1039/C4CS00219A>
57. Wu XL, He CL, Wu YD, Chen XS (2016) Synergistic therapeutic effects of Schiff's base cross-linked injectable hydrogels for local co-delivery of metformin and 5-fluorouracil in a mouse colon carcinoma model. *Biomaterials* 75:148–162. <https://doi.org/10.1016/j.biomaterials.2015.10.016>
58. Deng G, Tang C, Li F, Jiang H, Chen Y (2010) Covalent cross-linked polymer gels with reversible sol–gel transition and self-healing properties. *Macromolecules* 43(3):1191–1194. <https://doi.org/10.1021/ma9022197>
59. Cok AM, Zhou H, Johnson JA (2013) Synthesis of model network hydrogels via Tetrazine-Olefin Inverse electron demand Diels-Alder Cycloaddition. *Macromolecular Symposia* 329(1):108–112. <https://doi.org/10.1002/masy.201300008>
60. Casuso P, Odriozola I, Pérez-San Vicente A, Loínez I, Cabañero G, Grande H-J, Dupin D (2015) Injectable and self-healing dynamic hydrogels based on Metal(I)-Thiolate/Disulfide exchange as biomaterials with tunable mechanical properties. *Biomacromol* 16(11):3552–3561. <https://doi.org/10.1021/acs.biomac.5b00980>
61. Imato K, Irie A, Kosuge T, Ohishi T, Nishihara M, Takahara A, Otsuka H (2015) Mechanophores with a reversible radical system and freezing-induced mechanochemistry in polymer solutions and gels. *Angew Chem Int Ed* 54(21):6168–6172. <https://doi.org/10.1002/anie.201412413>
62. Roberts MC, Hanson MC, Massey AP, Karren EA, Kiser PF (2007) Dynamically restructuring hydrogel networks formed with reversible covalent crosslinks. *Adv Mater* 19(18):2503–2507. <https://doi.org/10.1002/adma.200602649>
63. Zhang Y, Tao L, Li S, Wei Y (2011) Synthesis of multiresponsive and dynamic chitosan-based hydrogels for controlled release of bioactive molecules. *Biomacromol* 12(8):2894–2901. <https://doi.org/10.1021/bm200423f>
64. Haldar U, Bauri K, Li R, Faust R, De P (2015) Polyisobutylene-based pH-responsive self-healing polymeric gels. *ACS Appl Mater Interfaces* 7(16):8779–8788. <https://doi.org/10.1021/acsami.5b01272>
65. Deng G, Ma Q, Yu H, Zhang Y, Yan Z, Liu F, Liu C, Jiang H, Chen Y (2015) Macroscopic organohydrogel hybrid from rapid adhesion between dynamic covalent hydrogel and organogel. *ACS Macro Lett* 4(4):467–471. <https://doi.org/10.1021/acsmacrolett.5b00096>
66. Guan Y, Zhang Y (2013) Boronic acid-containing hydrogels: synthesis and their applications. *Chem Soc Rev* 42(20):8106–8121. <https://doi.org/10.1039/C3CS60152H>
67. Xu J, Yang D, Li W, Gao Y, Chen H, Li H (2011) Phenylboronate-diol crosslinked polymer gels with reversible sol–gel transition. *Polymer* 52(19):4268–4276. <https://doi.org/10.1016/j.polymer.2011.07.015>
68. Chujo Y, Sada K, Naka A, Nomura R, Saegusa T (1993) Synthesis and redox gelation of disulfide-modified polyoxazoline. *Macromolecules* 26(5):883–887. <https://doi.org/10.1021/ma00057a001>
69. Chujo Y, Sada K, Saegusa T (1990) Reversible gelation of polyoxazoline by means of Diels–Alder reaction. *Macromolecules* 23(10):2636–2641. <https://doi.org/10.1021/ma00212a007>
70. Koehler KC, Anseth KS, Bowman CN (2013) Diels-Alder mediated controlled release from a Poly(ethylene glycol) based hydrogel. *Biomacromol* 14(2):538–547. <https://doi.org/10.1021/bm301789d>
71. Su J, Amamoto Y, Nishihara M, Takahara A, Otsuka H (2011) Reversible cross-linking of hydrophilic dynamic covalent polymers with radically exchangeable alkoxyamines in aqueous media. *Polym Chem* 2(9):2021–2026. <https://doi.org/10.1039/C1PY00176K>
72. Imato K, Nishihara M, Kanehara T, Amamoto Y, Takahara A, Otsuka H (2012) Self-healing of chemical gels cross-linked by diarylbibenzofuranone-based trigger-free dynamic covalent bonds at room temperature. *Angew Chem Int Ed* 51(5):1138–1142. <https://doi.org/10.1002/anie.201104069>

73. Nicolaÿ R, Kamada J, Van Wassen A, Matyjaszewski K (2010) Responsive gels based on a dynamic covalent Trithiocarbonate cross-linker. *Macromolecules* 43(9):4355–4361. <https://doi.org/10.1021/ma100378r>
74. Amamoto Y, Otsuka H, Takahara A, Matyjaszewski K (2012) Changes in network structure of chemical gels controlled by solvent quality through photoinduced radical reshuffling reactions of Trithiocarbonate units. *ACS Macro Lett* 1(4):478–481. <https://doi.org/10.1021/mz300070t>
75. Cornwell DJ, Smith DK (2015) Expanding the scope of gels—combining polymers with low-molecular-weight gelators to yield modified self-assembling smart materials with high-tech applications. *Mater Horizons* 2(3):279–293. <https://doi.org/10.1039/C4MH00245H>
76. de Loos M, van Esch J, Stokroos I, Kellogg RM, Feringa BL (1997) Remarkable stabilization of self-assembled organogels by polymerization. *J Am Chem Soc* 119(51):12675–12676. <https://doi.org/10.1021/ja972899z>
77. Eimura H, Yoshio M, Shoji Y, Hanabusa K, Kato T (2012) Liquid-crystalline gels exhibiting electrooptical light scattering properties: fibrous polymerized network of a lysine-based gelator having acrylate moieties. *Polym J* 44(6):594–599
78. George M, Weiss RG (2003) Low molecular-mass gelators with Diyne functional groups and their unpolymerized and polymerized gel assemblies. *Chem Mater* 15(15):2879–2888. <https://doi.org/10.1021/cm034099v>
79. Kim C, Lee SJ, Lee IH, Kim KT, Song HH, Jeon H-J (2003) Stabilization of supramolecular nanostructures induced by self-assembly of dendritic building blocks. *Chem Mater* 15(19):3638–3642. <https://doi.org/10.1021/cm021087l>
80. Moffat JR, Coates IA, Leng FJ, Smith DK (2009) Metathesis within self-assembled gels: transcribing nanostructured soft materials into a more robust form. *Langmuir* 25(15):8786–8793. <https://doi.org/10.1021/la900282k>
81. Diaz DD, Rajagopal K, Strable E, Schneider J, Finn MG (2006) “Click” chemistry in a supramolecular environment: stabilization of organogels by Copper(I)-catalyzed azide–alkyne [3+2] cycloaddition. *J Am Chem Soc* 128(18):6056–6057. <https://doi.org/10.1021/ja061251w>
82. Piepenbrock MOM, Clarke N, Foster JA, Steed JW (2011) Anion tuning and polymer templating in a simple low molecular weight organogelator. *Chem Commun* 47(7):2095–2097. <https://doi.org/10.1039/C0CC03439H>
83. Kolb HC, Finn MG, Sharpless KB (2001) Click chemistry: diverse chemical function from a few good reactions. *Angew Chem Int Ed* 40(11):2004–2021
84. Dasgupta D, Srinivasan S, Rochas C, Ajayaghosh A, Guenet JM (2009) Hybrid thermoreversible gels from covalent polymers and organogels. *Langmuir* 25(15):8593–8598. <https://doi.org/10.1021/la804185q>
85. Wang J, Wang H, Song Z, Kong D, Chen X, Yang Z (2010) A hybrid hydrogel for efficient removal of methyl violet from aqueous solutions. *Colloids Surf B Biointerfaces* 80(2):155–160. <https://doi.org/10.1016/j.colsurfb.2010.05.042>
86. Cornwell DJ, Okesola BO, Smith DK (2013) Hybrid polymer and low molecular weight gels—dynamic two-component soft materials with both responsive and robust nanoscale networks. *Soft Matter* 9(36):8730–8736. <https://doi.org/10.1039/C3SM51967H>
87. Cornwell DJ, Okesola BO, Smith DK (2014) Multidomain hybrid hydrogels: spatially resolved photopatterned synthetic nanomaterials combining polymer and low-molecular-weight gelators. *Angew Chem* 126(46):12669–12673. <https://doi.org/10.1002/ange.201405098>
88. Li P, Dou X-Q, Feng C-L, Zhang D (2013) Mechanical reinforcement of C2-phenyl-derived hydrogels for controlled cell adhesion. *Soft Matter* 9(14):3750–3757. <https://doi.org/10.1039/C3SM27727E>
89. Huang R, Qi W, Feng L, Su R, He Z (2011) Self-assembling peptide-polysaccharide hybrid hydrogel as a potential carrier for drug delivery. *Soft Matter* 7(13):6222–6230. <https://doi.org/10.1039/C1SM05375B>

## Chapter 6

# Inorganic Gels

**Abstract** This chapter focuses on the discussion of various inorganic gels including the formation mechanism, molecular systems and functional properties. The inorganic gels include silica-based gels, chalcogels and others. In the first section of the chapter, the concept of sol–gel process, which is a commonly used principle to explain the formation of inorganic gels, is introduced. In the following sections, three catalogues of inorganic gels are discussed in detail. For silica-based gels, the nanoparticles of silica derivatives are used as silica sources. The growth mechanism of silica gels from the nanoparticles and the key factors to determine the formation process are reviewed. Several representative silica gel systems are presented to show the versatility of the materials. In the following section, chalcogels are discussed and discussions focus on the preparation methods and catalytic performance of chalcogels. At last, a brief description about other gels including  $\text{AgVO}_3$  and  $\text{V}_2\text{O}_5$  gels is given.

**Keywords** Inorganic gels · Sol–gel process · Silica-based gels  
Chalcogels

The existence of inorganic gels dates back to 1846 when French chemist Ebelmen discovered the formation of gels by mixing  $\text{SiCl}_4$  with ethanol under wet air atmosphere [1]. Since the large-scale manufacture of silica gels first started in 1800s, inorganic gels have attracted significant research interests [2]. Apart from silica gels, Foerster made a jelly-like cupric oxide material by the hydrolysis of a concentrated solution of cupric ammonium acetate dated back to 1892 [3]. The observation of the cupric oxide jelly later embarked extended investigations on the formation of inorganic jellies with other saturated salt solutions [4]. Following the observation of a wide range of gel materials, the underlying fundamental knowledge, properties and applications have been gradually revealed. The advances in inorganic gel research significantly contributed to the fabrication of oxide materials using sol–gel method [5].

---

Ya Hu and Jianyong Zhang contributed together to this chapter.

Conventional wet gels encapsulating liquids can be converted into other gel forms through drying. Examples include xerogel formed after the shrinkage of original gel networks by drying under ambient pressure and aerogels which maintain gel networks by drying under supercritical conditions. Despite abundant existence of organic gels, inorganic gels have already evolved into an inseparable research branch of gel materials [6–8].

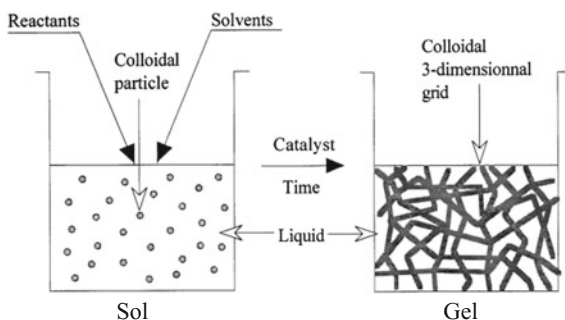
## 6.1 Sol–Gel Process for Gel Formation

Inorganic gels are often formed via the hydrolysis and condensation of oxides, in the form of solid colloidal particles. The colloid species that can undergo such sol–gel processes include silica and other metal oxides (e.g.  $\text{Al}_2\text{O}_3$ ,  $\text{TiO}_2$  and  $\text{ZrO}_2$ ). The formation of inorganic gels involves the linking of silicon or metallic atoms, similar to cross-linking between gelators via self-assembly or polymerization for polymer gels.

The sol–gel process starts with the formation of a colloidal suspension containing solid nanoparticles (Fig. 6.1). The nanoparticles are well dispersed in a suitable solvent leading to the macroscopic state of the solution. Subsequently, these dispersed nanoparticles are converted into three-dimensional networks by performing reactions to link them. While encapsulating the solvent, the solution is transformed into a colloidal gel via the gelation process.

Metallic salts are the first precursor used for the synthesis of inorganic gels via sol–gel processes. In aqueous medium, a metallic salt ( $\text{MX}_n$ ) composed of a metal (M) and  $n$  anions (X) can bond with water molecules forming solvated cations ( $\text{M}[\text{H}_2\text{O}]_n^{z+}$ ). In the hydrolysis step, the  $\text{H}_2\text{O}$  groups of the solvated cations are replaced with  $\text{OH}^-$  by losing protons. Following the hydrolysis, the metallic cations are connected by  $\text{M–OH–M}$  or  $\text{M–O–M}$  bonds via condensation reactions. In order to reveal the underlying mechanisms of these reactions, Livage and co-workers have proposed a partial charge model [6, 9]. As shown in Fig. 6.2a,  $\text{H}_2\text{O}$  molecules bonded with M are substituted by an  $\text{OH}^-$  directly. Subsequently, a transition of hydrogen bonds is proposed as a proton exchange mechanism to explain the

**Fig. 6.1** Schematic illustration of the sol–gel process for solid colloidal nanoparticles. Adapted with permission from Ref. [6]. Copyright 2002 American Chemical Society



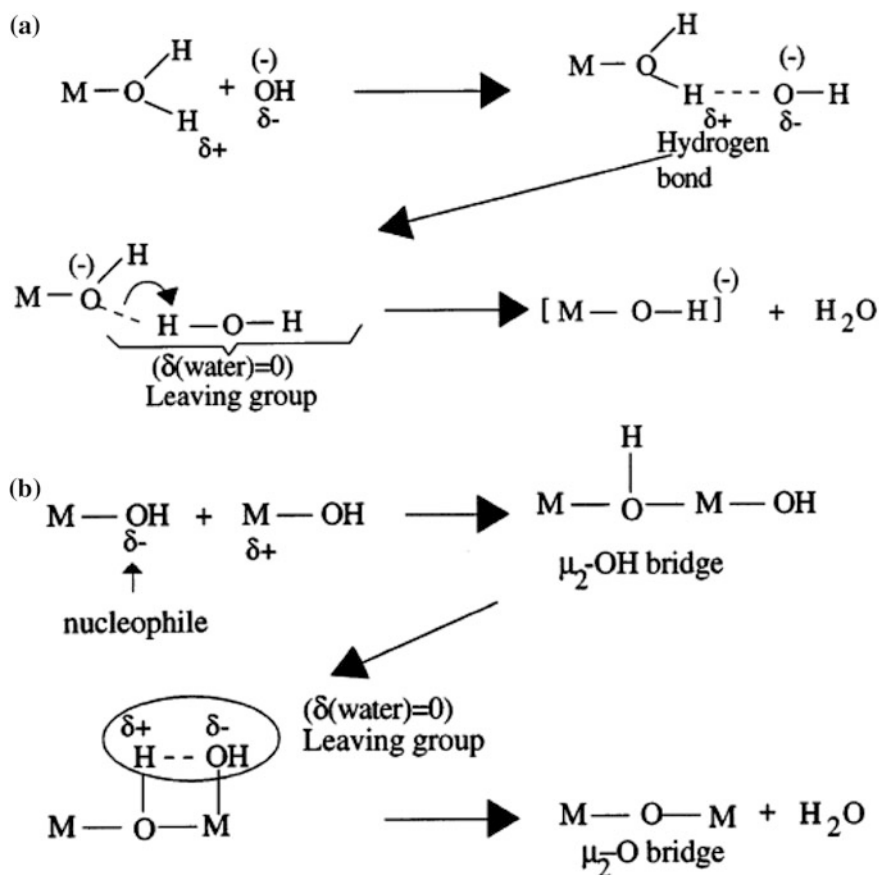
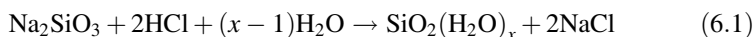


**Fig. 6.2 a** Schematic illustration for the partial charge model proposed by Livage and co-workers. Adapted with permission from Ref. [6]. Copyright 2002 American Chemical Society

formation of M–OH intermediates. Following the formation of the intermediates, several condensation reactions are activated for the formation of M–OH–M or M–O–M bonds (Fig. 6.2b). A key concept involved in this model is the redistribution of electronic clouds for the atoms of intermediates based on the electronic transfer mechanism proposed by Sanderson [10]. In this model, a group of neighbour atoms within an intermediate may separate as a leaving group when these atoms add a partial charge of an integral number (e.g. –1, 0 and 1). Next, the leaving group can be converted into an electrically neutral molecule, an anion or a cation depending on the magnitude of the partial charge.

## 6.2 Silica-Based Gels

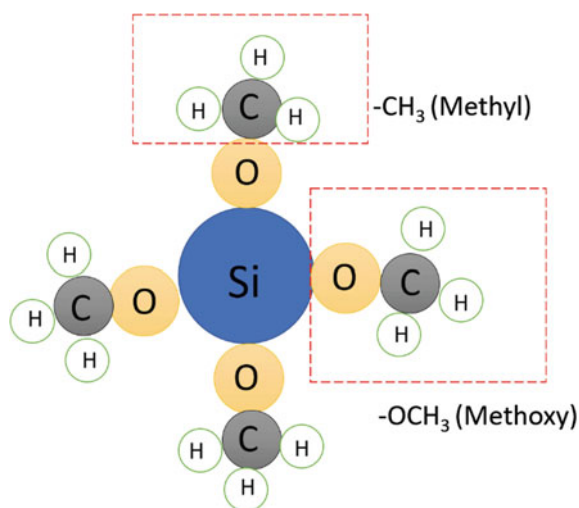
In early times,  $\text{SiO}_2$  were made from the chemical reaction between sodium metasilicate  $\text{Na}_2\text{SiO}_3$  and an acid (see reaction 6.1) [6, 11].



In order to obtain pure  $\text{SiO}_2$ , dialysis processes are often performed to remove  $\text{NaCl}$  following the reaction. Kistler first used this reaction to synthesize water glass-based aerogels by supercritical drying [11]. As a cheap method, this reaction was once modified by BASF to produce commercial silica-based aerogels [12]. The main disadvantage of the reaction lies in the use of water as a solvent which reduces the flexibility for the adjustment of the hydrolysis and condensation rates [6].

The preparation of silica gels often starts with the formation of a solution by dispersing nanoparticles in a suitable liquid, followed by interconnection of the particles. The most commonly used silica source is silicon alkoxide molecules, particularly tetramethoxysilane (TMOS) or tetraethoxysilane (TEOS). Figure 6.3 shows the packing arrangement of a TMOS molecule. The molecule is non-polar since all the dipole moments are neutralized resulting from the even distribution of the four methoxy groups. Upon contact with water, the alkoxide molecule first reacts with water forming  $\text{Si-OH}$  groups. Subsequently, the  $\text{Si-OH}$  condenses with another  $\text{Si-OH}$  or a  $\text{Si-OR}$  group to form a  $\text{Si-O-Si}$  bridge. Resulting from the formation of  $\text{Si-O-Si}$  bridges, multiple small TMSO molecules can be interconnected into silica nanoparticles. In a solution, the nanoparticles continue growing until reaching a critical size. Several factors play important roles in determining the magnitude of the critical size including temperature, the concentration of molecular

**Fig. 6.3** Schematic packing arrangement of a tetramethoxysilane molecule



species and the pH of the liquid medium [13]. Different nanoparticles can be interconnected into extended 3D networks through further condensation reactions between the alkoxy and hydroxyl groups on the particle surfaces. The resulting silicon alkoxide-based gel has been extensively used as a matrix to encapsulate cells in the area of biotechnology [14]. However, the application in cell encapsulation is limited by the pH adaptability of the silica gel structures [15]. The activity of intracellular enzymes of cells is significantly reduced while the gels are formed in an acidic solution. If the pH of the solution is adjusted to neutral prior to encapsulating cells, the gel structures may suffer from lack of diffusion leading to weak structural controllability.

To improve the encapsulation ability of silica gels while maintaining the bioactivity of guest bio-organisms, Mutlu and co-workers developed a novel silica gel based on silica nanoparticles cross-linked by silicon alkoxide molecules [16]. Figure 6.4 shows the schematic representation of the strategy to encapsulate catalytic bacteria within the silica-based network. In this preparation scheme, a silicon alkoxide species (e.g. TEOS) is used as a cross-linker for silica nanoparticles. To ensure the full hydrolysis and slow condensation of the silicon alkoxide solution, the pH of the solution and molecular ratio between water and silicon alkoxide molecules should be finely adjusted. In addition to silicon alkoxides, commercial solutions of silica nanoparticles (Ludox HS40, Ludox TM 40, Nexsil 85-40 and Hexsil 125-40 from Sigma-Aldrich) are employed for the preparation of gels. These purchased solutions vary in nanoparticle size and starting pH. By adding 1 M hydrochloric acid, the pH of the solutions can be adjusted to 7. This neutral pH conditions ensure the enzymes added into the system are still biologically active. In another flask, a bacteria suspension is prepared in water and subsequently added into the silica nanoparticle solutions. After mixing with the previously prepared silicon alkoxide solution, a transition into gels can be observed within seconds or hours. The gelation time is highly tunable depending on the formula of the mixed solutions. Further catalytic tests on the gel-bacteria composites show that the

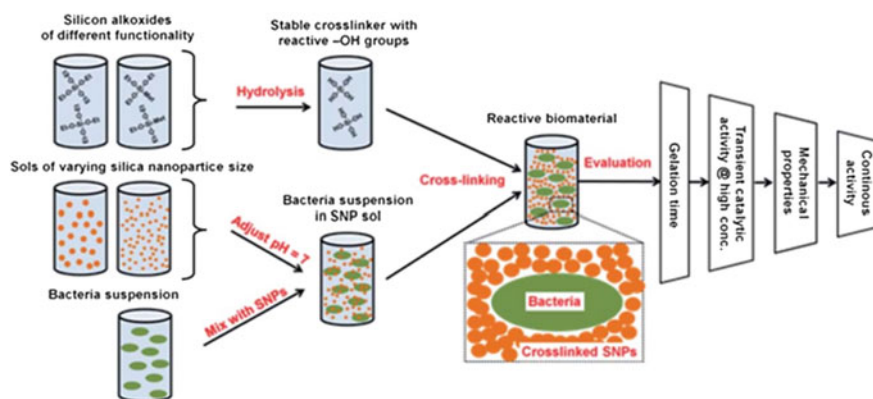


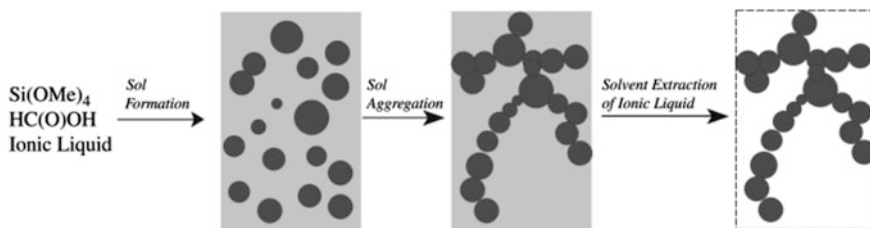
**Fig. 6.4** Schematic representation of experimental protocols to encapsulate bio-catalytically active bacterial in silica gels. Adapted from Ref. [16] with permission from The Royal Society of Chemistry

catalytic activity of the bacteria is still preserved. This composite material has potential applications in the elimination of water pollutants. The removal of atrazine at trace levels could be achieved successfully using the newly developed catalytic catalysts.

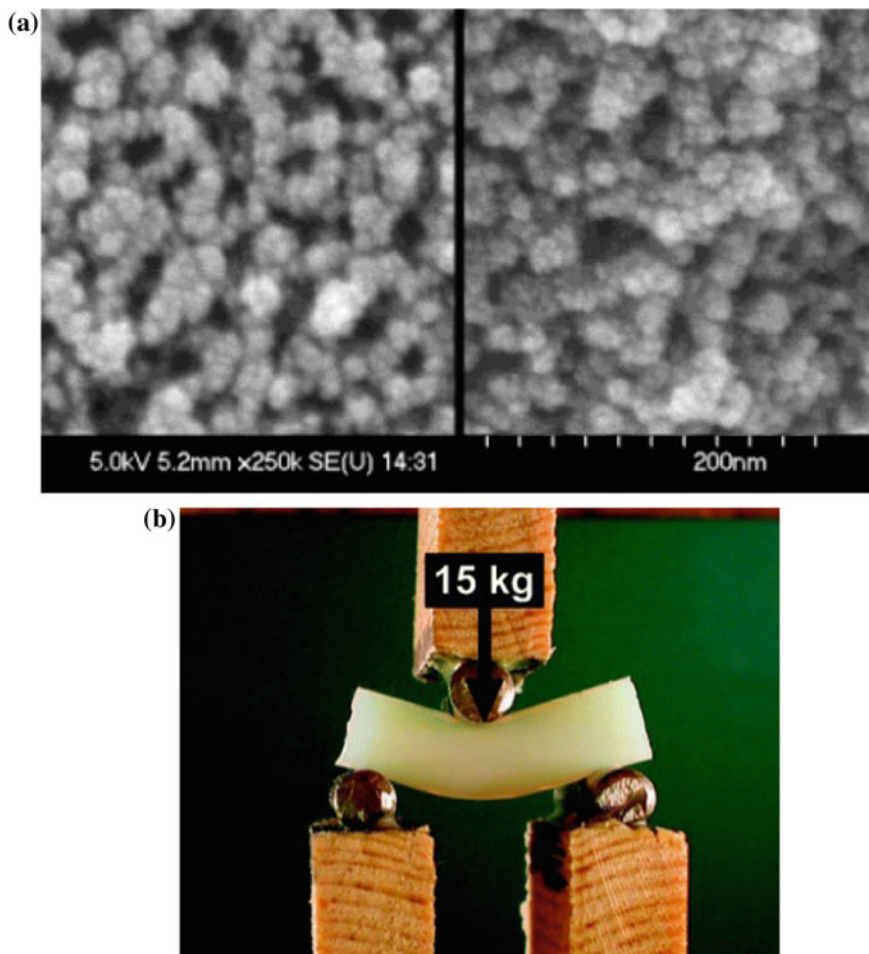
For most real applications, silica gels should be dried and used as aerogel. The preparation of silica aerogel is usually done by removing the liquid phase of the porous silica-based molecular network of silica wet gels. In this process, the volume percentage of the silica gel network that can be maintained reaches over 50% [17]. The liquid phase is typically removed by drying under supercritical conditions, but can also be done by adding surfactant molecules or using ionic liquids as solvents [18, 19].

Figure 6.5 shows the preparation scheme developed by Dai and co-workers for the formation of silica aerogels by using ionic liquids as solvents [18]. The silica precursor, TMOS, is mixed with the catalyst, formic acid and the ionic liquid, 1-ethyl-3-methylimidazolium bis[(trifluoromethyl)sulphonyl] amide ( $\text{EtMeIm}^+\text{Tf}_2\text{N}^-$ ). After an overnight gelling process, a silica wet gel is formed and subsequently cured at room temperature. The resulting transparent silica glass is monolithic and can be refluxed in acetonitrile to extract the encapsulated ionic liquid. The TMOS-based network of the aerogel is largely maintained following the ionic liquid removal. Compared with other aerogels prepared using different solvents and supercritical drying, the  $\text{N}_2$  sorption isotherm of this silica aerogel exhibits identical gas adsorption and desorption properties [20]. The successful extraction of the ionic liquid is suggested to result from the thermodynamically favourable interactions between TMSO particles and the liquid. Instead of forming chemical bonds with the TMSO network, the ionic liquid is only encapsulated within the network. Thus, the extraction of the ionic liquid from the gel network becomes facilitated. This ionic liquid method avoids the use of the expensive and energy-consuming supercritical drying process and has potential applications in the development of other aerogel materials.

Silica aerogels have attracted wide research interest because they are promising lightweight materials with enhanced mechanical properties. A strong silica aerogel has been developed by intruding diisocyanate (di-ISO) cross-linkers into the gel network [21]. The STM images in Fig. 6.6 show a comparison of morphological structures for silica aerogels prior to and following introducing di-ISO cross-linkers.



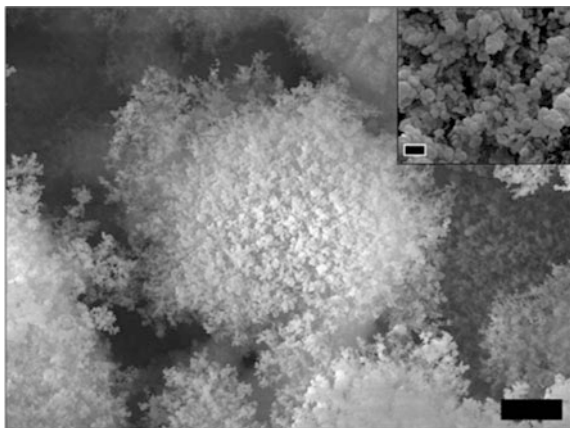
**Fig. 6.5** Schematic illustration for the formation of stable silica-based aerogels by using ionic liquids as solvents. Adapted from Ref. [18] with permission from The Royal Society of Chemistry



**Fig. 6.6** **a** Comparison of SEM images showing different microstructures of a native silica aerogel (left, density =  $0.169 \text{ g cm}^{-3}$ ) and a di-ISO cross-linked silica aerogel composite (right, density =  $0.380 \text{ g cm}^{-3}$ ). **b** Photograph of mechanically strong silica aerogels that can withstand 15 kg load. Adapted with permission from Ref. [21]. Copyright 2002 American Chemical Society

The native silica aerogels were prepared using tetramethoxysilane via base-catalyzed cross-linking reactions [22]. These silica aerogels are composed of interconnected particles with diameter ranging from 5 to 10 nm. Mesopores with diameters of around 50 nm are formed during the cross-linking of the particles. Following the formation of the silica aerogels, the gels are washed with ethanol, propylene carbonate and a mixture of propylene carbonate and poly(hexamethylene diisocyanate). After the cross-linking process with di-ISO, the interconnections between the silica particles are observed to become wider as compared with the image on the left. This significantly strengthens the robustness of the novel silica

**Fig. 6.7** SEM image illustrating the microscale structures agglomerated by fumed silica (scale bar, 5  $\mu\text{m}$ ). Inset: SEM image showing sub-micron structures (scale bar, 500 nm). Reproduced from Ref. [23] with permission from The Royal Society of Chemistry



composites. Figure 6.6b shows the photography of a three-point flexural bending method to test the strength of the di-ISO cross-linked silica aerogel with a density of  $0.447 \text{ g cm}^{-3}$ . Results from the mechanical test prove that a load of around 15 kg is required to break the monolith sample.

Colloidal silicon dioxide produced in a flame (called as fumed silica) is a widely investigated inorganic particle species for silica-based gel formation. The SEM images in Fig. 6.7 show the microstructures of fumed silica [23]. The fume silica aggregates are composed of primary particles with sizes ranging from 5 to 50 nm. These particles are fused into stable, branched secondary particles with large sizes ranging from 100 to 500 nm. Further stabilized by non-covalent bonding (e.g. hydrogen bonding and electrostatic interactions), the secondary particles are grown into aggregates with micrometre sizes [24, 25]. Fumed silica can be used as thickening and gelling agent in various liquid phases, such as organic solvents, ionic solutions and water [26, 27]. This versatile gelation property is closely correlated with the large surface area and surface hydrophilicity of the hierarchical structure of fumed silica [28].

An important application of fumed silica-based gels is working as electrolyte in batteries. Gençten and co-workers prepared a fumed silica-based gel working as an electrolyte for the valve-regulated lead-acid (VRLA) batteries [29]. For this application, the concentrations of silica, gel compositions, gelation conditions and additive species all play an important role in determining the performance of the batteries. Compared with colloidal silica, fumed silica-based gels exhibit better 3D gel structures, lower internal resistance, shorter gelling time and improved thixotropy. The authors tried to optimize the concentration of sulphuric acid and the ratios of inorganic additives using cyclic voltammetric and electrochemical impedance measurements. The results proved that the fumed silica-based gel electrolyte can be potentially applied as an electrolyte for VRLA batteries.

### 6.3 Chalcogels

Apart from inorganic gels made from oxides, Kanatzidis and co-workers have developed the application of sulphide and selenide clusters in gel formation [30]. The porous gel networks are stabilized by the interactions between these clusters and metal ions (termed as chalcogels). Figure 6.8 shows the molecular models of a range of chalcogenide-based clusters ( $[\text{MQ}_4]^{4-}$ ,  $[\text{M}_2\text{Q}_6]^{4-}$  and  $[\text{M}_4\text{Q}_{10}]^{4-}$  where  $\text{M} = \text{Ge}, \text{Sn}$  and  $\text{Q} = \text{S}, \text{Se}$ ) linked by platinum ions.  $\text{K}_2\text{PtCl}_4$  was chosen as a platinum source reacting with the chalcogenide-based clusters via metathesis reactions. Corresponding aerogels can be obtained by drying the resulting wet gels under supercritical conditions. Compared with conventional silica aerogels, the chalcogels have hydrophobic surfaces and exhibit better stability under humid atmospheres. Due these unique properties, the absorption of organic hydrophobic molecules can be efficiently absorbed by the chalcogels from solutions. Regarding optical properties, diffuse-reflectance solid-state ultraviolet-visible/near-infrared spectroscopy investigations show that the light absorption range of the chalcogels ranges from visible to infrared regions. Thus, the energy gap (0.8–2.0 eV) falls into the range of semiconductors. The chalcogels introduced in this work have highly tunable structures and properties, and thus have attracted extensive research interest to further explore this class of materials.

In addition to the metathesis reactions, Kanatzidis and co-workers have adopted an oxidative coupling reaction to prepare ion-exchangeable molybdenum sulphide ( $\text{MoS}_x$ ) chalcogel [31]. The chemical reaction shown in Fig. 6.9 describes the synthesis of  $\text{MoS}_x$  chalcogels by using  $\text{MoS}_4^{2-}$  clusters and  $\text{I}_2$ . If the stoichiometric ratio of  $\text{I}_2$  is lowered to 0.9, a  $\text{MoS}_x$  chalcogel can still be formed. In comparison with the  $\text{I}_2$  stoichiometric ratio of 1, the gel network contains residual  $\text{NH}_4^+$  ions to reach electrically neutral. Other cations, such as  $\text{K}^+$  and  $\text{Cs}^+$ , can be used to exchange the  $\text{NH}_4^+$  rendering it possible to functionalize the  $\text{MoS}_x$  chalcogels following synthesis. The resulting  $\text{MoS}_x$ -based wet chalcogels can also be converted into aerogels by supercritical drying with  $\text{CO}_2$ . As a result of the large amount

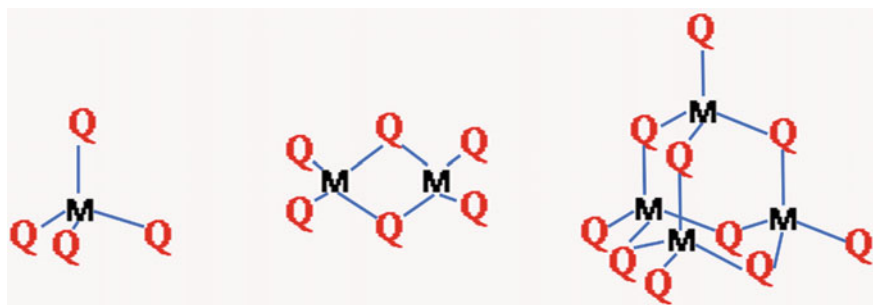


**Fig. 6.8** Schematic model of molecular building blocks used for the formation of chalcogels. M, metal centre (Ge, Sn); Q, chalcogenide atom (S, Se)

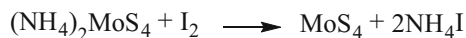


**Fig. 6.9** Chemical reaction between  $\text{MoS}_4^{2-}$  and iodine for the synthesis of  $\text{MoS}_x^-$  based chalcogel. Adapted with permission from Ref. [31]. Copyright 2015 American Chemical Society

of S–S bonding within the gel network, the  $\text{MoS}_x$  chalcogel can adsorb Hg vapour chemically by forming S–Hg–S bonds [32]. This Hg adsorption property has potential applications in eliminating mercury contamination emitted from coal burning. Another significant advantage of the  $\text{MoS}_x$  chalcogel is the ability to adsorb  $\text{I}_2$  vapour. This is related to the polarization of the inner Mo–S surface of the chalcogel. The  $\text{I}_2$  vapour is claimed to be mainly adsorbed via physical interactions.

The choice of preparation methods plays an important role in determining the structures of the resulting chalcogels and gel formation routes. Examples include the preparation of antimony sulphide (SbS) chalcogels using four different methods [33]. As shown in Fig. 6.10, the four synthetic methods include the hydrolysis of  $\text{SbS}_3^{3-}$  salts, the metathesis reaction between  $\text{SbS}_3^{3-}$  and  $\text{Sb}_3^+$ , the reaction between  $\text{Na}_2\text{S}$  and  $\text{Sb}_2\text{S}_3$  followed by hydrolysis and the reaction between  $\text{KOH}$  and  $\text{Sb}_2\text{S}_3$  followed by hydrolysis. All of these reaction routes lead to the formation of SbS-based chalcogels with difference in gelation time. More specifically, the gelation processes for SbS-I, SbS-III and SbS-IV are completed within a few hours while this for SbS-II requires 1 week. The prominent advantage of the SbS-based chalcogels lies in their high surface areas (nearly  $1700 \text{ m}^2 \text{ g}^{-1}$ ) as detected by  $\text{N}_2$  gas sorption experiments.

In addition to the diverse synthetic routes, chalcogels have attracted extensive research interest mainly because of their remarkable and highly tunable functional properties. These properties include the aforementioned  $\text{I}_2$  and Hg vapour adsorption [32], electrocatalytic and photocatalytic activity for hydrogen production [34, 35], selective removal of heavy metal elements [30] and hydrodesulphurization (HDS) catalysis [36]. In this section, several exemplary literatures investigating the properties of chalcogels are summarized and discussed.

Spongy chalcogels containing Ni–Mo–S, Co–Mo–S and Co–Ni–Mo–S have been prepared by metathesis reactions (Fig. 6.11) [36]. In these reactions,  $(\text{MoS}_4)^{2-}$  is used as precursors, and  $\text{Co}^{2+}$  and  $\text{Ni}^{2+}$  containing salts are used as linking agents. At room temperature, gel-phase materials can be obtained by mixing the solutions containing the precursors and linking agents followed by a 96 h ageing process. The gels prepared using the reactions (1), (2) and (3) were named as chalcogel-Ni-1, chalcogel-Co-1 and chalcogel-NiCo-1, respectively.

The photographs in Fig. 6.12a show the images of some of the wet gels and aerogels prepared by  $\text{CO}_2$  supercritical drying. In comparison, the chalcogels undergo no significant loss in volume showing stable connection between the secondary particles. The secondary particles are formed by the aggregation of primary particles produced by the reactions between  $(\text{MoS}_4)^{2-}$  and  $\text{Co}^{2+}/\text{Ni}^{2+}$  ions. Through hydrodesulphurization (HDS) processes, organosulphur compounds are removed from fossil fuels [37]. The catalytic activity of the chalcogels in the HDS

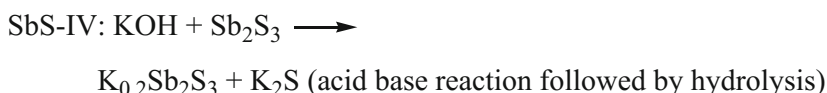
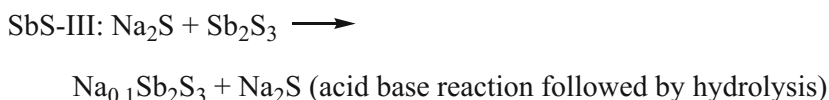
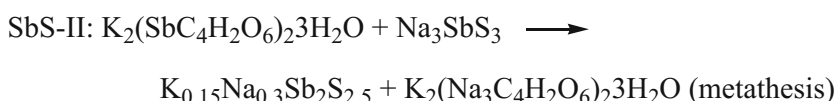
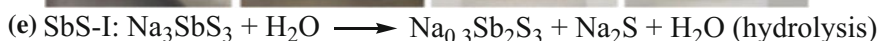
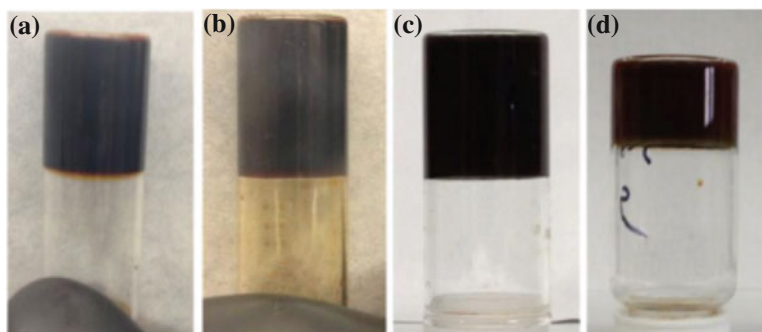


**Fig. 6.10** a–d Photographs of the corresponding gels and e four chemical reactions performed for the formation of SbS-based chalcogels (termed as SbS-I, SbS-II, SbS-III and SbS-IV). Adapted with permission from Ref. [33]. Copyright 2016 American Chemical Society

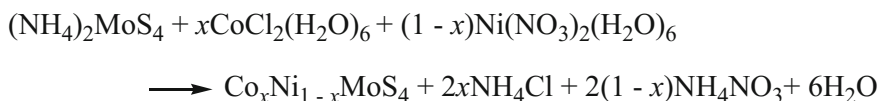


**Fig. 6.11** Metathesis reactions used to synthesis chalcogels containing Ni–Mo–S, Co–Mo–S and Co–Ni–Mo–S. Adapted with permission from Ref. [36]. Copyright 2009 Nature Publishing Group

process can be presented by the plots in Fig. 6.12b. Compared with the thiophene HDS activity of the commonly employed sulphide Co–Mo/Al<sub>2</sub>O<sub>3</sub> catalyst at 643 K, the chalcogel-Co-1 exhibits double catalytic performance as well as long-term stability (>48 h). This result demonstrates that the non-platinum chalcogel has

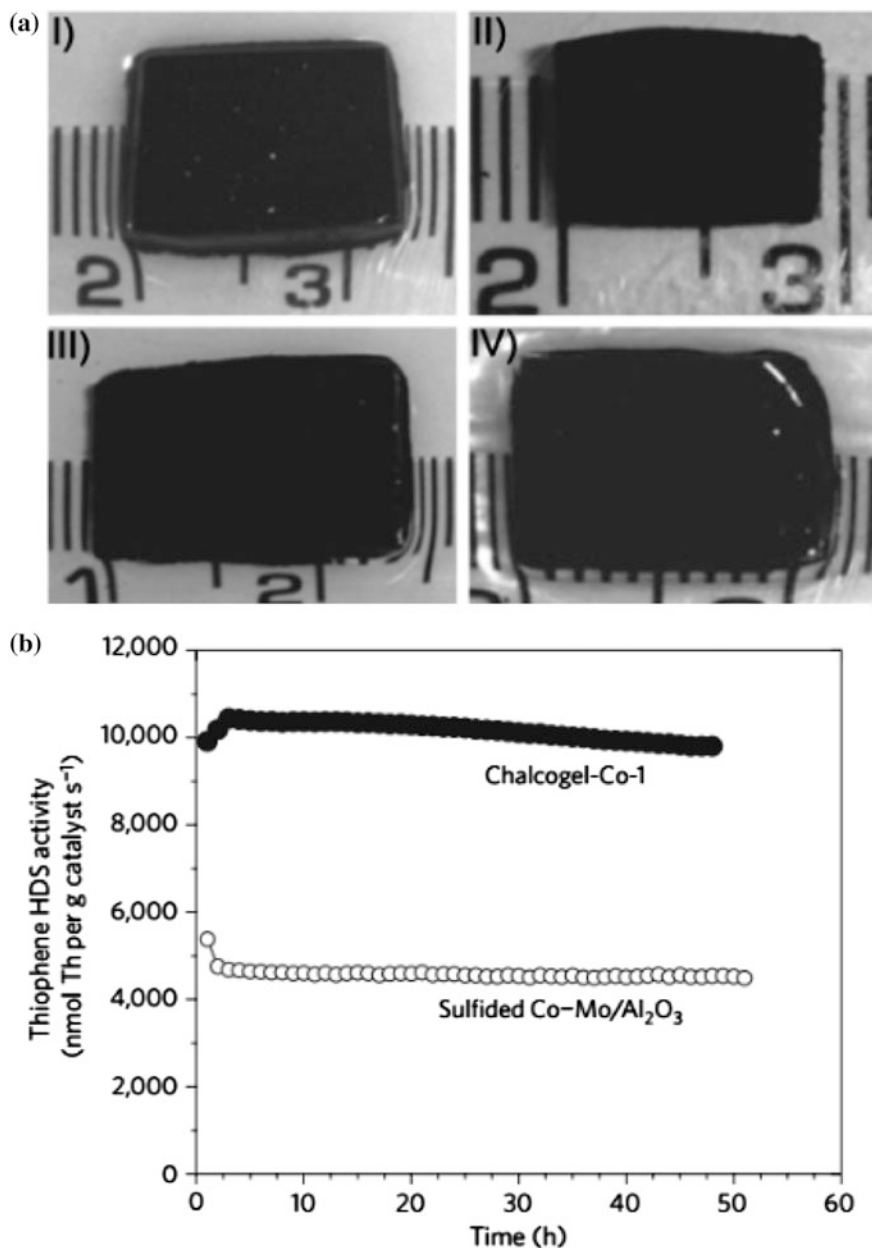


**Fig. 6.12** **a** Photographs of (I) chalcogel-Ni-1 hydrogel, (II) chalcogel-Ni-1 aerogel, (III) chalcogel-Co-1 hydrogel and (IV) chalcogel-NiCo-1 aerogel, and **b** thiophene HDS activity data for chalcogel-Co-1 (solid circle) and a sulphide Co-Mo/Al<sub>2</sub>O<sub>3</sub> catalyst (open circles). Adapted with permission from Ref. [36]. Copyright 2009 Nature Publishing Group

significant potential for clean energy applications. The excellent catalytic performance of the chalcogels is in correlation with the easy access to organic molecules resulting from the existence of large pores within the molecular networks.

In addition to HDS catalysis, chalcogels can also be applied in biologically important nitrogen fixation conventionally catalyzed by the enzyme nitrogenase [38, 39]. Figure 6.13b shows the nitrogen reduction process performing in biological organisms. In this process,  $H_2$  is produced while  $N_2$  is reduced under the catalysis of nitrogenase [40]. Later research reveals the composition of the active sites of nitrogenases as a Fe–Mo–S cluster [41]. A FeMoS-chalcogel can be synthesized using the scheme shown in Fig. 6.13b. Through the metathesis reaction between  $[Mo_2Fe_6S_8(SPh)_3Cl_6]^{3-}$  clusters and  $[Sn_2S_6]^{4-}$  ions, FeMoS-chalcogels are prepared in a mixture of *N*-methylformamide and *N,N'*-dimethylformamide. The formation of a FeMoS-chalcogel in black is confirmed by the tube inversion method. In order to test the catalytic performance of the FeMoS-chalcogel for nitrogen conversion, the chalcogel was deposited in an aqueous solution with  $N_2$  flowing through. The system was placed under the illumination of white light.

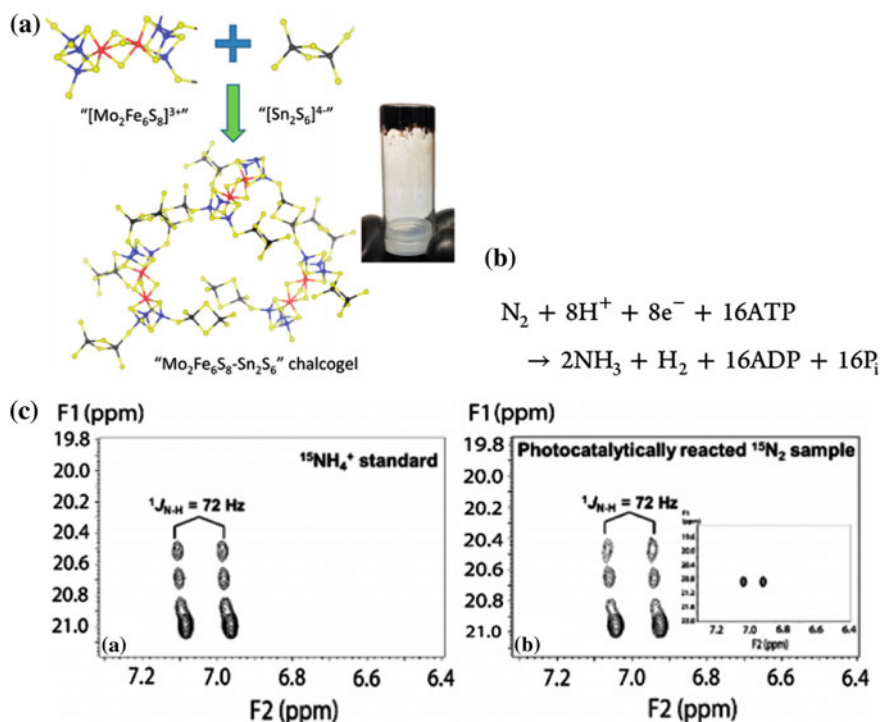


**Fig. 6.13** **a** Schematic illustration for the synthetic process of  $Mo_2Fe_6S_8-Sn_2S_6$  chalcogel (abbreviated as FeMoS-chalcogel), **b** chemical reaction showing nitrogen reduction process in biological organisms and **c** measurement of  $[^{15}NH_4]^+$  in the reaction solution using NMR. Adapted with permission from Ref. [38]. Copyright 2015 American Chemical Society

Isotope labelling experiments were performed to trace the nitrogen source of ammonia. In one set of experiments,  $^{15}\text{N}$  labelling was conducted for pyridinium chloride leading to the formation of  $^{14}\text{NH}_3$  ammonia. In the other set, labelled  $^{15}\text{N}_2$  gas was used for the nitrogen reduction under light illumination. Figure 6.13c presents the NMR results collected on standard  $[\text{}^{15}\text{NH}_4]^+$  solution and labelled  $^{15}\text{N}_2$  samples, respectively. In both cases, the characteristic peaks ( $J = 72$  Hz) corresponding to the  $^{15}\text{N}\text{-}^1\text{H}$  coupling are observed. Thus, the nitrogen source of ammonia is proved to nitrogen gas. This study illustrates the photocatalytic activity of the biomimetic FeMoS-chalcogels with FeMoS clusters as active sites. The FeMoS-chalcogels improves the original catalytic properties of nitrogenases by enabling strong white light absorption.

## 6.4 Other Inorganic Gels

Pal and co-workers prepared an  $\text{AgVO}_3$  inorganic gel without using any carbon-containing gelators (Fig. 6.14). The preparation for  $\text{AgVO}_3$  hydrogel starts by mixing the aqueous solutions of  $\text{AgNO}_3$  and  $\text{NH}_4\text{VO}_3$ . As a result of dipole–dipole interactions,  $\text{AgVO}_3$  molecules are produced leading to the formation of a cross-linked molecular network. Following encapsulation of water molecules within the networks,  $\text{AgVO}_3$  hydrogel is successfully prepared. The resulting  $\text{AgVO}_3$  hydrogel exhibits prominent adsorption for methylene blue (MB). As shown in Fig. 6.14b, an aqueous solution contaminated with MB is placed on the top of the  $\text{AgVO}_3$  hydrogel. Prior to adsorption, the upper solution is in dark blue showing a high concentration of MB in water. After 48 h, the colours of the  $\text{AgVO}_3$  hydrogel and upper solution change significantly (Fig. 6.14b). By tracing the concentration of MB in the upper solution using UV-Vis spectroscopy, the MB adsorption capacity for per unit amount of  $\text{AgVO}_3$  hydrogel was determined to reach  $580 \text{ mg g}^{-1}$ . In addition to organic dye removal, the  $\text{AgVO}_3$  hydrogel is also capable for heavy metal removal. Instead of placing a MB-contaminated aqueous solution, a solution containing  $\text{HgCl}_2$  or  $\text{Na}_3\text{AsO}_4$  salts were also tested. For both of the contaminants, the  $\text{AgVO}_3$  hydrogel acts as an effective sorption matrix for the hazardous waste removal.

Another example of inorganic gels is vanadium oxide ( $\text{V}_2\text{O}_5 \cdot n\text{H}_2\text{O}$ ) hydrogel, which comprises nanoribbons formed by the non-covalent cross-linking of vanadium oxide [43–45]. The size of the nanoribbons formed by cross-linked vanadium oxide is about over  $1 \mu\text{m}$  long and  $10 \text{ nm}$  wide [46]. The unique properties of vanadium oxide and the intrinsic porosity of the hydrogel enable a wide range of applications including self-cleaning, biological sensing and drug delivery [47, 48].

Further to inorganic  $\text{AgVO}_3$  and  $\text{V}_2\text{O}_5$  hydrogels, Fernandez and co-workers developed a composite hydrogel by mixing two solutions containing silver vanadium oxide ( $\beta\text{-AgVO}_3$ ) and slightly reduced vanadium oxide ( $\text{V}_{1.6}^{5+}\text{V}_{0.4}^{4+}\text{O}_{4.8}$ ), respectively [49]. By varying the ratio and concentrations of the two components, a range of composite hydrogels can be prepared. Examples include H1A10; the

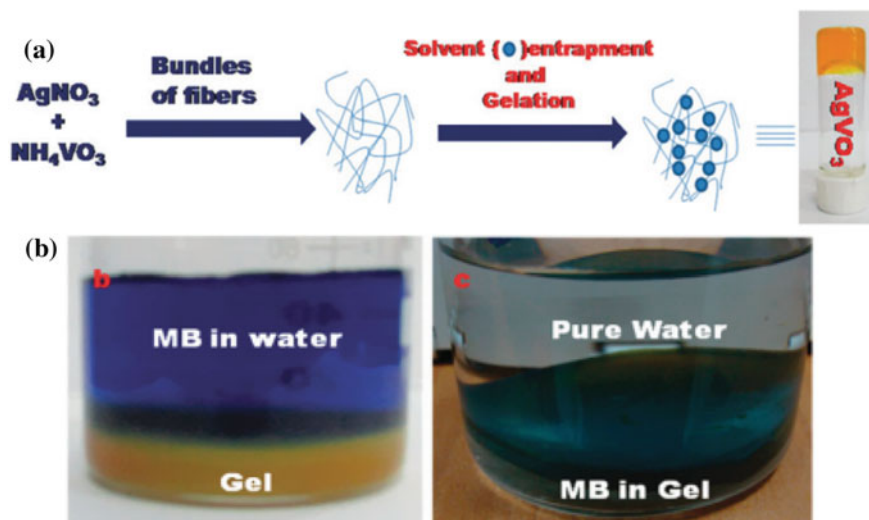


**Fig. 6.14** a Schematic illustration showing the preparation procedures for a  $\text{AgVO}_3$  hydrogel and b photographs of MB aqueous solution in contact with the  $\text{AgVO}_3$  hydrogel before (left) and after (right) MB removal. Reproduced from Ref. [42] with permission from The Royal Society of Chemistry

formula of which is  $\text{Ag}_{0.907}\text{V}_{1.016}\text{O}_3$ . Electron tomography analysis was conducted to study the 3D reconstruction of a single nanoribbon structure. As shown in Fig. 6.15a, the thickness of the nanoribbon and the location of Ag nanoparticles can be identified from the image. Under the illumination of an electron beam, a number of Ag nanoparticles are produced on the surface of the nanoribbon. The diameters

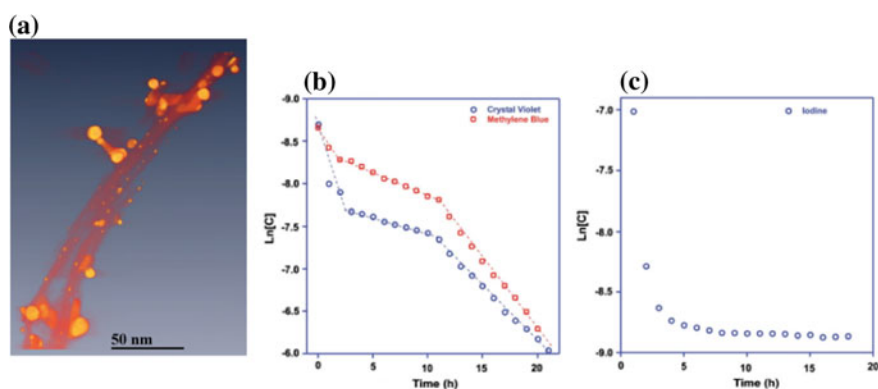


**Fig. 6.15** a Electron tomography 3D reconstruction of a single nanoribbon, b adsorption tests for the time-dependent concentrations of CV and MB using the H1A10 hydrogel and c adsorption tests for iodine. Reproduced from Ref. [49] with permission from The Royal Society of Chemistry

of the nanoribbons are in the range of a few nanometres upon the completion of nucleation and can increase to thousands of nanometres following growth process. The thickness of each nanoribbon is determined to be 5 nm [50]. The composite hydrogel has high adsorption capability against crystal violet (CV), methylene blue (MB) and radioactive iodine. Figure 6.15b presents the adsorption profile against CV and MB, in which three adsorption stages are clearly identified including 0–3, 3–11 and 11–20 h. By fitting the curves as first-order kinetic processes, the kinetic adsorption rates are calculated. The adsorption behaviour against radioactive iodine is different from those against CV and MB (Fig. 6.15c). The adsorption rate for iodine reaches high values during the first 3 h of the adsorption process.

## References

1. Ebelmen M (1846) *Ann Chim Phys* 16:129–166
2. Beelen TPM (1996) Inorganic particle gels. *Curr Opin Colloid Inter Sci* 1(6):718–725. [https://doi.org/10.1016/S1359-0294\(96\)80073-2](https://doi.org/10.1016/S1359-0294(96)80073-2)
3. Weiser H (1923) Cupric oxide Jellies. *J Phys Chem* 27(7):685–691
4. Finch L (1914) Cupric oxide jellies. *J Phys Chem* 18(1):26–33
5. Danks AE, Hall SR, Schnepf Z (2016) The evolution of ‘sol–gel’ chemistry as a technique for materials synthesis. *Mater Horizons* 3(2):91–112. <https://doi.org/10.1039/C5MH00260E>
6. Pierre AC, Pajonk GM (2002) Chemistry of aerogels and their applications. *Chem Rev* 102(11):4243–4266. <https://doi.org/10.1021/cr0101306>
7. Chung I, Kanatzidis MG (2014) Metal chalcogenides: a rich source of nonlinear optical materials. *Chem Mater* 26(1):849–869. <https://doi.org/10.1021/cm401737s>
8. Bag S, Arachchige IU, Kanatzidis MG (2008) Aerogels from metal chalcogenides and their emerging unique properties. *J Mater Chem* 18(31):3628–3632. <https://doi.org/10.1039/B804011G>
9. Livage J, Henry M, Sanchez C (1988) Sol–gel chemistry of transition metal oxides. *Prog Solid State Chem* 18(4):259–341. [https://doi.org/10.1016/0079-6786\(88\)90005-2](https://doi.org/10.1016/0079-6786(88)90005-2)
10. Sanderson RT (1951) An interpretation of bond lengths and a classification of bonds. *Science* 114(2973):670–672
11. Kistler S (1932) Coherent expanded-aerogels. *J Phys Chem* 36(1):52–64
12. Herrmann G, Iden R, Mielke M, Teich F, Ziegler B (1995) On the way to commercial production of silica aerogel. *J Non-Cryst Solids* 186 (Supplement C):380–387. [https://doi.org/10.1016/0022-3093\(95\)90076-4](https://doi.org/10.1016/0022-3093(95)90076-4)
13. Carcouët CCMC, van de Put MWP, Mezari B, Magusin PCMM, Laven J, Bomans PHH, Friedrich H, Esteves ACC, Sommerdijk NAJM, van Benthem RATM, de With G (2014) Nucleation and growth of monodisperse silica nanoparticles. *Nano Lett* 14(3):1433–1438. <https://doi.org/10.1021/nl404550d>
14. Nassif N, Bouvet O, Rager MN, Roux C, Coradin T, Livage J (2002) Living bacteria in silica gels. *Nat Mater* 1(1):42
15. Finnie KS, Bartlett JR, Woolfrey JL (2000) Encapsulation of sulfate-reducing bacteria in a silica host. *J Mater Chem* 10(5):1099–1101
16. Mutlu BR, Yeom S, Tong H-W, Wackett LP, Aksan A (2013) Silicon alkoxide cross-linked silica nanoparticle gels for encapsulation of bacterial biocatalysts. *J Mater Chem A* 1(36):11051–11060. <https://doi.org/10.1039/C3TA12303K>
17. Dorcheh AS, Abbasi M (2008) Silica aerogel; synthesis, properties and characterization. *J Mater Process Tech* 199(1):10–26

18. Dai S, Ju YH, Gao HJ, Lin JS, Pennycook SJ, Barnes CE (2000) Preparation of silica aerogel using ionic liquids as solvents. *Chem Commun* 3:243–244. <https://doi.org/10.1039/A907147D>
19. Guo Y, Guadalupe RA (1999) Functional silica aerogel from metastable lamellar composite. *Chem Commun* (4):315–316. <https://doi.org/10.1039/A807762B>
20. Morris CA, Anderson ML, Stroud RM, Merzbacher CI, Rolison DR (1999) Silica sol as a nanogel: flexible synthesis of composite aerogels. *Science* 284(5414):622–624
21. Leventis N, Sotiriou-Leventis C, Zhang G, Rawashdeh A-MM (2002) Nanoengineering strong silica aerogels. *Nano Lett* 2(9):957–960. <https://doi.org/10.1021/nl025690e>
22. Leventis N, Elder IA, Long GJ, Rolison DR (2002) Using nanoscopic hosts, magnetic guests, and field alignment to create anisotropic composite gels and aerogels. *Nano Lett* 2(1):63–67. <https://doi.org/10.1021/nl015637a>
23. Patel A, Mankoč B, Sintang MB, Lesaffer A, Dewettinck K (2015) Fumed silica-based organogels and ‘aqueous-organic’ bigels. *RSC Adv* 5(13):9703–9708
24. Wu X-J, Wang Y, Yang W, Xie B-H, Yang M-B, Dan W (2012) A rheological study on temperature dependent microstructural changes of fumed silica gels in dodecane. *Soft Matter* 8(40):10457–10463
25. Gun'ko V, Mironyuk I, Zarko V, Turov V, Voronin E, Pakhlov E, Goncharuk E, Lebeda R, Skubiszewska-Zięba J, Janusz W (2001) Fumed silicas possessing different morphology and hydrophilicity. *J Colloid Interface Sci* 242(1):90–103
26. Raghavan SR, Walls H, Khan SA (2000) Rheology of silica dispersions in organic liquids: new evidence for solvation forces dictated by hydrogen bonding. *Langmuir* 16(21):7920–7930
27. Zheng Z, Song Y, Yang R, Zheng Q (2015) Direct evidence for percolation of immobilized polymer layer around nanoparticles accounting for sol–gel transition in fumed silica dispersions. *Langmuir* 31(50):13478–13487
28. Binks BP, Horozov TS (2005) Aqueous foams stabilized solely by silica nanoparticles. *Angew Chem* 117(24):3788–3791
29. Gençten M, Dönmez KB, Şahin Y, Pekmez K, Suvacı E (2014) Voltammetric and electrochemical impedimetric behavior of silica-based gel electrolyte for valve-regulated lead-acid battery. *J Solid State Electro* 18(9):2469–2479. <https://doi.org/10.1007/s10008-014-2507-y>
30. Bag S, Trikalitis PN, Chupas PJ, Armatas GS, Kanatzidis MG (2007) Porous semiconducting gels and aerogels from chalcogenide clusters. *Science* 317(5837):490–493. <https://doi.org/10.1126/science.1142535>
31. Subrahmanyam KS, Malliakas CD, Sarma D, Armatas GS, Wu J, Kanatzidis MG (2015) Ion-exchangeable molybdenum sulfide porous chalcogel: gas adsorption and capture of iodine and mercury. *J Am Chem Soc* 137(43):13943–13948. <https://doi.org/10.1021/jacs.5b09110>
32. Oh Y, Morris CD, Kanatzidis MG (2012) Polysulfide chalcogels with ion-exchange properties and highly efficient mercury vapor sorption. *J Am Chem Soc* 134(35):14604–14608. <https://doi.org/10.1021/ja3061535>
33. Subrahmanyam KS, Malliakas CD, Islam SM, Sarma D, Wu J, Kanatzidis MG (2016) High-surface-area antimony sulfide chalcogels. *Chem Mater* 28(21):7744–7749. <https://doi.org/10.1021/acs.chemmater.6b02913>
34. Staszak-Jirkovsky J, Malliakas CD, Lopes PP, Danilovic N, Kota SS, Chang K-C, Genorio B, Strmcnik D, Stamenkovic VR, Kanatzidis MG, Markovic NM (2016) Design of active and stable Co–Mo–S<sub>x</sub> chalcogels as pH-universal catalysts for the hydrogen evolution reaction. *Nat Mater* 15(2):197–203. <https://doi.org/10.1038/nmat4481>
35. Liu J, Kelley MS, Wu W, Banerjee A, Douvalis AP, Wu J, Zhang Y, Schatz GC, Kanatzidis MG (2016) Nitrogenase-mimic iron-containing chalcogels for photochemical reduction of dinitrogen to ammonia. *Proc Natl Acad Sci USA* 113(20):5530–5535. <https://doi.org/10.1073/pnas.1605512113>
36. Bag S, Gaudette AF, Bussell ME, Kanatzidis MG (2009) Spongy chalcogels of non-platinum metals act as effective hydrodesulfurization catalysts. *Nat Chem* 1(3):217–224

37. Startsev AN (1995) The mechanism of HDS catalysis. *Catal Rev* 37(3):353–423. <https://doi.org/10.1080/01614949508006446>
38. Banerjee A, Yuhas BD, Margulies EA, Zhang Y, Shim Y, Wasielewski MR, Kanatzidis MG (2015) Photochemical nitrogen conversion to ammonia in ambient conditions with FeMoS-chalcogenides. *J Am Chem Soc* 137(5):2030–2034. <https://doi.org/10.1021/ja512491v>
39. Seefeldt LC, Hoffman BM, Dean DR (2009) Mechanism of Mo-dependent nitrogenase. *Ann Rev Biochem* 78(1):701–722. <https://doi.org/10.1146/annurev.biochem.78.070907.103812>
40. Yang Z-Y, Khadka N, Lukoyanov D, Hoffman BM, Dean DR, Seefeldt LC (2013) On reversible H<sub>2</sub> loss upon N<sub>2</sub> binding to FeMo-cofactor of nitrogenase. *Proc Natl Acad Sci USA* 110(41):16327–16332. <https://doi.org/10.1073/pnas.1315852110>
41. Einsle O, Tezcan FA, Andrade SLA, Schmid B, Yoshida M, Howard JB, Rees DC (2002) Nitrogenase MoFe-protein at 1.16 Å resolution: a central ligand in the FeMo-cofactor. *Science* 297(5587):1696–1700. <https://doi.org/10.1126/science.1073877>
42. Mondal C, Ganguly M, Pal J, Sahoo R, Sinha AK, Pal T (2013) Pure inorganic gel: a new host with tremendous sorption capability. *Chem Commun* 49(82):9428–9430. <https://doi.org/10.1039/C3CC45555F>
43. Commehines X, Davidson P, Bourgaux C, Livage J (1997) Orientation of liquid-crystalline suspensions of vanadium pentoxide ribbons by a magnetic field. *Adv Mater* 9(11):900–903. <https://doi.org/10.1002/adma.19970091110>
44. Chandrappa GT, Steunou N, Cassaignon S, Bauvais C, Livage J (2003) Hydrothermal synthesis of vanadium oxide nanotubes from V<sub>2</sub>O<sub>5</sub> gels. *Catal Today* 78(1):85–89. [https://doi.org/10.1016/S0920-5861\(02\)00298-5](https://doi.org/10.1016/S0920-5861(02)00298-5)
45. Alonso B, Livage J (1999) Synthesis of vanadium oxide gels from peroxovanadic acid solutions: a 51 V NMR study. *J Solid State Chem* 148(1):16–19. <https://doi.org/10.1006/jssc.1999.8283>
46. Livage J (1991) Vanadium pentoxide gels. *Chem Mater* 3(4):578–593. <https://doi.org/10.1021/cm00016a006>
47. Chen J, Yoshida M, Maekawa Y, Tsubokawa N (2001) Temperature-switchable vapor sensor materials based on N-isopropylacrylamide and calcium chloride. *Polymer* 42(23):9361–9365. [https://doi.org/10.1016/S0032-3861\(01\)00523-7](https://doi.org/10.1016/S0032-3861(01)00523-7)
48. van Bommel KJC, Stuart MCA, Feringa BL, van Esch J (2005) Two-stage enzyme mediated drug release from LMWG hydrogels. *Org Bio Chem* 3(16):2917–2920. <https://doi.org/10.1039/B507157G>
49. Fernandez de Luis R, Martinez-Amesti A, Larrea ES, Lezama L, Aguayo AT, Arriortua MI (2015) Composite [small beta]-AgVO<sub>3</sub>@V<sub>1.65</sub>+V<sub>0.44</sub>+O<sub>4.8</sub> hydrogels and xerogels for iodide capture. *J Mater Chem A* 3(39):19996–20012. <https://doi.org/10.1039/c5ta04189a>
50. Song J-M, Lin Y-Z, Yao H-B, Fan F-J, Li X-G, Yu S-H (2009) Superlong β-AgVO<sub>3</sub> nanoribbons: high-yield synthesis by a pyridine-assisted solution approach, their stability. *Electr Electrochem Prop ACS Nano* 3(3):653–660. <https://doi.org/10.1021/nn800813s>

# Index

## A

Acid, 3, 12, 25, 31, 36, 38, 39, 41, 42, 47, 50, 68, 81–84, 86–88, 95, 96, 103, 107–109, 119–121, 126, 127, 141, 145, 158, 163, 164, 167, 169, 172–175, 182, 183, 194–196, 198

Acylhydrazone, 122, 124–127, 131–133, 145, 173

Acylhydrazone bonding, 145, 147, 173, 174

Addition, 10, 20, 25, 28, 31, 37, 38, 41–51, 62, 67, 71, 74, 75, 84, 85, 87, 89, 95, 97, 98, 101, 105, 120, 122–124, 130–134, 145, 154, 157, 158, 164, 166, 171, 172, 175, 179, 180, 183, 199, 200, 203, 204

Adsorption, 12, 36, 39, 81, 105, 106, 131, 143, 169, 182, 196, 200, 204, 205, 206

Aerogel, 81, 88, 105, 143, 144, 196, 197, 198, 202

$\text{Ag}^+$ , 3, 47, 62, 65, 89, 100, 107, 131, 140, 166

$\text{Ag}^+$ –alkene interaction, 47

Aggregation-caused quenching, 13

Aggregation-induced emission, 88, 105, 143

Aggregation-induced enhanced emission, 12

$\text{AgVO}_3$ , 204, 205

Alkoxide, 194, 195

Alkoxyamine, 176, 177

Amide, 29, 63, 65, 68, 84, 89, 90, 98, 122, 179, 196

Amine-functional polymer, 158

Amphiphile, 124

Amphiphilic, 47, 48, 62, 63, 74

Anion, 43–45, 82, 98, 122, 133, 193

Anthracene dimerization, 120, 139

Antimony, 200

Atom force microscopy, 4

Azobenzene, 16–22, 41, 87, 88

## B

Base, 3, 25, 38, 119, 141, 172, 197

Bidentate ligand, 97

Bimetallic, 93, 131

Biomedical material, 183

Bispyridine, 167

Boronic ester, 119, 120, 140, 141, 173–175

Bulky molecule, 105

## C

Cage, 77, 139, 167, 169, 170

Cage molecule, 139

Calix[4]arene, 145, 147

Capillary reactor, 145

Carbene, 70

Carbon, 13, 23, 76, 90, 107, 109, 204

Carboxylate, 81, 84–86, 95–97, 105, 106

Catalysis, 13, 28, 81, 100, 109, 139, 165, 200, 203

Catalyst, 3, 13, 65, 90, 108, 145, 177, 196, 201, 202

Catechol, 120, 165, 166

Cation, 4, 39, 47, 79, 98, 127, 135, 166, 193

$\text{Cd}^{2+}$  ion, 95, 98, 107

Chalcogels, 199–201, 203, 204

Characterization, 4

Chemical gel, 157, 171

Chemical stimuli, 29, 37, 38, 44, 99, 128

Chiral, 25, 28, 45, 47, 50, 67, 68, 73, 75, 77, 93, 130, 131, 145, 182

Chiral amino alcohol, 50

Chirality, 12, 28, 29, 36, 37

Chitosan, 158, 172

Cholesterol, 18, 32, 35, 41, 65, 122, 128, 129

Chromophore, 13, 16, 122, 123

Cisplatin, 62, 138

- Click chemistry, 126, 180  
CN<sup>-</sup>, 130, 132, 133  
Component, 1, 12, 29, 39, 69, 127, 161, 164, 166, 172, 176, 181, 183, 195  
Contact lense, 154, 155, 157  
Coordination bonding, 61  
Coordination cage, 76  
Coordination interaction, 140  
Coordination polymer, 62, 79, 81, 82, 90, 93, 95, 98, 108, 110  
Copper(I), 63, 90, 96, 99, 177, 180, 181  
Copper(II), 50, 70, 95, 96, 98  
Coupling reaction, 108, 109, 199  
Covalent bond, 3  
Covalent interaction, 153, 162  
Cr(VI), 99, 100  
Critical gelator concentration, 4  
Cross-linking, 79, 85, 90, 122, 153–159, 163, 165–167, 172, 174, 176, 177, 179, 181, 183, 192, 197, 204  
Crystallization, 13, 62, 101, 184  
Cu<sup>2+</sup>, 47, 66, 67, 69, 70, 72–74, 76, 83, 89, 91, 95, 98, 128–134  
Cu–Cu interaction, 74  
Cycloaddition, 17, 108, 145, 180, 181  
Cyclodextrin, 50
- D**  
Dendron, 25, 26, 122–124, 131  
Deswelling, 13, 15, 20  
Detection, 48, 65, 73, 76, 88, 100, 104, 105, 107, 123, 133  
Diacetylene, 17, 23, 179, 180  
Diarylbibenzofuranone, 176, 178  
Diarylethene, 16, 27  
Diels–Alder cycloaddition, 119  
Diels–Alder reaction, 175, 176  
Differential scanning calorimetry, 4  
Discrete gelator, 62, 121  
Disulfide, 120  
Dithienylethene, 17, 28, 29  
Driving force, 2–4, 25, 31, 47, 142, 164, 165  
Dye, 22, 40, 105, 106, 135, 181, 182, 204  
Dynamic covalent chemistry, 3, 119, 139, 171, 172  
Dynamic covalent polymer, 141, 145
- E**  
Elastic modulus, 6, 169, 183  
Electroactive, 41, 42  
Electrocatalytic activity, 200  
Electrocyclic reaction, 17  
Electrode, 76, 107, 110  
Electrolyte, 84, 106, 198
- Enantioselective, 50, 51, 68, 73, 145, 147  
External stimuli, 10, 35, 61, 62, 121, 124, 153, 157, 169
- F**  
Fe<sup>3+</sup>, 3, 41, 81, 85, 87, 88, 95, 103, 105, 109, 110, 133, 134, 165, 166  
Ferrocene, 36, 40, 41, 70, 71, 124  
Flory lattice model, 160  
Flory–Rehner theory, 159  
Fluorescent switch, 29, 130, 132, 133  
Fluoride, 29, 43–45, 105, 122  
Fluoride ion, 29  
4-dimethylaminopyridine, 74
- G**  
Gel, 1, 2, 4, 5, 9, 11–13, 15, 18–21, 23, 25–38, 40–52, 61–63, 65–69, 71, 73–77, 79, 81–90, 92–96, 98–103, 105–110, 119, 122–127, 129–136, 138–143, 145–148, 155, 156, 158, 159, 162–167, 169, 171–184, 191, 192, 195, 196, 198–200  
Gelator, 1–5, 9–11, 13, 16, 19–23, 25, 27–29, 31, 32, 35–38, 40–52, 62, 63, 66, 68, 69, 73, 74, 76, 84, 89, 90, 96, 110, 126, 128, 129, 131, 133, 136, 140, 145, 162, 165, 181–184  
Gel–sol transition, 15, 19–21, 25, 29, 34, 40–43, 62, 67, 68, 71, 79, 89, 105, 122, 124, 129, 131, 143  
Gel–to–sol phase transition, 10, 11, 43, 47  
Gel–to–sol transformation, 69  
Gel–to–sol transition, 4, 11, 12, 36, 45–47, 50, 51, 74  
Gluconamide, 62  
G–quartet, 127, 128, 138  
Grapheme, 71  
Guanosine, 126–128, 135, 136
- H**  
Heat-responsive, 10  
Helicity, 28  
Heterocycle, 24, 89  
Heterometallic, 69, 92, 95, 96, 105, 106  
Hg<sup>2+</sup>, 72, 100, 131, 133  
Hg vapor, 200  
Hierarchical porosity, 81, 85, 105, 143  
Host–guest, 50, 71, 74, 139  
Host–guest interaction, 46  
Hybrid gel, 83, 107, 163, 181–184  
Hydrazide, 99, 105, 126, 128, 145  
Hydrazone, 124, 126, 128, 145  
Hydrogel, 20, 38–40, 50, 69, 73, 74, 110, 125, 126, 135–138, 141, 145, 157, 162–164,

- 166, 167, 172–176, 181–184, 202, 204–206
- Hydrogen bonding, 1, 3, 5, 11, 13, 16, 19, 25, 31, 37, 40, 42–45, 47–50, 61, 63, 68, 71, 76, 79, 84, 90, 95, 98, 100, 104, 121, 122, 124, 125, 131, 135, 140, 155, 158, 162–165, 167, 168, 178, 179, 198
- Hydrolysis, 84, 120, 191, 192, 194, 195, 200
- Hydrophilic, 48, 50, 155, 157, 158, 176
- Hydrophilicity, 25, 162, 198
- Hydrophobic interaction, 65, 68
- I**
- I<sub>2</sub> vapor, 200
- Imidazole, 17, 76, 89, 103, 109, 110, 139
- Imide, 31, 122
- Imine bonding, 120–122, 124, 129, 172, 173
- Inorganic gel, 1, 191, 204
- Ion, 38, 39, 43, 46, 47, 70, 91, 93–95, 97, 105, 110, 163, 166, 183, 199
- Ionic liquid, 196
- Irradiation, 20–22, 25–28, 31, 43, 86, 87, 122, 131, 139, 140, 148, 177, 179, 180
- L**
- Lead(II), 83
- Ligand, 25, 43, 46, 66, 69, 70, 74, 76, 79, 82, 84–86, 90, 93, 95, 98, 99, 101, 109, 140, 164–167, 169, 170
- Light responsive, 16, 86
- Logic gate, 29
- Low molecular weight gelator, 2, 61, 121, 178
- Luminescence, 34, 66, 69, 85, 88, 95, 99, 101
- M**
- Macrocycle, 93, 140
- Mechanical property, 145
- Mechanical stimuli, 34, 96, 98
- Mechanical stress, 10, 29, 34–37, 42, 98
- Mesoporosity, 81, 88, 105
- Metal ion, 81, 84, 89, 92, 96, 124, 131
- Metallogel, 46, 62, 63, 70, 71, 74, 76, 84, 91, 98, 100, 103–105, 131, 132, 134, 165, 170
- Metal–metal interaction, 73, 76
- Metal-organic, 3, 4, 48, 52, 61–63, 65, 68, 72–74, 79–83, 85–90, 93–95, 97, 98, 100, 101, 105, 106, 108, 109, 129, 130, 140, 158, 164–167, 169
- Metal-organic bond, 3
- Metal-organic cage, 167
- Metal-organic framework, 52, 82, 101
- Metal-organic gel, 63, 73, 76, 86, 93, 95, 99, 100, 107
- Metal oxide, 192
- Metathesis, 120, 199, 200, 201, 203
- Microfluidic, 145
- Microporosity, 81, 105
- Molybdenum, 199
- Monodentate ligand, 74
- Morphology evolution, 83, 90, 92
- Multistimuli-responsive, 41
- N**
- Nanofibre, 42, 74, 79
- Nanoparticle, 195
- Nanoribbon, 205
- Nanotube, 79
- Naphthalene-diimide, 12, 39, 48
- Naphthalimide, 22, 32, 122
- N-containing ligand, 73
- Neutral species, 3, 38, 48
- N-heterocyclic carbene, 70
- Nitrite, 76
- Nitrogen fixation, 203
- Non-covalent, 198
- Non-covalent interaction, 3, 9, 10, 23, 29, 37, 48, 61, 121, 126, 154
- O**
- Organogel, 25, 26, 47–49, 103–105, 122, 132, 173, 174
- Organometallic, 70, 71
- Oxide, 62, 89, 191
- P**
- Palladium(II), 31, 70
- Pd<sup>2+</sup>, 62, 77, 90, 92, 95, 103, 108–110, 169, 170
- Peptide, 31, 34, 42, 70, 141, 142, 183, 184
- Perylene, 13
- Photocatalytic activity, 200, 204
- Photochromic, 24, 49, 86, 122
- Photoisomerization, 20–22, 86
- Photoluminescent, 86
- Photopolymerization, 23, 180, 183
- Photoreactive, 145
- Photoresponsive, 16–19, 24, 26, 41, 86, 141, 183
- pH-responsive, 38, 39, 107, 165
- Physical gel, 157, 158, 171
- Physical stimuli, 37
- $\pi$ – $\pi$  interaction, 3, 13, 19, 42, 47, 89, 95, 122, 140

$\pi$ - $\pi$  stacking, 9, 13, 16, 19, 21, 25, 27, 31, 42, 46, 48, 61, 62, 65, 66, 68–71, 73–77, 79, 94, 97, 121, 124, 125, 132, 166

Picric acid, 88

Pillararene, 74

Pincer, 50, 70, 76, 167

Platinum, 75, 199

Platinum(II), 32, 34, 50, 62, 65, 70, 71, 75

Platinum-acetylide, 71

Polyacrylamide, 155, 157

Polyethylene glycol diacrylate, 157

Polymer gel, 155, 159, 160, 162, 163, 165, 166, 168, 171–173, 175–177, 181, 183

Polyoxybutylene, 157

Polyoxyethylene, 157

Polysiloxane, 155

Porosity, 28, 106, 143, 167, 204

Porphyrin, 143, 145

Post-modification, 103, 108–110

Potassium(I), 84

Pt...Pt interaction, 75–77

Pyrazole, 89, 98

Pyrene, 13, 71, 122–124

Pyridine, 62, 69, 70, 73–76, 89, 90, 95, 96, 98, 120, 131, 140, 170

Pyridyl, 62, 70, 89, 96, 98, 101, 169

Pyrophosphate, 73

## Q

Quantum dot, 13, 34, 101

Quinolinol, 65, 66, 68

## R

Redox, 38, 40–43, 66, 68–71, 84–86, 89, 96, 119, 124, 141, 174

Responsive, 10, 19, 27, 29, 37, 40–43, 46, 47, 50–52, 74, 77, 86, 99, 122, 129, 131–133, 141, 153, 157, 162, 172, 182, 183

Reversibility, 13, 38, 51, 119, 181

Reversible, 3, 10, 12, 15, 16, 19–21, 24, 25, 27–29, 31, 36–38, 40–43, 46, 50, 62, 63, 66, 68–71, 74, 79, 86, 89, 104, 119–122, 126–128, 132, 133, 139–141, 145, 158, 162, 163, 165, 167, 171–176

Rheological study, 5

Rhodamine B, 105, 125, 172

Rotaxane, 63

## S

Scanning electron microscopy, 4

Schiff base, 47, 120

Selective sensing, 73

Selenide, 199

Self-healing, 35–37, 73, 83, 85, 90, 92, 93, 101, 162, 169, 172, 177

Self-repairing, 177

Self-sustainability, 98

Silica gel, 195, 196

Silicone, 155, 156, 179, 180

Silver ion, 46, 65, 79

Silver nanoparticle, 62, 131

Solar cell, 106

Sol-gel process, 192

Sol-gel transition, 79, 172

Solvophobic effect, 4

Sonication, 29–34, 37, 42, 43, 50, 89, 90, 165

Sonogel, 31

Sorption, 85, 105, 143, 196, 200, 204

Spectroscopy, 36, 37, 165, 169, 180, 182, 199, 204

Spirooxazine, 24, 26

Spiropyran, 16, 17, 24–26

Stilbene, 16–18, 21, 22, 145

Stimuli-responsiveness, 46, 47, 162, 171

Sulfide, 101, 199, 200, 201, 202

Supercritical drying, 5, 13, 194, 196, 200

Supramolecular chirality, 18, 20, 28, 67

Supramolecular gel, 6, 10, 12, 77, 99, 131, 181

Supramolecular interaction, 1, 13, 16, 31, 108

Swelling, 13, 15, 20, 154, 155, 158, 159, 174, 177

## T

Tautomerism, 129

Tb<sup>3+</sup>, 93, 94, 99, 134

Temperature-responsive, 10

Template, 2, 81, 106, 107, 128, 135, 180

Terpyridine, 50, 72–75, 93, 95, 97, 163

Terpyridyl, 32, 74, 75, 97

Tetramethoxysilane, 194, 197

Tetraphenylethene, 88, 143

Tetrapodal ligand, 95

Tetrathiafulvalene, 40, 41, 69

Tetrazole, 77, 89, 93

T<sub>gel</sub>, 4, 10, 47, 131

Thermal stimuli, 128

Thermoreversible, 10, 61, 62, 121, 125, 143

Thiol, 174, 175

Thiophene, 40, 41, 201, 202

Thixotrophy, 198

Thixotropic, 35–37, 73, 98, 140

Tissue engineering, 10, 162, 183

Titanocene, 70

Toughness, 119, 162, 163, 165

Toxic gases, 93

Trans-cis isomerisation, 19

Transmission electron microscopy, 73

Triazole, 63, 89

Tridentate ligand, 72, 76, 97

Tripeptide, 68

Tripodal ligand, 95

Trithiocarbonate, 177

Trivalent metal ion, 81, 82, 85, 88

Two-component gel, 39

## U

Ultrasound, 29–32, 34, 90, 122, 140

Urea, 13, 40, 43, 45, 50, 51, 62, 89

## V

Vanadium oxide, 204

Van der Waals interaction, 9, 74, 89, 125, 158

Viscoelastic property, 75, 158

Visual recognition, 97

## X

Xerogel, 13, 16, 62, 79, 84, 85, 91, 99, 101, 105–107, 140, 192

X-ray diffraction, 5, 37

## Z

Zinc(II), 95

Zn<sup>2+</sup>, 47, 68, 72, 73, 90, 95, 97, 101, 103, 105, 128–130, 133, 166